# Mechanism of Passivity Breakdown in Seawater

Comprehensive Final Technical Report
on Contract Nos.

N00014-90-J-1947
May 1, 1990 to December 30, 1995

and

N00014-94-1-0209
December 1, 1993 to August 31, 2000

Submitted to

Office of Naval Research
800 N. Quincy Street
Arlington, VA 22217-5660

Attention:

Dr. A. John Sedriks
Materials Division, Code 1131M

Submitted by

Stephen C. Dexter
Professor
College of Marine Studies
University of Delaware ◆ Lewes, DE 19958

UNIVERSITY OF DELAWARE

# Mechanism of Passivity Breakdown in Seawater

## Comprehensive Final Technical Report

On Grant Numbers:

N00014-90-J-1947
May 1, 1990 to December 30, 1995

And

N00014-94-1-0209
December 1, 1993 to August 31, 2000

Submitted to:

Office of Naval Research
800 N. Quincy Street
Arlington, VA 22217-5660

Attention:
Dr. A. John Sedriks
Materials Division, Code 1131M

Submitted by:

Stephen C. Dexter
Professor
College of Marine Studies
University of Delaware
Lewes, DE 19958

# REPORT DOCUMENTATION PAGE

*Form Approved*
*OMB No. 0704-0188*



| 1. REPORT DATE *(DD-MM-YYYY)* | 2. REPORT DATE | 3. DATES COVERED *(From - To)* |
|---|---|---|
| 16/02/01 | Final Technical | 01/05/90-31/08/00 |

**4. TITLE AND SUBTITLE**

Mechanism of Passivity Breakdown in Seawater

**5a. CONTRACT NUMBER**

**5b. GRANT NUMBER**

N00014-90-J-1947 & N00014-94-1-0209

**5c. PROGRAM ELEMENT NUMBER**

**6. AUTHOR(S)**

Stephen C. Dexter

**5d. PROJECT NUMBER**

**5e. TASK NUMBER**

**5f. WORK UNIT NUMBER**

**7. PERFORMING ORGANIZATION NAME(S) AND ADDRESS(ES)**

College of Marine Studies
University of Delaware
Lewes, DE 19958

**8. PERFORMING ORGANIZATION REPORT NUMBER**

**9. SPONSORING/MONITORING AGENCY NAME(S) AND ADDRESS(ES)**

Office of Naval Research
800 North Quincy Street
Arlington, VA 22217-5660

**10. SPONSOR/MONITOR'S ACRONYM(S)**

**11. SPONSORING/MONITORING AGENCY REPORT NUMBER**

**12. DISTRIBUTION AVAILABILITY STATEMENT**

Approved for public release: distribution unlimited

**13. SUPPLEMENTARY NOTES**

**14. ABSTRACT** Natural marine biofilms shift the open circuit potential of passive alloys and enhance their cathodic properties. It has been shown that this affects both the initiation and propagation of localized corrosion of these alloys. The increase in cathodic properties also produces an increase of 5 to 8 times in the galvanic corrosion rate of anodic materials connected to passive alloys with biofilms. Critical pitting and breakdown potentials are also affected by biofilm formation but the mechanism for this effect is uncertain. Solid state microelectrode techniques using square wave voltammetry have been developed for measuring chemical profiles through the biofilm thickness. Laser confocal microscopy has been used to image the community of microbes at the sites of chemical measurement. The mechanism for these effects is believed to involve continual redox cycling of manganese dioxide within the biofilm matrix. It has been shown that a combination of chemical and biological reoxidation of reduced manganese species is able to account for the observed corrosion rates.

**15. SUBJECT TERMS** Passivity Breakdown, Biofilms, Corrosion Initiation, Corrosion Rate, Ennoblement, Seawater, Manganese Dioxide, pH, peroxide, microelectrodes, confocal microscopy, interfacial chemistry, Weldements, Passive Film

| 16. SECURITY CLASSIFICATION OF: | | | 17. LIMITATION OF ABSTRACT | 18. NUMBER OF PAGES | 19a. NAME OF RESPONSIBLE PERSON |
|---|---|---|---|---|---|
| a. REPORT | b. ABSTRACT | c. THIS PAGE | | | Stephen C. Dexter |
| UU | UU | UU | UU | 162 | 19b. TELEPONE NUMBER *(Include area code)* (302) 645-4261 |

# Table of Contents:

# I. Introduction

Research in our lab during the decade of the 1990s has concentrated on how microorganisms in natural marine biofilms can influence the process of passivity breakdown on corrosion resistant (passive) alloys and the rates of marine corrosion involving those alloys. Three types of questions were asked during the course of this research. First, we wanted to determine the degree to which microbial activity at the metal surface in a typical coastal marine environment could influence passivity breakdown. In order to do this, we designed experiments to measure the effect of biofilm formation on the open circuit potential (OCP), the breakdown potential for localized corrosion initiation and the initiation time. Second, we wanted to document whether or not the action of microbes in biofilms had an influence on the localized corrosion rate of the passive alloy after initiation, or on the galvanic corrosion rate of more anodic materials in contact with the passive alloy. These things will be referred to in this report as the phenomenon, or the effect of, biofilms. Third, we wanted to determine the mechanisms by which the organisms were able to accomplish these effects.

This report is organized into five major sections. Following this introductory section, some background will be given about work on the phenomenon during the 1980s and early 90s with support from E.P.R.I. and Sea Grant. This work set the stage for the ONR sponsored effort. Section III will relate results from the ONR sponsored work to extend our knowledge of the phenomenon. During the course of the ONR work, we became involved from time to time in developing new methodologies for use in the research. These developments will be discussed in Section IV. The bulk of the ONR sponsored work was devoted to an investigation of the mechanisms, which will be presented in Section V. Finally, in Section VI, a summary will be presented on the questions asked during the research and the degree to which they have been answered.

## II. Background

The background for the ONR sponsored work summarized in this report was prepared by our research during the 1980s on how natural marine biofilms affect the open circuit potential (OCP) of passive metals and alloys, a phenomenon called ennoblement. Then in the late 1980s and early 1990s we extended that work to see what effect biofilms might have on the initiation and propagation of crevice corrosion.

During the work on ennoblement, we showed that the OCPs of all passive alloys tested including UNS S30400, S30403, S31600, S31603, S31703, S31803, N08904, N08367 (6XN), S44660 (29-4C), S44735, N10276 (C-276) and Titanium R50250 were eventually ennobled in the presence of biofilms (Dexter, 1985; Dexter, et al., 1988; Dexter and Gao, 1988; Dexter and Zhang, 1990). Ennoblement of the OCP occurred in fresh, brackish and sea waters as long as corrosion initiation did not interfere. The rate of ennoblement was slower in fresh than in sea water, but the amount of ennoblement was inversely related to the salinity of the electrolyte (Dexter, 1992). The most noble potentials reached were also highest and most consistent in fresh water. Thus, it was concluded that ennoblement of the OCP decreased the salinity level below which a given alloy should be resistant to localized corrosion initiation (Dexter, 1992). Theoretically, this information could be used to decide the upper salinity limits for application of any given alloy. In practice, however, this is hard to do for two reasons. First, there are seasonal and tidal salinity fluctuations in any natural estuarine environment. Second, complex industrial equipment, such as heat exchangers, that are often fabricated from passive alloys may themselves create salinity gradients due to variations in temperature and flow rate.

Dexter and Zhang (1991) and Dexter, Zhang and Chandrasekaran (1994) reported that ennoblement was the most persistent and reproducible under darkened or continuously low light level conditions. Tests done on alloy N10276 under a translucent roof exposed to daily light/dark cycling showed large fluctuations in the ennobled potential. The most noble potentials were usually recorded at night, while the potential typically dropped by up to 200 mV during the daylight hours. This behavior was rationalized in terms of the photosynthetic activity of bacterial and algae in the biofilm.

It had been shown by Johnsen and Bardal (1985), Scotto (1985, 1989), Dexter and Gao (1988) and Holthe, et al. (1988) that the cathodic kinetics of passive alloys were enhanced during the ennoblement process in addition to changes in the OCP. But there was no data to show whether or not that would effect localized corrosion initiation and propagation. We bagan by looking at crevice corrosion initiation. Dexter, Lucas and Gao (1986) showed that dissolved oxygen in the crevice solution could be depleted by the action of microorganisms in the crevice water at about the same rate as it is depleted in the process of maintaining the passive film. Thus, there is a biological component in the first step in crevice corrosion initiation for any alloy immersed in natural saline waters. They concluded that this effect was of little practical importance because the oxygen depletion time by electrochemical means alone is already much shorter than the desired lifetime of the alloy.

Tests on alloys S30400 and S31600 revealed that crevice initiation times were reduced when natural marine biofilms were allowed to form on the boldly exposed external cathode surface of crevice corrosion samples (Zhang and Dexter, 1992, 1993, 1995a, 1995b; Dexter, 1992). In order to perform such tests, an effective control experiment has to be devised in which the chemistry and geometry are kept the same, but biofilm formation is retarded. Several types of control tests were tried during this research, and the effectiveness of various control procedures is review further in Section IV of this Report. In many crevice corrosion tests the initiation time was statistically significantly reduced in the presence of natural biofilms vs. control. There was a lot of variability in the data, however, and while the difference was obvious in some tests, it was less so in others. Nevertheless, it was concluded from the tests that ennoblement of the OCP in the presence of natural biofilms usually caused the alloy to reach its breakdown potential for crevice initiation faster than when the test was repeated under control conditions.

The results on crevice propagation were much more definitive. Propagation rates after initiation were significantly and consistently enhanced as shown by Zhang and Dexter (1992, 1993, 1995). Crevice propagation densities were increased by one to three orders of magnitude vs. control for alloys S30400, S31603, S31725 and N08904. The effect was also reflected in greater weight loss, as well as higher maximum and average depths of attack on test alloys with biofilms on the exterior cathode surface vs. control. Theoretical weight losses calculated from the measured current densities and Faraday's Law were in good agreement with the measured weight losses.

It was not clear during the course of this work whether the effects of biofilms on crevice initiation and propagation were due to the same mechanism. While ennoblement of the potential, leading to a decrease in initiation time, could result from things that change either the thermodynamic or kinetic factors of the cathodic electrochemistry, an increase in propagation rate clearly required an increase in kinetics. Thus, by the mid 1990s it was becoming clear that any mechanism trying to explain the overall effect of biofilms would have to account for thermodynamic and kinetic effects.

**Papers published from early non-ONR sponsored work:**

S. C. Dexter, 1985, "Fouling and Corrosion," Proceedings, EPRI Condenser Biofouling and Control Symposium, Held at Orlando, FL, in June 1985, pp. 2-28 to 39, published November, 1985.

S. C. Dexter, K. E. Lucas and G. Y. Gao, 1986, "The Role of Bacteria in Crevice Corrosion Initiation," Proceedings, International Conference on Biologically Induced Corrosion, NACE, Held: Gaithersburg, MD, June 10-12, 1985, pp. 144-153, Pub. June, 1986.

S. C. Dexter, 1988, "Role of Microfouling Organisms in Marine Corrosion," Presented as Plenary Lecture at 7th Intl. Congr. On Marine Corrosion and Fouling, Valencia, Spain, November, 1988. (Proceedings never published)

S. C. Dexter and G. Y. Gao, 1988, "Effect of Seawater Biofilms on Corrosion Potential and Oxygen Reduction on Stainless Steels", Corrosion, Vol. 44, No. 10, p. 717.

F. Mansfeld, B. Little and S. C. Dexter, 1989, "Discussion on Effect of Seawater Biofilms on Corrosion Potential and $O_2$ Reduction of Stainless Steel", Corrosion, 45(10), p. 786.

S. C. Dexter and H-J. Zhang, 1990, "Effect of Biofilms on Corrosion Potential of Stainless Alloys in Estuarine Waters", Proc. 11th Intl. Corrosion Congress, Florence, Italy, April 1990, p. 4.333.

H-J. Zhang and S. C. Dexter, 1992, "Effect of Marine Biofilms on Crevice Corrosion of Stainless alloys," Paper #400, CORROSION/92, Nashville, TN, April 92.

S. C. Dexter and S-H Lin, 1992, "Effect of Marine Biofilms on Cathodic Protection," International Biodeterioration, Vol. 29, No. 3, pp. 231-249.

S. C. Dexter and S-H. Lin, 1992, "Calculation of Seawater pH at Polarized Metal Surfaces in the Presence of Surface Films," Corrosion, Vol. 48, No. 1, pp. 50-60.

S. C. Dexter, 1992, "Implications of Biological Effects to Localized Corrosion of Stainless Alloys," Proceedings 1st Pan American Congress on Corrosion and Protection, Mar del Plata, Argentina, October, 1992, p. 485-500.

H-J. Zhang and S.C. Dexter, 1993, "Effect of Biofilms on Crevice Corrosion of Stainless Alloys in Coastal Seawater, Proc. 12th International Corrosion Congress, Vol. 5B, NACE, International, Houston, TX, pp. 3761-3772.

S. C. Dexter, H-J. Zhang and P. Chandrasekaran, 1994, "Biofouling Effects on Corrosion of Stainless Alloys in Seawater," Biodeterioration Research 4, G.C. Llewellyn, W.V. Dashek and C.E. O'Rear, Eds., Plenum Press, New York, pp. 553-571.

D. C. Hansen, S. C. Dexter and J. H. Waite, 1995, "The Inhibition of Corrosion of S30403 Stainless Steel by a Naturally Occurring Catecholic Polymer," Corrosion Science, Vol. 37, No.9, p. 1423.

H-J Zhang and S. C. Dexter, 1995, "Effect of Biofilms on Crevice Corrosion of Stainless Steels in Coastal Seawater," Corrosion, Vol. 51, No. 1, 1995, pp. 56-66.

H-J. Zhang and S. C. Dexter, 1995, "Effect of Marine Biofilms on Initiation Time of Crevice Corrosion for Stainless Steels," CORROSION/95 Paper No. 285, NACE International, Houston, TX.

**Other References Cited:**

Holthe, R., E. Bardal and P.O. Gartland, 1988, "Time dependence of Cathodic Properties of Stainless Steels, Titanium, Platinum and 90-10 CuNi in Seawater," Corrosion/88 Paper No. 393, NACE, International, Houston, TX.

Johnsen, R. and E. Bardal, 1985, Corrosion, 41, p. 296.

Scotto, V., R. DiCintio and G. Marcenaro, 1985, Corrosion Science, 25, p. 185.

Scotto, V., 1989, Proc. E.P.R.I. Workshop on Microbial-Induced Corrosion, EPRI ER-6345, Palo Alto, CA, p. B-1.

# III. ONR Sponsored Work on the Phenomenon of Ennoblement

## III.A. Critical Pitting Potential and Its Relation to OCP

In seawater, a major reason for structural failure of stainless steels is due to localized pitting and crevice corrosion. Theoretically, the open circuit corrosion potential, Ecorr, can not be more noble than Ecpp without initiating passivity breakdown. Thus, potential ennoblement caused by biofilms was expected to increase the probability of pit and crevice corrosion initiation. This effect was demonstrated by Dexter and Zhang (1995a). However, there were also cases where the ennobled Ecorr was higher than Ecpp of the same alloy measured in seawater of the same bulk salinity (Zhang, 1993). It was suspected that factors in addition to chloride activity must become important at the metal surface under a marine biofilm where the water chemistry may be different from that of the bulk water. Therefore, one of the first things addressed with ONR support was the effect biofilms may have on the relation between the open circuit potential and the pitting and breakdown potentials associated with the onset of localized corrosion. The results of that work were presented at the 1995 NACE Conference on Microbiologically Influenced Corrosion and published in the proceedings volume for the conference (Zhang and Dexter, 1995b). Excerpts from that paper are as follows:

The flat samples used for this work were immersed part way, leaving an air water interface on the sample surface. Pitting potentials were measured potentiostatically in a one-liter corrosion-testing cell. Whenever pitting initiated on the flat submerged face of the coupon the associated potential was taken as a critical pitting potential, Ecpp. When pits initiated at the air-water interface or at an edge or corner of the sample, the associated potential was taken as a breakdown potential, Eb. Thus, the final Ecpp value was taken as the most noble potential at which pitting on the flat submerged face of the coupon did not initiate within two hours after a 20 mV increase in the potential. Initiation was confirmed under a stereo microscope at 50 x. Likewise, the final Eb was taken as the most noble potential at which corrosion did not initiate elsewhere on the sample.

For alloy S30400, the average Ecpp of the biofilmed samples (425 ± 24 mV SCE) was 95 mV higher than that of the bare samples (330 ± 35 mV). The t-test showed that these differences were significant (at $P = 0.002$). This result is not surprising since bacteria produce nitrates and sulfates. Further, many bacteria accumulate large amounts of inorganic phosphate in the form of granules of polyphosphate. When bacteria die, those phosphates will be released into the biofilm. $Na_2S0_4$ and $NaNO_3$ (concentrations as low as 0.0125 M) are known to be pitting inhibitors for stainless steels. The presence of these corrosion inhibitors in biofilms would certainly increase Ecpp for S30400.

For alloy S31600, the Ecpp values of the biofilmed samples (500 mV) were not much different from those of the bare samples (480 ± 17 mV) and the t-test showed that the difference was not statistically significant ($P = 0.200$). The reason for this is unknown, but it is possible that the inhibitor concentration produced in the biofilm was not high enough to affect the higher Ecpp for S31600.

The breakdown potential data for alloy S30400 showed that Eb increased from 60 mV for the bare sample to 260 ± 20 mV for those with biofilms. For alloy S31600 Eb increased a smaller amount from 300 mV for the bare sample to 390 ± 14 mV for those with biofilms. These values agreed favorably with our previous observations that corrosion at the air-water interface was observed for S30400 and S31600 after Ecorr reached the potentials of about 250 and 350 mV SCE respectively.

Comparing values of Ecpp and Eb for samples with biofilms, the average Ecpp for alloy S30400 was 165 mV higher than Eb. For S31600 samples with biofilms the average Ecpp value was 110 mV higher than Eb. This agrees with common experience that localized corrosion initiates more readily at corners, edges and interfaces than on the boldly exposed face of the sample. Ecpp values for stainless steels are usually measured with bare samples in chemical solutions, and the effect of biofilms are not considered. The results in this paper showed that marine biofilms did increase Ecpp for S30400. Therefore, Ecpp for stainless steels, especially the low resistance steels such as S30400, should be measured using samples with biofilms instead of bare samples.

The Ecpp tests using various values of pH and peroxide on bare S30400 samples in seawater showed that there were no statistically significant systematic differences in the Ecpp values for pH from 2.9 to 7.2 and for peroxide up to 4 ppm. This is consistent with earlier measurements of Leckie and Uhlig (1966) and Fokin, et al., (1965) and Kolotyrkin, et al., (1963) that Ecpp for 18Cr-8Ni type alloys was not greatly affected in 0.1 N NaCl solutions. Little et al. (1991) reported that Ecpp for S30400 decreased from about 300 mV at pH 8 to zero mV SCE at pH 2.8. However, they used 10% acetic acid to adjust the pH of their synthetic seawater. It would have required at least 30% by volume of this acid to reach pH 2.8 in artificial seawater, while the volume of 1 N HCl required to adjust pH from 7.8 to 2.9 in our natural seawater tests was less than 0.35%. Thus, the final composition of the artificial seawater used by Little et al. (1991) was significantly different from that of natural seawater, and their results may not correspond to what happens in a natural biofilm.

From this work we concluded that: 1) Biofilms significantly increased the critical pitting potential (Ecpp) for S30400 in seawater, while they had little effect on Ecpp for S31600; 2) Critical pitting potentials for low resistance stainless steels such as S30400 should be measured using samples with biofilms if the results will be used to predict the initiation of pitting in natural seawater; 3) The lack of direct effect of pH and peroxide (singly or in combination) on Ecpp of alloy S30400 is compatible with the ennoblement mechanism calling for low pH and peroxide in marine biofilms.

## References Cited

Fokin, M., M. Kurtepov, V. Bochkareva, Sbomik po Korozii, (1965), Moscow.

Kolotyrkin, Ya M., G.V. Golovina, G.M. Florianowich, Dokl. Akad. Nauk SSSR, 148, (1963), p. 1106.

Leckie, H., H. Uhlig, J. Electrochem. Soc.. 113 (1966), p. 1262.

Little, B., R. Ray, P. Wagner, Z. Lewandowski, W. Lee, W. Characklis, F. Mansfeld, Biofouling 3, (1991): pp54-55.

Zhang, H-J., 1993, "Effect of biofilms on localized corrosion of stainless@alloys" (Ph.D Dissertation, University ofDelaware, p.59.

Zhang, H-J., S.C. Dexter, 1995a, "Effect of marine biofilms on initiation time of crevice corrosion for stainless steels," Corrosion/95, paper no.285 (Houston, TX:NACE).

Zhang, H-J. and S. C. Dexter, 1995b, "Effect of Biofilms on Critical Pitting Potentials for Stainless Steels S30400 and S31600 in Seawater," Proc. 1995 International Conference on Microbiologically Influenced Corrosion, New Orleans, LA, May, 1995, P. Angel, et al., eds., NACE International, Houston, TX, pp. 70/1 - 70/8.

### III.B. Ennoblement of Alloys with n- and p-Type Passive Films

Marine and fresh water biofilms usually shift the open circuit potential (OCP) of stainless steels in the electropositive direction by several hundred millivolts. One of the reasons for this ennoblement is thought to be the presence of Mn in biofilms. Earlier work by Maruthamuthu had suggested that differences in the amount of ennoblement from one alloy to the next could be due to variations in the electronic structure of their passive films. As a Post-Doctoral Investigator in Dr. Dexter's lab, Dr. Maruthamuthu pursued the passive film question further, investigating ennoblement of two stainless steels, UNS NO8367 (6XN, having an n-type passive film) and NO6455 (C4 with a p-type film). This work will be presented at the Spring 2001 NACE Meeting as COR/2001 Paper No. 256. The following are selected exerpts from that paper.

$MnO_2$ was coated (See Section IV for the procedure) onto the oxide films of both alloys. As shown in Figure III.B.1 the $MnO_2$ coating resulted in a higher OCP (+750 mV SCE) on n-type alloy NO8367 than on the p-type NO6455 (+360 mV). This is consistent with the interpretation that $MnO_2$ reduction is easier on the n-type passive film, which is rich in free electrons, than on the p-type film. Figure III.B.2 shows mixed potential vs. time for the same alloys with equal immersed areas of $MnO_2$ coating and bare oxide film.

OCP measurements were also made for equal area $MnO_2$ coated coupons in the presence of 0.3mM EDTA. For alloy NO8367 the potentials shifted to a maximum range of +500 to 550 mV SCE within 2000 sec. Two additional samples had been kept in seawater for 7 days after $MnO_2$ coating. For those samples the potential shifted to the +400 mV level. For 3 control samples without $MnO_2$ coating the potentials shifted a smaller amount to about -100 mV SCE. In contrast the potentials of $MnO_2$ coated NO6455 samples shifted to a maximum of about 400 mV upon addition of EDTA. The potential shift in this case, however, was consistently more gradual with time. A single 6-day-old $MnO_2$ coated coupon of NO6455 was also tested. The potential of this older coupon rose to a lesser value (about +300 mV) than that of the fresh ones under the same conditions. Three control samples without $MnO_2$

coatings were also subjected to EDTA additions. The potentials of these coupons changed in the positive direction by a small amount.

Coupons with $MnO_2$ coatings exposed to natural seawater developed similar potential shift to that of the samples without $MnO_2$ coatings. Samples of $MnO_2$ coated NO8367 exhibited a negative shift over the first 2 days, followed by the usual ennoblement to the +400 to 450 mV range. The control samples in filtered seawater all showed a continuous negative drift after the initial 2-day decrease. In contrast, the $MnO_2$ coated NO6455 coupons in natural seawater showed a gradual positive shift to about 350 mV over the 15-day exposure period, while the control samples were relatively unaffected during the exposure. This indicates that without the biofilm, $MnO_2$ alone cannot produce a lasting positive shift in the potential. This result is consistent with the effect of EDTA on the $MnO_2$ coated coupons.

Cathodic polarization curves run on the two alloys revealed reduction peaks for Fe, Mn and Cr oxides. The Fe and Mn reduction peaks were thought to be due to the availability and flow of electrons between the n-type passive oxide film and the n-type $MnO_2$ coating. These peaks were consistently absent for the p-type alloy NO6455. Since p-type films are deficient in free electrons, the $MnO_2$ coating on those alloys was thought to supply electrons to the oxide film for chromium reduction. The results are consistent with the idea that bacteria, having a net negative surface charge, accumulate reduced manganese ions for re-oxidation.

Based on the results of this study, the differences in ennoblement tendencies above were attributed to differences in electronic structure between the two types of semiconducting passive films, particularly with regard to the availability of free electrons. The behavior of $MnO_2$ coated coupons of the two test alloys immersed in natural seawater was similar upon the formation of biofilms to what it had been for each alloy with EDTA additions. This implied that microorganisms and/or polymers within natural biofilms have chelating properties similar to EDTA. It was proposed that a contributing factor in ennoblement comes from interactions between bacterially produced $MnO_2$ and polymers in the biofilm. This process, in turn, may be influenced by the electronic structure of the passive film. The iron and manganese reduction peaks on alloy N08367 were due to the ease of electron flow between the passive film and the $MnO_2$ film, which are both n-type. In contrast, on alloys such as N06455 with p-type passive films having a low concentration of free electrons, $MnO_2$ reduction was more difficult, resulting in less ennoblement in the presence of both $MnO_2$ films and natural biofilms. When $MnO_2$ is present, however, it may supply electrons to the p-type oxide film for chromium ion reduction. The results help to explain why alloys with p-type passive films have been observed to ennoble less and more slowly than those with n-type films.

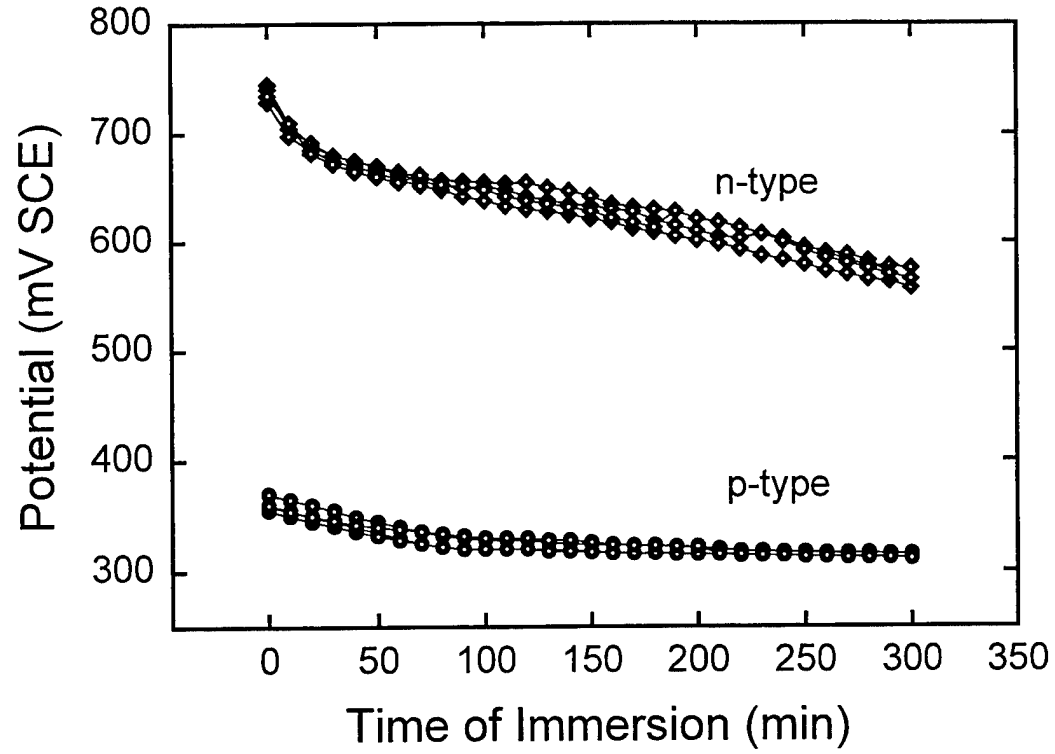


Figure III.B.1. OCP measurements for n- and p-type alloys with fully coated $MnO_2$

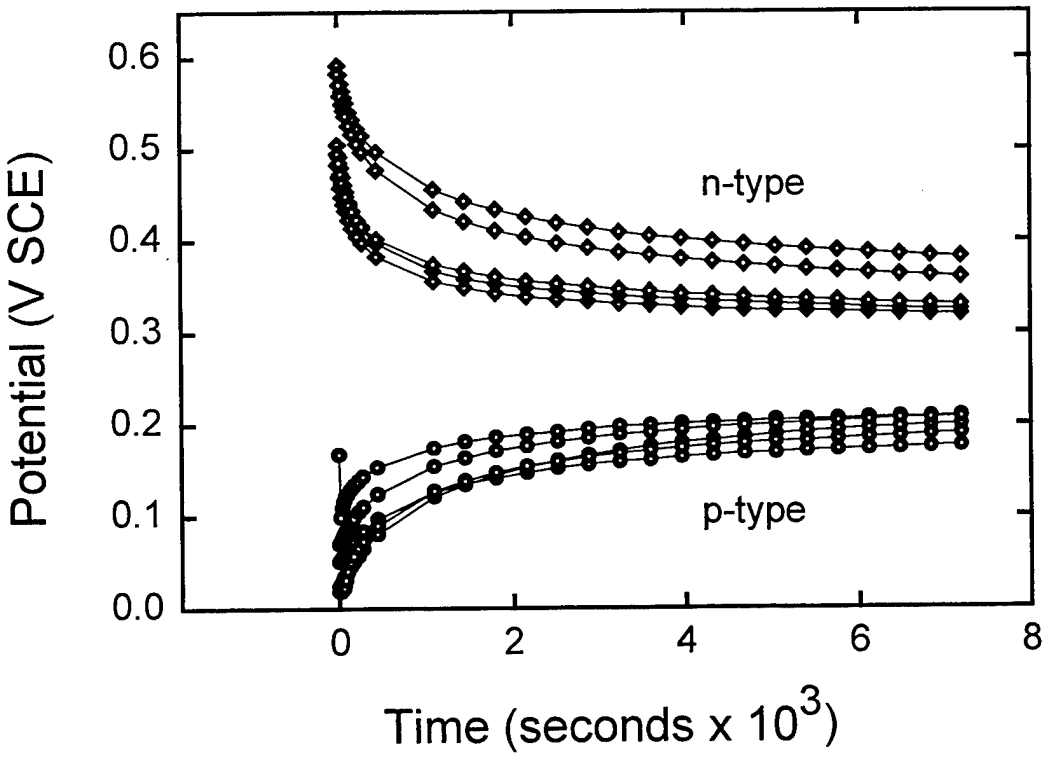


Figure III.B.2. Mixed potential between $MnO_2$ and passive film for n- and p-type alloys.

### III.C. Biological Settlement Patterns on Weldments

In natural aqueous environments corrosion and microbial settlement take place together on immersed metal surfaces. Most investigators would agree that the two phenomena can and do influence each other. For at least two decades, however, there has been controversy in the literature as to whether the settlement patterns of microorganisms on metal surfaces are determined by electrochemical activity, or cause it. This has lead to a number of questions about cause and effect. Are microorganisms attracted preferentially to sites of pre-existing electrochemical activity? Alternatively, does the formation of microcolonies on the metal surface serve to initiate electrochemical activity at the sites of those colonies? Moreover, why do microbial colonies appear to form preferentially associated with certain metallurgical features, such as welds?

The tendency in the 1980s was to blame the microbes for initiating corrosion whenever they were found to be present at a corrosion site. Dexter (1988, 1993) pointed out in marine systems, that organisms in the general biofilm remote from the corrosion site were often more involved with corrosion initiation than those found within the corrosion products at the site. Little, et al. (1996) has warned repeatedly that it is dangerous to decide that a certain organism caused a given incidence of corrosion just because it was found at the corrosion site. Yet it was commonly agreed that organisms present on the metal surface often had an important influence on both initiation of corrosion (eg., see the discussion of crevice initiation in Section II above) and its propagation rate (see Section III.D below).

The question has become particularly pertinent to the important industrial corrosion problem of the development of deep pits under discrete "biodeposits" associated with the welds on stainless steel tanks and piping. The question has been raised as to whether microbial settlement or corrosion initiation comes first. Do the microbes first form the biodeposit at the weld for some unknown reason, creating chemical conditions favorable for corrosion initiation? Or rather, do the biodeposits form in response to corrosion initiation? In either case it is widely agreed that the microorganisms are involved in determining the severity of corrosion. Dexter (1988, 1993, and 1995) suggested the following sequence for the process. The initial biofilm forms randomly over the entire wetted metal surface. That film is then instrumental in ennobling the open circuit potential of the metal to the point where electrochemical activity starts at the weakest locations on the passive film. Microbes are attracted in great numbers to the active sites, forming microbial colonies and eventually the observed biodeposits. The physical presence of the colonies/biodeposits shields and isolates the active site, promoting the initiation of stable localized corrosion. The chemistry developed by the microorganisms within the biodeposit then serves to accelerate the corrosion rate.

Experimental work on this subject with specific application to stainless steel weldments was done in Dr. Dexter's lab with ONR support during the MS Thesis research of Dheeraj Sakhuja (1997), and by Post-Doctoral student, Dr. Eashwar. Parts of this work were presented at Corrosion/99 and published as Conference Paper no. 174 (Eashwar and Dexter, 1999). Excerpts from that paper and from Sakhuja's thesis are as follows.

The purpose of this work was not to explain the mechanism of microbial attack but rather to address bacterial settlement patterns in relation to anodic electrochemical activity. Experiments were designed in such a way that the metal surface could be made electrochemically more anodic, but with or without initiating active corrosion. Stainless steel weldments were chosen as the test materials not only because of their industrial importance but to take advantage of their intrinsic character that renders some defined areas (such as heat affected zone) more vulnerable, and therefore electrochemically more active, than the parent metal. Thus, the basic idea of the work was to examine bacterial settlement on a material that had zones of different electrochemical activity. Anodic polarization was used as a tool for enhancing the activity in two different test media (coastal seawater and fresh pond water). This allowed the extent and intensity of electrochemical reactions to be varied widely.

Welded coupons of UNS S30400 stainless steel were 50 x 100 x 3 mm with the weld bead running across the width at 25 mm from the bottom end as shown in Figure III.C.1. The progression of bacterial numbers with time in three different zones (parent metal away from the weld, heat affected zone, HAZ, adjacent to the weld and the weld bead itself) was measured for exposures in seawater and fresh water. In all three zones in both environments, there was an increase in bacterial numbers with time. Figure III.C.2 shows bacterial numbers at seven locations running in a line perpendicular to the weld. Locations 1 and 2 are in the parent metal above the weld in Figure III.C.1. Location 3 is within the HAZ above the weld,. Location 4 is on the weld bead. Location 5 is within the HAZ below the weld, and locations 6 and 7 are in the parent metal below the weld. Note from Figure III.C.2 that bacterial settlement occurred more rapidly in the heat-affected zone (HAZ) and at the root of the weld as compared to the parent metal. In seawater the bacterial numbers that developed in the HAZ were nearly an order of magnitude higher than those in the other zones. In the pond water however, no discernible differences in bacterial settlement patterns on the three zones were observed.

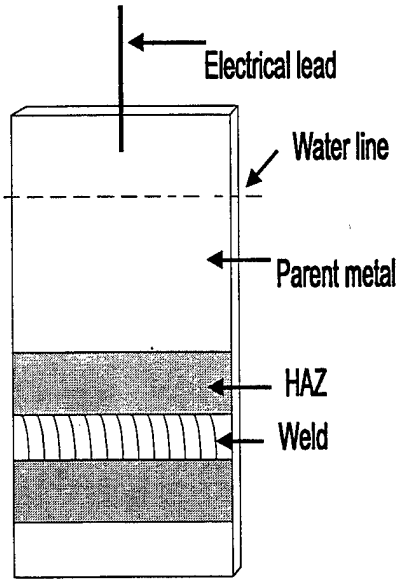


Figure III.C.1 – Welded stainless steel sample showing general features and zones.

Initial microbial settlement patterns were random in all three zones as depicted in Figure III.C.3. With increasing time of exposure, however, preferential attachment of bacteria to a network of surface cracks was routinely observed for the least corrosion resistant alloy, S30400 stainless steel, freely immersed in seawater as shown in Figure III.C.4 Starting at about 100 hours of immersion, dense bacterial colonies were also observed to develop within the HAZ on alloy S30400, especially when the heat tint film from the welding process was not removed prior to exposure. On the more corrosion resistant alloy S31600 random attachment paying no attention to the surface cracks or HAZ was observed. On both alloys, and in both environments preferential attachment could be induced by anodic polarization to 0mv SCE. This potential was below that required to initiate stable corrosion in either environment. In the less corrosive fresh pond water, bacterial settlement was more random, until application of anodic polarization, which triggered bacterial settlement patterns analogous to the sea water system. Supplementary experiments on bacterial response to pre-initiated corrosion sites in the form of pits and scratches reinforced the idea that bacteria preferentially colonize areas of anodic electrochemical activity and/or metal ion release. These results strongly suggest that non-random settlement around the weld and HAZ on alloy S30400 was triggered by electrochemical activity.

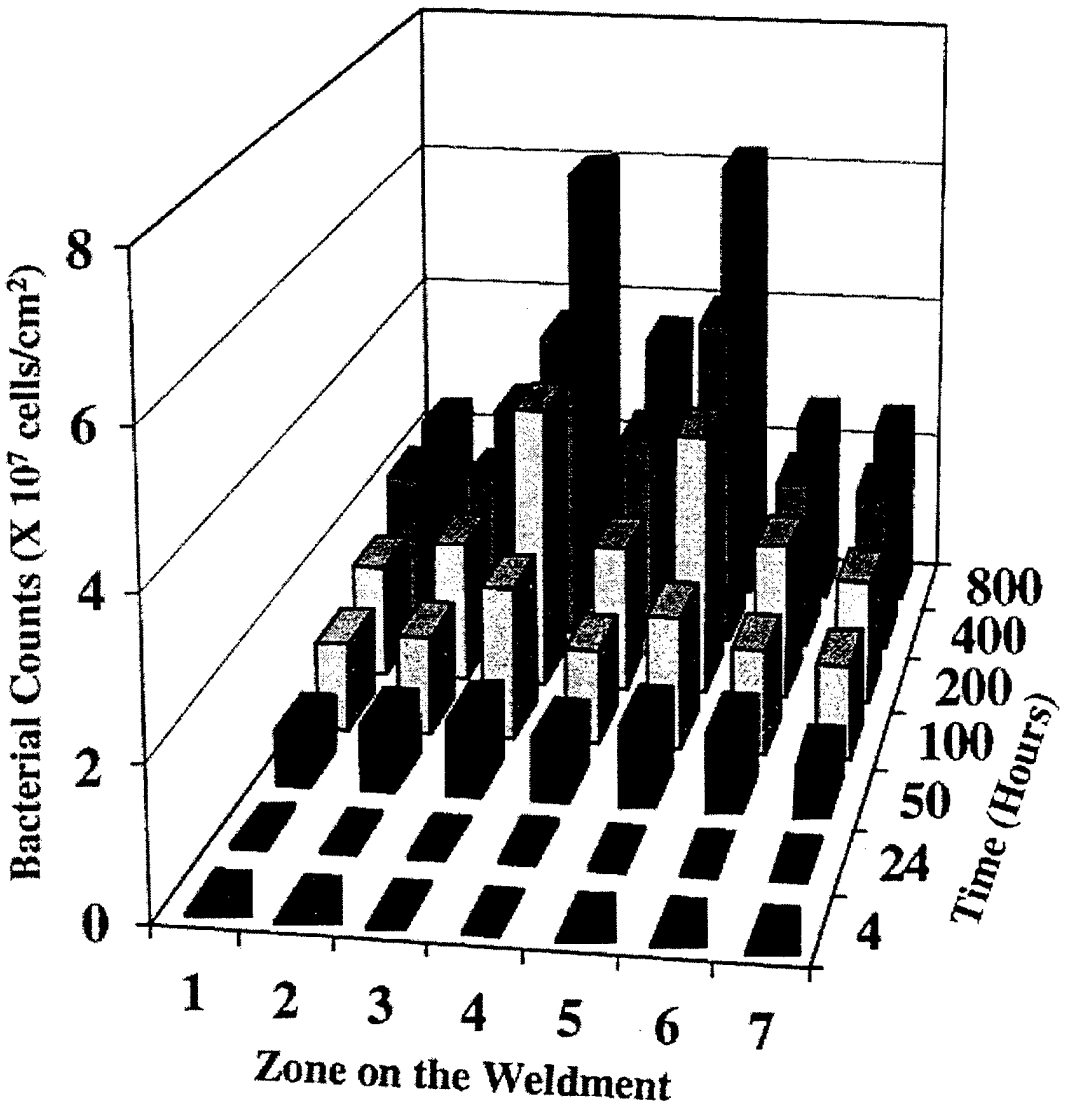


Figure III.C.2. Bacterial counts obtained in various zones on welded coupons.

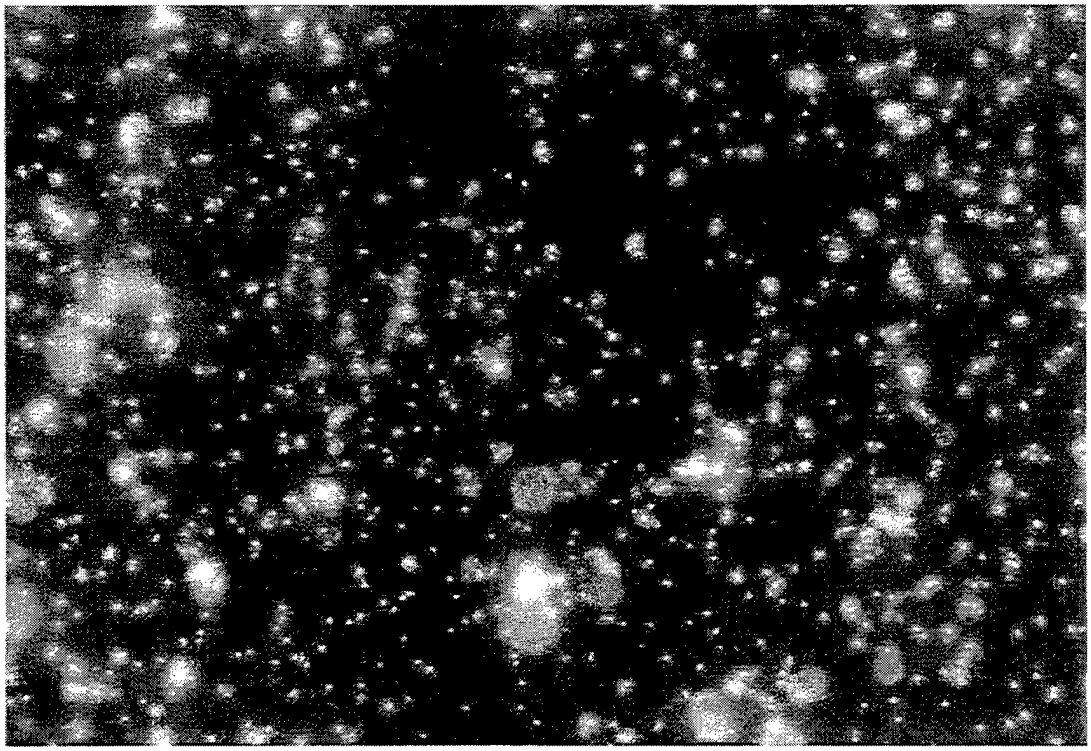

Figure III.C.3. Random settlement pattern on welded S31600 coupon in seawater.

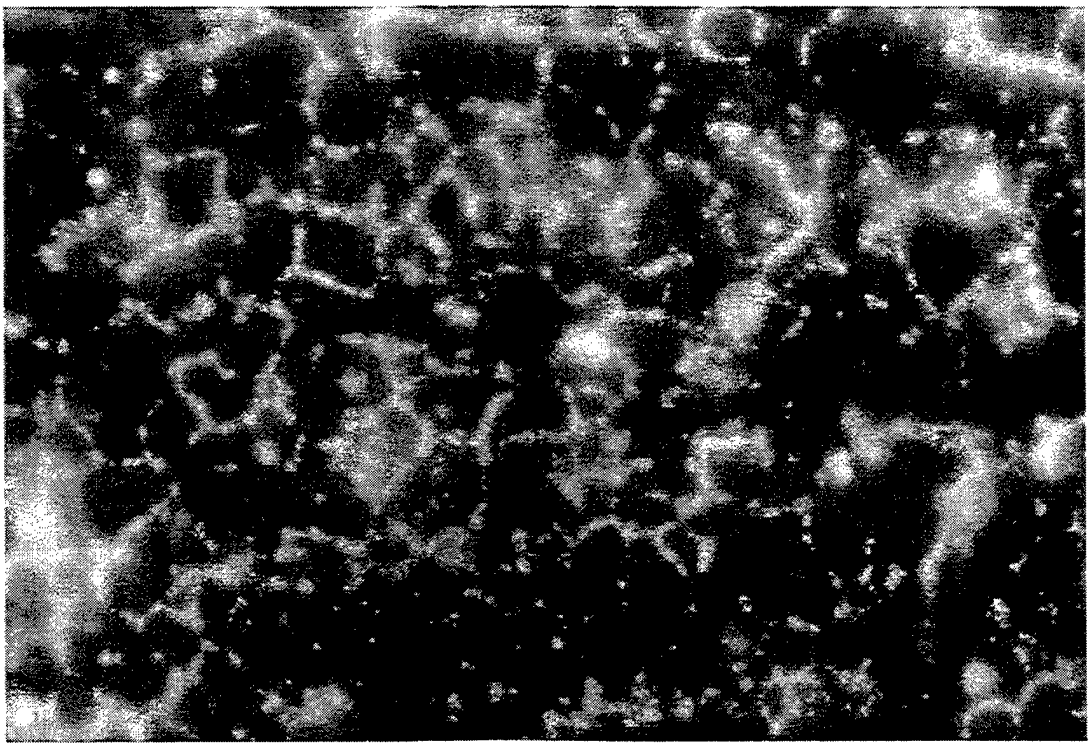

Figure III.C.4. Preferential settlement to surface cracks on S30400 coupon.

Other welded samples of S30400 were immersed for the purpose of monitoring the open circuit corrosion potential until corrosion initiation had occurred. Potential versus time curves for four samples each exposed to natural seawater and control seawater are shown in Figure III.C.5. The control water was produced by a filtering and low temperature pasteurizing process to retard biofilm formation without changing the chemistry of the bulk water. These and other control procedures and their effectiveness are discussed further in Section IV of this Report. It can be seen from Figure III.C.5 that the coupons exposed in the natural seawater gradually ennobled to about +300 mV SCE within 400 hours of exposure. Within 700 hours all of their potentials had dropped and stabilized at about –120 mV SCE. This drop in potential indicated that stable localized corrosion had initiated, and this was confirmed by visual inspection. In contrast, no ennoblement was observed for the samples exposed in the control water, and corrosion had not initiated on any of those samples even after 900 hours of immersion. After one month of exposure, epifluorescent microscopy with DAPI staining was used to make bacterial counts on samples exposed to both natural and control waters. The results are shown in Figure III.C.6. The difference of nearly two orders of magnitude was found to be statistically significant (t-test, $p < 0.05$). The results in Figures III.C.5 and 6 suggest that the electrochemical activity responsible for non-random settlement at the weld and HAZ started in response to ennoblement of the OCP from formation of the general biofilm.

Upon termination of the experiment, the surface condition of the coupons was recorded photographically, and one of them exposed in natural seawater is shown in Figure III.C.7. Note that the corrosion pit has formed along the upper edge of the weld, and its appearance is just beginning to develop the vertical tiger striping pattern so commonly observed on the surface of corroded industrial weldments.

It is difficult to relate the present results on small coupons to the literature on corrosion initiation of large weldments. Nevertheless, the results presented here show ennoblement of the OCP in both fresh- and sea-waters in response to initial biofilm formation. They also show enhanced settlement and microcolony formation at sites of electrochemical activity induced by anodic polarization with a potentiostat. It is reasonable to expect that polarization due to biofilm formation (ennoblement) would have the same effect. In none of the experiments during this work were large microbial colonies observed to form prior to some sort of electrochemical activity, but often they formed in response to it. Thus, these results favor the proposed sequence of initial random settlement, ennoblement, electrochemical activity, colony formation, localized corrosion initiation, biodeposit formation and corrosion acceleration.

This illustrates the need to address more carefully the progression of bacterial attachment before, during and after corrosion initiation if one wants to convincingly establish biological effects on corrosion. Further work needs to be done to precisely address the nature of bacterial attraction to sites of anodic electrochemical activity.

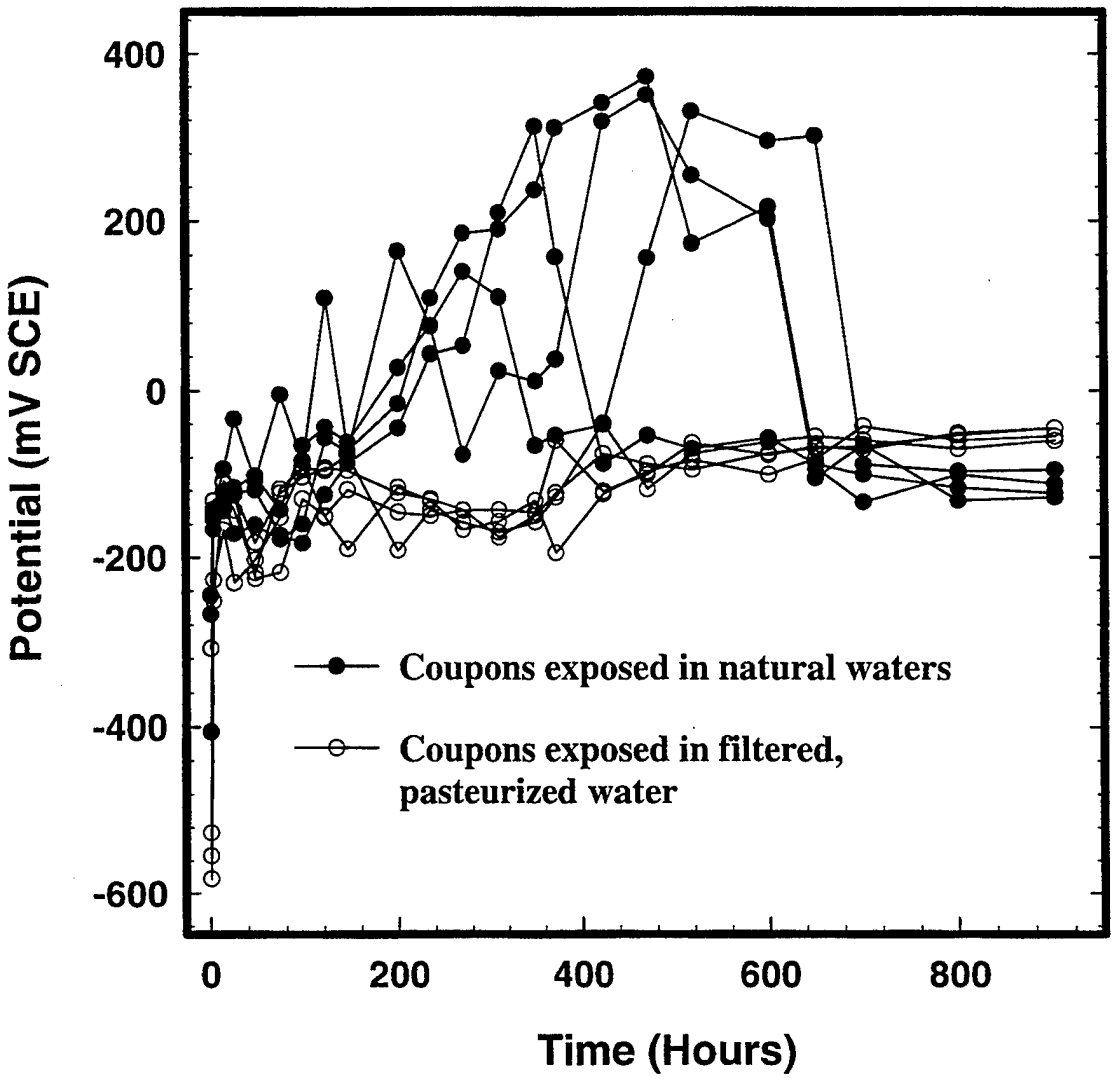


Figure III.C.5. Ennoblement of open circuit potentials with time for welded S30400 coupons immersed in natural and control seawaters.

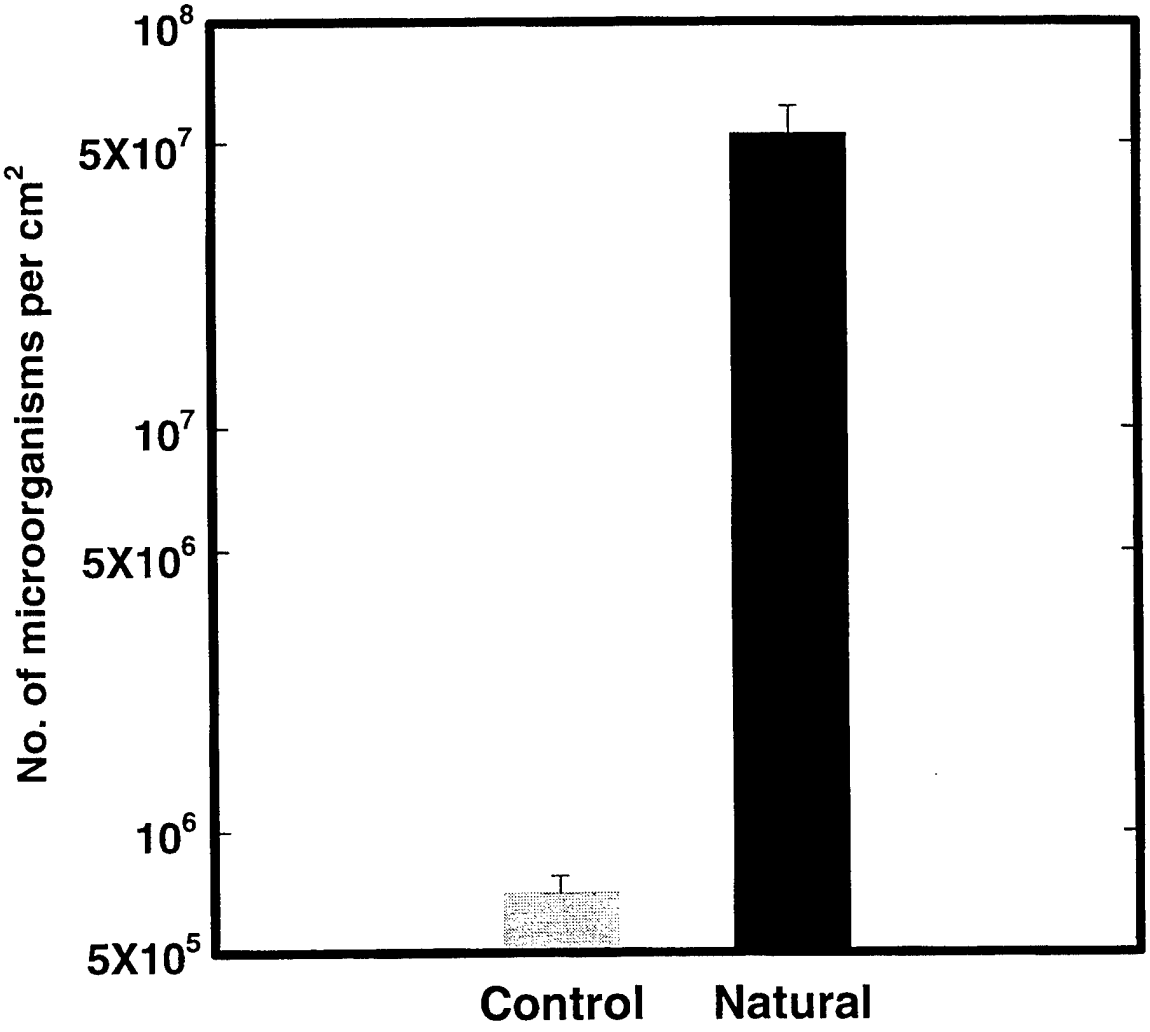


Figure III.C.6. Bacterial counts on welded S30400 coupons after one month of exposure to natural and control seawaters.

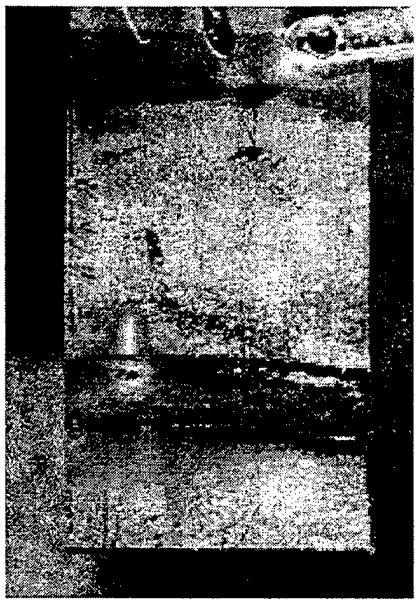

Figure III.C.7. Corrosion pit at weld on S30400 coupon. Note the development of the characteristic vertical tiger striping pattern.

## References Cited


Dexter,S. C., 1993, "Role of Microfouling Organisms in Marine Corrosion", Biofouling, Vol. 7, pp. 97-127.

Dexter, S. C., 1995, "Effect of Biofilms on Marine Corrosion," in Bioextraction and Biodeterioration of Metals, C. Gaylarde and H. Videla, Eds., Cambridge University Press, pp. 129-167.

Dexter, S. C., 1988, "Role of Microfouling Organisms in Marine Corrosion," Presented as Plenary Lecture at 7th Intl. Congr. On Marine Corrosion and Fouling, Valencia, Spain, November, 1988. (Proceedings never published)

Eashwar, M. and S. C. Dexter, 1999, "Relation of Bacterial Settlement Patterns to Anodic Activity on Stainless Steel Weldments," Paper No. 174, CORROSION/99, NACE, International, Houston, TX.

Little, B.J., P.A. Wagner, K.R. Hart, R. Ray, 1996, "Spatial Relationships Between Bacteria and Localized Corrosion," Corrosion/96 Paper No. 278 (Houston, TX: NACE International).

### III.D. Effect on Galvanic Corrosion

Another major thrust of the ONR sponsored work in the 1990s was to determine whether the action of a natural marine biofilm on passive metal surfaces would have any effect on galvanic corrosion. This was in parallel with the work described in Section II above on the effects of biofilms on crevice corrosion propagation. Based on cathodic and anodic polarization curves first published by Mollica, et al (1988) and Scotto (1985, 1989) and confirmed by our group (see: Dexter et al, 1993; Dexter, 1995; Zhang and Dexter, 1995) it was predicted that the galvanic corrosion rate of copper should be enhanced by biofilms on a passive cathode. It was also predicted from the polarization data that the galvanic corrosion rate of zinc should not be affected by biofilms on the cathode. No clear prediction could be made from the polarization results, however, for the galvanic corrosion rates of steel and aluminum.

Preliminary experiments done with ONR support in the early 1990s (Dexter, et al, 1993) indicated that biofilms did enhance the galvanic corrosion rates of steel and 3003 aluminum connected to stainless steel panels with biofilms. These results also confirmed the predicted lack of an effect on zinc. Based on these results a much more thorough investigation was initiated using copper, steel, 3003 aluminum and zinc as the test anodes. This work has been published in several papers (LaFontaine and Dexter, 1997; Dexter and LaFontaine, 1998a, 1998b; Dexter, 1998, 1999) Excerpts from those papers are as follows:

Of all the anodic materials used in this study, copper produced the greatest differences in corrosion currents between couples with biofilms on the cathode surface and the control couples without biofilms. As shown in Figure III.D.1, corrosion currents for all couples decreased steadily as corrosion product films built up. During the first 10-12 days corrosion currents were highly variable as the couples equilibrated with the seawater. Average corrosion currents shown in Table 2 were calculated for the period from day 12 to day 60. Currents were 2 to 3 decades higher for copper couples with biofilms on the cathode than for the corresponding control couples. Statistical t-tests were performed on data from the copper couples for days 12, 19, 27 and 60. The differences for these days shown in Figure 3 were all significant, with the calculated P-values for the t-statistic being $2.23 \times 10^{-4}$, $1.00 \times 10^{-2}$, $4.23 \times 10^{-3}$, and $3.00 \times 10^{-3}$, respectively. Weight losses observed on copper anodes coupled to biofilmed NO8367 were also significantly higher (P-value $6.55 \times 10^{-3}$) than those on control coupons (Table III.D.1). Copper anodes coupled to biofilmed cathodes were visibly more corroded than those coupled to control cathodes. The biofilms themselves are described, including epifluorescent micrographs, in the paper. Color photographs of the weight loss coupons are also shown in the paper.

After copper, structural steel was the next most noble of the five materials used as anodes in this study. Significant differences in corrosion current developed between biofilmed and control couples after the first 10-12 days of immersion (Figure III.D.2). P-values for corrosion currents on days 12, 19, 27 and 60 were $1.80 \times 10^{-3}$, $2.08 \times 10^{-5}$, $1.0 \times 10^{-2}$ and $3.90 \times 10^{-4}$ respectively. Average corrosion currents for biofilmed couples ranged from 4.26 to 5.00 mA, compared to those of control couples, which ranged from 0.835 to 0.890 mA (Table III.D.2). Weight losses on the 1018 steel coupons coupled to biofilmed cathodes were

approximately 5 times higher than those found on 1018 steel coupons coupled to control cathodes (Table III.D.2), and these differences were significant with $P = 1.26 \times 10^{-4}$. The difference was also confirmed by visual inspection of the test and control coupons. The galvanic behavior of 3003 aluminum was similar to that of 1018 steel, and the data are shown in the published papers.

Corrosion currents for all zinc couples, both biofilmed and control, were similar to eachother (Figure III.D.3). Average corrosion currents for all zinc couples were within the range of 5.62 to 6.16 mA, and those for biofilmed couples were not significantly different from control. Weight loss values for all zinc coupons ranged from 6.21 to 6.85 grams, and the P-value of 0.33 showed that there were no significant weight loss differences. There were also no visible differences in corrosion damage between samples from biofilmed and control couples.

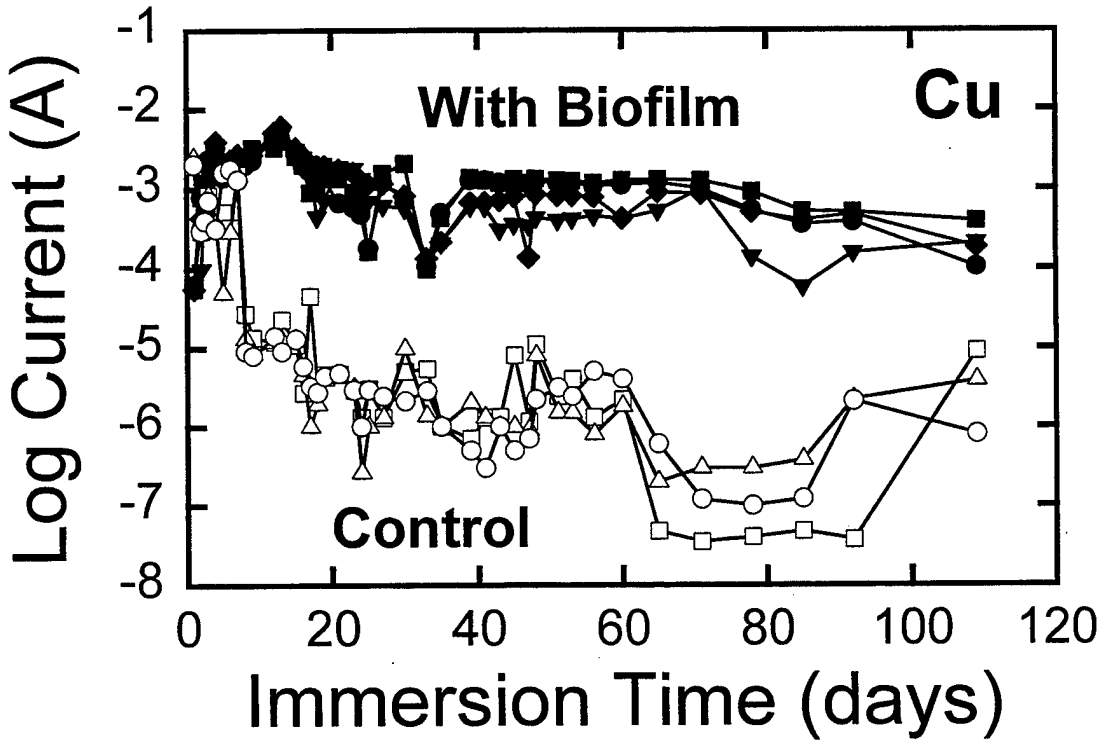


Figure III.D.1 Corrosion currents for galvanic couples with copper.

**Table III.D.1 Galvanic Corrosion Data for Copper Anodes**

| COUPLE | AVERAGE CORROSION CURRENT (mA) (days 12 to 60) | AVERAGE CORROSION POTENTIAL (mV vs. SCE) | WEIGHT LOSS (grams) |
|---|---|---|---|
| Biofilm 1 | 0.78 +/- 0.38 | -135 +/- 39.6 | 6.39 |
| Biofilm 2 | 0.57 +/- 0.40 | -155 +/- 46.4 | 3.84 |
| Biofilm 3 | 1.11 +/- 0.48 | -11.1 +/- 83.4 | 5.75 |
| Biofilm 4 | 0.95 +/- 0.40 | -9.83 +/- 77.5 | 4.67 |
| Control 1 | 0.0025 +/-0.0027 | -145 +/-70.6 | 2.10 |
| Control 2 | 0.0016 +/- 0.0017 | -129 +/-88.8 | 1.93 |
| Control 3 | 0.0020 +/-0.0013 | -145 +/- 74.2 | 2.37 |

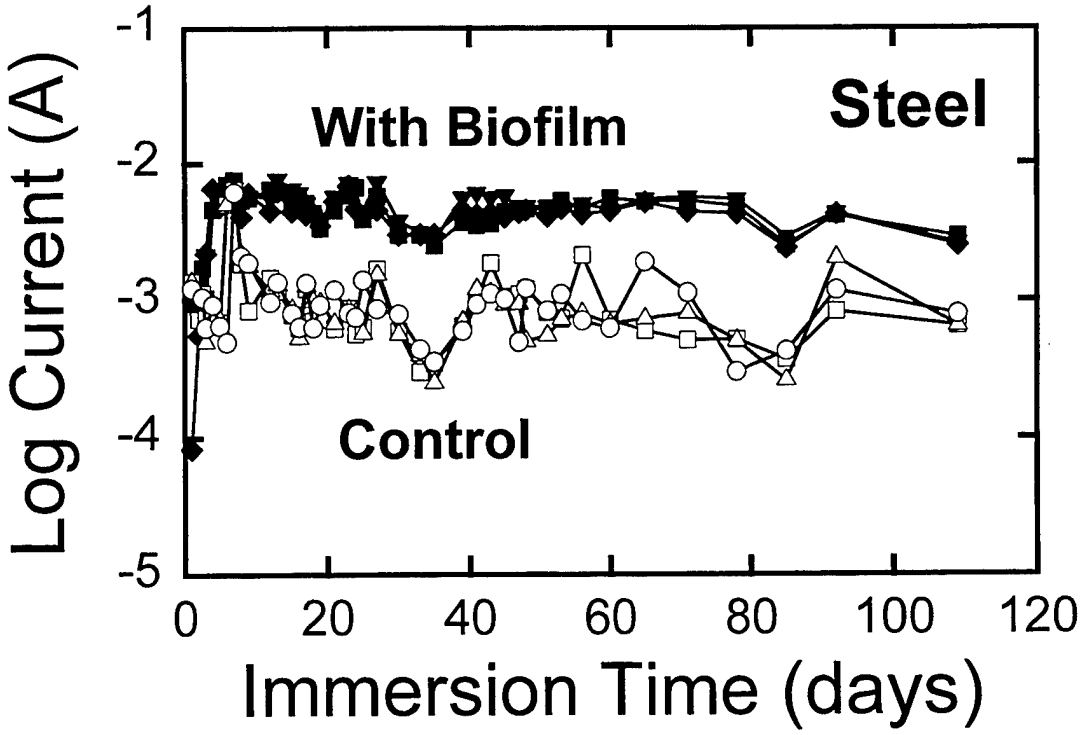


Figure III.D.2 Corrosion currents for galvanic couples with steel.

## Table III.D.2 Galvanic Corrosion Data for 1018 Steel Anodes

| COUPLE | AVERAGE CORROSION CURRENT (mA) (days 12 to 60) | AVERAGE CORROSION POTENTIAL (mV vs. SCE) | WEIGHT LOSS (grams) |
|---|---|---|---|
| Biofilm 1 | 4.26 +/- 0.92 | -700 +/- 26.5 | 9.7 |
| Biofilm 2 | 5.00 +/- 1.3 | -699 +/- 33.9 | 10.8 |
| Biofilm 3 | 4.54 +/- 1.1 | -698 +/- 21.8 | 9.2 |
| Control 1 | 0.875 +/- 0.44 | -733 +/- 29.7 | 2.1 |
| Control 2 | 0.835 +/- 0.38 | -735 +/- 31.9 | 1.9 |
| Control 3 | 0.890 +/- 0.35 | -732 +/- 32.6 | 2.6 |

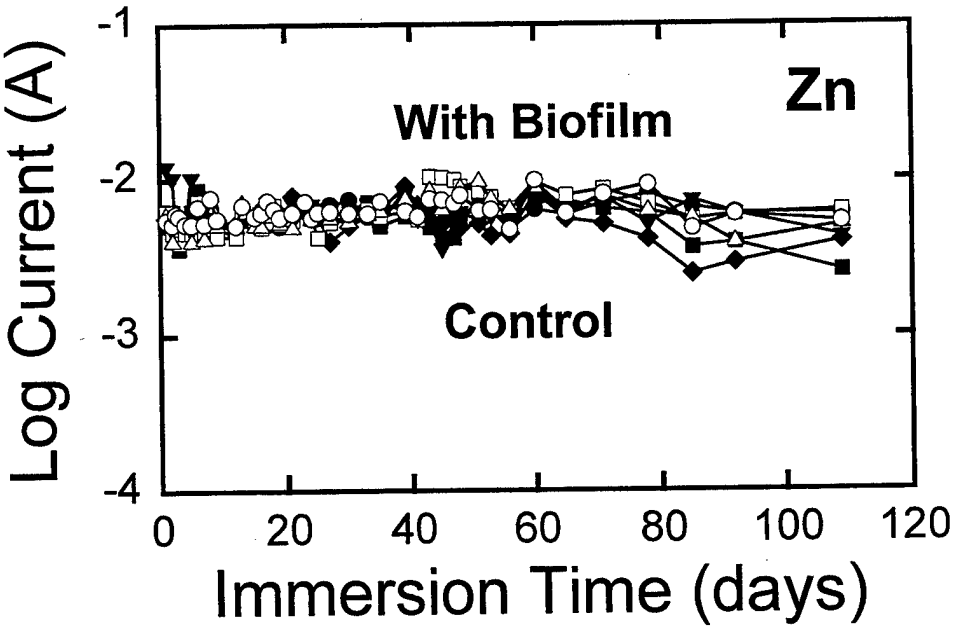


Figure III.D.3 Corrosion currents for galvanic couples with zinc. Note that the differences between biofilm and control samples shown in Figures III.D.1 and 2 for copper and steel anodes have disappeared.

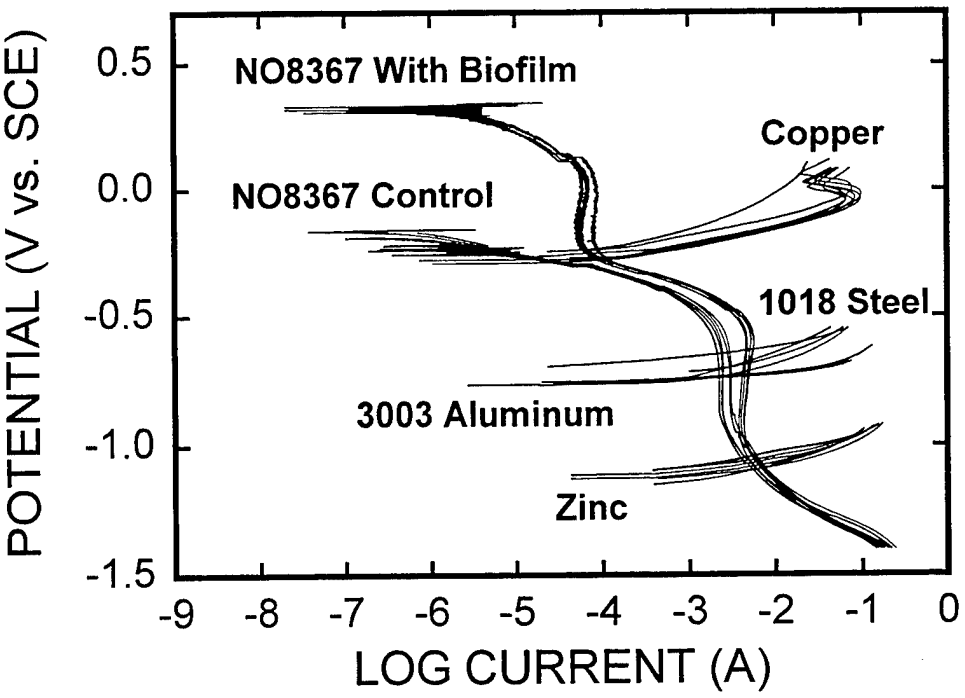


Figure III.D.4 Cathodic polarization curves for UNS alloy NO8367 with biofilm and without (control) and anodic polarization curves for copper, steel, aluminum and zinc. Anodic curves were taken from the corroded coupons at the end of the exposure period.

Polarization curves measured for corroded anodes and biofilmed cathodes are shown in Figure III.D.5. At potentials more noble than approximately -900 mV, the curves for all biofilmed NO8367 cathode coupons were shifted to the right vs. control. This shift was most severe at potentials more noble than -250 mV. The increase in the limiting current on biofilmed coupons between -300 and -900 mV (Figure 10) is significant, with P-values for the t-tests being below 3.0 x 10-5 at potentials of -400 and -700 mV SCE. The increase in current at these potentials as a result of the presence of a biofilm correlates well with the measured increases in galvanic currents and weight losses for the steel and aluminum anodes.

The increase in cathodic reduction kinetics due to the presence of a biofilm was found to diminish at potentials more active than about –1,000 mV vs. SCE (See Figure III.D.4). At these active potentials, the interface pH may increase due to enhanced OH- ion production from oxygen reduction as well as hydrogen evolution. An increase in pH to above 9 at the metal-biofilm interface would inactivate most marine microorganisms. Under the heavy metal hypothesis there could be two reasons why the cathodic polarization curves with and without biofilms on the metal surface merge at potentials more negative than –1000 mV. Either microbial recycling of Mn is prevented by the higher pH, or hydrogen evolution becomes the predominant cathodic reaction at the more negative potentials as it does when in competition with the oxygen reduction reaction.

The implications of biofilm effects for control of galvanic corrosion in natural aqueous environments or for cathodic protection by sacrificial anodes are dependent on the situation. Microbial films form on virtually all metal surfaces in natural waters. If the cathodic surface is well covered with a paint coating, however, biofilm effects on the cathodic properties of the metal will be negated. If the passive metal surface is not coated, the effect of a biofilm will be determined by the mixed potential of the couple. For couples with mixed potentials more noble than about -850 mV SCE, the data presented here indicate that corrosion of the anodic member of the couple will be increased due to the action of biofilms. The data also indicate that biofilms will increase the current necessary to protect stainless steel from pitting at a potential of -400 mV SCE, and that they will increase consumption of the steel anodes often used for that purpose. For couples with anodes of zinc, or a more active material, however, the data indicate that the mixed potential should be active enough for there to be no increase in anode consumption. The practice of keeping surfaces clean is certainly reinforced by the results of this study. Allowing highly corrosion resistant passive alloy surfaces to foul just because that is not expected to increase their own corrosion rate or susceptibility may lead to an increased corrosion rate on an adjacent metal which is in galvanic contact.

Some stainless steels have OCP values more active than Cu-Ni alloys and many bronzes when the clean materials are first immersed in seawater. This implies that stainless steel would be the anode in a galvanic couple when these materials are first immersed. The data presented here, as well as that in the general literature on the ennoblement phenomenon, imply that the polarity of such galvanic couples would be reversed for any stainless steel that had become ennobled without initiation of localized corrosion prior to being joined with one of these Cu-Ni or bronze alloys in a galvanic couple. Such a reversal in polarity might not happen, however, if the galvanic couple was established immediately upon first immersion, and localized corrosion initiated on the stainless steel while it was the anode. The data presented here do not give any reliable basis on which to predict the effect of biofilms on galvanic couples in which both members of the couple are passive alloys.

These experimental results confirmed the predictions of an increase in the galvanic corrosion rate of copper with no effect on that of zinc. They also showed that the rates of galvanic corrosion of steel and aluminum were increased by the activity of biofilms on the cathode. Thus, the entire action of biofilms cannot be understood on the basis of how they effect just the electrochemical potential of a given alloy. One also has to be able to explain how the galvanic current density is increased, not just in laboratory tests, but also for months at a time in the field. These experiments also showed that there is more to predicting the rate of marine corrosion in surface waters in the presence of biofilms than just measuring the water chemistry and dissolved oxygen concentration.

**References Cited:**


Dexter, S. C., P. Chandrasekaran, H-J Zhang and S. Wood, 1993, "Microbial Corrosion in Marine Environments: Effect of Micro-fouling Organisms on Corrosion of Passive Metals", Proc. 2nd USA/Argentina Workshop on Biocorrosion and Biofouling, Buckman Laboratories International, Inc., Memphis, TN, pp. 171-180.

Dexter, S. C., 1995, "Effect of Biofilms on Marine Corrosion," in Bioextraction and Biodeterioration of Metals, C. Gaylarde and H. Videla, Eds., Cambridge University Press, pp. 129-167.

Dexter, S. C., 1998, "Contribution of Biofilms to the Rate of Marine Corrosion," LATINCORR 98 Paper No. S19-08, 3rd Latin American Region Corrosion Congress, Cancun, Mexico, August, 1998.

Dexter, S. C., 1999, "Role of Biofilms in Determining the Rate of Localized Marine Corrosion," in Critical Factors in Localized Corrosion III, A Symposium in Honor of the 70th Birthday of Jerome Kruger, R. G. Kelly, P. M. Natishan, G. S. Frankel, and R. C. Newman, Eds., PV 98-17, The Electrochemical Society, Pennington, NJ, 1999, pp. 339-352.

Dexter, S.C. and J.P. LaFontaine, 1998, "Effect of Natural Marine Biofilms on Galvanic Corrosion Predicted Using Potentiodynamic Polarization Curves, CORROSION/98 Paper No. 288, NACE, International, Houston, TX.

Dexter, S. C. and J. P. LaFontaine, 1998, "Effect of natural marine biofilms on galvanic corrosion," Corrosion, Vol. 54, No. 11, p. 851.

LaFontaine, J.P. and S.C. Dexter, 1997, "Effect of Marine Biofilms on Galvanic Corrosion," in Proc. Tri-Serv. Conf. on Corrosion, November, 1997, Wrightsville Beach, NC.

Mollica, A., G. Ventura, E. Traverso, V. Scotto, 1988, "Cathodic Behavior of Nickel and Titanium in Natural Seawater," 7th Intl. Biodeterioration Symp., Cambridge, UK.

Scotto, V., R. DiCintio, G. Marcenaro, 1985, Corrosion Science, 25, 3: p. 185.

Scotto, V., 1989, "Electrochemical Studies on Biocorrosion of Stainless Steel in Seawater," EPRI Workshop on Microbial Induced Corrosion, G. Licina, ed., Electric Power Research Institute, Palo Alto, CA, p. B.1.

Zhang, H-J and S. C. Dexter, 1995, "Effect of Biofilms on Crevice Corrosion of Stainless Steels in Coastal Seawater," Corrosion, Vol. 51, No. 1, 1995, pp. 56-66.

## III.E. Effect of Biofilms on Manganese Bearing Stainless Steels

Work in this section was in support of the developing Navy interest in non-magnetic, welded, stainless steel ship hulls. In order to obtain non-magnetic properties and avoid the deleterious effects on corrosion of delta ferrite formation upon welding, the alloys of choice were to include the manganese bearing stainless steel, Nitronic 50, and the superaustenitic, 6% molybdenum alloy, 6XN, which also contains some manganese.

It has recently been determined that manganese and iron concentrated at the millimolar level by the organisms within marine biofilms on passive metals play a large role in the corrosion behavior of those alloys in both the welded and non-welded conditions in seawater. The alloys tested previously, however, have been the ordinary 300 series stainless steels with some super austenitics and super ferritics. These alloys all contain less than 2% by weight of manganese, but there is abundant manganese available to the microbes in the water at our exposure site. Thus, it is of both practical and academic importance to determine if manganese will have a deleterious effect on corrosion of the manganese bearing alloys of navy interest. Since naval ships go into many types of environments, it will also be important to determine if the source of manganese (from the environment vs. the metal) makes any difference in its effect on corrosion.

For this purpose, the objectives of the work were to: 1) Determine the effect of biofilms on OCP and on corrosion initiation at welds of Nitronic 50 using alloy 6XN as a control, 2) determine the effects of biofilms and manganese on the properties of Nitronic 50 as a galvanic cathode. and 3) determine if it matters how much manganese is in the alloy when it is present or absent in the environment.

### III.E.1. Effect of Biofilms on Nitronic Series Alloys

The working hypothesis for these experiments was that Mn and Fe concentrated within the biofilm matrix on the Nitronic series of manganese bearing stainless steels would be involved in the mechanism by which microorganisms accelerate the cathode reaction as it has been in all other stainless steels we have tested. Data were collected during the Ph.D. Dissertation work of Dr. Kunming Xu (2000) on the behavior of Nitronic Alloys 33, 40 and 50, along with 6XN which served as the control. These alloys contain different percentages of manganese as shown in Figure III.E.1.

Potentiodynamic anodic polarization curves for three coupons each of the three Nitronic alloys in seawater of 30 ppt salinity are shown in Figure III.E.2. The data were obtained by polarizing flat metal coupons under aerated seawater conditions. The breakdown potential of each sample was taken as the potential value when the current density reached 0.001 $A/cm^2$. Thus, the breakdown potentials were: 212 ± 26 mV for Nitronic 33, 733 ± 23mV for Nitronic 40 and 1075 ± 16 mV for Nitronic 50. In each case corrosion initiation at the breakdown potentials occurred on the flat, boldly exposed surfaces of the coupons below the air/water interface. Note that Nitronic33, which contains the highest amount of Mn, had the lowest

breakdown potential. Nitronic 50, which contains lowest amount of Mn and 2.5% of Mo, possessed the highest breakdown potential.

Nitronic series stainless alloys and AL6XN were immersed in natural seawater during the summer months. Their open circuit potentials were measured over time as shown in Figures III.E.3 to 6. For Nitronic 50, Nitronic 40 and AL6XN coupons Figures III.E.3, 4 and 5 respectively), open circuit potentials increased with time due to biofilm formation. Within 2 weeks of their immersion, open circuit potentials reached over +300 mV versus SCE, and remained in the range of +320 to +430 mV. This is in agreement with previous reports in the literature on passive alloys under biofilm forming conditions (Zhang and Dexter, 1995). However, for Nitronic 33 (Figure III.E.6), the open circuit potentials increased to about +100 mV within the first three days of immersion and then dropped sharply. Since the potentials in Figure III.E.6 were only being measured once a day, the peak values immediately prior to corrosion breakdown were probably missed. Thus, it is not surprising that the breakdown potential of 212 mV recorded in Figure III.E.2 was not shown. After corrosion initiation, the potentials for Nitronic 33 fluctuated within the range of -200 mV to -50 mV. These low potential values indicated that the metal had probably undergone localized corrosion. Microscopic observation confirmed that there were many localized corrosion sites at the metal surfaces. This behavior is similar to that of type 304 stainless steel (Zhang and Dexter, 1993).

From these data it can be concluded that the ennoblement behavior of the Nitronic Series alloys under biofilm forming conditions in seawater is similar to that of other stainless alloys tested previously. No work has yet been done on Nitronic series alloy weldments.

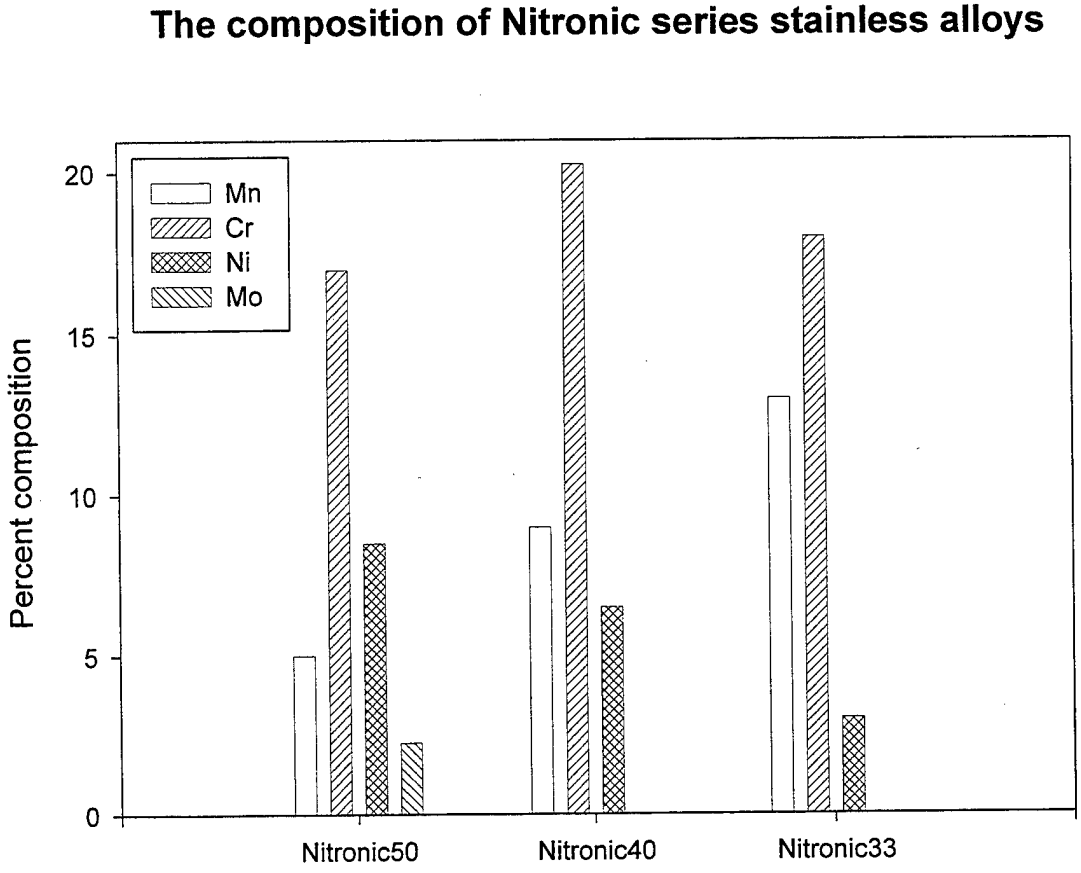


Figure III.E.1. The major elemental composition of Nitronic series stainless alloys.

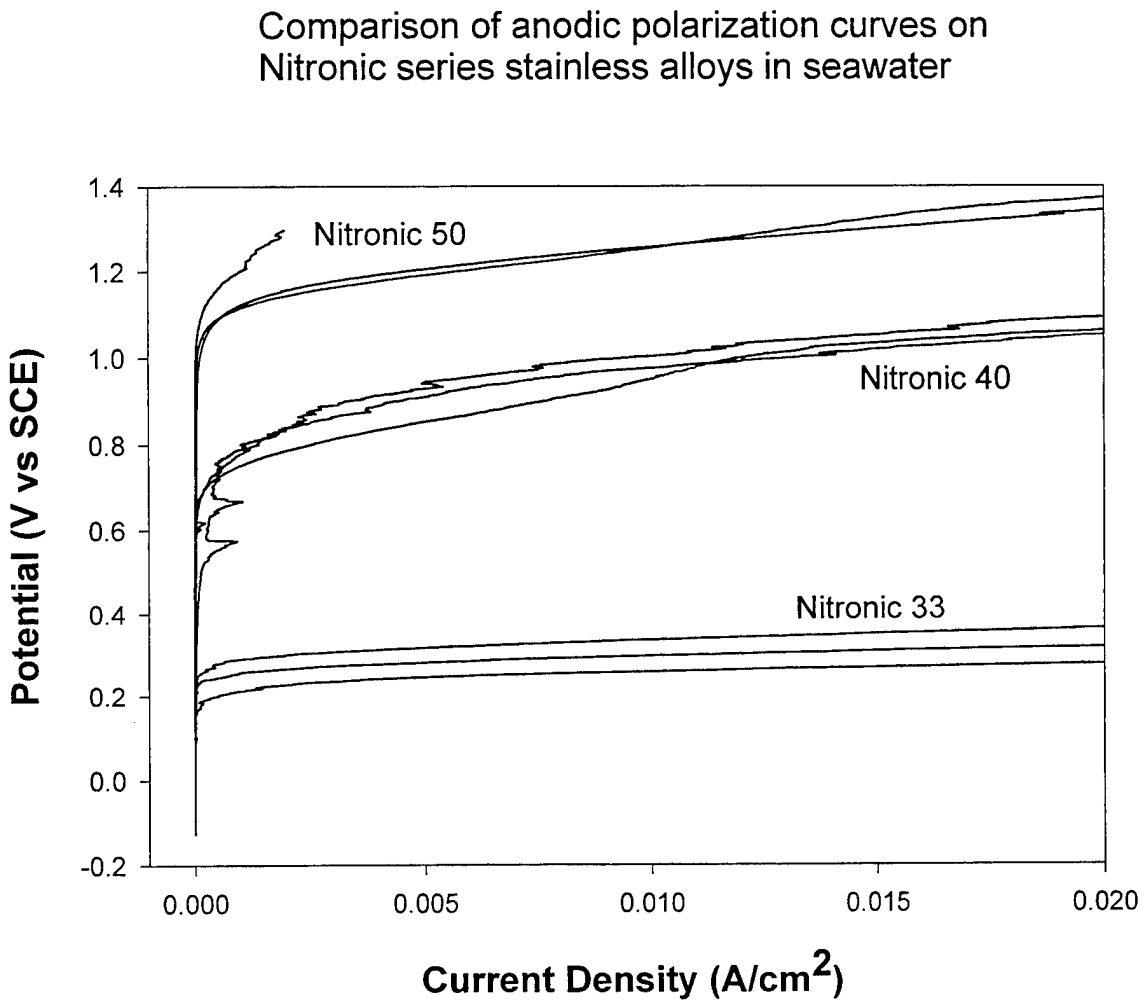


Figure III.E.2. The anodic polarization curves of Nitronic series stainless alloys in seawater.

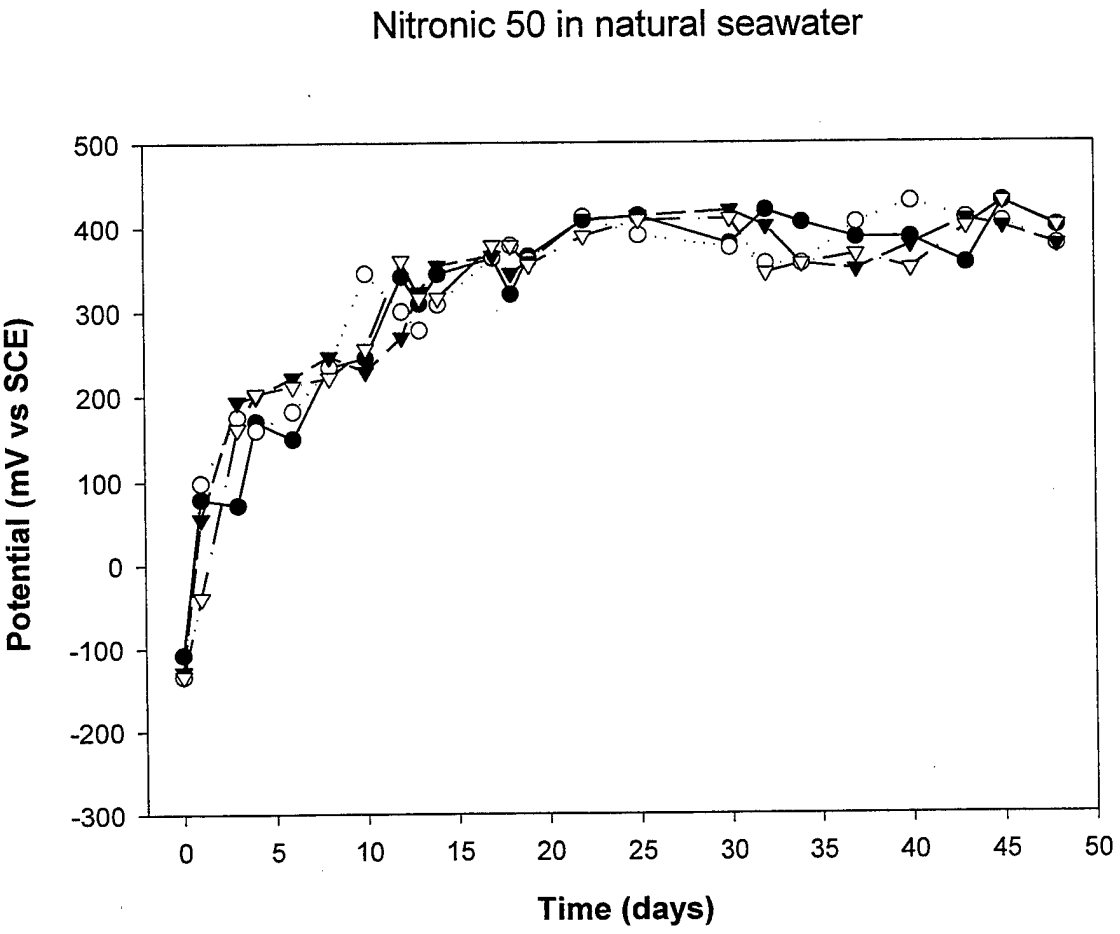


Figure III.E.3. Open circuit potential of Nitronic 50 stainless alloy coupons in seawater versus time.

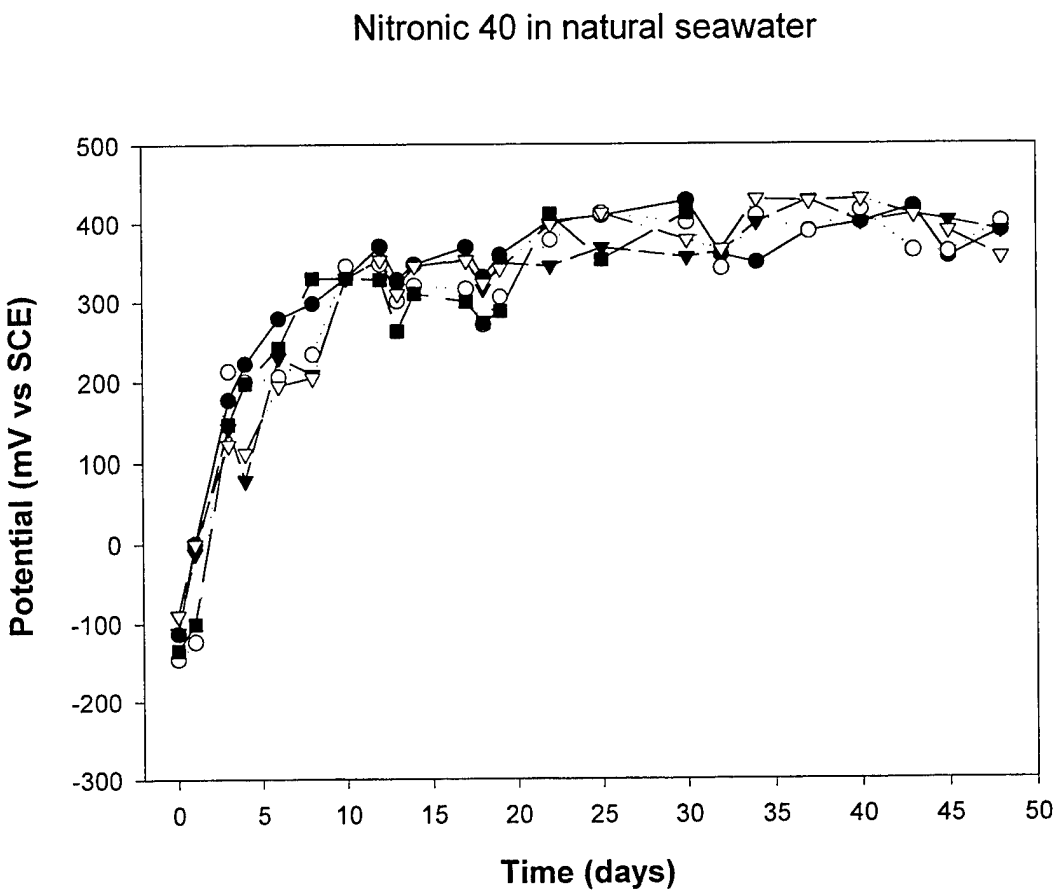


Figure III.E.4. Open circuit potential of Nitronic 40 stainless alloy coupons in seawater versus time.

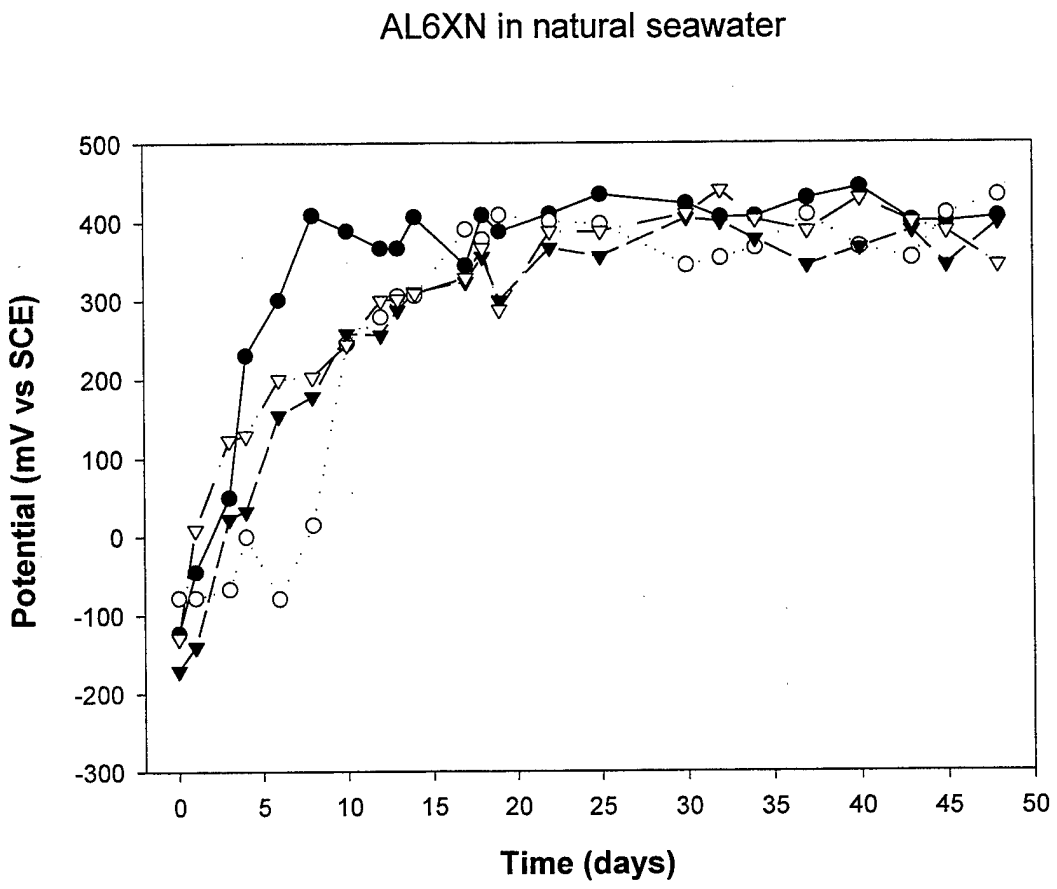


Figure III.E.5. Open circuit potential of AL6XN stainless alloy coupons in seawater versus time

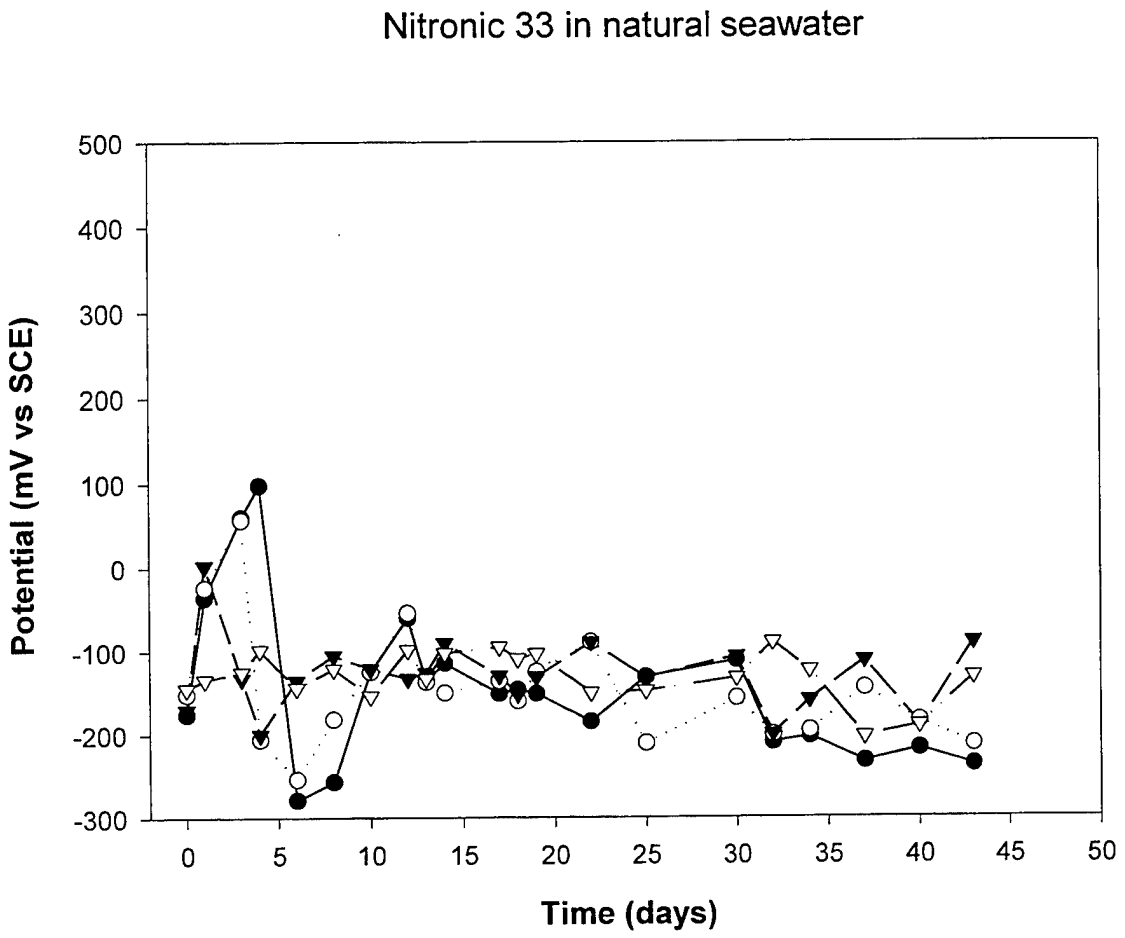


Figure III.E.6. Open circuit potential of Nitronic 33 stainless alloy coupons in seawater versus time.

### III.E.2. Cathodic Properties of Nitronic 50 and Effect of $MnO_2$

It was thought that Nitronic 50 would follow the same pattern as 6XN and other stainless alloys that have been tested in that the action of biofilms will cause it to become more severe as a cathode, thus accelerating the rates of crevice and galvanic corrosion of less noble metals connected to it. Work on the cathodic properties of Nitronic alloys was done during the Ph.D. work of Dr. Xu (2000) as well as during the MS Thesis work of David Ruppel (1999).

Dr. Xu performed cathodic polarization experiments on bare metal coupons, as well as on coupons with biofilms and $MnO_2$ coatings. Bare coupons of Nitronic 50 were exposed in seawater for 3 months before running the polarization curves. As shown in Figures III.E.7 and III.E.8, the cathodic polarization properties for Nitronic 50 and Nitronic 40 have very similar patterns. The OCP for coupons with biofilms was about +400 mV, whereas that for the bare metal coupons was the usual -100 to –200 mV. The difference is due to microbial ennoblement of the OCP on the coupons with biofilms. The bare metal coupons showed two Tafel slope regions separated by the normal diffusion limited region:

1) The Tafel slope region for oxygen reduction ranged from -0.20 V to -0.40 V.
2) The diffusion limited region ranged from -0.50 V to -0.90 V. In this region the current density represented the limiting current for oxygen reduction at the quiescent hydrodynamic conditions of the experiment.
3) The Tafel slope region of hydrogen evolution ranged from -1.10 V downwards.

The polarization curves for coupons with biofilms were more complex than those of bare metal coupons. In addition to generally higher current densities in the first two regions of the curve as described above, the polarization curve of biofilmed coupons shows a clear reduction peak in the potential range from +0.20 V to -0.20 V. This additional current peak is attributed to the biofilm effect. Although just a single curve is presented in each of the figures they represent typical cathodic polarization patterns for these two Nitronic alloys.

It cannot be discerned from the data presented what chemical species within the biofilm contributed to the current peak in the potential range from +0.20 V to –0.20 V. However, as shown in Figure III.E.9, an $MnO_2$ coating on the metal surface produced a similar effect on the polarization curve. This indicates that the reduction peak is probably associated with manganese chemical species within the biofilm.

The cathodic behavior revealed in these polarization curves is consistent with data on other passive alloys in the published works of many investigators from our own lab and internationally. Thus, we conclude that the cathodic behavior of the Nitronic alloys in seawater under biofilm forming conditions is similar to that of many other alloys previously tested.

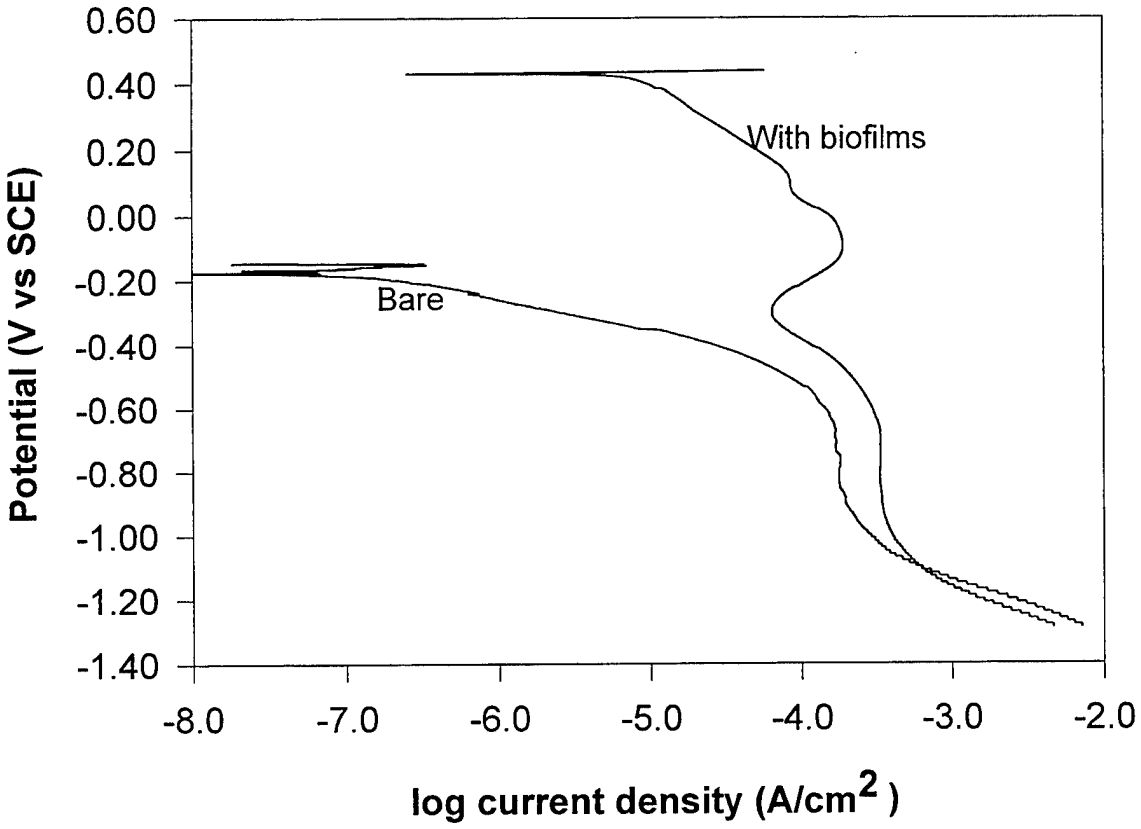


Figure III.E.7. Cathodic polarization curves of Nitronic 50 alloy with and without biofilms.

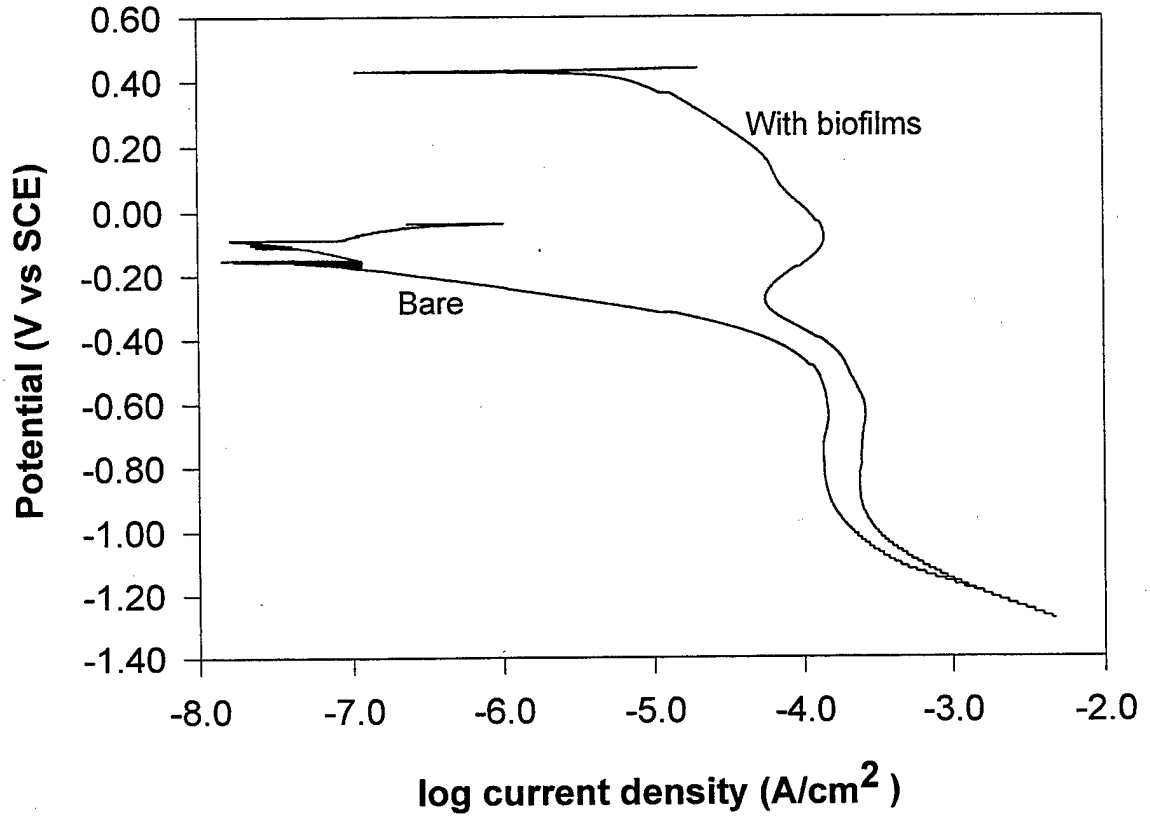


Figure III.E.8. Cathodic polarization curves of Nitronic 40 alloy with and without biofilms.

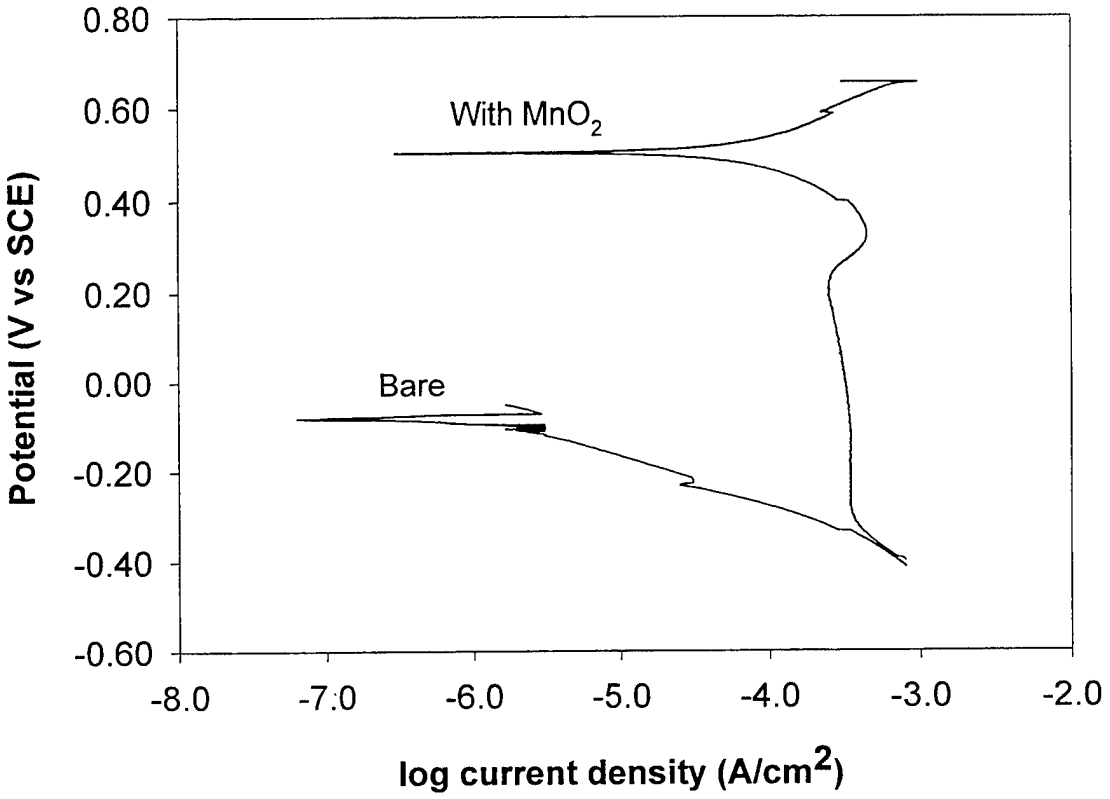


Figure III.E.9. Cathodic polarization curves for Nitronic 50 alloy with and without a $MnO_2$ coating film.

As part of his MS Thesis research David Ruppel examined how biofilms grown on Nitronic 50 and alloy C4 (16 Cr, 55 Ni, 15.5 Mo, zero Mn) affected their cathodic properties in galvanic couples. He compared this to the well-known effect (Dexter and LaFontaine, 1998) of biofilms on alloy 6XN.

An experiment was performed where biofilm-coated and control cathodes of C-4, Nitronic 50 and 6XN were coupled to aluminum anodes in August and September, a total of 53 days. The current densities in these galvanic couples are shown in Figure III.E.10. Rapid increases in the current of control couples on days 16 and 34 occurred because the control cathodes were not changed before a biofilm developed. Note that the control current returned to normal each time a freshly cleaned cathode was inserted (See the discussion on control techniques in Section IV of this Report). This emphasizes the fact that biofilms develop quickly in warm water, and may subsequently affect the corrosion rate. Even though the current readings were variable, the increase in galvanic current for the test couples with biofilms on the cathode was consistent with previous work on alloy 6XN cathodes (Dexter and LaFontaine, 1998). Weight loss of the aluminum anodes connected to the two Nitronic alloys and 6XN (control) are shown in Table III.E.1.

Based on the weight loss data in the table and the galvanic currents in Figure III.E.10 one can conclude that the galvanic corrosion rates were accelerated vs. control by the formation of natural biofilms on all three cathode alloys. Using the weight loss data, one can see that the effect of the biofilm was largest at about a factor of 8 on 6XN, and this was consistent with previous tests on that alloy cathode (Dexter and LaFontaine, 1998). The effect was smaller (factor of about 3) for the Nitronic 50 cathodes, and it was the smallest (factor of about 2.4) for C4.

In light of the fact that alloy C4 ennobles very little due to the p-type properties of its passive film (see section III.B above) it is interesting that the galvanic current is still accelerated when it is the cathode in a galvanic couple. This is consistent with our hypothesis that the ennoblement phenomenon consists of two parts: the effect of biofilms on the OCP of an alloy and the effect on the cathodic kinetics. On a given alloy in a given environment these effects may or may not have the same mechanism.

Based on the data in Figure III.E.10 and Table III.E.1, we again reach the conclusion that the effect of natural marine biofilms on Nitronic series alloys is nominally the same as has previously been documented for other passive metals. Further work will be required to determine if the smaller increase in galvanic current in the presence of biofilms on Nitronic 50 as compared to 6XN is significant for either scientific or engineering purposes.

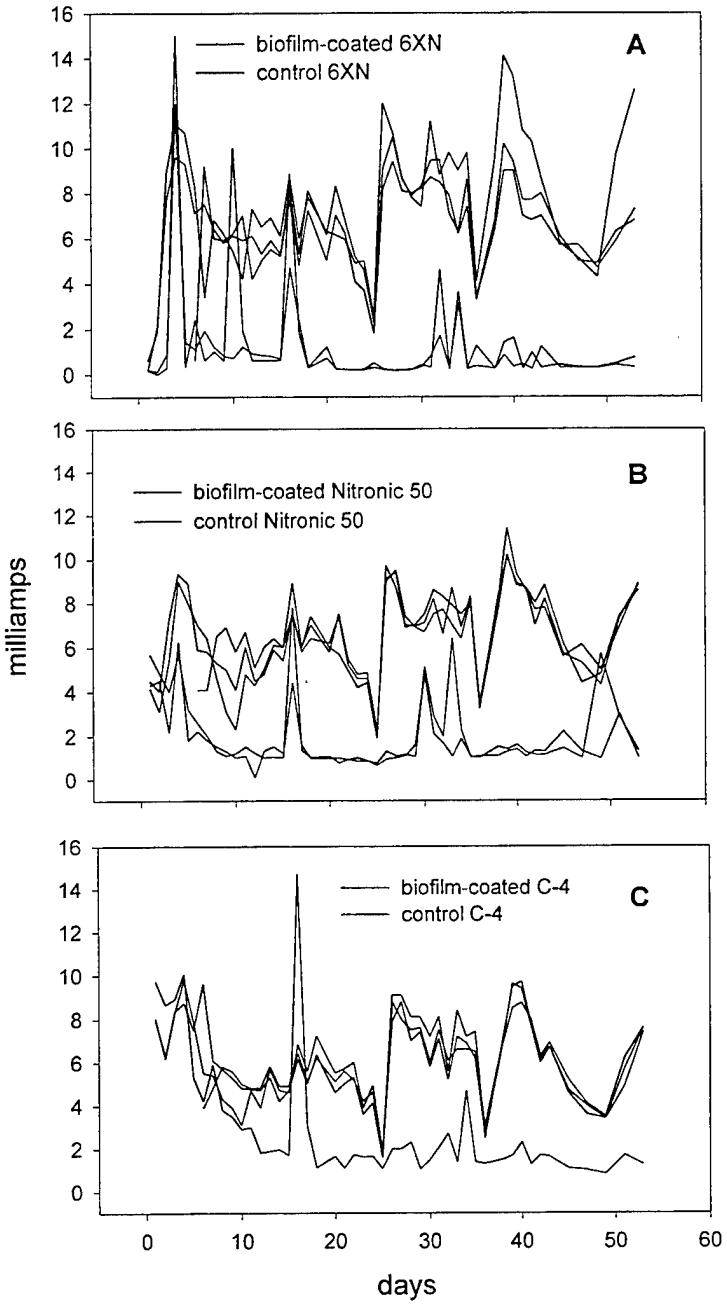


Figure III.E.10. Galvanic corrosion currents between aluminum and A) 6XN, B) Nitronic 50, C) C-4 during 53 day immersion test started in July.

Table III.E.1 Weight loss data for aluminum anodes connected to C4 Nitronic 50 and 6XN cathodes with biofilms.

| | Weight Loss (g) | | |
|---|---|---|---|
| Cathode Alloy | Test | Control | Ratio Test/Control |
| C4 | 3.0 ± 0.2 | 1.5 (1 point) | 2.4 |
| Nitronic 50 | 3.78 ± 0.07 | 1.31 ± 0.05 | 2.89 ± 0.15 |
| 6XN | 3.9 ± 0.25 | 0.5 ± 0.1 | 8 ± 1.6 |

### III.E.3. Source of the Manganese

The working hypothesis here was that the source of manganese is unimportant – it could come from either the environment or the alloy. Thus, if manganese were abundant in the environment, it might not matter what the Mn concentration was in the metal. If, however, Mn was absent in the environment, then manganese as an alloying constituent in the alloys could be important. There might even be a threshold concentration of manganese in the alloy above which it will become concentrated enough in the biofilm to contribute significantly.

Work done to date provides only a partial answer to this question. The data of Ruppel in Figure III.E.10 and Table III.E.1 above were taken in seawater with total manganese in the 3 to 6 μM range. These data showed that the effect of biofilms on galvanic corrosion currents increased in order for cathodes of C4, Nitronic 50 and 6XN. Yet the concentration of manganese in those alloys went in the order of C4 (none), 6XN (0.2 % by weight) and Nitronic 50 (4 %). Thus, at least up to 4 % by weight of manganese in the alloy appears to be insignificant as long as there is manganese in the environment. This supports the hypothesis that low concentrations of manganese in the alloy are unimportant to the ennoblement process as long as manganese is present in the environment.

Part of the thesis work of Dr. Xu involved using the ICP-AES technique to quantify the total concentrations of manganese and iron in seawater at our exposure site and in the biofilms

grown on passive alloy surfaces immersed in that seawater. Metal coupons were immersed in seawater from our usual estuarine exposure site as well as from the recirculating seawater system in the Cannon Marine Studies Laboratory. These waters have been described in numerous publications. The estuarine water is coastal Atlantic seawater on the incoming tide and the effluent from the local salt marsh on the outgoing tide. The water from the building recirculating system is fresh coastal Atlantic Ocean seawater taken from a site remote from the Delaware Bay plume and refreshed weekly.

As shown in Table III.E.2, the concentrations of manganese and iron in Shellfish laboratory seawater (6 to 8 μM) are about three times higher than in Cannon laboratory seawater (1 to 3 μM). All biofilms developed in these two seawaters contained millimolar levels of total manganese and iron. At first glance it would seem that the biofilms grown Nitronic 40 and 50 contained more manganese and iron in the estuarine water than in the Lab water. According to the statistical t-test, however, there are no significant differences in the manganese contents between the two sets of biofilms. For example, the probability that you are incorrect in stating that the Mn concentrations in biofilms from the two seawater sources are significantly different is 69.95% for biofilms on Nitronic 50 and 78.30% for biofilms on Nitronic 40 (much larger than common criteria of 5%).

For each biofilm sample, the total concentration of iron was higher than that of manganese. The reason for this difference is probably that the biofilms trap particulate material, which generally contains a much higher concentration of iron than manganese because manganese is more easily dissolved than iron (Stumm and Morgan, 1996). Since the elemental composition of the Nitronic alloys indicates that iron content is much higher than that of manganese in the alloys, it is also possible that iron from the alloy has contributed to that accumulated in the biofilm. Further experiments using trace metal clean waters would be required to determine if this was a possibility.

At the time of the measurements, all coupons with biofilms had OCP values close to +300 mV. The difference was that it took two months for the OCP to reach +300 mV in Cannon laboratory seawater, whereas it took only three weeks in estuarine seawater. Since the biological activity is much higher in the estuarine water than in the Lab water, it can be inferred that biofilm activity is involved in accumulating heavy metals near the alloy surface. Theoretically, manganese and iron may come from seawater or from the alloys. The result using two different water sources hinted that manganese and iron accumulated similarly within biofilms regardless of their contents in the waters.

Further experiments using higher manganese alloys (such as Nitronic 40 with 8 to 9 % Mn) and lower manganese waters need to be done in order to prove whether or not manganese can contribute to the ennoblement process if it is absent in the environment.

**Table III.E.2 Total concentrations of manganese and iron in seawater and in biofilms that formed on Nitronic stainless alloys.**

| Experiments using Estuarine seawater: | Mn Conc. | Fe Conc. | OCP (mV vs SCE) | Exposure time (days) |
|---|---|---|---|---|
| Estuarine Seawater #1 | 5.84 μM | 6.50 μM | | |
| #2 | 6.07 μM | 7.26 μM | | |
| #3 | 3.16 μM | 4.53 μM | | |
| Biofilms on Nitronic 50 #1 | 2.44 mM | 13.5 mM | +312 | 21 |
| #2 | 3.02 mM | 15.4 mM | +311 | 21 |
| #3 | 11.9 mM | 26.5 mM | +285 | 21 |
| Biofilms on Nitronic 40 #1 | 10.8 mM | 17.3 mM | +302 | 21 |
| #2 | 12.2 mM | 14.8 mM | +305 | 21 |
| #3 | 8.15 mM | 51.6 mM | +293 | 21 |
| Experiments using Cannon lab seawater: | | | | |
| Seawater (Cannon lab) #1 | 2.08 μM | 2.75 μM | | |
| #2 | 1.05 μM | 1.39 μM | | |
| #3 | 2.33 μM | 3.04 μM | | |
| Biofilms on Nitronic 50 #1 | 4.01 mM | 17.2 mM | +298 | 60 |
| #2 | 3.30 mM | 9.6 mM | +298 | 60 |
| #3 | 2.10 mM | 16.9 mM | +254 | 60 |
| Bioiflms on Nitronic 40 #1 | 1.4 mM | 2.1 mM | +295 | 60 |
| #2 | 4.30 mM | 11.5 mM | +290 | 60 |
| #3 | 3.12 mM | 15.2 mM | +271 | 60 |

## References Cited


Dexter, S. C. and J. P. LaFontaine, 1998, "Effect of natural marine biofilms on galvanic corrosion," Corrosion, Vol. 54, No. 11, p. 851.

Ruppel. T. D. 1999. "The Effect of Manganese in Biofilms on Galvanic Corrosion Currents." Master's Thesis, University of Delaware.

Stumm, W. and J. J. Morgan. 1996. *Aquatic Chemistry*. John Wiley & Sons, Inc., New York.

Xu, K., 2000, "Effect of Biofilm Heterogeneity on Corrosion Behavior of Passive Alloys in Seawater." Ph.D. Dissertation, University of Delaware.

Zhang, H-J. and S. C. Dexter. 1993. Effect of biofilms on crevice corrosion of stainless alloys in coastal seawater, Proc. 12$^{th}$ International Corrosion Congress, Vol. 5B, NACE international, Houston, TX, pp. 3761-3772.

Zhang, H-J. and S. C. Dexter. 1995. Effect of biofilms on crevice corrosion of stainless steels in coastal seawater, *Corrosion,* 51: 56-66.

# IV. Tests and Methods Developed

During the course of this work it has been necessary to develop several techniques, which will be reported in this section.

## IV.A. Control Techniques for Biocorrosion Tests in Natural Environments

Proving that the organisms in natural marine biofilms do or do not have a significant effect on corrosion initiation and propagation requires simultaneous running of control tests in which the effects of the microbes is removed without changing the bulk water chemistry. This topic has been addressed in all of the published papers from our lab, but a summary of the techniques used and their strengths and weaknesses was given by Dr. Dexter in the Proceedings of the 1996 NACE Topical Research Symposium on Crevice Corrosion (Dexter, 1996). Text from the appropriate section of that paper is reproduced below. The references have been removed to save space, but they are available in the original paper.

The most difficult problem to solve when doing experiments to demonstrate an effect (or lack thereof) of microorganisms on crevice corrosion is to devise an effective method for making the measurements with the same geometry and chemistry but without the organisms. Ideally, one should have a sterile control experiment running concurrently, and under the same chemical and geometrical conditions as the one in the natural environment. However, it is quite difficult to maintain truly sterile conditions in such corrosion experiments. The problem is compounded as the required duration of the experiment becomes longer and the volume of water involved larger. For the long duration (several months) and large volumes of water required for most crevice corrosion experiments, it becomes impractical (some would say impossible) to maintain truly sterile conditions with no change in chemistry of the water. Given these difficulties, the objective of the control experiment changes from that of having no organisms present to that of delaying the onset of microbial effects long enough to do a meaningful experiment. If it is impossible for practical purposes to have an absolutely sterile control experiment, then some way must be found to have a control condition that is demonstrably effective in order for the data generated to be interpretable.

Several techniques, none of which are perfect, have been developed for creating such an effective, rather than absolute, control condition. These techniques all involve one, or a combination of, three approaches: 1) do the testing in a simulated electrolyte, 2) treat the natural water, or 3) treat the specimen surface. If the natural electrolyte is seawater, the first inclination will be to use a 3.5% NaCl solution as the control water. This approach will not sterilize the water, but the organisms will be different from those in the marine environment. Thus, whatever biofilm does form will behave differently than a natural marine biofilm. This simple solution provides an electrolyte that is chemically stable over long periods of time, but it does not reproduce either the inorganic or organic chemistry of seawater very well. A chemical improvement is to use artificial seawater, such as the ASTM Standard Specification for Substitute Ocean Water D 1141-75. Other artificial seawaters that more accurately reproduce the chemistry of open ocean water than ASTM seawater also are available. In general, however, the more chemically accurate the artificial formulation is, the more difficult it is to make, and the less stable it is over time. Moreover, no artificial seawater can

reproduce the organic chemistry of natural seawater. It is important to realize that biofilms eventually form even in artificial waters, and the investigator must be able to demonstrate that the level of biofilm control achieved is sufficient for the purposes of a given experiment.

The next approach to making an effective control is usually to modify the natural water itself in such a way as to eliminate the microorganisms, or to delay their tendency for biofilm formation over the desired length of the experiment. Many methods have been tried, but no one has devised an easy way to maintain sterile conditions without also changing the water chemistry. Biofilm formation can be prevented by continuous photo-oxidation or addition of biocides to kill or inhibit the organisms, but these techniques also change the chemistry of the water. Perhaps the most successful technique has been to sterilize the water by combination of mechanical filtration at the 0.2 (or even 0.1) micro-meter level with a low temperature (75 to 80 °C) pasteurization. This does not guarantee continued sterility of the water but it does delay the formation of a biofilm for 4 to 8 weeks. This combination of filtration and pasteurization is usually the method of choice for short term (< 1 month) laboratory experiments. The disadvantage is that this control water has to be changed every 2 or 3 days to keep it fresh. Since filtration at the 0.2 μm level is a slow process, this means that new water must be continuously under preparation, and the experimental logistics become difficult if the volume of water required for a given experiment is more than about 5 liters.

The final approach to creating an effective control experiment involves periodic removal of the biofilm from the metal surface by physical or chemical treatment. Techniques such as periodic wiping or scraping, chemical cleaning and autoclaving the metal samples have been tried with varying degrees of success. These techniques are all temporary, and they must be repeated frequently in order to be effective. Recently, Zhang and Dexter (1995) found that the control condition for long term crevice corrosion experiments requiring large volumes of water could be maintained by a combination of pasteurizing the control water and recycling the cathodes. Two identical cathode panels were prepared for each experiment. These cathode panels were exchanged approximately every three days. The panel that was removed was immediately immersed in fresh water at 60°C for one hour, then air dried and kept in a desiccator until it was time for the next exchange. At that time the treated panel was connected into the circuit before disconnecting the old panel in order to avoid an open circuit condition on the anode. This simple method was found to be nearly as effective and much less labor intensive than filtering the water. The disadvantage was that the current and potential record for the assembly showed large (although short-term) fluctuations each time the cathodes were changed, and each anode was momentarily connected to twice the normal area of cathode. None of the control methods described above are ideal, and the one chosen for a given experiment will depend on the intended purpose and duration of the experiment.

It is realized that the control condition never exists in real, open seawater or industrial applications. Some have said that our results are only of academic interest because the biofilm can never really be eliminated in practice. This may be true, but our results have shown that biofilms are the reason for the long-standing observation that natural seawater is more corrosive than chemical solutions used to simulate it in the laboratory. Our data also show what could be gained in marine corrosion control by just eliminating the action of microbes in the biofilm.

## IV.B. Development of Microelectrodes

The work to develop voltammetric microelectrodes suitable for measuring chemical profiles of Fe, Mn, $O_2$ and S species within natural marine biofilms was done by Dr. K. Xu (1997) during the course of his MS Thesis research. The work was presented at the NACE Spring meeting in 1997 (Xu, Dexter and Luther, 1997) and published in Corrosion (Xu, Dexter and Luther, 1998). Exerpts from that paper are now presented.

A gold-based mercury microelectrode was prepared by electroreducing $Hg^{2+}$ on a gold wire of 25 μm diameter encased in glass. The electrode reaction and analytical sensitivity for dissolved $O_2$, Mn, Fe, S (-II), and $H^+$ using square wave voltammetry are investigated. The use of this voltammetric microelectrode takes advantage of fast scan voltammetric methods for the simultaneous measurement of the key redox species during a single potential scan from -0.1 V to -1.7 V (SCE). Various interfering factors and experimental parameters of the voltammetric measurements are discussed. By mounting the working electrode on a computerized micromanipulator, vertical microprofiles of the redox species were measured at 10 μm depth resolution across seawater biofilms formed on metal coupons. Results revealed the heterogeneous nature of the biofilm and complex microbially mediated heavy metal (Mn and Fe) cycles within the biofilm system.

Traditional membrane microelectrodes can not measure dissolved Mn and Fe species due to their working principles. The microelectrodes used to date for biofilm studies can be classified into potentiometric and polarographic type electrodes according to their working theory. The potentiometric type electrode for determining the concentration of a single analyte is based on the Nernst equation that the electrode potential varies linearly with the log of the analyte concentration. The potentiometric ion-selective electrode generally contains an ion selective membrane or a gas-permeable membrane. Each membrane is designed to develop an electrical potential in response to a specific ion. So far ion-selective microelectrodes are limited to the determination of two reference electrode related ions (Ag+, Cu2+), the stable ions within alkali (H+, L+, Na+, K+, NH4+) and halogen groups (F-, Cl-, Br-), and several pH-sensitive gas molecules (NH3, H2S, CO2). The membrane oxygen microelectrode is the most commonly used polarographic type microelectrode. At a potential of around -0.5 V vs SCE, the faradaic current flow through the electrode is diffusion-limited and proportional to the concentration of dissolved oxygen in the solution. Like potentiometric type microelectrodes, polarographic type microelectrodes are not suitable for measuring transition metal species in natural environments.

Recently, Brendel and Luther (1995) have developed a gold amalgam voltammetric microelectrode for the determination of dissolved Fe, Mn, $O_2$, and S(-II) in porewaters of marine and freshwater sediments. Most of their work was performed with a microelectrode of 300 μm tip diameter. Microprofile measurements of redox species within thin biofilms, however, require microelectrodes of smaller tip diameters. Based on the known structure of the biofilms (Lewandowski, et al., 1992, 1995), the anticipated physical scale of the chemical variability to be measured should be less than 50 μm. For microelectrode construction, as the size of the wire and glass decreases, the quality of the wire-to-glass junction becomes crucial due to the increase of circumference to area ratio ($2\pi R / \pi R^2$). Gold sealed in glass is sensitive

to the match between the coefficients of thermal expansion for the gold-glass junction at the electrode tip. Severe mismatch often lead to formation of micro cracks in the sealing glass (Sawyer and Roberts, 1974). Thus the methods for constructing the small sized microelectrodes had to be improved. In this work we developed gold-based mercury amalgam microelectrodes of 25 μm diameter tip for use with square wave voltammetry in making chemical measurements within seawater biofilms. Our main objective was to develop this technique for biocorrosion studies. We show that small sized Hg-Au microelectrodes can be constructed by making modifications to the procedure used for large microelectrodes. We also show that electrode contamination can be removed by proper electrochemical conditioning steps, and the effects of various interfering factors can be overcome. By profiling key redox species within seawater biofilms, this work demonstrates the value of the voltammetric microelectrode technique in characterizing chemical changes within biofilms on metal surfaces.

### IV.B.1. Electrode construction

Microelectrodes were constructed in a method similar to Brendel and Luther (1995). Soft glass capillaries of 1 mm o.d. (0.68 mm i.d.) were used for this work. The end of a 15 cm long capillary was heated and pulled to a diameter of less than 50 μm. A gold wire with a diameter of 25 μm was then inserted, and the glass tip was melted to seal the gold. Since the melting point of glass is higher than that of gold, breaks in the gold wire inside the capillary may occur. These were avoided by proper adjustment of the heating temperature. Once cooled the excess glass and melted gold were ground away to expose the gold wire section. Because heating and grinding often resulted in microcracks of sealing glass at the tip, a stereo microscope was used to examine the status of the electrode tip during the above processes.

After the electrode was ground flat and smooth, a 0.5 mm diameter silver wire was fixed to the gold inside the glass with a conductive epoxy. After drying, the electrode was then sealed at the top of the glass with a non-conductive epoxy. Upon washing briefly in 1: 1 nitric acid solution, the electrode was plated with mercury by electroreducing $Hg^{2+}$ in 0.1 M $Hg(NO_3)^2$ / 0.03 M $HNO_3$ electrolyte at a potential of -0.1 V (vs SCE) for 1 min. The electrode was checked under the microscope to assure that a mercury film of around 8 μm thickness had formed over the gold wire. After this, the electrode was placed in 1N NaOH solution, and a potential of -9.0 V (with DC output of 200 μA) was applied for a period of 30 seconds. This polarization step reduced H+ and Na+ ions as well as gold and mercuric oxides that might have formed during the mercury deposition, it was found to give the electrode better reproducibility and lower minimum detection limits for chemical measurements. The structure of the gold-based mercury microelectrode is shown in Figure 1. Such a solid state microelectrode, when stored in deionized water, could often be used for several weeks without affecting its performance.

### IV.B.2. Square wave voltammetry

Square wave voltammetry was performed using a model DLK-100 electrochemical analyzer from Analytical Instrument Systems, Inc. The instrument and its accompanying software enabled the application of various scanning waveforms to the working electrode. They also

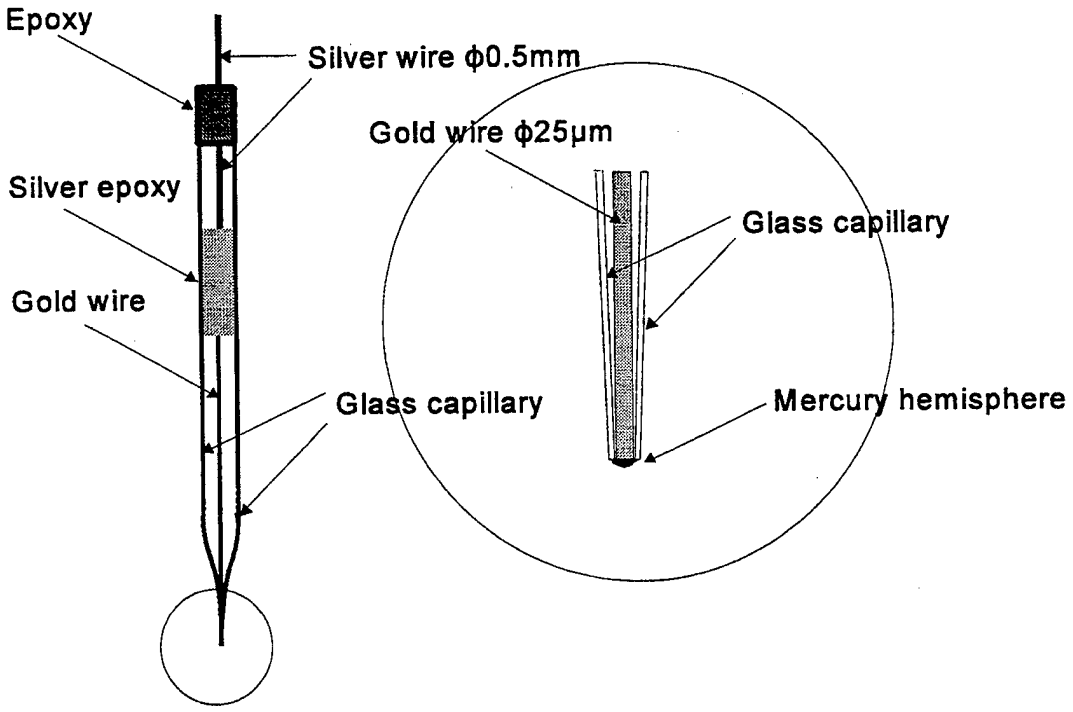


**Figure 1 - A schematic diagram of the gold-based mercury microelectrode**

enabled the measurement of voltammetric signals at several current detection ranges (from 10 nA to 10 mA) for best signal to noise ratio. The working electrode was a gold-based mercury microelectrode of 25 μm diameter as constructed above. A 1 mm diameter platinum wire and a saturated calomel electrode (SCE) were used as counter and reference electrodes, respectively.

In general, square wave voltammetry not only provides reversibility information of the measured analyte as also revealed by cyclic voltammetry, but gives larger current signals than other scanning waveforms. Its waveform is a staircase wave superimposed on a symmetrical square wave of the same phase and frequency (Figure 2). To obtain the best faradaic current to charging current ratio, the signal is sampled at the end of each pulse to yield forward and reverse currents. The resultant current is obtained by subtracting the reverse current from the forward current.

### IV.B.3. Electrode calibration

In order to calibrate the microelectrode under similar conditions to that of the biofilm electrolyte, all standards were made from seawater taken from the water tank where the biofilms were developed. The seawater had a salinity of approximately 28 ppt with pH 7.0, which was first filtered through a 0.4 μm Nuclepore filter. Dissolved oxygen concentration

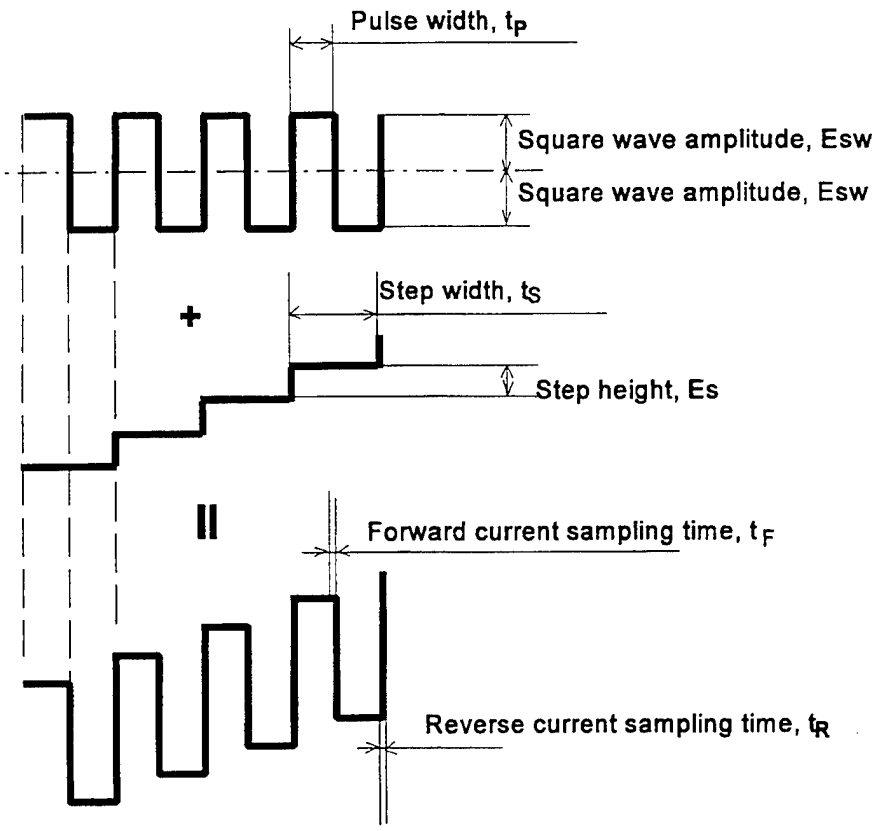


**FIGURE 2 - The waveform of square wave voltammetry is the sum of a simple symmetrical square wave and a staircase wave of the same phase and frequency.**

was determined using the Winkler titration method (Grasshoff, 1983). Analytical grade chemicals $MnCl^{2}{\cdot}4H_2O$, $Fe(NH_4)^{2}(SO_4)^{2}{\cdot}6H_2O$ and $Na_2S$ were used to prepare standards for dissolved Mn, Fe, and S(-II) calibration. For dissolved Fe calibration, oxygen was purged using inert argon gas, and the electrolyte pH was adjusted to 5.5 by adding diluted (0.01N) HCl solution. S(-II) was calibrated in deaerated seawater at neutral pH. 0.01N HCl solution was also used for adjusting the seawater pH for the electrode pH calibration. pH buffer solutions were not used to stabilize the pH value because some of the buffers can give voltammetric peaks near -1.4 V, which would interfere with the pH signal. Instead, the standard pH values were determined using a digital pH meter before and after the voltammetric measurements to ensure that they remained constant.

It was not necessary to calibrate the electrode for all the analytes each time it was used, provided that it retained good reproducibility in seawater solution and gave a linear relationship between peak current and analyte concentration. Since the ratio of slopes (nA/μM) between any two analytes remained relatively constant, the "pilot ion method" (Meites, 1965) was used to avoid the tedious calibration procedure for all analytes. Such simplified electrode calibration was carried out before and after the field measurements.

### IV.B.4. Voltammetric measurements in biofilms

Experiments were conducted to measure vertical microprofiles of redox chemical species within the biofilms. In the laboratory, the biofilm coupon was immersed horizontally in seawater inside a petri dish. Both the counter and reference electrodes were then inserted into seawater beside the coupon. After proper calibration, the working microelectrode was mounted on a computer-controlled micromanipulator and lowered vertically into the seawater. The three electrodes were arranged in such a way that the distance between any two of them was less than 1 cm. The three-electrode voltammetric cell was set up inside a specially designed faradaic cage, which allowed for micropositioning of the working electrode. The working electrode was stepped into the biofilm at 10 μm depth intervals (with 0.4 μm resolution), and square wave voltammograms were then generated at each depth.

The diameter of the microelectrode tip was so small that it was hard to see when immersed in water, and impossible to see when immersed in the biofilm. This made it difficult to establish the absolute height of the electrode tip above the surface of the metal coupon. Fortunately, the electrode gave a large spike of current at a potential below -1.0 V when the mercury hemisphere got close to the metal surface. The electrode itself was durable enough to withstand such "soft contact" without losing its calibration. Thus, the procedure for making profiles perpendicular to the metal surface was to start in the water above the outer surface of the biofilm, approaching the metal surface in 10 μm intervals. When the current spike occurred, the absolute positions at which each measurement were taken were back calculated with a precision of ±5 μm. It is possible to increase that precision by reducing the size of the interval over the last few steps, at the cost of increasing the total time required for measuring the profile.

The sensitivity of the voltammetric microelectrode in square wave voltammetry, as in traditional polarographic methods, is determined by the ratio of faradaic current to charging current. In general, reversible redox species have lower minimum detection limits than irreversible species. However, the peak current (Ip) of a specific ion also depends on the surface area of the sensing electrode, the properties of the supporting electrolyte, and the choice of experimental parameters. The relationship between Ip and the electrode area was usually expressed by the equation (Bond, 1980):

$$Ip = nFACf^{1/2} \psi$$

where $\psi$ is a dimensionless current function, A is the electrode surface area, f is the square wave frequency, C is analyte concentration and other symbols have their usual meanings. While it is true that faradaic current decreases with decreasing the surface area of the sensing electrode, the analytical sensitivity of the small-sized microelectrode is, however, increased. First, small surface area enhances analyte polarization and thus permits application of fast scan rates, which in turn increases the Ip signal. Second, enhanced polarization also means sharper voltammetric peaks and decreased iR drop over the electrolyte. Third, reducing surface area generally reduces electrode double layer capacitance and the background charging current. All these factors result in a better signal to noise ratio of the small microelectrode.

The relationship between peak current and analyte concentration is linear over a wide concentration range. Listed in Table 1 are typical slope values (nA/μM) and linear concentration ranges for dissolved $O_2$, $H_2O_2$, Mn, Fe, S (-II), and H+ species in square wave voltammetry. These data were collected at a scan rate of 60 mV/s.

TABLE 1
Electrode Reaction And Analytical Sensitivity Of
The Hg-Au Microelectrode For Redox Species In Seawater

| Electrode Reaction | Ep (V) | Linear Range (μM) | Slope (nA/μM) |
|---|---|---|---|
| $O_2 + 2H^+ + 2e^- \rightarrow H_2O_2$ | -0.28 | 5 to 300 | 0.0090 |
| $HS^- + Hg \leftrightarrow HgS + H^+ + 2e^-$ | -0.62 | 0.05 to 100 | 2.0 |
| $Fe^{3+} + e^- \leftrightarrow Fe^{2+}$ | -0.3 to -0.8 | 2 to 4000 | 0.068 |
| $H_2O_2 + 2H^+ + 2e- \rightarrow 2H_2O$ | -1.23 | 5 to 300 | 0.0090 |
| $2H^+ + 2e- \rightarrow H_2$ | -1.38 | $10^{-4.3}$ to $10^{-1}$ M | 0.020 |
| $Fe^{2+} + Hg + 2e^- \rightarrow Fe$ (Hg) | -1.43 | 15 to 4000 | 0.0072 |
| $Mn^{2+} + Hg + 2e^- \leftrightarrow Mn$ (Hg) | -1.55 | 5 to 1000 | 0.011 |

A square wave voltammogram of oxygen reduction in seawater electrolyte is shown in Figure 3. Current signals can be discerned from the forward and reverse currents as well as from the resultant current, which is the difference of the former two currents. Ideally, one might expect the current peaks at potentials of -0.28V and -1.22V to have roughly the same height, and the areas under the two peaks to be about equal because 1 mole $O_2$ reduces into 1 mole $H_2O_2$, which then reduces to $H_2O$ during the two step reduction. However, because $H_2O_2$, as an intermediate species, is not strictly diffusion controlled at the electrode surface during the reduction processes, its voltammetric peak tends to be broader and lower than that of oxygen. The peak current ratio of $H_2O_2$ to $O_2$ in seawater solution is normally about 0.90 and remains constant. Thus the peroxide concentration in an unknown sample can be measured within 10 % precision by comparing the peroxide peak with oxygen peak.

Square wave voltammograms for Mn and Fe are shown in Figure 4 and 5. The linear regression coefficients, $r^2$, for Mn and Fe measurements were 0.996 and 0.994 in the calibrated concentration ranges, respectively. The minimum detection limits for $HS^-$, $Mn^{2+}$, and $Fe^{2+}$, as shown in Table 1, were calculated from their square wave voltammograms. Obviously, much lower detection limits can be achieved by using square wave anodic (or cathodic) stripping voltammetry that provides a preconcentration step. The linear relationship between the voltammetric current and analyte concentration was found to break down at high

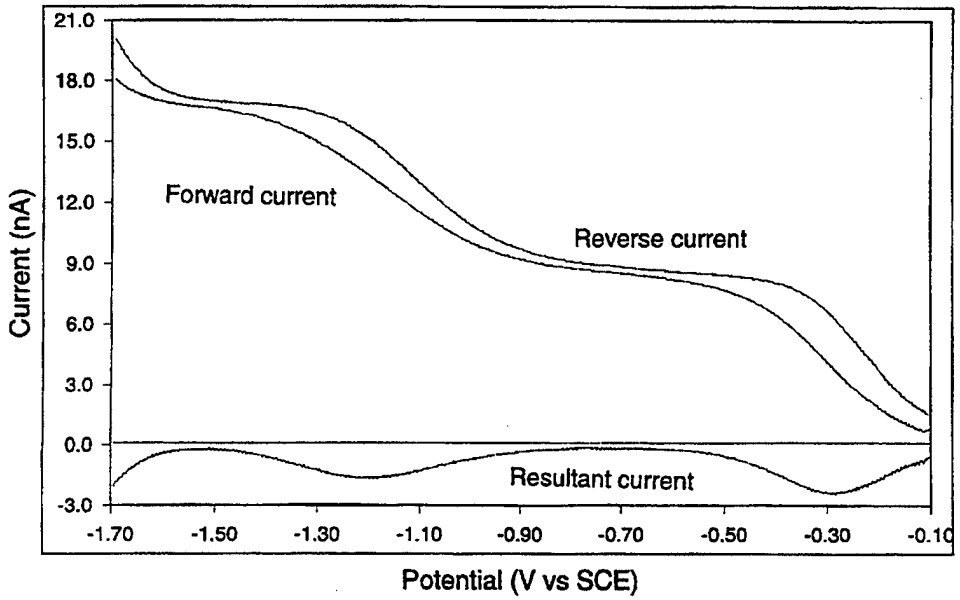


FIGURE 3 - Square wave voltammogram obtained from a microelectrode in seawater at a scan rate of 20 mV/s. The forward and reverse currents are plotted as positive currents and the resultant current as nagative current. Dissolved $O_2$ is reduced to $H_2O_2$ at -0.28 V, which is then reduced to $H_2O$ at potential near -1.22 V.

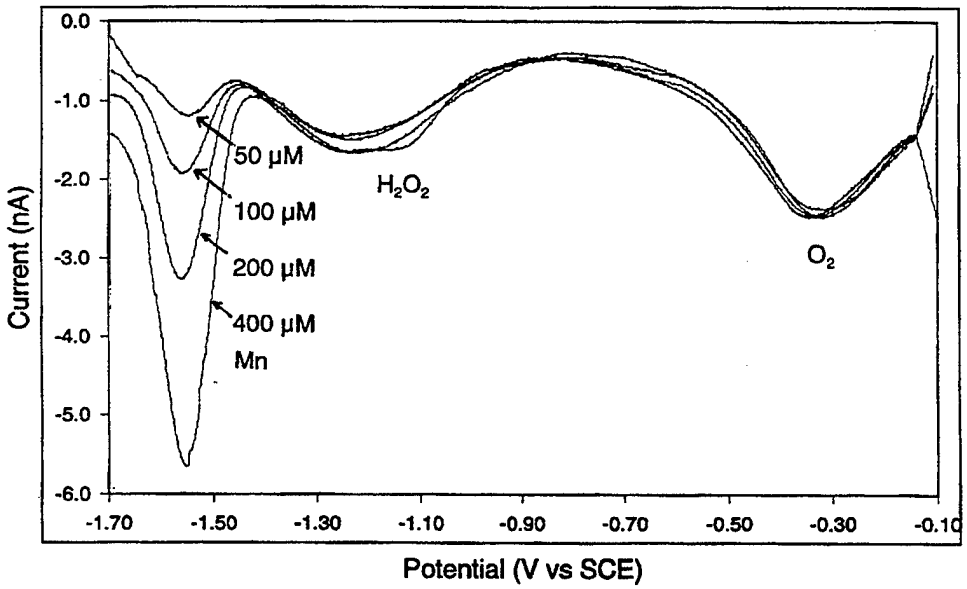


FIGURE 4 - Sqaure wave voltammograms for dissolved Mn in seawater electrolytes. The heights of voltammetric peaks shown at -1.55 V are proportional to the standard $Mn^{2+}$ concentrations with a linear regression coefficient ($r^2$) of 0.996.

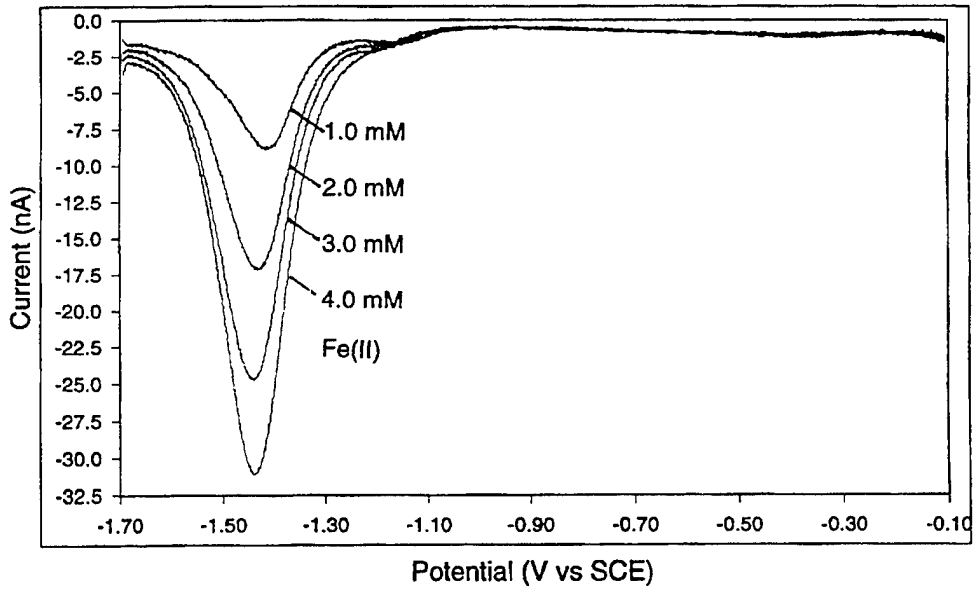


FIGURE 5 - Square wave voltammograms for dissolved Fe in deaerated seawater at pH 5.5. The peak currents and the standard $Fe^{2+}$ concentrations are in good linear relationship ($r^2 = 0.994$).

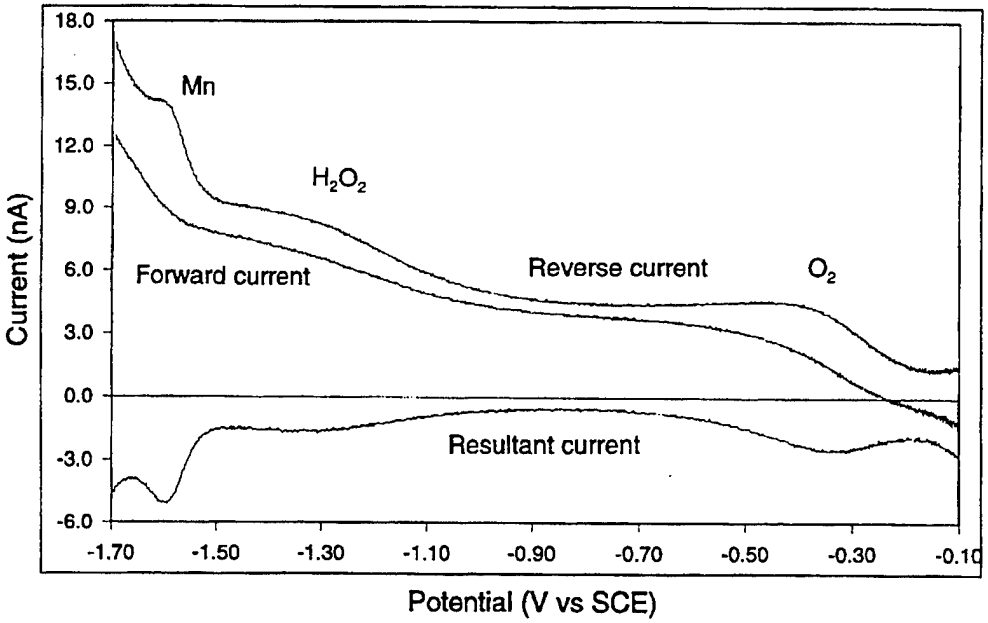


FIGURE 6 - Square wave voltammogram obtained from a microelectrode deployed in a seawater biofilm formed on a stainless alloy coupon. Dissolved Mn was detected in the presence of low oxygen within the biofilm.

analyte concentrations. The voltammetric measurement of high concentrations of dissolved Mn, Fe, and sulfide is usually prohibited by the occurrence of splitting wave and the formation of electrode plaque.

$Fe^{2+}$ reduction can be regarded as an irreversible process in square wave voltammetry. The dissolution of Fe into the sensing mercury may decrease the overvoltage of redox species at the mercury surface, and produce abnormally high voltammetric current while shifting analyte Ep to a more positive potential. Such Fe contamination can be removed by applying a conditioning potential at -0.2 V before the voltammetric measurement. In contrast, S (-II) oxidation is highly reversible at the mercury surface. It gives a sharp current peak at potential of -0.62 V in square wave voltammetry. High sulfide concentrations often influence the performance of the solid state microelectrode. This can be overcome by conditioning the electrode at -1.0 V before taking measurements. Electrode plaque by Mn is rarely encountered in the actual analyses.

### IV.B.5. Effects of experimental parameters

The goal of choosing the proper experimental parameters in a specific voltammetric measurement is to obtain a good signal to noise ratio. Higher square wave frequency means faster scan rate, which generally produces a larger Ip signal. In a biofilm system abundant with organic matter, too large a charging current often results in the distortion of voltammetric curves and peaks especially near the initial potential and final potential. While better peak shape can generally be achieved by decreasing the scan rate, it takes a longer time to run a single potential scan. Too slow a scan rate may generate undesirable noise and increase the susceptibility of the electrode to plaque formation when measuring ferrous and sulfide species. Based on the investigation of Ip versus frequency for all the key redox species, we found 60 Hz to be an optimal scanning frequency in the biofilm measurements.

The potential increment or step height was fixed at 1 mV to ensure enough data points for good resolution. Changing square wave amplitude may influence the current signal of reversible and quasi-reversible species. In general, higher square wave amplitude produces a larger current signal in forward as well as in reverse scan, but in the mean time it may also increase the offset distance of Ep potentials between the forward and reverse curves. The latter phenomenon can cause the resultant wave to split into two peaks. Square wave amplitude of 24 mV was chosen in all measurements.

In a biofilm system abundant with bacterial extracellular polymers, the effects of organic metal complexation and electrode contamination are expected. The adsorption of organic matter to the working electrode may slow down the diffusion of the electroactive reactants, increase the electrolyte resistance and electrode charging capacitance, and diminish the effective surface area of the sensing mercury. Hence organic fouling often decreases the analytical sensitivity of the working electrode. Previous work in our group has found that organic adsorption can be eliminated efficiently through the conditioning step at the sodium reduction potential, e.g., -2.1 V vs SCE (Brendel and Luther, 1995).

Since both Mn and Fe may have several dissolved species and oxidation states within the biofilm, quantitative interpretation of the voltammetric measurements of these dissolved metal species must be taken with caution. Many Mn(III) organic complexes are reduced through a two step process. First Mn(III) to Mn(II) conversion occurs at potential -0.5 to -1.2 V, and then Mn(II) to Mn(0) reduction occurs at a potential near -1.55V (Magers, et al, 1978; Luther, et al., 1994). Thus the peak for the reduction of Mn(II) to Mn(0) is not specific for the Mn(II) redox state (Luther, et al., 1994). While the precise Ep position of a certain Mn complex also depends on the property of the specific organic ligand, the reduction peak detected in natural biofilms (Figure 6), which occurs near -1.55 V, is defined as total soluble Mn rather than only free Mn2+ ion.

Organic complexation generally shifts the ferrous reduction potential in the negative direction. High concentrations of $Fe(NH_4)^2(SO_4)^2 \cdot 6H_2O$ at seawater pH were observed to form ferrous ammonia complexes, which were reduced at -1.64 V. In square wave voltammetry, Fe (III) to Fe (II) reduction occurs at roughly the same potential as sulfide oxidation. However, due to the high sensitivity of mercury to sulfide, the sulfide peak is usually much sharper than that of ferric species, which usually covers a broad potential range from -0.1 V to -0.8 V (Figure 7 and 8). Ferric organic complexes were also found to give sharper voltammetric peaks than ferric hydroxide colloids. The reversibility of Fe (III) to Fe (II) conversion varied from highly reversible (Figure 7) to quasi-reversible or even irreversible (Figure 8) depending on the Fe (III) complexation and oxygen exposure conditions. The slope value (nA/μM) for ferric colloids formed in deaerated seawater is presented in Table 1 for reference.

In this work it was demonstrated that the gold-based mercury amalgam microelectrode can be used for measurement of dissolved $O_2$, $H_2O_2$, Mn, Fe and S(-II) in marine biofilms. Using square wave voltammetry, the microelectrode showed excellent reproducibility for chemical measurements in seawater and biofilms. Electrode plaque from adsorption of electroactive analytes and organic matter could be removed with proper electrochemical conditioning steps. The microelectrode has provided the first detailed information on Mn and Fe at 10 μm vertical resolution across the thickness of natural biofilms. Suitability of voltammetric microelectrodes for characterizing detailed changes in redox chemical species in electrolytes close to the metal surface will make it a powerful tool in the study of biocorrosion.

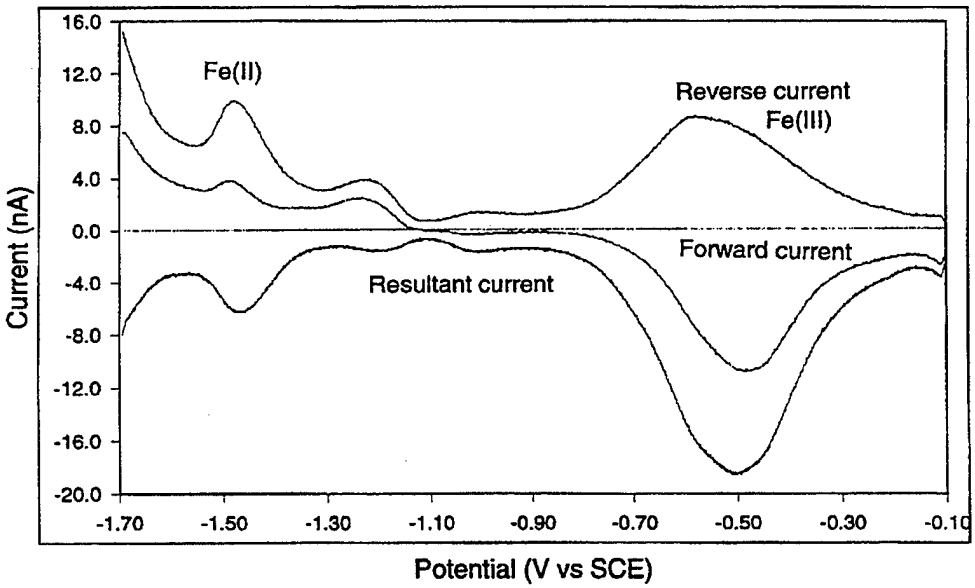


FIGURE 7 - Square wave voltammogram of Fe (II) added to deaerated seawater. Ferrous oxidation in the presence of trace oxygen resulted in the formation of Fe(III) colloids. The Fe (III) to Fe (II) reduction was highly reversible. Similar voltammetric curves were detected within seawater biofilms.

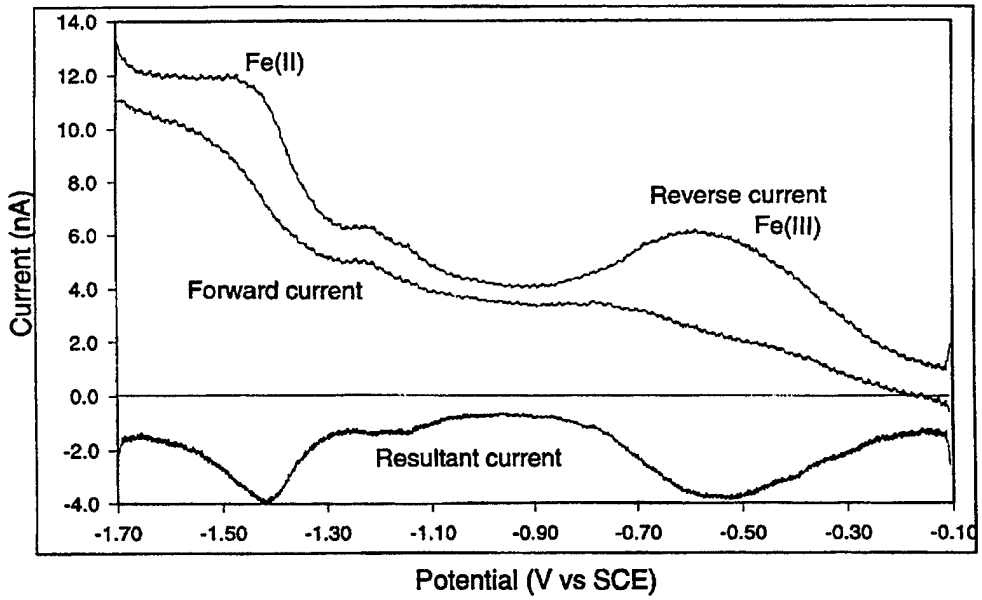


FIGURE 8 - Square wave voltammogram of Fe (II) added to aerated seawater. Rapid ferrous oxygenation resulted in the formation of Fe (III) colloids which were irreversibly reduced over a broad potential range from -0.2 V to -0.8 V. Such irreversible Fe (III) signals were also detected within seawater biofilms.

## IV.C. Correlating Data from Microelectrodes and Confocal Microscopy

After documenting the chemistry at a given location, the microelectrode was withdrawn vertically into the bulk solution and then translated horizontally to the corner of the coupon. In this way the X- and Y-coordinates were recorded for the location of the chemical profile. The same metal coupon was then prepared for confocal microscopy by fixing in paraformaldehyde and staining with the cell-permeating nucleic acid dye, Syto 13.

It was desired to use the Zeiss LSM 510 confocal microscope to image the organisms in the biofilm at the same location at which the chemical profiles were taken. A protocol for finding the same X, Y coordinates in the confocal was worked out by Dr. Xu in the course of his Ph.D. Dissertation work (Xu, 2000). In doing this a biofilm image was first obtained near the reference corner of the sample using the low-magnification 10X objective. A 500 μm scale bar was then placed on the image in both the X and Y directions. Using these scale bars, the image was then moved to the correct X and Y coordinates with the confocal in fast scanning mode. Once at the proper location, the final biofilm images were obtained by replacing the low power objective with 40X or 60X oil-immersion objectives or a long working distance 40X water-immersion objective.

An estimate of the precision by which the X and Y coordinates of the chemical profiles could be relocated in the confocal microscope was obtained by multiple measurements of the full width of the metal coupon by both techniques and statistical analysis of the data. Ten biofilmed coupons were used in this test. The results of the width measurements are presented in Table 3.4. Column 3 in this table showed the difference between data obtained with the two systems. Regardless of +/- sign, the average value is 28 μm. This error is a reflection of the uncertainties associated with locating a metal corner using the two systems. From Table 3.4, the standard deviation, $\sigma$, of the difference column is 37 μm. According to standard normal curve, this means that confocal microscopy is capable of locating a specific X-Y coordinate recorded by the microelectrode measurement system with a precision of ±37 μm with probability of 68.3% or at a precision of ±111 μm ($3\sigma$) with probability of 99.7%. Because the biofilm images taken under the Plan-Apochromat 40X objective lense had a size of 231 x 231 $\mu m^2$, the field of image taken under the confocal microscope covered the specific X-Y coordinate where chemical measurements were conducted within the 99% confident limit.

It was estimated that the limiting factor in determining the precision of the overall measurement was the radius of curvature of the coupon corners and edges. On the final images, a circle 25 μm in diameter was drawn at the center of the image field. This circle, matching the diameter of the microelectrode itself, was designated as the most probable location of the chemical profile. The field of view in a 40X objective corresponded very closely to the 99% confidence limit for locating the site of the chemical profile. An intermediate square was also drawn on each image representing the 80% confidence range. Chemical profiles with corresponding confocal images will be shown in Section V. This information will be presented at the Spring ECS meeting in Washington, DC in the Symposium on Corrosion Sensors.

**Table 3.4 Width of metal coupons obtained by microelectrode measurements and by confocal microscopic measurements. The difference of these measurements was used for evaluating the precision of spatial correlation using the two techniques.**

| Microelectrode measurements (μm) | Microscopic measurements (μm) | Difference (μm) |
|---|---|---|
| 16109 | 16097 | 12 |
| 16093 | 16079 | 14 |
| 16414 | 16337 | 77 |
| 16120 | 16135 | -15 |
| 16108 | 16118 | -10 |
| 16033 | 16038 | -5 |
| 15904 | 15862 | 42 |
| 16055 | 16128 | -53 |
| 16244 | 16222 | 22 |
| 16367 | 16401 | -34 |
| | Absolute mean = | 28 μm |
| | Standard deviation = | 37 μm |

## IV.D. Method for Creating Artificial Manganese Dioxide Films

$MnO_2$ coatings were prepared for use during the works of David Ruppel and Dr. Maruthamuthu according to the procedure established by Perez-Benito, et al. (1989) from the reaction:

$$8MnO_4^- + 3S_2O_3^{-2} + 2H^+ \rightarrow 8MnO_2 + 6SO_4^{-2} + H_2O \qquad (1)$$

The $MnO_2$ formed in this reaction is made up of 50-nm or smaller $MnO_2$ clusters rather than $MnO_2$ molecules. Thus, it will be referred to as polymeric $MnO_2$. A 2 mM homogeneous solution of polymeric MnO2 was made by dissolving 632 mg $KMnO_4$ in 1500 ml of high-purity deionized water (ASTM type I, 18 MΩ). A second solution was prepared by dissolving 1.86 g $Na_2S_2O_3$ in 100 ml of high-purity deionized water. Exactly 21.0 ml of $Na_2S_2O_3$ solution was added to the $KMnO_4$ via a burette—5% more $Na_2S_2O_3$ than was needed for a stoichiometrically complete reaction. This assured that all of the $KMnO_4$ was reduced to $MnO_2$, erring on the side of excess $S_2O_3^{-2}$ rather than $MnO^{4-}$. High-purity deionized water was then added to bring the volume to 2 liters. The polymer is stable as a soluble entity for many months in high purity water, but precipitates in a matter of days or hours in salinities as low as 0.5 parts per thousand (Luther, et al., 1989).

Coating of the test coupons with $MnO_2$ was performed by immersing a polished and passivated coupon in a mixture containing 1mM $MnO_2$ and 10 mM NaCl for 20 to 24 hours. The NaCl concentration was empirically chosen to give slow precipitation of the $MnO_2$ onto the coupon. Slow precipitation was needed to produce the smaller, more electroactive $MnO_2$ particles that are needed for the electrochemical reaction, and which would be similar to $MnO_2$ particles in the natural environment. The quantity of $MnO_2$ deposited on the coupons was measured by dissolving the $MnO_2$ from four replicate coupons in acidified oxalic acid ($H_2C_2O_4$). This solution was then analyzed for total manganese by inductively coupled plasma-optical emission spectroscopy (ICP-OES), which gave a value of 255 ± 35 μM, or13 μmol of Mn in 50 ml of solution. On a typical coupon of 32.5 cm2 surface area, this translated to 390 ± 50 nmol of Mn per $cm^2$.

## IV.E. Other Papers on Methods

During the course of our research two other papers were written in the general area of measurement techniques for use in MIC investigations:

S. C. Dexter, D. J. Duquette, O. W. Siebert and H. A. Videla, 1991, "Use and Limitations of Electrochemical Techniques for Investigating Microbiological Corrosion," Corrosion, Vol. 47, No. 4, pp. 308-318.

S. C. Dexter, 1995, Section V, Chapter 43, "Microbiological Effects," in Corrosion Tests and Standards, Application and Interpretation, R. Baboian, Ed., ASTM Manual Series: MNL 20, American Society for Testing and Materials, Philadelphia, pp. 419-429.

### References Cited in Section IV


Bond, A. M., 1980, Modern Polarographic methods in Analytical Chem. Marcel Dekker, Inc.

Brendel, P. J. and G. W. Luther III, 1995, Envir. Sci. & Tech., Vol. 29, 751-761.

Dexter, S. C., 1996, "Effect of Biofilms on Crevice Corrosion," Proc. COR/96 Topical Research Symposium on Crevice Corrosion, NACE, Houston, TX, pp. 367-383.

Grasshoff, K., 1983, Methods of seawater analysis, Verlag Chemie: Berlin, p. 60-72.

Lewandowski, Z., F. Roe, T. Funk, and D. Chen, 1992, Chemistry near microbially colonized metal surfaces. Proc. Biocorrosion & Biofouling, NSF-Conicet workshop.

Lewandowski, Z., P. Stoodley, and F. Roe, 1995, "Internal mass transport in heterogeneous biofilms, recent advances," CORROSION 95, paper no. 222, (Houston, TX: NACE International).

Luther, G. W. III, D. B. Nuzzio and J. Wu, 1994, Analytical Chimica Acta, 284, p. 473-480.

Luther, G. W., D. T. Ruppel and C. Burkhard (1999) Reactivity of Dissolved Mn(III) Complexes and Mn(IV) Species with Reductants: Mn Redox Chemistry Without a Dissolution Step? In Sparks, D. L. and T. J. Grundl (Eds.) *Minera-Water Interfacial Reactions: Kinetics and Mechanisms*. ACS Symposium Series 715, American Chemical Society. Washington D. C. pp. 265-280.

Magers, K. D. Smith, C. G.; Sawyer, D. T., 1978, Iorg. Chem., 17: p. 515-523,

Meites, L., 1965, Polarographic Techniques, Interscience Publishers, New York.

Perez-Benito, J. F., E. Brillas and R. Pouplana (1989) Identification of a soluble form of colloidal manganese(IV). *Inorg. Chem.* **28**: 390-392.

Sawyer, D. T. and L. J. Roberts, 1974, Experimental electrochemistry for chemists. Wiley, New York, p. 86-88.

Xu, K., 1997, "Development of Hg-Au Microelectrodes for the Determination of Dissolved Mn, Fe, O2, and S(-II) in Marine Biofilms." MS Thesis, University of Delaware.

Xu, K., S.C. Dexter and G.W. Luther, 1997, "Development of Voltammetric Microelectrodes for use in Corrosion Studies," Paper No. 300, CORROSION/97, NACE, International, Houston, TX.

Xu, K., S. C. Dexter and G. W. Luther, III, 1998, "Voltammetric microelectrodes for biocorrosion studies," Corrosion, Vol. 54, No. 10, p. 814.

Zhang, H-J and S. C. Dexter, 1995, "Effect of Biofilms on Crevice Corrosion of Stainless Steels in Coastal Seawater," Corrosion, Vol. 51, No. 1, 1995, pp. 56-66.

## V. Mechanisms of Ennoblement

One of the main purposes of our ONR sponsored work has always been to investigate mechanisms by which the biofilms that form on metal surfaces immersed in seawater are involved in the breakdown of passivity on passive metals and alloys. As detailed in Section II above, by the time ONR funding started in 1990, it was already well established that biofilms were able to raise (or ennoble) the open circuit corrosion potential of many alloys, thus increasing the probability of passivity breakdown in the presence of chloride ions. The results of our work from 1990 to 1995 will be described only briefly here as they were dealt with in our 1996 Final Technical Report.

Among the early mechanisms proposed to explain the ennoblement phenomenon were ones involving enhancement of the cathodic oxygen reduction reaction. This had been proposed to take place by: 1) organo-metallic catalysis (Johnsen and Bardal, 1985), 2) catalysis by bacterially produced enzymes (Scotto, et al., 1985), or 3) enhancement of the oxygen reaction by a decrease in pH (Dexter, 1988). The original working hypothesis that we proposed to test in 1990 was that all three of these mechanisms were capable of producing ennoblement by enhancing the dissolved oxygen reduction reaction. Our ideas of that time period about the mechanisms of potential ennoblement were presented and discussed in the following papers:

S. C. Dexter, 1988, "Role of Microfouling Organisms in Marine Corrosion," Presented as Plenary Lecture at 7th Intl. Congr. On Marine Corrosion and Fouling, Valencia, Spain, November, 1988. (Proceedings never published)

P. Chandrasekaran and S.C. Dexter, 1993, "Mechanism of Potential Ennoblement on Passive Metals by Seawater Biofilms," CORROSION/93, Paper No. 493, NACE, International, Houston, TX.

S. C. Dexter, 1993, "Role of Microfouling Organisms in Marine Corrosion", Biofouling, Vol. 7, pp. 97-127.

We made considerable progress in determining that most of the observed ennoblement of the corrosion potential on passive metals in seawater could be explained by the pH mechanism. In fresh water, however, the pH mechanism could account for only about half of the observed ennoblement. Thus, while we still believed that the primary mechanism involved low pH, we began research on other mechanisms that could provide supplementary ennoblement in cases where low pH was inadequate. In this regard we began to look at mechanisms involving hydrogen peroxide and heavy metal catalysis of the oxygen reduction reaction. Based on our research results up to that time, the new Working Hypothesis under which our research proceeded was that: 1) The primary ennoblement mechanism is acidification at the metal surface due to the bacterial metabolism. 2) Under conditions in which acidification alone does not produce enough ennoblement to account for observation, the secondary mechanism comes from reduction of peroxide produced on a continual basis by respiration of the organisms in the biofilm and regulated at a low (non-toxic) concentration by the bacterial

respiratory enzyme system. 3) A tertiary mechanism for ennoblement might involve catalysis by organo-metallic compounds of the porphyrin type.
At that time we believed that most of the observed ennoblement could be explained by a combination of acidification and continual, low-level peroxide formation, perhaps supplemented further by organometallic catalysis. The results and arguments for the pH, peroxide, low oxygen mechanism were presented and published in the following papers:

P. Chandrasekaran and S.C. Dexter, 1993, "Factors Contributing to Ennoblement of Passive Metals Due to Biofilms in Seawater," Proc. 12th International Corrosion Congress, Vol. 5B, NACE, International, Houston, TX, pp. 3696-3707.

S. C. Dexter, P. Chandrasekaran, H-J Zhang and S. Wood, 1993, "Microbial Corrosion in Marine Environments: Effect of Micro- fouling Organisms on Corrosion of Passive Metals", Proc. 2nd USA/Argentina Workshop on Biocorrosion and Biofouling, Buckman Laboratories International, Inc., Memphis, TN, pp. 171-180.

P. Chandrasekaran and S. C. Dexter, 1994, "Bacterial Metabolism in Biofilm Consortia," Paper # 276, CORROSION/94, NACE, International, Houston, TX.

P. Chandrasekaran and S. C. Dexter, 1994, "Thermodynamic and Kinetic Factors Influenced by Biofilm Chemistry Prior to Passivity Breakdown," Paper # 482, CORROSION/94, NACE, International, Houston, TX.

S. C. Dexter, 1994, "Mechanism of Ennoblement by Biofilms on Active/Passive Alloys Immersed in Seawater," in Proc. Tri-Service Conference on Corrosion, June, 1994, Orlando, FL.

S. C. Dexter, H-J. Zhang and P. Chandrasekaran, 1994, "Biofouling Effects on Corrosion of Stainless Alloys in Seawater," Biodeterioration Research 4, G.C. Llewellyn, W.V. Dashek and C.E. O'Rear, Eds., Plenum Press, New York, pp. 553-571

Again, the results of this work were presented in our 1996 Final Technical Report so most of the details will not be presented here. Highlights of three important observations will be summarized, however, in order to put subsequent work in perspective.

### V.A. The pH, Peroxide, Oxygen Mechanism

Experiments were carried out to understand more about the synergistic contributions of peroxide and pH towards ennoblement of the OCP of platinum in deaerated Delaware Bay seawater (0.55 ± 0.05 ppm (17 ± 1 mM) O2) at various combinations of pH and peroxide. Figure V.A.1 shows the OCP of platinum in deaerated natural seawater (0.55 ppm oxygen). Condition 1 shows the data at pH 8.3. A decrease in pH to 5 (condition 2) produced a jump in OCP to over 300 mV as would be expected from the Nernst equation. Addition of 2.4 mM peroxide at pH 5 gave no further increase in potential (condition 3). A further decrease in pH to 2.9 without peroxide addition increased the potential to about 350 mV (condition 4).

However, it was not until a combination of pH 2.9 and 2.4 mM peroxide was tried that the potential of over 400 mV observed on biofilmed platinum was obtained (condition 5).

The effect of combinations of peroxide and pH under oxygen saturated conditions was somewhat different. A decrease in solution pH caused a noble shift in OCP of platinum in oxygen saturated solutions similar to its effect in deaerated solutions. The addition of peroxide in oxygen saturated solutions, however, caused an active shift in OCP. The same type of results was also obtained by Hoare (1968). The full amount of ennoblement observed on platinum under natural biofilms could only be reproduced when the proper concentration of peroxide was added to deaerated, low pH solutions.

### V.A.1. Heavy Metals

The earliest data on Mn and Fe in biofilms grown at our location was obtained by EDAX. Further data were taken by Inductively coupled plasma atomic emission spectroscopy. In spite of the careful handling procedures, the blank showed small heavy metal concentrations, which were subtracted from the experimental values. The concentrations of iron and manganese on a bare coupon and in biofilms formed for 2 to 24 months did not follow any trend with respect to thickness, age of the biofilm, or OCP of the coupon (Table V.A.1). However, it is important to note that iron and manganese accumulation began within the first two months of exposure to natural seawater. While the presence of heavy metals had been documented in the biofilm, the correct role for them in the mechanism of ennoblement had not yet been envisioned.

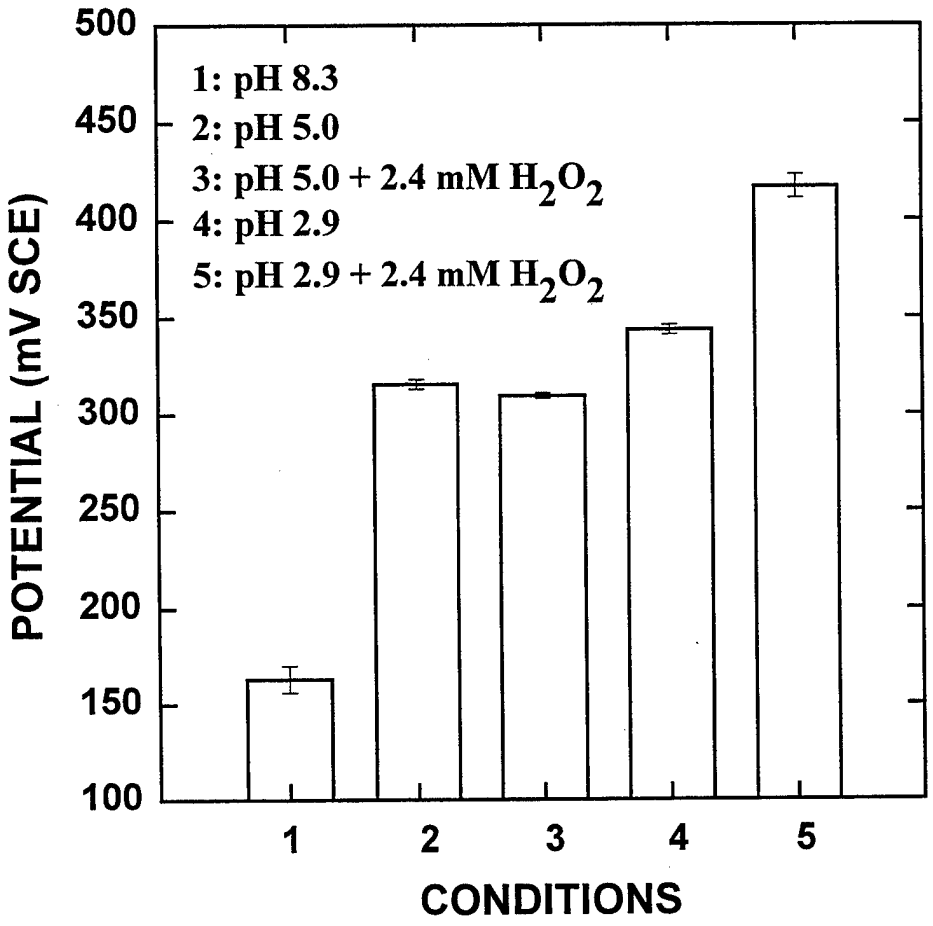


Figure V.A.1. OCP of platinum in deaerated natural seawater at various pH and peroxide levels.

Table V.A.1. Concentrations of Fe and Mn in natural marine biofilms on platinum for different periods of exposure.

| Age of Biofilm (Months) | Film Thickness (μm) | Fe Conc. (mM) | Mn Conc. (mM) | OCP of Coupon (mV SCE) |
|---|---|---|---|---|
| 0 (bare coupon) | None | -- | -- | 160 ± 50 |
| 2 | 29 | 29 | 13 | 251 |
| 5 | 58 | 25 | 23 | 425 |
| 5 | 44 | 9 | 22 | 441 |
| 24 | 48 | 7 | 14 | 463 |
| 24 | 67 | 11 | 19 | 432 |

## V.A.2. pH in Marine Biofilms

The evidence for low pH within marine biofilms consists of two types of measurements as recently published in the Journal, Biofouling (Dexter and Chandrasekaran, 2000). The first type of evidence was obtained using pH indicating dyes. In order to get a general indication of the pH possible within natural assemblage biofilms under our conditions, scrapings from our biofilms were mixed with marine agar incorporating pH-indicating dyes as described above. The colors developed by the colonies of microorganisms as they grew in the agar were taken to indicate the pH range of the metabolites. The results are shown in Table V.A.2. Note that about one third of the colonies that grew in the agar with bromophenol blue were yellow in color, indicating that the pH was less than three. None of the colonies that grew gave an indication of pH greater than 6.4, the pH above which chlorophenol red turns red. This data shows that the pH within some colonies of the natural marine biofilms grown at our location could be in the acid range.

The second type of evidence for low pH was measurements taken directly by Iridium-Iridium oxide type micro-electrodes. Profiles of pH through the natural biofilm perpendicular to the metal surface were measured for many randomly selected locations. Measurements were started in the bulk water, and data points were taken at 10 μm intervals every 15 seconds until the microelectrode tip touched the metal surface. Four of these profiles, each representing one of the types of pH behavior frequently observed, are shown in Figures V.A.2a to V.A.2d. In Figure V.A.2a the local pH near the metal surface was just mildly acidic and the gradient was not steep. At other locations (data not shown) the pH readings remained essentially the same as in the bulk water. In Figures V.A.2b to d, however, the pH profile is steep, and the local pH is quite acidic. The exact location of the biofilm-water interface in these profiles was not known. However, the

Table V.A.2. pH of Metabolites from colonies grown on marine agar.

| pH Indicating Dye in the Agar | Total Number of Colonies | Number of Colonies in Each pH Range | % Showing Acid pH |
|---|---|---|---|
| Phenol Red (below 6.8 yellow above 8.2 red) | 37 | 26 yellow<br>Zero red<br>Remainder white | 70.3 |
| Chlorophenol Red (below 4.8 yellow above 6.4 red) | 14 | 5 yellow<br>Remainder white | 35.7 |
| Bromocresol Green (below 3.8 yellow above 5.4 blue) | 32 | 12 yellow<br>Remainder<br>Bluish white | 37.5 |
| Bromophenol Blue (below 3.0 yellow above 4.6 blue) | 28 | 10 yellow<br>Remainder<br>Bluish white | 35.7 |
| None | 31 | 6 yellow<br>Remainder white | Not Applicable |

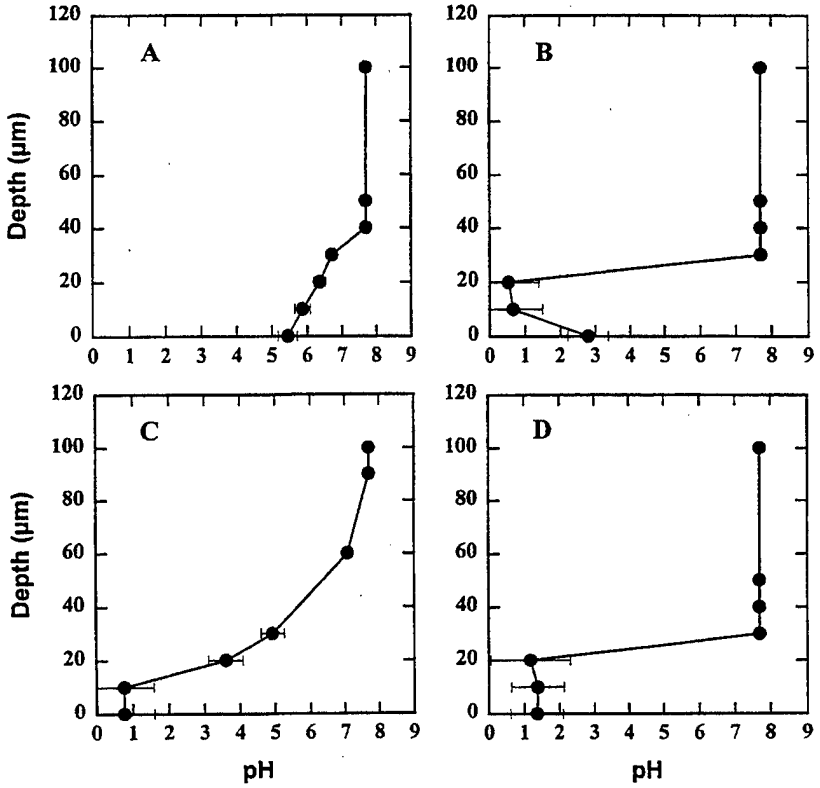


Figure V.A.2. Profiles of pH measured at four different locations within a natural biofilm on platinum. The coupon was ennobled to +510 mV vs SCE.

region of the profile in which the pH began to change rapidly was taken as the interval in which the tip moved into the film (e.g., 30 to 40 μm in Figure V.A.2a and 20 to 30 μm in Figure V.A.2b). At the final step, the microelectrode tip actually touched the platinum coupon surface. The microelectrode was usually robust enough to withstand this contact partially because the platinum coupon was not mounted rigidly, and was, thus, able to move vertically. Distances from the coupon surface shown in the pH profiles were back calculated from the step at which contact occurred. The uncertainty of each vertical position was taken as half the distance of the final step (± 5 μm). There was an additional uncertainty related to the instrumental accuracy (± 0,4 μm) of the micromanipulator. The sum of these two errors in the vertical position of the microelectrode tip is about the same as the size of the data points plotted. The horizontal error bars are the standard error for the pH measurements in the biofilm as calculated from the calibration curves.

The problem that was not yet recognized at that time this data was taken was that, while the pH could be quite low in places within biofilms, those areas are highly localized, and there is probably not enough total acidity to account for the observed ennoblement in any given environment.

## References Cited

Dexter, S. C. and P. Chandrasekaran, 2000, "Direct Measurement of pH Within Marine Biofilms on Passive Metals," Biofouling, Vol. 15, No. 4, pp. 313-325.

Dexter, S. C., 1988, "Role of Microfouling Organisms in Marine Corrosion," Presented as Plenary Lecture at 7th Intl. Congr. On Marine Corrosion and Fouling, Valencia, Spain, November, 1988. (Proceedings never published)

Hoare, J.P., 1968, "The Electrochemistry of Oxygen," Wiley-Interscience, New York.

Johnsen, R. and E. Bardal, 1985, Corrosion, Vol. 41, No. 5, p. 296.

Scotto, V., R. DiCintio and G. Marcenaro, 1985, Corrosion Science, Vol. 25, No. 3, p. 185.

## V.B. Mechanism in Transition

During the mid-1990s the focus of our research on the mechanisms of ennoblement gradually shifted from ideas based on pH changes to those centered on the effects of the heavy metals, Fe and Mn. Two factors drove this transition. First was the development of a new general model for the structure of biofilms by the group under Dr. Lewandowski at Montana St. University. Second was the growing realization from our own work that the ennoblement mechanism had to account not only for the noble shift in OCP of passive metals, but an increase in the corrosion rate as well. While we were satisfied that the mechanisms we had been working on were able to account for the shift in OCP, something additional was needed to account for an increase in the sustained current needed to support the higher observed corrosion rates in the presence of biofilms.

In 1993 our working hypothesis for the ennoblement mechanism was based on the pH-peroxide model. We hypothesized that ennoblement of the OCP of passive metals and alloys to values greater than +300 mV SCE by microbial biofilms less than about 100 μm in thickness required sharp gradients in both pH and dissolved oxygen within the biofilm. As illustrated schematically in Figure V.B.1, the biofilm was still seen as having a layered structure. The outer layers were thought to be aerobic and at near neutral pH, while the portion of the film immediately adjacent to the metal surface was thought to be acidified, with a generally low oxygen concentration, possibly becoming anaerobic over large portions of the metal surface. Under these conditions, the primary contribution to ennoblement was thought to come from the thermodynamic effect of pH itself on the OCP. A very important secondary contribution was to come from the cathodic reaction. This was envisioned as a combination of the acidic form of the oxygen reduction reaction, Equn (1), and the reduction of hydrogen peroxide to water, Equn (2). Both of these reactions have more noble redox potentials than the oxygen reaction at neutral to basic pH.

$$O_2 + 4H^+ + 4e^- \rightarrow 2H_2O \qquad E° = 1.229 \text{ V SHE} \qquad (1)$$

$$H_2O_2 + 2H^+ + 2e^- \rightarrow 2H_2O \qquad E° = 1.776 \text{ V SHE} \qquad (2)$$

The metabolic action of the biofilm itself was then seen as both the primary source and regulator of peroxide through the superoxide dismutase/catalase (or peroxidase) enzyme system of the aerobic organisms in the outer layers of the film. We further hypothesized that peroxide, being a powerful oxidizer, was involved in maintaining the low pH within the film through its action on reduced chemical species in the film. Finally we hypothesized that the suite of conditions described above for producing ennoblement could only be achieved by a variety of different types of microorganisms in consortia as found in biofilms grown from natural waters. The outer portions of the biofilm would contain mostly general aerobic microorganisms consuming oxygen. Beneath these in the reduced oxygen portion of the biofilm would be the Fe and Mn reducers and the fermenters. Finally, at the base of the biofilm, in the anaerobic niches or sublayer would be the sulfate reducers.

Note that the biofilm at this time was still envisioned as a layered structure with some horizontal variability. We now know that this structure is basically incorrect, and that the

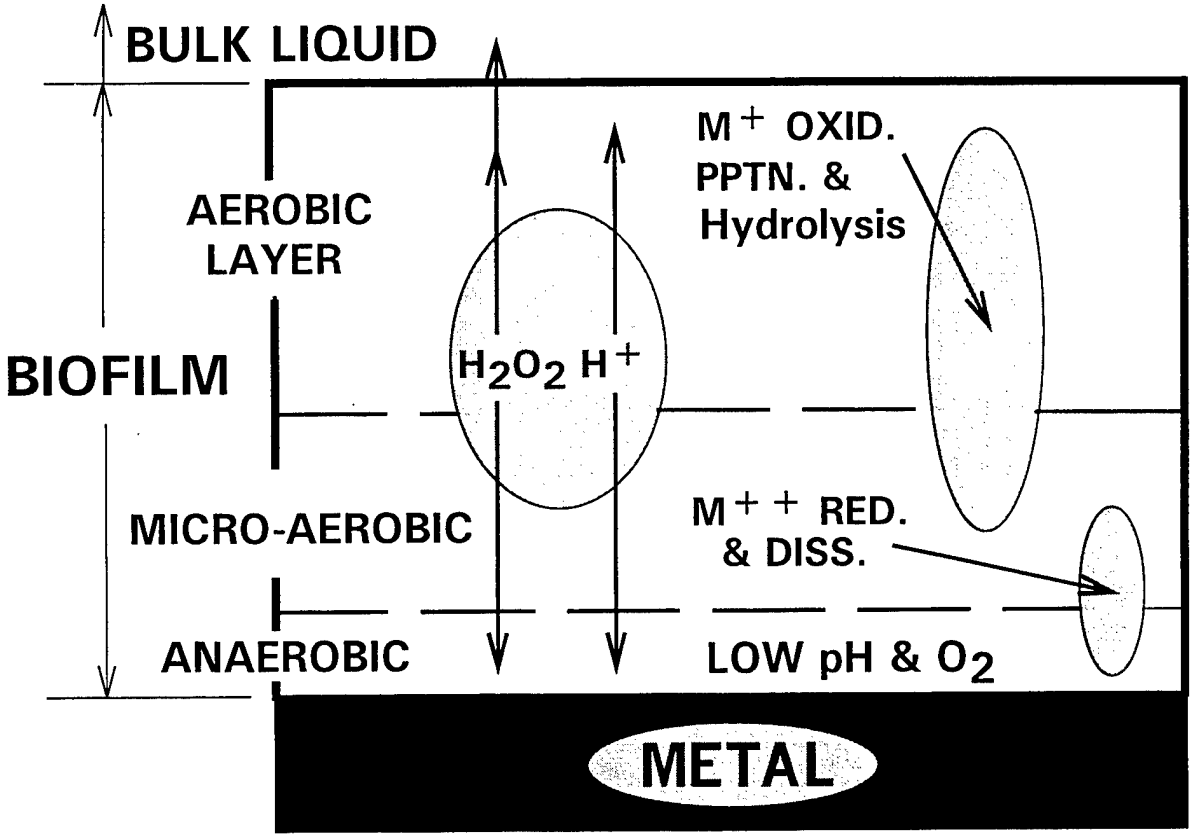


Figure V.B.1. Schematic diagram of layered biofilm structure and reactions involved in supporting the early pH, peroxide, oxygen model of ennoblement.

new and valid structure would make it unlikely that the above mechanism could carry the primary load of ennoblement. Note also that Fe and Mn are specifically mentioned here as important, but they are envisioned as instrumental in producing both peroxide and low pH as the primary agents for ennoblement, rather than being the agent themselves.

During the course of that work in the mid-1990s, it became clear that:

1) The biofilm structure was not continuous layers, but rather a thin base film overlain by a heterogeneous columnar structure that accommodated intense microcolonies and allowed near bulk water conditions to reach the metal surface (or near it at least) between the columns. Thus, mass transport to and from the microcolonies and bulk water could take place horizontally as well as vertically (Lewandowski, et al., 1995).

2) The rate of crevice corrosion was systematically increased by biofilms in addition to a decrease in the initiation time (Zhang and Dexter, 1995). Thus, any overall mechanism would have to account for increased current capacity as well as ennoblement of the OCP.

Thus, we began to realize that, while the above mechanisms worked for the OCP, something additional was necessary to account for the current capacity.

## V.C. Heavy Metals and the Manganese Dioxide Mechanism

In the early 1990s we had forseen that biofilms could cause ennoblement by the introduction of redox systems other than oxygen. At that time we stated:

> "There is a large number of possibilities here that could be investigated. One criterion that would have to be met by any proposed reaction, however, is that it would have to supply a reduction current larger than that of oxygen at air saturation in order to account for the observed data. Since likely reactions capable of meeting this criterion have not yet been identified, this approach will be considered only if the work proposed here convincingly demonstrates that organo-metallic catalysis, enzymatic catalysis and acidification are not viable mechanisms for corrosion potential ennoblement."

In our 1997 ONR Proposal we noted that Dexter and LaFontaine (1998) had shown an increase in the limiting cathodic reduction current at potentials between -300 and –900 mV SCE. We then went on to reason that:

> "... the increase in limiting current is not likely due to an increase in oxygen transport to the metal surface. If anything, the biofilm would act as an additional physical barrier to oxygen diffusion. Dickinson and Lewandowski (1996) found numerous Mn rich deposits on stainless steel coupons ennobled by fresh water biofilms. In abiotic experiments with $MnO_2$ on clean coupons they found almost identical electrochemical effects as found on naturally biofilmed coupons. Chandrasekaran and Dexter (1994) also found elevated levels of Fe and Mn in biofilms from Lower Delaware Bay waters. Thus, reduction of Mn as well as other heavy metals may be responsible for the increase in the limiting current. It is proposed, therefore, that the biofilm introduces reduction of heavy metals as a new redox reaction with an elevated limiting current density in the –300 to –900 mV range as compared to that of the oxygen system. This mechanism is under further investigation."

The MS Thesis research by David Ruppel was intended to determine if the increased Galvanic Current could be due to the presence of Manganese dioxide. Results from that work have recently been submitted for publication in Corrosion Journal. Pertinent sections of that paper are quoted below.

A recent explanation for ennoblement and increased current capacity involves the deposition of high oxidation state Fe and Mn via metal oxidizing bacteria living in the biofilm (Dickinson and Lewandowski, 1996; Linhardt, 1996). Metal oxidizing bacteria, or chemolithotrophs, found in suboxic and anoxic environments, metabolize the reduced forms of metals ($Mn^{+2}$, $Fe^{+2}$) that naturally occur in aquatic environments, producing the oxidized forms ($Mn^{+4}$, $Fe^{+3}$). Metal oxidizing bacteria are common to many aquatic systems, including coastal seawater, lakes, thermal springs, wetlands and soils (Ghiorse, 1984). Dickinson &

Lewandowski (1996) and Linhardt (1996) found numerous Mn and Fe oxidizing bacteria and Mn-rich deposits on ennobled stainless steel coated with fresh water biofilms. Chandrasekaran (1995) and Xu *et al.* (1998) also found elevated levels of Fe and Mn in biofilms formed in lower Delaware Bay waters. Milli-molar concentrations were measured in the biofilm matrix as compared with μM or nM concentrations found in bulk seawater. Dickinson & Lewandowski (1996) observed that, upon chemical dissolution of such Mn-rich deposits, the potential of the metal dropped to pre-biofilm levels. Additionally, they found that when bare stainless steel was coated with a $MnO_2$ paste, the OCP and current capacity increased to values characteristic of coupons with biofilms. These findings suggested that Mn enrichment could increase current capacity and hence the corrosion rate of Al and steel coupled to biofilm-coated cathodes. Numerous reactions with Mn oxides and (oxy)hydroxides would be kinetically fast enough to increase current capacity Dickinson and Lewandowski, 1996; Dickinson, et al., 1996; Stumm and Morgan, 1981; Luther, et al., 1999).

Manganese is the fifth most abundant metal on earth (Montgomery, 1992), thus it is available to participate in large-scale reactions in a variety of environments. Manganese in biofilms is significant because the redox potentials of its species occur at the natural pε-pH boundaries, allowing Mn to participate in environmental electron exchange reactions Nealson and Saffarini, 1994). The solubility of Mn species is fundamental to its chemical reactivity. The reduced form ($Mn^{+2}$) is soluble, while the oxidized form ($Mn^{+4}$) is usually considered to be insoluble in aerobic, aquatic systems. This is not always the case, however, as a soluble form of polymeric $MnO_2$ has recently been documented (Luther, et al., 1999), and Kostka *et al.* (1995) were among the first to work with a soluble form of $Mn^{+3}$ in environmental systems.

In light of the recent increase in understanding about the role of manganese in biofilms as outlined above, the present work was focused on the effects of $MnO_2$ reactions on passive alloy surfaces. It was particularly desirable to test the hypothesis that $MnO_2$ concentrated at the metal surface by natural biofilms is capable of: a) supplying enough current, and b) sustaining it long enough to account for the observed increases in galvanic corrosion rates of aluminum and steel.

### V.C.1. Results

Reader please note: All Figures in Section V.C are numbered consecutively within this section. The OCP of $MnO_2$-coated coupons was more noble than the control coupons by approximately 700 mV, regardless of oxygen concentration (Figure 1). This effect of $MnO_2$ on the OCP of stainless steel has also been observed by other investigators (Dickinson, et al., 1996; Olesen, et al., 2000). Under air-saturated conditions, polarization curves of $MnO_2$-coated coupons showed greater current densities (by a factor of about 2 at –700 mV SCE) than did the control coupons. The same was true for oxygen-saturated conditions, with the difference being a factor of 4 at –700 mV. The $MnO_2$ coating also increased current density under nitrogen-saturated conditions for all applied potentials more noble than –700 mV SCE, at which point they became similar. While both $MnO_2$ and oxygen were able to increase current density, the effect of oxygen in addition to $MnO_2$ was statistically insignificant at potentials more noble than –300 mV SCE. As the level of polarization continued to potentials

more active than –300 mV SCE, the current density contributed by dissolved oxygen became more important.

Prior work in the immersion tanks with Lower Delaware Bay seawater had shown that biofilm growth on the cathode panel of galvanic couples increased the corrosion rate of anodic materials, as compared to those connected to clean, control cathodes Dexter and LaFontaine, 1998b). The purpose of this work was to determine the role of $MnO_2$ in that effect. To this end, galvanic coupling was simulated in the same water by potentiostatic polarization. Samples of UNS NO8367, with and without an abiotically produced $MnO_2$ coating, were polarized at a constant potential of – 500 mV SCE, yielding current density vs. time plots.

As shown in Figure 2 under air-saturated conditions, each curve showed an initial transient current spike before settling to a stable current within 2-3 minutes after application of the potential. Each of the curves in Figure 2 represents the average of three runs on independent samples. Error bars representing the standard error of the mean are shown for each curve at 3, 6 and 9 minutes. The curves in Figure 2 revealed differences between the first and second polarization runs of the $MnO_2$-coated samples as well as between those and the control samples without $MnO_2$ coatings. The final currents after ten minutes of polarization for the first and second runs on $MnO_2$-coated samples and uncoated controls are shown in Table 1. Analyzing the data with ANOVA (analysis of variance) followed by a Tukey's HSD revealed that the final currents resulting from the first and second polarizations of the $MnO_2$-coated coupons were significantly different from one another. These were also significantly different from the final currents from the control coupons ($P<0.05$).

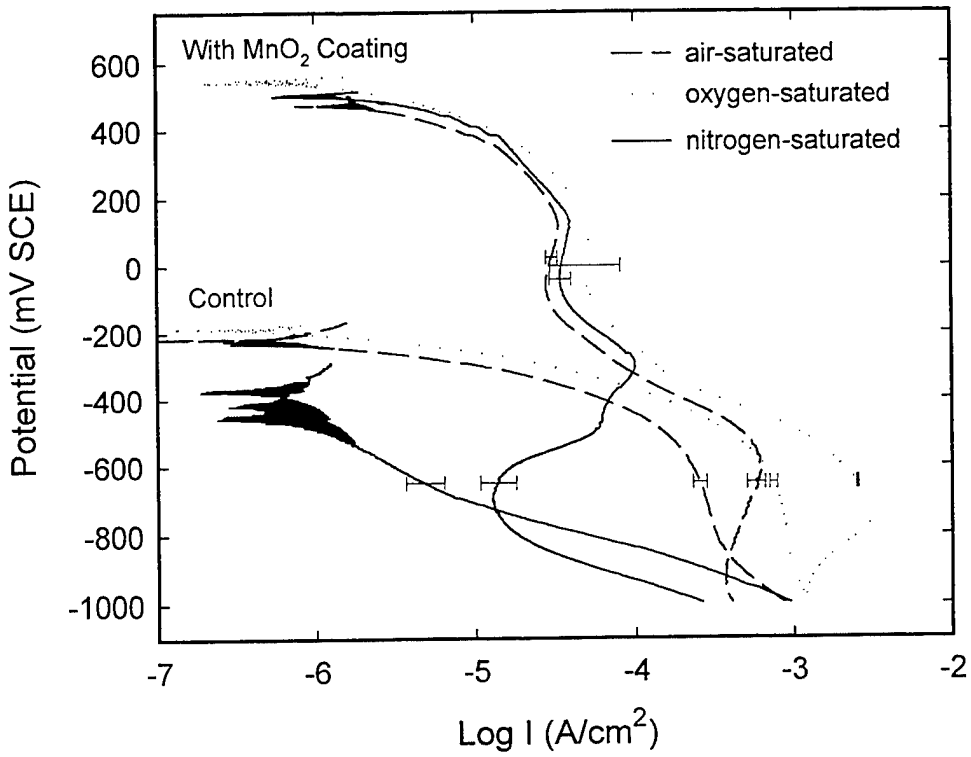


Figure 1. Average cathodic polarization curves of $MnO_2$-coated and control NO8367 in seawater of varying dissolved oxygen concentrations.

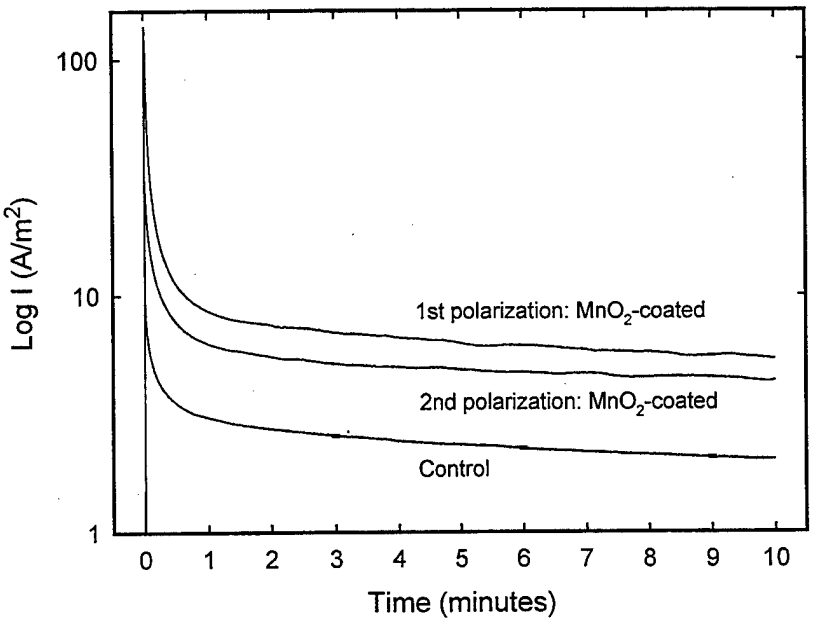


Figure 2. Potentiostatic polarization of control and $MnO_2$-coated NO8367 in air-saturated seawater at -550 mVSCE.

**TABLE 1:** Final current densities after 10-minute polarization of UNS NO8367 at –550 mV SCE under air-, nitrogen- and oxygen-saturated conditions.

| | Current Density ($mA/cm^2$) | | |
|---|---|---|---|
| | Air-saturated | $N_2$-saturated | $O_2$-saturated |
| 1st polarization—$MnO_2$-coated | 0.533 ± 0.001 | 0.093 ± 0.002 | 1.21 ± 0.01 |
| 2nd polarization—$MnO_2$-coated | 0.43 ± 0.01 | 0.044 ± 0.002 | 1.12 ± 0.01 |
| Control | 0.20 ± 0.02 | 0.0013 ± 0.0002 | 0.59 ± 0.06 |

Polarization curves for the samples in nitrogen-saturated seawater are shown in Figure 3, and the current densities after ten minutes of polarization are shown in Table 1. These current densities for the first and second polarizations of $MnO_2$-coated coupons under nitrogen-saturated conditions were significantly different from one another and from the controls ($P<0.05$). They were also six times lower than those measured under air-saturated conditions.

During the polarization runs in nitrogen-saturated seawater, a brown film was observed to form on the auxiliary platinum anode. This film was insoluble in a solution of 10% HCl in deionized water. The film was soluble, however, in acidified oxalic acid, indicating that it was probably $MnO_2$. In order to determine if it was possible that the brown film had come from the $MnO_2$ deposited on the cathode, total Mn concentration in the nitrogen-saturated seawater was measured by ICP. Before insertion of the $MnO_2$ coated coupon, the Mn concentration in the water varied from 16 to 163 ± 2 nM depending on the tidal cycle. Mn concentration was then measured again in the same seawater after immersion and polarization of an $MnO_2$ coated coupon. In two separate trials, the Mn concentration increased by 95 and 207 ± 2 nM above that in the ambient water, showing that Mn was being transferred (probably as Mn+2) to the bulk water during polarization.

Current densities from polarizations on $MnO_2$-coated coupons in oxygen-saturated seawater (Figure 4) revealed much higher current densities than in the other conditions. The final current densities after ten minutes of polarization are shown in Table 1. Interestingly, ANOVA and Tukey's HSD tests revealed that the current densities from the first and second polarizations of $MnO_2$-coated UNS NO8367 under oxygen-saturated conditions were not significantly different from one another ($P>0.05$). The current densities of the $MnO_2$-coated coupons, however, were significantly different from those of the controls.

Integrating under the current density vs. time curves from Figures 2-4 yielded total charge transferred during the 10-minute polarization—a measure of the net influence of the $MnO_2$ coating. These data for the oxygen-saturated, air-saturated and nitrogen-saturated conditions are shown in Table 2. Under all experimental conditions, the highest average charge transferred was during the first polarization run, and the lowest was on the control coupons. Average charge transferred also increased systematically from nitrogen-saturated to air-saturated to oxygen-saturated conditions.

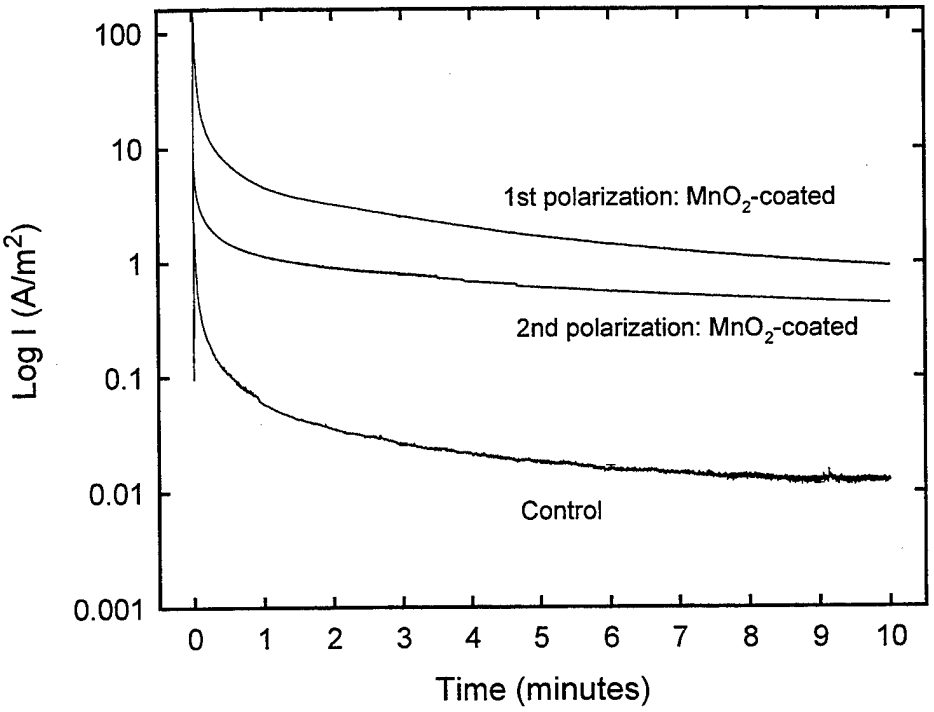


Figure 3. Potentiostatic polarization of control and $MnO_2$-coated NO8367 in nitrogen-saturated seawater at -550 mVSCE.

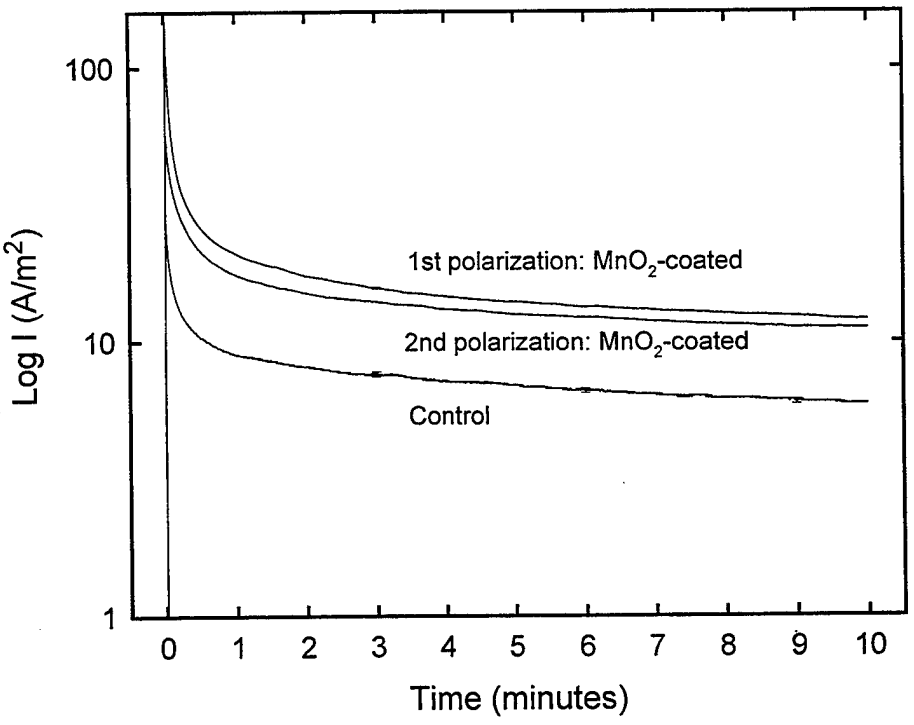


Figure 4. Potentiostatic polarization of control and $MnO_2$-coated NO8367 in oxygen-saturated seawater at -550 mVSCE.

**TABLE 2:** Total charge transferred after 10-minute polarization of UNS NO8367 at –550 mV SCE.

| | Total Charge transferred ($mC/cm^2$) | | |
|---|---|---|---|
| | Air-saturated | $N_2$-saturated | $O_2$-saturated |
| 1st polarization—$MnO_2$-coated | 440 ± 7 | 175 ± 4 | 970 ± 16 |
| 2nd polarization—$MnO_2$-coated | 318 ± 7 | 46 ± 1 | 840 ± 16 |
| Control | 150 ± 13 | 2.3 ± 0.2 | 443 ± 48 |

Natural biofilms were grown on N08367 coupons to see how their polarization behavior would compare to that of $MnO_2$-coated coupons. Each coupon was polarized twice, waiting one hour between runs. A second set of polarizations was run after a four-day recovery period back in the immersion tank. The data shown in Figure 5 indicate that the transient peak heights observed within the first few seconds of polarization (60 mA) were greater than those from the $MnO_2$-coated coupons (18 mA). It is also apparent from the data that the individual curves were less reproducible than those for the $MnO_2$ coupons. In addition, no systematic differences were visually apparent between the first and second polarization runs on a given day, or between the initial set of runs and those done four days later. The same statement can be made for the values of the final current densities after ten minutes of polarization and the total charge transferred as shown in Table 3. Statistical analysis (ANOVA and Tukey's HSD) of the polarization curves in Figure 5 and the data in Table 3 confirm the judgment made by visual inspection. None of the data in Figure 5 and Table 3 were statistically significantly different from any of the others ($P>0.05$).

**TABLE 3:** Current density and total charge transferred after 10-minute polarization of biofilm-coated UNS NO8367 at –550 mV SCE.

| | | Current Density ($mA/cm^2$) | Charge Transferred ($mC/cm^2$) |
|---|---|---|---|
| Day 1 | 1st polarization | 0.33 ± 0.01 | 520 ± 50 |
| | 2nd polarization | 0.28 ± 0.02 | 310 ± 20 |
| Day 4 | 1st polarization | 0.31 ± 0.03 | 430 ± 65 |
| | 2nd polarization | 0.27 ± 0.02 | 265 ± 25 |

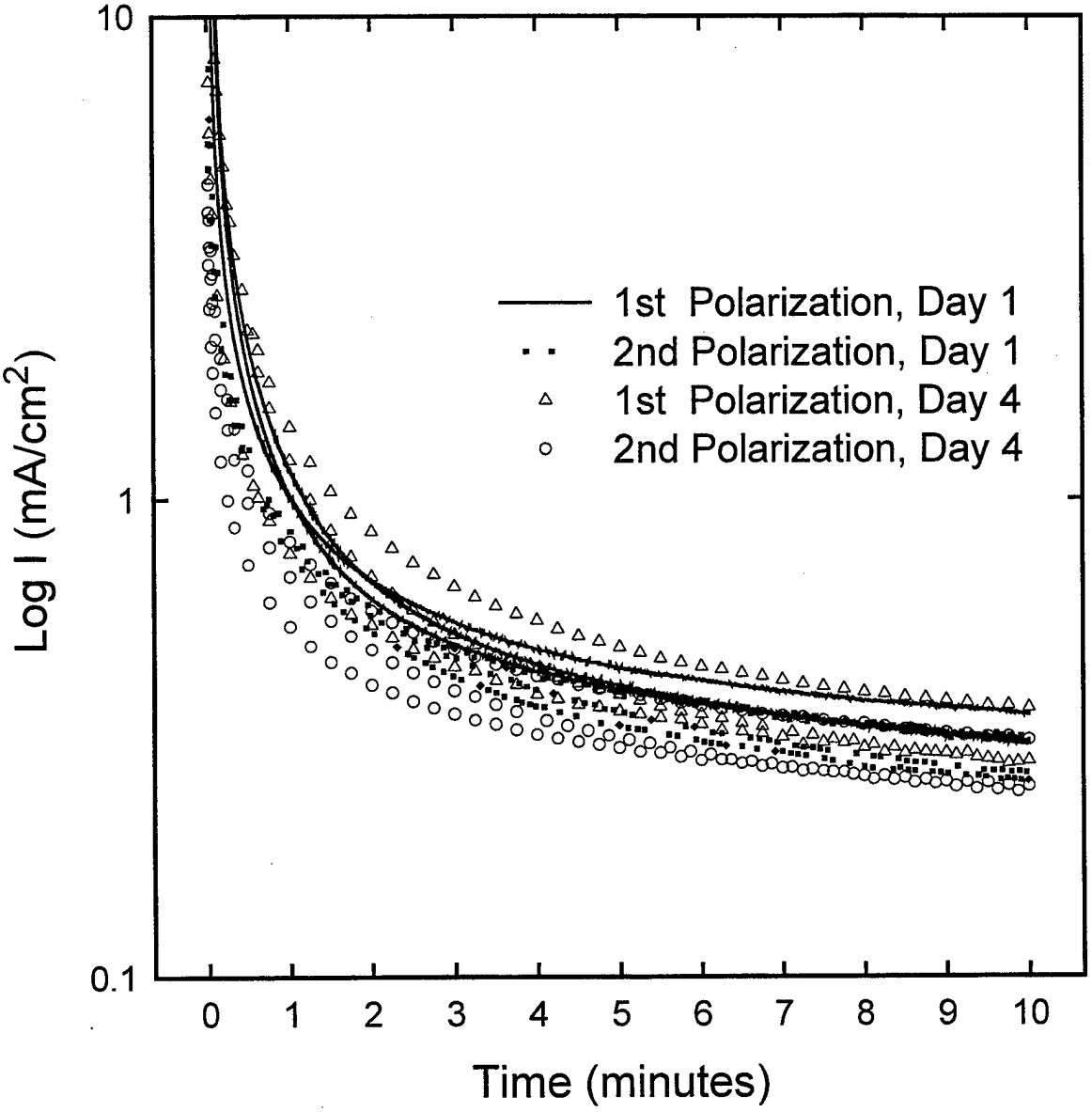


Figure 5. Potentiostatic polarization of biofilm-coated NO8367 in air-saturated seawater at -550 mV SCE. Second set of of curves (open points) were run four days after the first.

## V.C.2. Discussion

The data presented demonstrate that $MnO_2$ coated onto the surface of passive metal coupons is capable of increasing both the OCP of the coupon and the current that can be drawn from it. Consider now what can be deduced from the data concerning the magnitude of the manganese effect, its relation to the effect of oxygen and its capacity for explaining the observed increase in galvanic corrosion rates in the presence of natural biofilms (Dexter and Lafontaine, 1998b).

At first thought it might be expected that the contributions to current density from $MnO_2$ and oxygen, while additive, would act independently of one another. Referring to Table 1, the contribution to current density from $MnO_2$ alone, without the influence of oxygen can be taken as the current from the first polarization run for the $MnO_2$-coated coupons under nitrogen-saturated conditions. This value was 0.093 $mA/cm^2$. The contribution to current density from oxygen alone, without the influence of $MnO_2$ can be taken as the control current under air-saturated conditions. This value was 0.20 $mA/cm^2$, approximately twice that from $MnO_2$ alone. Adding these two numbers together yields 0.293 $mA/cm^2$, and this combined value is nearly a factor of 2 less than the 0.533 $mA/cm^2$ for the $MnO_2$ coated coupon polarized under air-saturated conditions. A similar result can be seen using the corresponding values for the second polarization run, or the data for the total charge transferred in Table 2. In each case the differences become larger if one substitutes the oxygen-saturated data for the air-saturated values. Thus, it is obvious that the combined effect of $MnO_2$ and oxygen was greater than the sum of the individual effects, and one can conclude that there is a synergy between the effects of oxygen and $MnO_2$.

The most straight forward explanation for an increased current density of $MnO_2$ coated coupons vs. control under air and oxygen-saturated conditions is that $MnO_2$ provides an additional reduction reaction, producing either $Mn^{+2}$ or $Mn^{+3}$ during the cathodic polarization process. The Pourbaix (1974) diagram for the Mn-water system indicates that the potential at which $MnO_2$ begins to be reduced at pH 7.5 is –210 mV SCE, which agrees with the observed results. This alone could explain an additive increase in current density between control and $MnO_2$-coated coupons, but it cannot explain the synergistic effect.

The fact that Mn and oxygen are synergistic, and not simply mathematically additive, may be explained by the fact that dissolved oxygen can be involved in reoxidizing the newly formed $Mn^{+2}$. Thus, a single $MnO_2$ molecule may contribute many times to the total charge transferred during a polarization run. The rate of chemical re-oxidation of $Mn^{+2}$, however, is slow (on the order of weeks or months) unless biologically mediated or in the presence of $MnO_2$, which has an autocatalytic effect (Stumm and Morgan, 1981). In most cases, this slow oxidation rate precludes the reaction from contributing to the overall electron transfer process in natural systems. In various anoxic environments, however, $Mn^{+2}$ oxidation rates can be many orders of magnitude faster than would be observed from abiotic reactions alone (Neaslon, et al., 1988). Tebo (1991) found that the oxidation rate of $Mn^{+2}$ in the anoxic Black Sea was five to six times faster than from autocatalytic oxidation on the surface of $MnO_2$, suggesting microbial catalysis contributes to the oxidation process. The conditions found in

the Black Sea (an oxic/suboxic interface) are similar to those found in biofilms. Xu (2000) found that manganese in natural biofilms grown at our Lower Delaware Bay exposure site was usually associated with areas of low oxygen (about 10 μmolar) and elevated peroxide.

The kinetics of the inorganic manganese oxidation reaction can be described by the rate law:

$$-d[Mn^{+2}]/dt = k_o[Mn^{+2}] + k[Mn^{+2}][MnO_2] \qquad (2)$$

where the rate of $Mn^{+2}$ oxidation is dependent on the concentrations of both $Mn^{+2}$ and $MnO_2$. Thus, the presence of $MnO_2$ on the coupon catalyzes the oxidation of $Mn^{+2}$ on a time scale that allows a continuous contribution to current density.

One might then ask why the current density for the control coupon in Figure 1 was greater than that of the $MnO_2$-coated coupon in nitrogen-saturated seawater at potentials more active (negative) than –700 mV SCE. Upon examining the polarization curve for the $MnO_2$ coated sample under nitrogen-saturation in Figure 1, it appears that, without oxygen present to continually re-oxidize $Mn^{+2}$, the initial supply of $MnO_2$ became depleted by the time the polarization reached –700 mV SCE. Thus, at more active potentials in the absence of oxygen, reduction of water to form $H_2$ gas became the dominant cathodic reaction.

At potentials more positive than –700 mV in the potentiodynamic polarization curves (Figure 1), the current densities from $MnO_2$ coated coupons were always greater than control, indicating that $MnO_2$ contributed to the reduction reactions at the cathode. Increasing dissolved oxygen levels also resulted in correspondingly higher current densities on both control and $MnO_2$-coated coupons. Thus it appears that the reduction products of $MnO_2$ interacted with oxygen to contribute to current density. This is consistent with observations from the potentiostatic polarizations in Figures 2 through 4 that $MnO_2$ increased the current capacity while being partially depleted in the process. This conclusion is based on the fact that the second polarization of $MnO_2$-coated coupons yielded significantly lower current densities than the first in each condition except oxygen-saturated. The second potentiostatic polarization in oxygen-saturated conditions was not statistically different from the first based on ANOVA and Tukey's HSD test.

The quantity of manganese in biofilms has been measured by several means. Chandrasekaran and Dexter (1994) used ICP techniques to measure the total Mn in biofilms scraped from metal surfaces. They found concentrations of 10 to 20 mM. Much of that manganese, however, was present in the inorganic particulates trapped in the biofilm matrix, and it would not have been measured as a soluble species. For example, Xu, et al. (1998) and Xu (2000) used microelectrode techniques to show that dissolved $Mn^{+2}$ was present in low oxygen areas of the biofilm at the 20 to 50 μM level. While all of that soluble manganese would have been available for reoxidation, the distribution of it was spotty within the biofilm matrix.

The amount of $MnO_2$ deposited on the test coupons in the present work was calculated from the ICP-OES measurements to be about 0.4 μmol/cm$^2$. Taking the estimated thickness of the deposited film to be 0.1 mm, the concentration of Mn in the film becomes 40 mM. This is

higher than, but generally comparable to the 10 to 20 mM total Mn measured in natural biofilms by ICP (Chandrasekaran and Dexter, 1994).

The amount of $MnO_2$ deposited can also be estimated by calculating the total charge transferred (Table 2) from potentiostatic polarizations of $MnO_2$-coated coupons. This will be done using the data for nitrogen-saturated conditions in order to minimize the synergistic re-oxidizing effect of oxygen. Assuming reaction (3) below is occurring on the coupon surface during the potentiostatic polarization:

$$4H^+ + MnO_2 + 2e^- \rightarrow Mn^{+2} + 2H_2O \qquad (3)$$

it is clear that two equivalents (moles of electrons) are consumed for every mole of $MnO_2$ reduced. The charge transferred during potentiostatic polarization of an $MnO_2$-coated coupon under nitrogen-saturated conditions was $175 \pm 4$ mC/cm$^2$ (Table 2). Subtracting the $2.3 \pm 0.2$ mC/cm$^2$ for the control measurement, equation (4) then gives the quantity of $MnO_2$/cm$^2$ on the coupon:

$$(0.173\ C/cm^2)(1\ equiv/96{,}500\ C)(1\ mol\ MnO_2/2equiv) = 0.9\ \mu mol\ MnO_2/cm^2 \qquad (4)$$

This estimate (0.9 μmol/cm$^2$) based on the polarization data is larger by a factor of 2.3 than the 0.4 μmol/cm$^2$ value obtained from ICP-OES. In the presence of oxygen this disparity could be explained by the autocatalytic effect of $MnO_2$ on $Mn^{+2}$. However, this mechanism cannot occur under the nitrogen-saturated conditions where the maximum value of dissolved oxygen was 3μM. The mass balance calculations clearly indicate that the total charge transferred was greater than could be produced by a 2-electron transfer of all the $MnO_2$ on the coupon. This is especially true when one considers that some brown film was always left on the coupons after polarization, indicating that not all of the coated $MnO_2$ was released into solution. Thus, there must have been an additional mechanism for reforming $MnO_2$.

Equations (5) to (7) below describe the well known reduction of $MnO_2$ via a soluble $Mn^{+3}$ intermediate:

$$4H^+ + MnO_2 + 1e^- \rightarrow Mn^{+3} + 2H_2O \qquad (5)$$

$$2H_2O + 2Mn^{+3} \rightarrow MnO_2 + Mn^{+2} + 4H^+ \qquad (6)$$

$$2H_2O + Mn^{+2} + O_2 \rightarrow Mn^{+3} + 4OH^- + 1e^- \qquad (7)$$

Equation (5) describes the one-electron reduction of $MnO_2$ to a soluble $Mn^{+3}$ species, which is metastable and will quickly disproportionate to $Mn^{+4}$ and $Mn^{+2}$ in seawater (equation 6) unless complexed by strong organic ligands (Luther, et al., 1999). These reactions explain the

production of $MnO_2$ and $Mn^{+2}$ in the absence of dissolved oxygen. If oxygen is present, it can re-oxidize $Mn^{+2}$ back to $Mn^{+3}$ (equation 7) where equation (6) can occur again. If oxygen is not present, $Mn^{+3}$ disproportionation alone can still account for the results since $MnO_2$ can never be fully depleted. Figure 6 shows this Mn cycle including both inorganic and biological processes. These inorganic and electrochemical recycling reactions explain how $MnO_2$ can be reformed in nearly anoxic conditions, effectively contributing more charge transfer than could be produced by the simple reduction of $MnO_2$ to $Mn^{+2}$.

The value of total charge transferred under nitrogen saturation (Table 2) was used above in Equation (4) to calculate the quantity of $MnO_2$ on the coupon assuming a two-electron transfer. It can also be used to calculate the quantity of $MnO_2$ for the one-electron transfer reaction represented by Equation (5). The result is 1.8 μmol $MnO_2/cm^2$, and this value is 4.6-fold greater than the $MnO_2$ on the coupon calculated by ICP-OES analysis (0.4 μmol/$cm^2$). This would mean that in the case of a one-electron transfer reaction, the $MnO_2$ is being recycled almost five times during the ten-minute polarization run. According to equations (5) through (7) the mechanism for this chemical recycling under our nitrogen saturated conditions was disproportionation.

Recently, Olesen, et al. (2000) have discussed the thermodynamics of solid phase Mn(III, IV) compounds. Possible manganese reduction and re-oxidation reactions included were the two-electron transfer reduction of $MnO_2$ directly to $Mn^{+2}$ as originally proposed by Linhardt (1996) and the one-electron transfer reduction of $MnO_2$ to solid MnOOH. They then analyze further reduction of solid MnOOH to $Mn^{+2}$ by a one-electron transfer reaction:

$$MnOOH + 3H^+ + e^- \rightarrow Mn^{+2} + 2H_2O \qquad (8)$$

Or by disproportionation:

$$2MnOOH + 2H^+ \rightarrow MnO_2 + Mn^{+2} + 2H_2O \qquad (9)$$

They conclude that disproportionation of the solid MnOOH by equation (9) is unlikely because the free energy of formation was positive under their conditions, and that reduction by equation (8) would allow for reoxidation in the presence of manganese oxidizing bacteria to keep the redox cycle going.

While we do not disagree with their thermodynamic discussion on solid phases, our data and calculations indicate that there are mechanisms available for recycling $MnO_2$, even in the absence of a biofilm. These include reoxidation of $Mn^{+2}$ on $MnO_2$ surfaces by oxygen in aerated solutions and disproportionation of a soluble form of $Mn^{+3}$ in deaerated solutions. Our data support $Mn^{+3}$ disproportionation. The solution analysis data showed that $Mn^{+2}$ went into solution when $MnO_2$ coated coupons were polarized in nitrogen-saturated solutions, but not when the solutions contained oxygen. Moreover, it was observed that a brown film formed on the platinum anodes when polarizing in nitrogen-saturated conditions. Oxalic acid dissolution of the brown product indicated that this was oxidized Mn(III or IV) solids. Thus, we conclude that the brown film formed when $Mn^{+2}$ migrated to the anode and was re-oxidized by oxygen formed there from the breakdown of water. This could occur without disproportionation of $Mn^{+3}$ by direct reduction of $MnO_2$ to $Mn^{+2}$. However, the fact that the

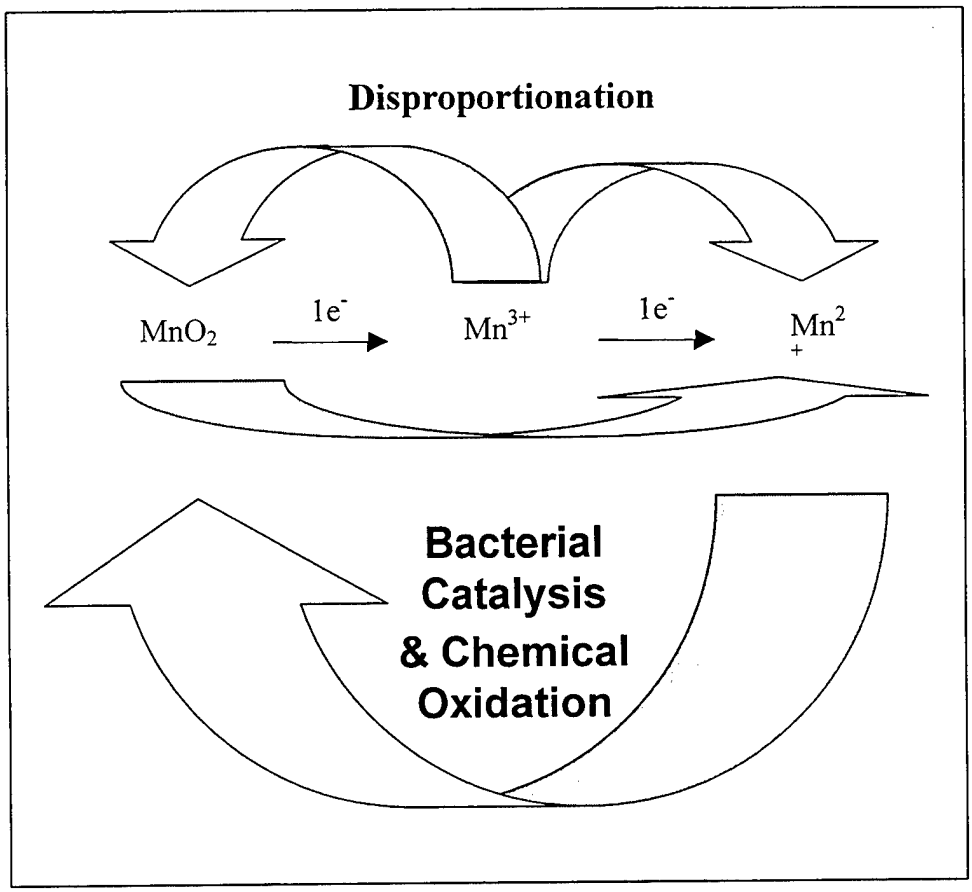


Figure 6. Schematic diagram of manganese cycling in a biofilm.

current produced was 4.6 times higher than that necessary to reduce all the $MnO_2$ on the cathode means that even in these abiotic and very low oxygen solutions, something was regenerating $MnO_2$ on the cathode surface. We propose as shown in Figure 7(A) that this happened by formation of a soluble $Mn^{+3}$ intermediate at the cathode surface (Equation 5), followed by disproportionation to replace $MnO_2$ at the cathode and put $Mn^{+2}$ into solution (Equation 6). Some of the $Mn^{+2}$ in solution then diffused to the anode to form $MnO_2$ or MnOOH. Note that in Figure 7(B) there is no mechanism for renewing $MnO_2$ on the cathode surface. Thus, it becomes depleted, and the total cathodic current available is limited to that for reducing the $MnO_2$ originally deposited. In contrast, the $MnO_2$ on the cathode in Figure 7(A) is continuously replenished by the disproportionation reaction, and the total current available is larger than that represented by the $MnO_2$ deposited in agreement with the amplification by 4.6x observed.

Coupons with natural biofilms were included in the polarization test program to see how their performance compared to those with $MnO_2$ coatings. The purpose of polarizing each biofilm-coated coupon twice with a one-hour delay and then again four days later was to determine the ability of microorganisms to regenerate the chemical conditions in the biofilm on both a

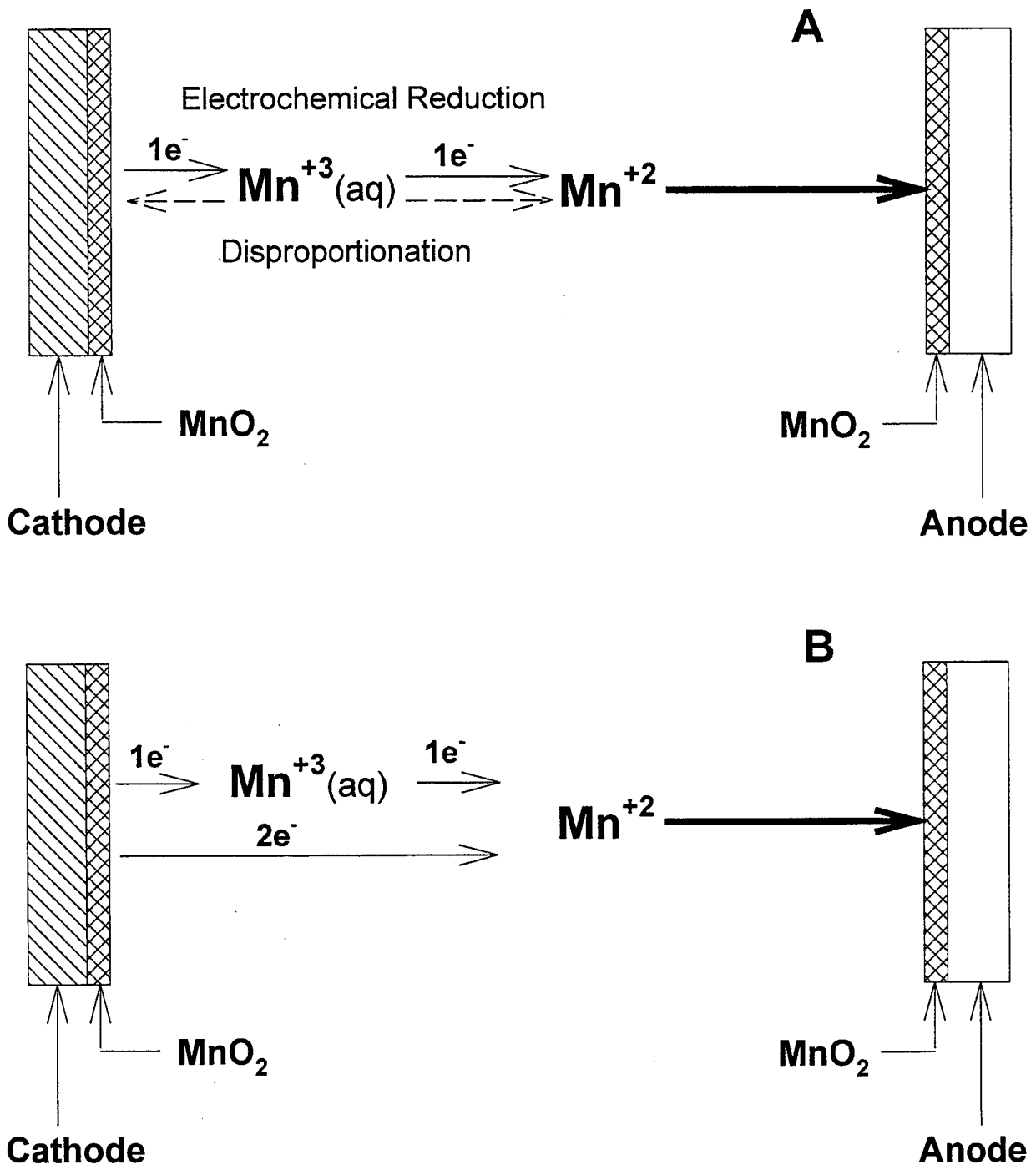


Figure 7. Reactions to form $MnO_2$ (or MnOOH) on the anode in deaerated solutions:
A) with disproportionation, $MnO_2$ on the cathode is reformed.
B) without disproportionation, $MnO_2$ on the cathode becomes depleted.

short term basis (one hour) and a longer term basis (four days). As was shown in Table 3, there was a small decrease in current density and charge transferred between the first and second polarization runs on both days 1 and 4. During the interval between days 1 and 4, however, the biofilm recovered nearly all its capacity to supply current in response to polarization. In fact, if one looks at all the polarization curves together (Figure 5) there were no statistically significant differences between them. This is in contrast to the behavior of coupons with chemically produced $MnO_2$ coatings under air- and nitrogen-saturated conditions (Figures 2 and 3). In these cases there were statistically significant decreases in current capacity between the first and second polarization runs even with the abiotic manganese recycling mechanisms outlined above. Only under oxygen saturated conditions (Figure 4) were the differences between the first and second runs comparable to those for coupons with natural biofilms. Looking at the values of current density from Tables 1 and 3, one can see that the currents supplied by the $MnO_2$ coated coupons under air-saturation (0.5 $mA/cm^2$) were similar to those for coupons with natural biofilms (0.3 $mA/cm^2$). $MnO_2$ coated coupons under nitrogen-saturation produced less current (0.1 $mA/cm^2$) than coupons with natural biofilms, while $MnO_2$ coated coupons under oxygen-saturation produced more (1.2 $mA/cm^2$). For comparison, the long-term galvanic couples having anodes of aluminum or carbon steel and cathodes of stainless steel with biofilms drew an average current density at the cathode of 0.02 $mA/cm^2$ (0.004 $mA/cm^2$ control with no biofilm) for periods of 2 to 3 months.

While this work produced no direct evidence of a link between bacterial metabolism and increased current capacity, the rapid recovery of the current capacity on biofilm-coated coupons after polarization suggests that there is one. The data have shown that chemical reoxidation can certainly provide some of the increase in current observed for natural biofilms. The chemical system accomplished this by a combination of direct reoxidation of $Mn^{+2}$ by oxygen in the presence of $MnO_2$ and disproportionation of $Mn^{+3}$ to keep the $MnO_2$ from becoming depleted. In the abiotic system, however, chemical reoxidation could only produce rapid enough results to match those of the natural biofilms under oxygen-saturated conditions, which do not exist in natural marine systems. On the contrary, the dissolved oxygen near the metal surface within natural biofilms has generally been found to be low. Specifically, Xu (2000) found that the dissolved oxygen at locations where manganese was found tended to be around 10 μM, which is similar to the oxygen concentration of the nitrogen-saturated solutions in the present work. Thus the rapid regeneration of current capacity for natural biofilms, as shown in Table 3, requires more than just the chemical reoxidation and disproportionation mechanism presented here.

Natural biofilm systems have several advantages over the chemical system used in the present work for manganese cycling. First, the polymer matrix of a natural biofilm will tend to keep Mn from escaping into the bulk solution as it did in our chemical tests. Moreover, it has recently been demonstrated (Mandernack, et al., 1995) that certain strains of a marine Bacillus were capable of rapid oxidation of $Mn^{+2}$ directly to $Mn^{+4}$. Natural biofilm systems would, thus, have the capability of combining the chemical mechanisms for manganese recycling shown in this work with direct biologically mediated reoxidation. Redox cycles of other chemical species such as iron and nitrogen could also contribute to the total cathodic current in many natural biofilm systems. These latter reactions might predominate in a given

aquatic system in which manganese was low or absent. Additional research will be needed to determine the proportions of current carried by each reaction when all three are present.

Unfortunately, a direct comparison of the currents due to Mn cycling in this work with those observed earlier for galvanic corrosion was not possible due to the much longer time frame of the galvanic corrosion tests. Thus, a quantitative determination of the proportion of galvanic current that was carried by $MnO_2$ recycling could not be made from the data presented. The data in Tables 1 and 3, however, showed that the short-term current density for the $MnO_2$ coated coupons under air saturated conditions was similar to that for the coupons with natural biofilms. Therefore, the present data are consistent with the idea that $MnO_2$ recycling (perhaps augmented by iron and nitrogen cycling) within natural biofilms is sufficient to account for both ennoblement of the OCP of passive metals and alloys and the observed long-term galvanic corrosion rates. If Mn is absent in a given environment, previous works by many authors have shown alternate mechanisms by which the OCP may be ennobled. No one has yet proposed, however, an alternate mechanism by which the galvanic current can be elevated over a sustained period of time. Further work will be required to determine if iron and nitrogen cycling, which are certainly important processes in salt marsh sediments, can sustain a substantial proportion of the galvanic current observed in the presence of biofilms.

### V.C.3. Conclusions

The data presented demonstrate that $MnO_2$ adsorbed on the surface of passive metal coupons was capable of increasing both the OCP of the coupon and the current that can be drawn from it, even in the absence of biofilms. While it is reasonable to expect that bacteria in biofilms are capable of cycling Mn, the $MnO_2$ data indicate that there are also abiotic mechanisms. The increase in current capacity from $MnO_2$ was greater with higher concentrations of dissolved oxygen in the electrolyte. The observed effect of $MnO_2$ on current density was greater than could be accounted for by reduction of all the $MnO_2$ deposited. Comparison of the total charge passed upon a 10-minute polarization with the amount of $MnO_2$ deposited indicated that each $Mn^{+2}$ ion was being abiotically recycled 2 to 5 times during the polarization process. Under abiotic conditions, disproportionation of a soluble $Mn^{+3}$ intermediate to $MnO_2$ and $Mn^{+2}$, could account for the increased current density in anoxic solutions. Re-oxidation of $Mn^{+2}$ by oxygen accounted for the increased current density in oxic solutions.

The current supplied by abiotic $MnO_2$ coated coupons under air-saturated conditions was similar to that provided by coupons with natural biofilms. However, the rapid regeneration of current capacity demonstrated by natural biofilms could only be matched by the abiotic system under oxygen-saturated conditions. This requires more than just the chemical mechanisms presented here, and it is reasonable to conclude that this would involve biological reoxidation. Direct comparison of the currents due to Mn cycling in this work with those observed earlier for galvanic corrosion was not possible due to the much longer time frame of the galvanic corrosion tests. Nevertheless, the present data are consistent with the idea that $MnO_2$ recycling (perhaps augmented by iron and nitrogen cycling) within natural biofilms is sufficient to account for the observed long-term galvanic corrosion rates.

## References Cited


Chandrasekaran, P. and S.C. Dexter, 1994, "Bacterial Metabolism in Biofilm Consortia: Consequences for Potential Ennoblement,"Corrosion/94, Paper No. 276 (Houston, TXL NACE).

Chandrasekaran, P. (1995) Mechanism of Potential Ennoblement on Passive Metals Due to Biofilms in Seawater. Doctoral dissertation, University of Delaware.

Dexter, S.C. and J.P. LaFontaine, 1998, "Effect of Natural Marine Biofilms on Galvanic Corrosion Predicted Using Potentiodynamic Polarization Curves, CORROSION/98 Paper No. 288, NACE, International, Houston, TX.

Dexter, S. C. and J. P. LaFontaine (1998b) Effect of natural marine biofilms on galvanic corrosion. *Corrosion*, **54**, 11: 851-861.

Dickinson, W.H., Z. Lewandowski, Biofouling 10, 1-3(1996): p. 79.

Dickinson, W. H. and Z. Lewandowski (1996) Manganese biofouling and the corrosion behavior of stainless steel. *Biofouling*, **10**: 79-93.

Dickinson, W. H., F. Caccavo and Z. Lewandowski (1996) The ennoblement of stainless steel by manganic oxide biofouling. *Corrosion Science*, **38**, 8: 1407-1422.

Ghiorse, W. C. (1984) Biology of iron and manganese depositing bacteria. *Ann Rev Microbiol.* **38**: 515-550.

Kostka J. E., G. W. Luther, III and K. H. Nealson (1995) Chemical and biological reduction of Mn(III)-pyrophosphate complexes—potential importance of dissolved Mn(III) as an environmental oxidant. *Geochim. Cosmochim. Acta.* **59**: 885-894.

Lewandowski, Z., P. Stoodley, F. Roe, "Internal mass transport in heterogeneous biofilms," CORROSION/95, paper no. 222, (Houston, TX: NACE International, 1995).

Linhardt, P. (1996) Failure of chromium-nickel steel in a hydroelectric power plant by manganese-oxidizing bacteria. In: Heitz *et al.* (Eds.), *Microbially Influenced Corrosion of Materials*. Springer-Verlag Berlin Heidelberg.

Luther, G. W., D. T. Ruppel and C. Burkhard (1999) Reactivity of Dissolved Mn(III) Complexes and Mn(IV) Species with Reductants: Mn Redox Chemistry Without a Dissolution Step? In Sparks, D. L. and T. J. Grundl (Eds.) *Minera-Water Interfacial Reactions: Kinetics and Mechanisms*. ACS Symposium Series 715, American Chemical Society. Washington D. C. pp. 265-280.

Mandernack, K. W., J. Post and B. M. Tebo (1995) Manganese Mineral Formation by Bacterial Spores of the Marine *Bacillus*, strain SG-1: Evidence for the Direct Oxidation of Mn(II) to Mn(IV). Geochimica et Cosmochimica Acta, 59, No. 21, pp. 4393 to 4408.

Montgomery, C. W. (1992) *Environmental Geology*. Third edition, Wm. C. Brown Publishers. Dubuque, IA.

Nealson, K. H. and D. Saffarini (1994) Iron and manganese in anaerobic respiration: Environmental significance, physiology and regulation. *Ann Rev Microbiol.* **48**: 311-343.

Nealson, K., B. Tebo and R. Rosson (1988) Occurrence and mechanisms of microbial oxidation of manganese. *Advances in Applied Microbiology.* **33**: 279-318.

Olesen, B.H., R. Avci and Z. Lewandowski (2000) Manganese Dioxide as a Potential Cathodic Reactant in Corrosion of Stainless Steels, Corrosion Science, 42, 2000, p. 211-227.

Pourbaix, M. (1974) *Atlas of Electrochemical Equilibria in Aqueous Solutions*. NACE, International, Houston, TX. pp. 97-105, 286-292.

Stumm W. and J. J. Morgan (1981) *Aquatic Chemistry*, 2nd ed. John Wiley & Sons, New York, NY. pp. 465-468.

Tebo, B. (1991) Manganese(II) oxidation in the suboxic zone of the Black Sea. *Deep Sea Res.* **38**: S883-S905, suppl. 2.

Xu, K., S. C. Dexter and G. W. Luther (1998) Voltammetric microelectrodes for biocorrosion studies. *Corrosion*, **54**, 10: 814-823.

Xu, K. Ph.D. Dissertation, University of Delaware, June, 2000.

Zhang, H-J and S. C. Dexter, 1995, "Effect of Biofilms on Crevice Corrosion of Stainless Steels in Coastal Seawater," Corrosion, Vol. 51, No. 1, 1995, pp. 56-66.

## V.E. Development of Biofilm Community Structure

In seawater environments, a mature biofilm is composed of microorganisms, the by-products of their metabolism, trapped detrital materials and corrosion products. Traditionally, it had been believed that aerobic heterotrophic bacteria colonize the outer portion of the biofilm, consuming oxygen and producing metabolites, whereas obligate anaerobic heterotrophic bacteria and sulfate-reducing bacteria reside in the depths of the film (Jorgenson et al., 1986; Parkes, 1987; Gaylarde and Videla, 1987). Aerobic and anaerobic microorganisms were seen as having complementary metabolic pathways forming a synergistic community on an immersed metal surface. Many investigators have delineated such a biofilm structure as a homogeneous, multi-layered film (Hamilton and Maxwell, 1986; Costerton and Geesey, 1986). Under this old concept, the electrochemical condition of a metal surface with a mature biofilm was dominated by the metabolic activity of sulfate-reducing bacteria.

With the use of CSLM, our current concept of biofilm structure has changed in recent years. The new understanding of biofilm structure depicts large physical heterogeneities starting with a thin base layer of organisms embedded in extracellular polymeric substances (EPS). Depending on the velocity of fluid flow, that base layer may be anywhere from 10 to 100 μm in thickness, and it may cover from less then 20% to more than 90% of the metal surface. On top of the base film is a columnar, or cauliflower-like structure extending out into the bulk fluid. Between and around columnar entities is a network of microchannels through which water may flow (Lewandowski et al., 1995). In the current study, it was found that biofilms developed in Delaware Bay seawater conformed to the above heterogeneous model. Microbial populations and chemical concentrations were non-uniformly distributed within a biofilm. The physical thickness of 4 month old biofilms was in the range of 20 to 130 μm. Microscopic observations indicated that a biofilm might contain diverse microbial populations including coccoidal, rod-shaped, chain-forming and filamentous microorganisms.

In the present work biofilms were grown on Nitronic 50 metal surfaces in natural seawater for periods of 3, 7, 14, 28, and 42 days. These biofilms were fixed with paraformaldehyde and stained with Syto 13 before imaging. As shown in Figure V.E.1, the first pioneering settlers were coccoidal and short rod-shaped microorganisms. Within one week of immersion, few microorganisms of other shapes were observed. This observation was based on more than twenty images obtained under the confocal microscope. This might be due to the fact that the majority of microorganisms in seawater are coccoidal and rod-shaped bacteria. Filamentous microorganisms generally occurred in a later stage. This is in agreement with the observation by Marszalek et al. (1979), who suggested that the progressive microbial attachment starts with coccoidal and rod-shaped bacteria, followed by stalked bacteria and then filamentous microorganisms.

Another observable fact of biofilm development was that the density of bacteria colonizing a surface increased with time. Figure V.E.2 shows the result of cell enumerations conducted using epifluorescent microscopy. The number of microorganisms on a 3 day old biofilm was at the level of 2 x 105 cells/cm2. By 2 weeks, their number increased to about 12 x 105 cells/cm2. By four weeks, the bacterial counts reached 20 x 105 cells/cm2. These data were the average of bacterial counts in 15 fields. Under the epifluorescent microscope, each field

was chosen to include at least 20 bacteria but avoid the areas of microbial colonies. Bacterial counts at microcolonies were generally much higher than those at locations without colonies. Thus, the bacterial counts represented background numbers. They were very accurate for young biofilms (less than 2 weeks) but somewhat underestimated the bacterial densities for old biofilms, where many microcolonies had formed

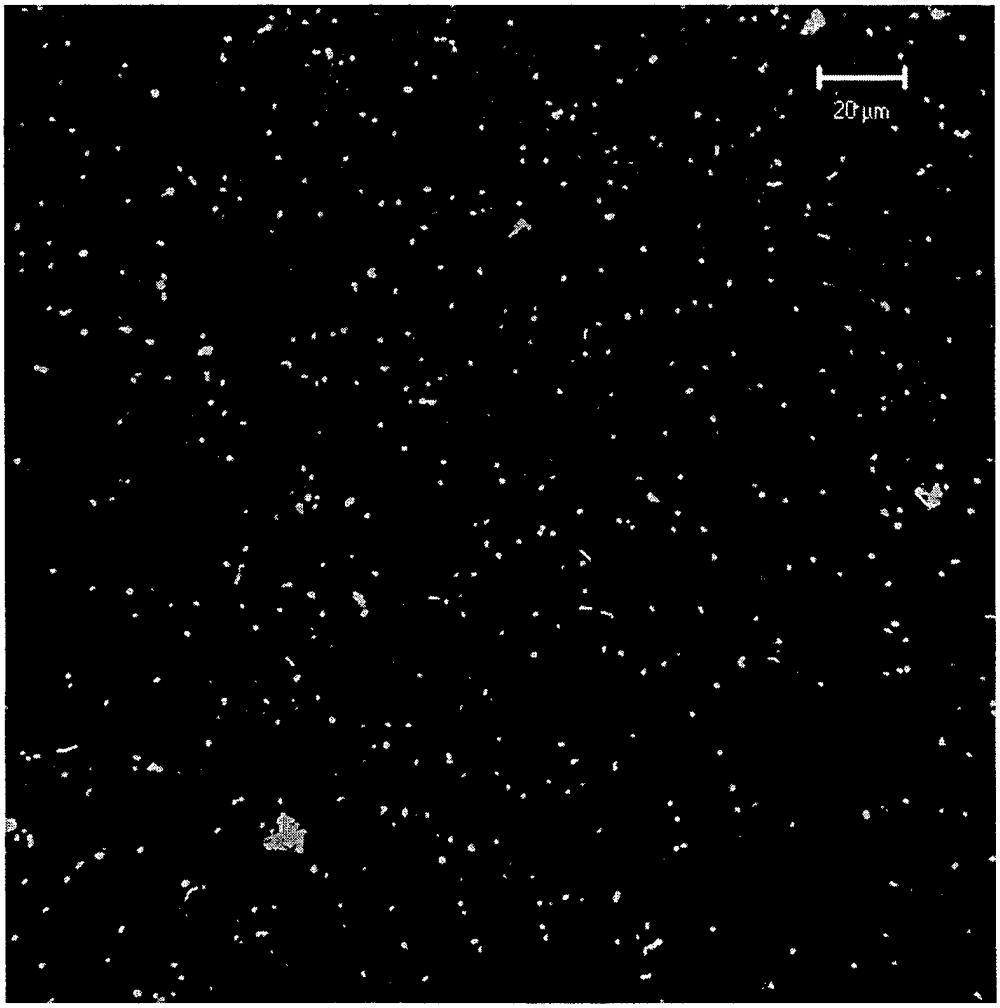


Figure V.E.1. Random settlement of microbial cells on Nitronic 50 alloy immersed in natural seawater for 7 days.

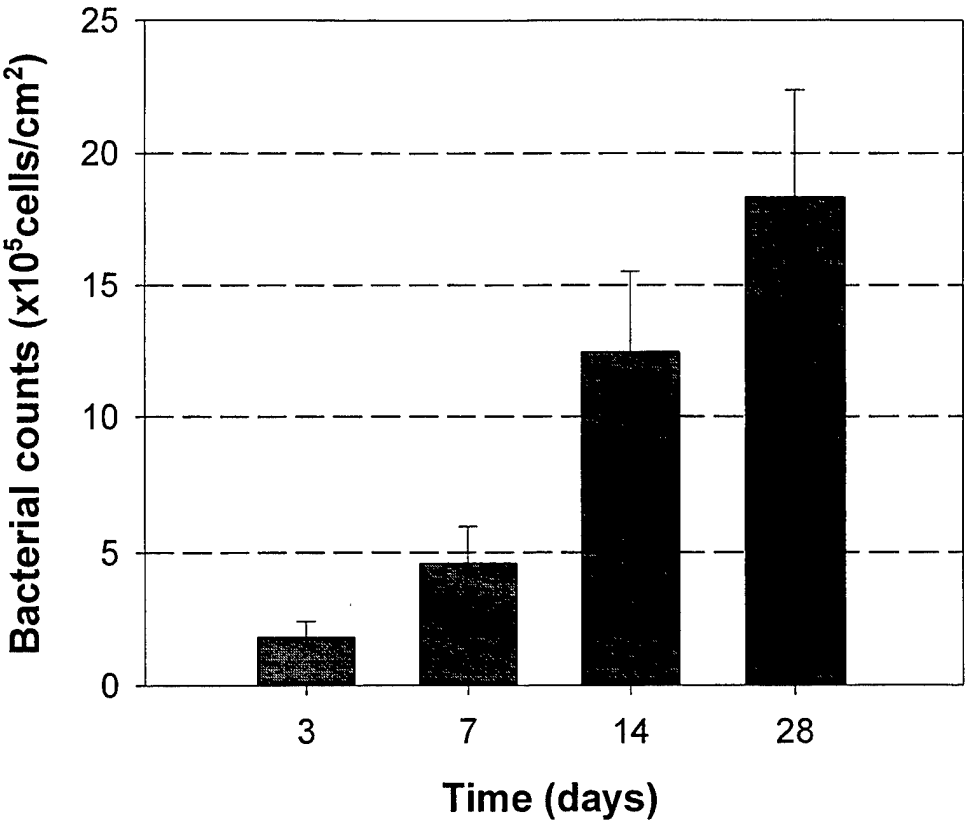


Figure V.E.2. The number of microorganisms settling on Nitronic 50 metal surfaces immersed in natural seawater as counted under an epifluorescent microscope.

The microbial settlement pattern on a metal surface showed significant change after 2 weeks of exposure. Besides random attachment, microorganisms that settled on the metal surface at an early stage started to grow. They proliferated till they formed a cell cluster. The importance of discrete multiplication overtook that of random settlement in a mature biofilm.

As shown in Figures V.E.3 and V.E.4, many microbial cells colonized a metal surface forming a discrete microcolony. This suggests that they were the result of microbial growth and division rather than random attachment of individual cells from the bulk seawater. These two figures show similar patterns in microbial morphology. There are several coccoidal microcolonies, in which each cell has a size of about 1.1 μm in diameter. The cocci juxtapose so orderly that they were apparently resulting from cellular divisions in situ. All cells in such homologous aggregates look more or less identical in appearance. For each cell,

the staining agent (Syto 13) is uniformly spread over the entire cell. There are not organelle features, such as different color or intensity, observed inside the cell. This is characteristic of prokaryotic microorganisms because prokaryotes do not possess a true nucleus, and the nuclear material (DNA) in these microorganisms is scattered all over the cell. Also shown in the figures are filamentous microorganisms, chain-forming microorganisms and other smaller cocci.

Figure V.E.5 shows some rod-shaped bacteria (bacilli) along with some cocci. The bacilli have a size of about 1 μm x 5 μm. They belong to large bacteria category according to *The Prokaryotes* handbook (Starr and Schmidt, 1981). The majority of the commonly encountered bacteria measure about 0.5 by 3 μm for the rod form. However, bacteria may show great variation in size depending on growth and nutrient conditions. Alternatively, it is also possible that several smaller cells are encapsulated within one rod, but this is not clear from the picture.

Figures V.E.6 and V.E.7 show filamentous microcolonies along with some cocci within the biofilm. It is known that bacterial shape depends to a certain extent upon physiological state and environmental factors such as temperature, age, and nutrients (Characklis et al., 1990). Brock (1966) hypothesized that rod-shaped and filamentous organisms increased efficiency of nutrient uptake since most bacteria found in lakes and oceans, where the concentration of organic material is low, are filamentous or rod-shaped. It is also known that many metal-oxidizing bacteria, such as Gallionella sp. Leptothrix sp. and Sphaerotilus sp., are filamentous (Lutey, 1992).

Figure V.E.8 shows two coccoidal colonies with some filamentous microorganisms in a 42 day biofilm. The area of the microcolony at left lower corner is about 20 μm in diameter and the microbial colony is composed of about 200 cocci. Another microcolonies at the left center is composed of more than 100 cells. There are also some relatively large cocci shown in the picture. Figure V.E.9 shows some combinations of coccoidal and filamentous microorganisms. In general, the distribution of microorganisms within the biofilms is not uniform. Discrete microcolonies were the most significant phenomenon found in a mature biofilm.

It is hard to identify the species of the bacteria just based on the shape and morphology. However, it is commonly believed that heterotrophic bacteria are the most important types found in marine biofilms (Characklis, et al.,1990). Unlike photosynthetic bacteria, which utilize sunlight as a source of energy, heterotrophs require reduced organic compounds as their energy source. Since our biofilms were grown at Shellfish laboratory in the dark, it is reasonable to expect that the majority of the microorganisms are heterotrophic bacteria.

To further capture the discrete multiplication pattern, microbial counts were also conducted using epifluorescent microscopy. Figures V.E.10 and V.E.11 show typical microbial distribution data found within biofilms. The observations on biofilms indicated that the distribution of microbial cells at a metal surface in a 7 day biofilm was mostly random and uniform, whereas the distribution of a one month old biofilm was highly heterogeneous. Thus, microbial multiplication was an important factor leading to the heterogeneity of a biofilm.

## References Cited


Brock, T. D. 1966. *Principles of Microbial Ecology*, Prentice-Hall, Englewood Cliff, NJ, pp. 1-300.

Characklis, W. G., K. C. Marshall, and G. A. McFeters. 1990. The microbial cell, in *Biofilms*, edited by W. G. Characklis and K. C. Marshall, John wiley & sons, Inc, pp. 131-160.

Costerton, J. W. and G. C. Geesey. 1986. The microbial ecology of surface colonization and of consequent corrosion, in *Biological Induced Corrosion*, NACE-8, edited by S. C. Dexter, pp. 223-232.

Gaylarde, C. C. and H. A. Videla, 1987. *Int. Biodet.*, 23: 91-104.

Hamilton, W. A. and S. Maxwell. 1986. Biological and corrosion activity of SRB in natural biofilms. Proceedings of Biologically Induced Corrosion, NACE International, Houston, TX, pp. 131-136.

Jorgensen, B. B., Y. Cohen, and N. P. Revsbech. 1986. Transition from anoxygenic to oxygenic photosynthesis in a Microcoleus chthonoplastes cyanobacterial mat, Appl. Environ. Microbiol. 51: 408-417.

Lewandowski, Z., P. Stoodley, and F. Roe. 1995. Internal mass transport in heterogeneous biofilms recent advances, CORROSION/95, paper No. 222. NACE International, Houston, TX.

Lutey, R. W. 1992. Identification and detection of microbiologically influenced corrosion. Proc of NSF-CONICET workshop, Biocorrosion & Biofouling, edited by H. A. Videla, Z. Lewandowski, and R. W. Lutey. Nov, 1992, Argentina, pp. 146-158.

Marszalek, D. S., S. M. Gerchakov, and L. R. Udey. 1979. Influence of substrate composition on marine microfouling. *Appl. Environ. Microbiol.* 38: 987-995.

Parkes, R. J. 1987. *Soc. Gen. Microbiol. Symp.*, 41: 147-177.

Starr, M. P. and J. M. Schmidt. 1981. Prokaryote diversity, in *The Prokaryotes*, an handbook on habitats, isolation, and identification of bacteria, edited by M. P. Starr, H. Stolp, H. G. Truper, A. Balows, and H. G. Schlegel, Vol. 1, pp. 1-200.

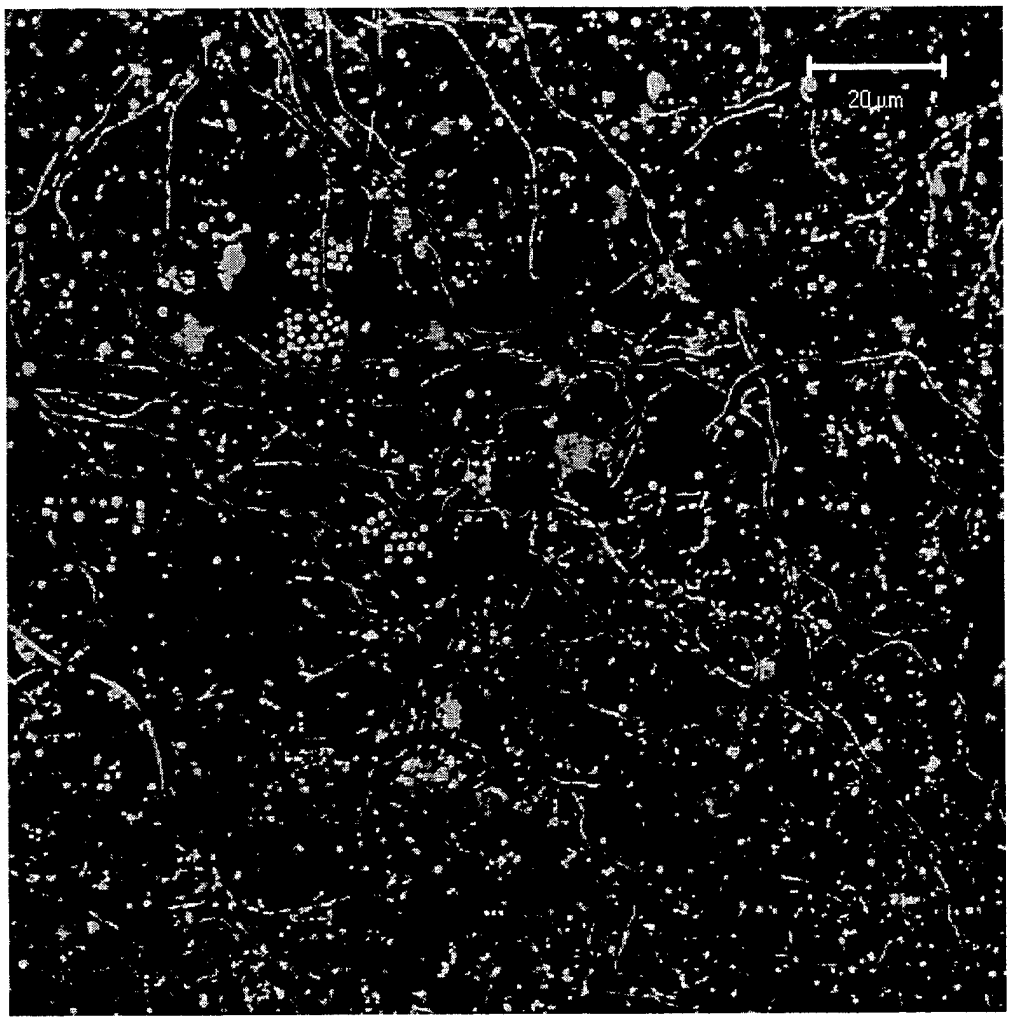


Figure V.E.3. Some coccoidal microbial colonies and filamentous microorganisms observed on a Nitronic 50 metal surface immersed in natural seawater for 28 days.

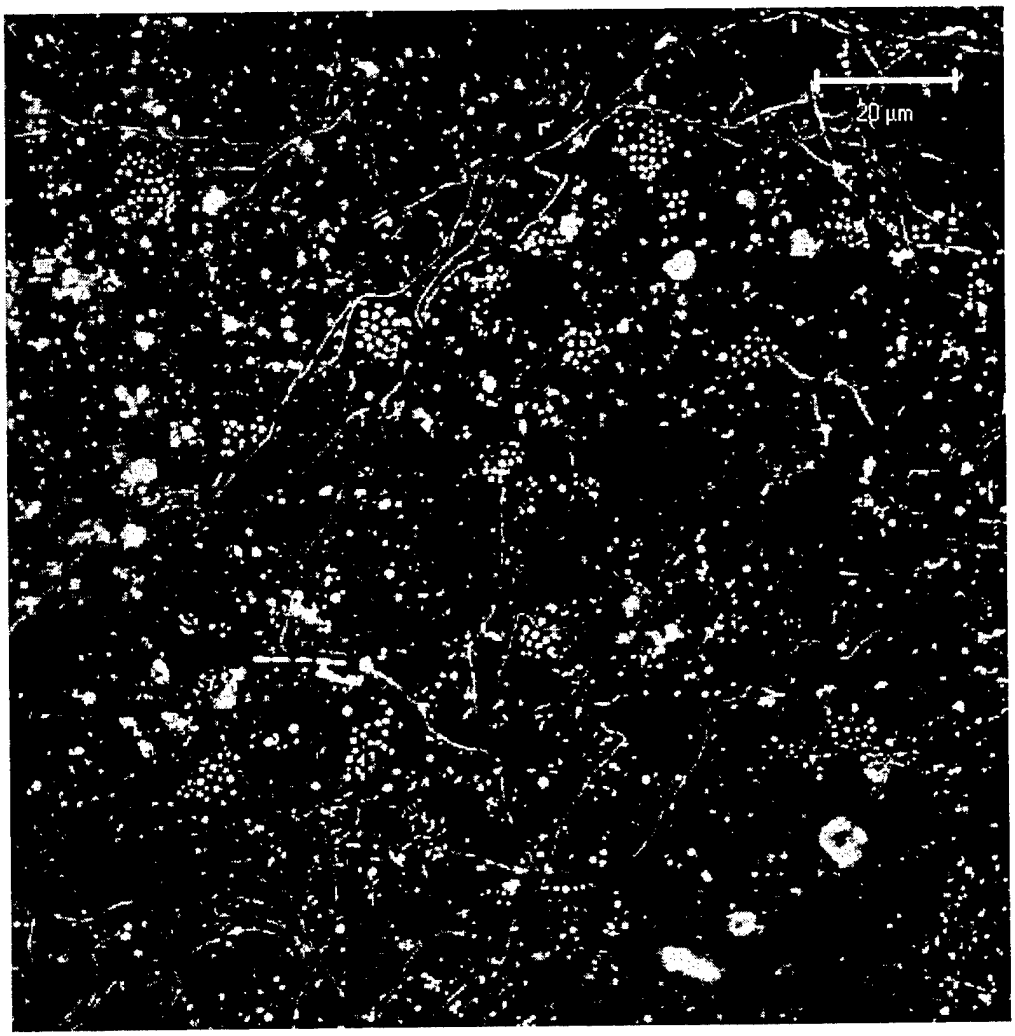


Figure V.E.4. Some coccoidal microbial colonies and filamentous microorganisms observed on a Nitronic 50 metal surface immersed in natural seawater for 28 days.

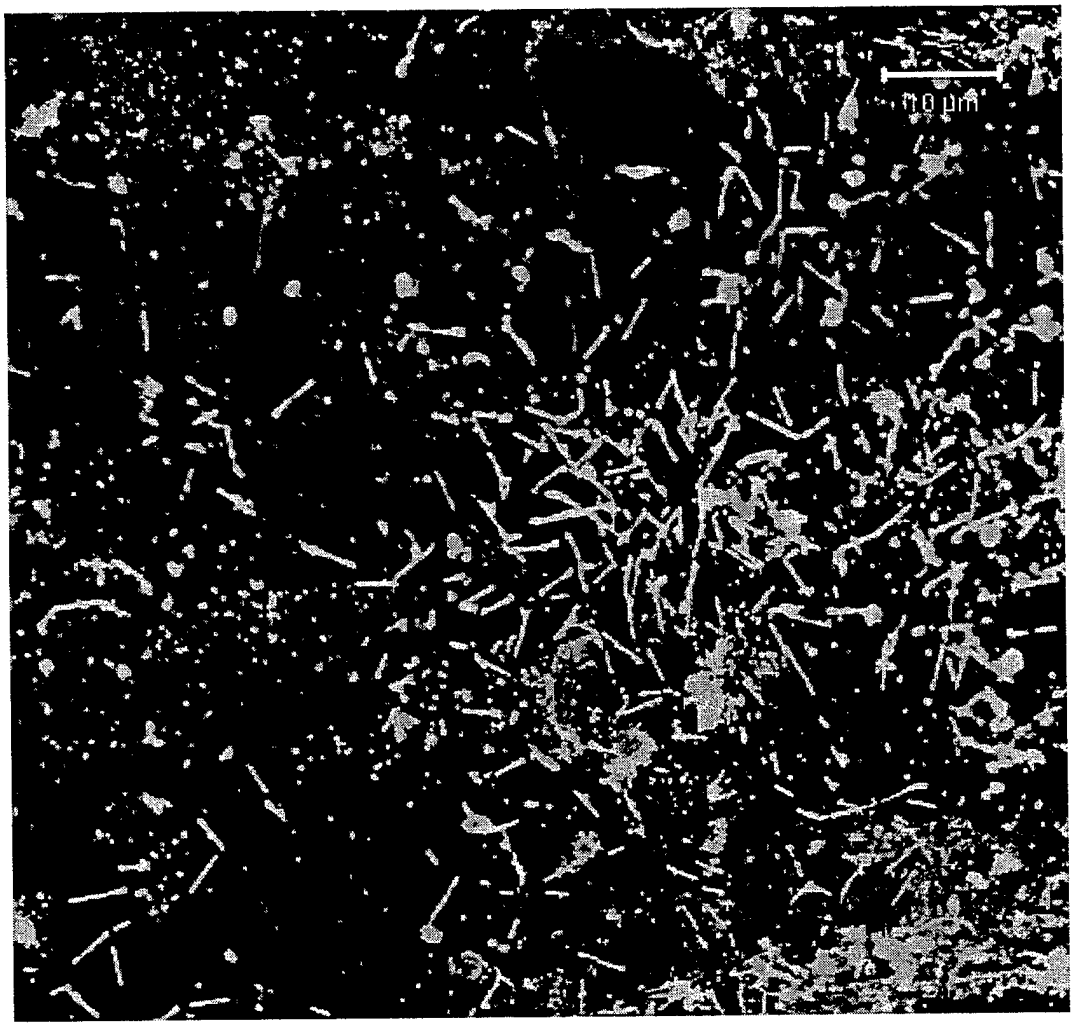


Figure V.E.5. Some rod-shaped microbial colonies observed on a Nitronic 50 metal surface immersed in natural seawater for 28 days.

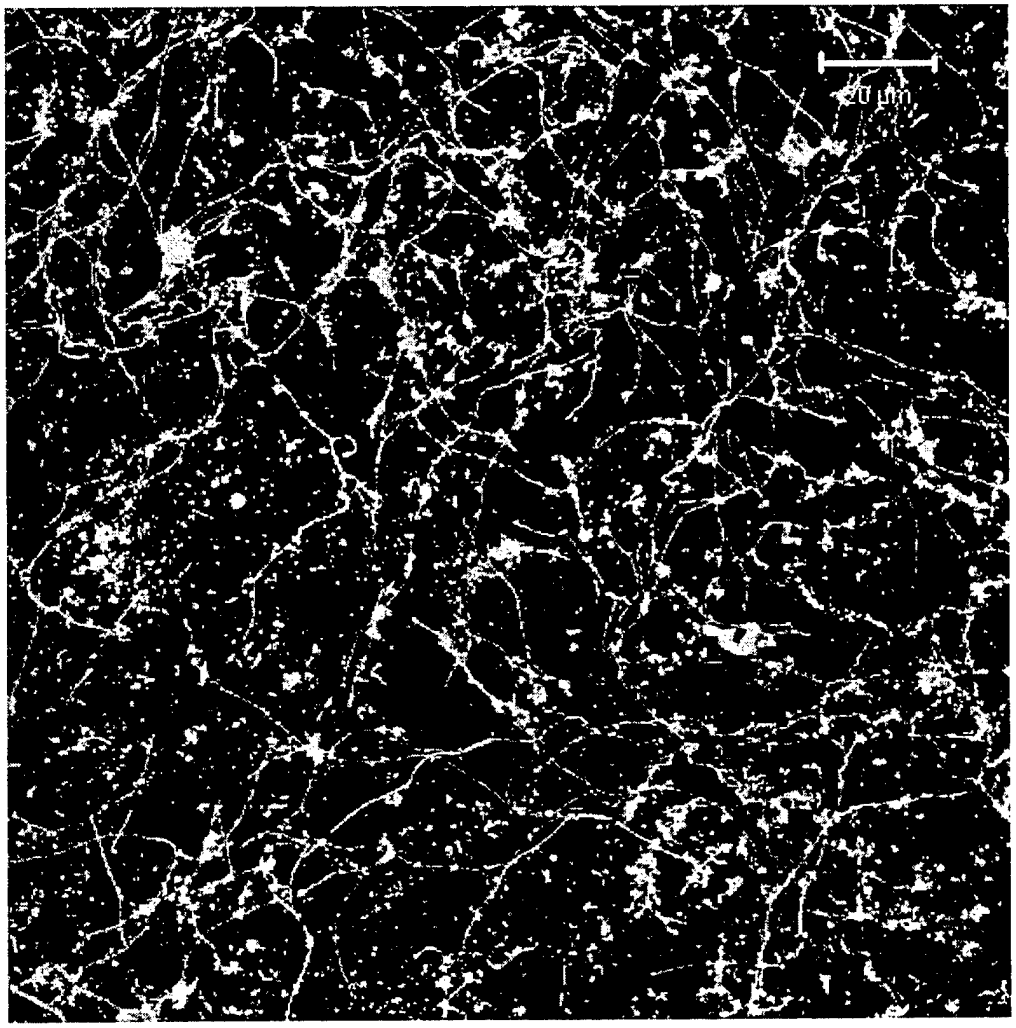


Figure V.E.6. Some filamentous microbial colonies observed on a Nitronic 50 metal surface immersed in natural seawater for 28 days.

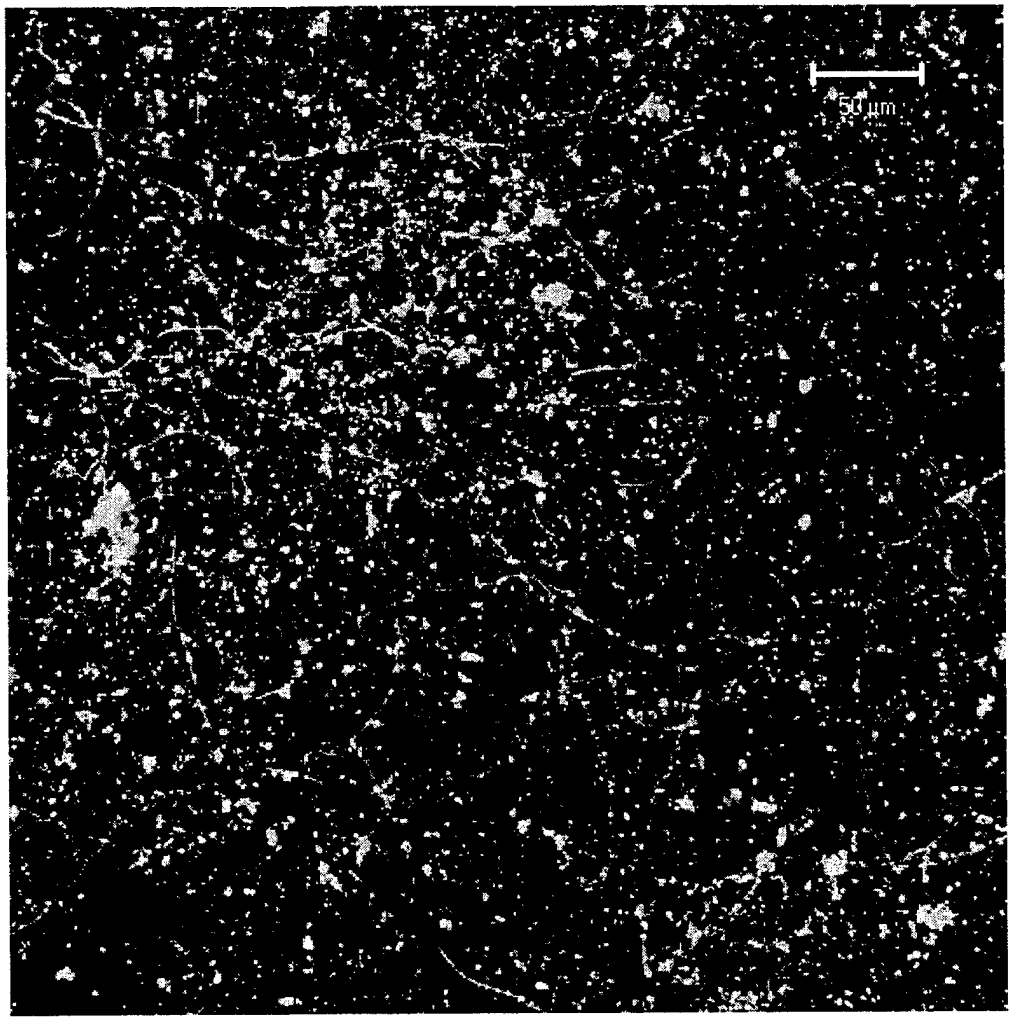


Figure V.E.7. Some filamentous microbial colonies observed on a Nitronic 50 metal surface immersed in natural seawater for 42 days.

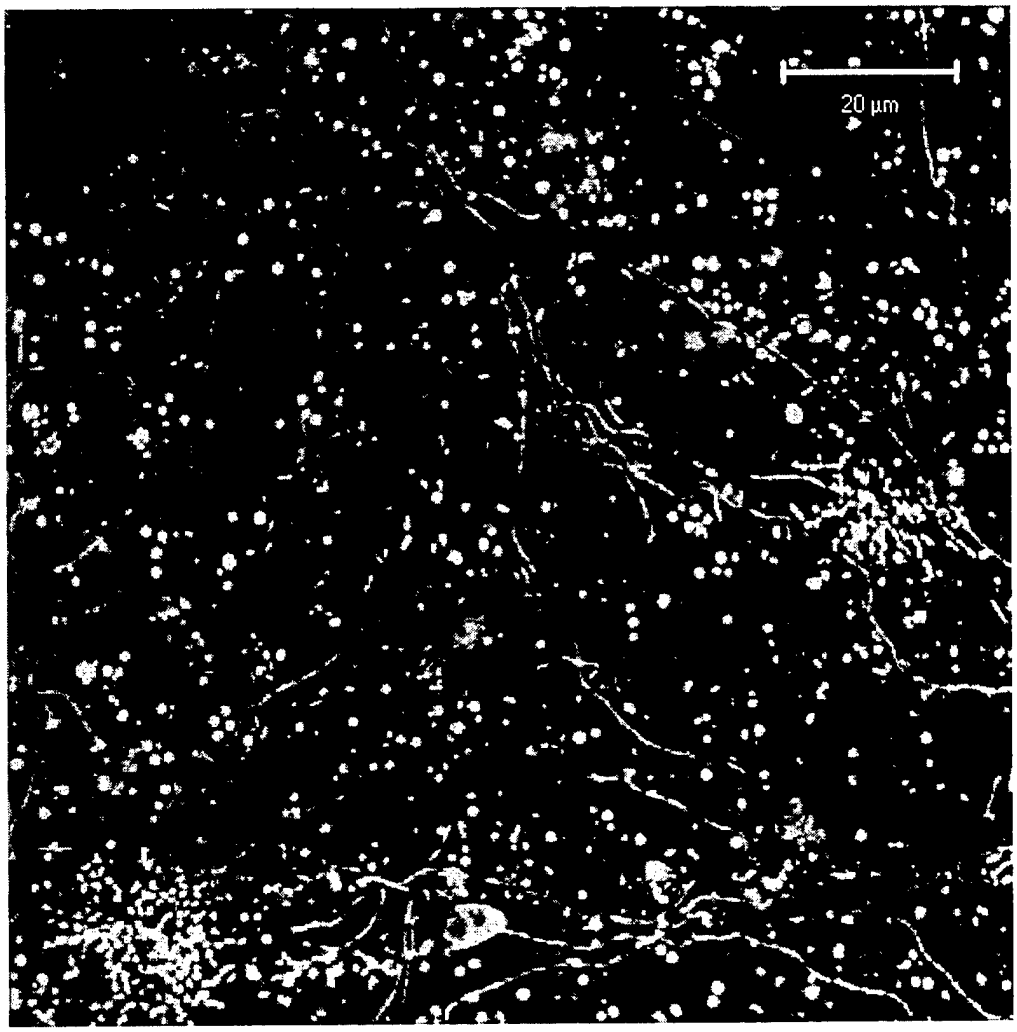


Figure V.E.8. Two microbial colonies and some filamentous microorganisms observed on a Nitronic 50 metal surface immersed in natural seawater for 42 days.

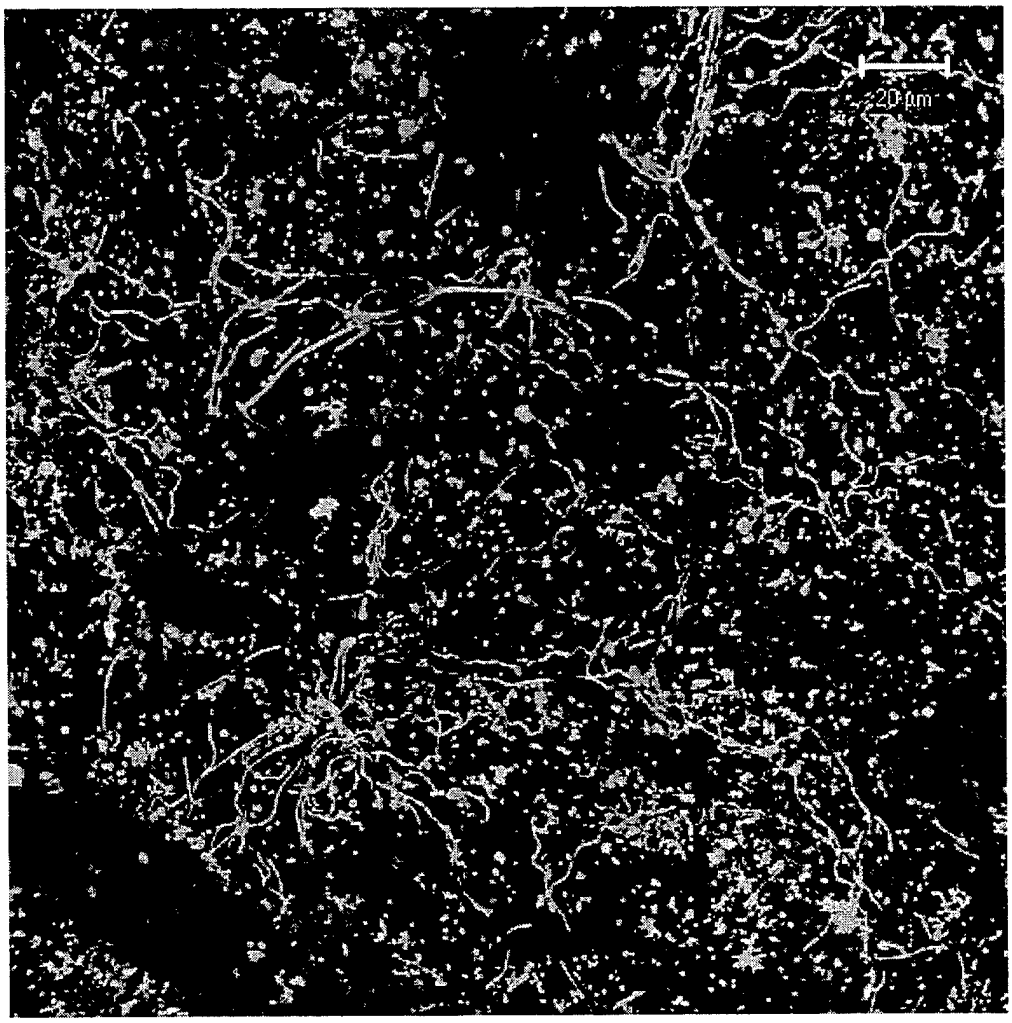


Figure V.E.9. Some filamentous and coccoidal microorganisms observed on a Nitronic 50 metal surface immersed in natural seawater for 42 days.

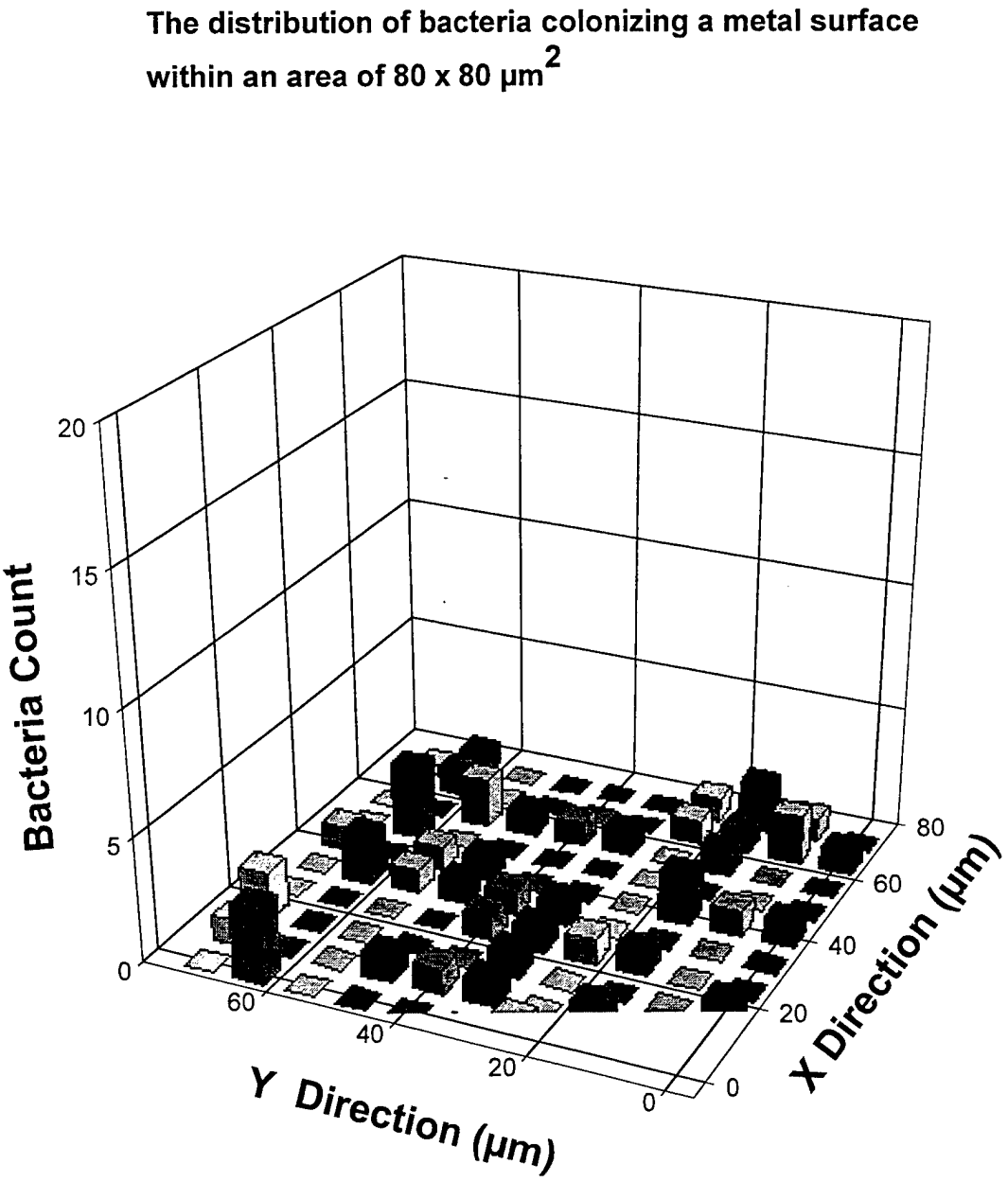


Figure V.E.10. The distribution of microorganisms settling on a Nitronic 50 metal surface immersed in natural seawater for 7 days as counted under an epifluorescent microscope.

**The distribution of bacteria colonizing a metal surface within an area of 80 x 80 $\mu m^2$**

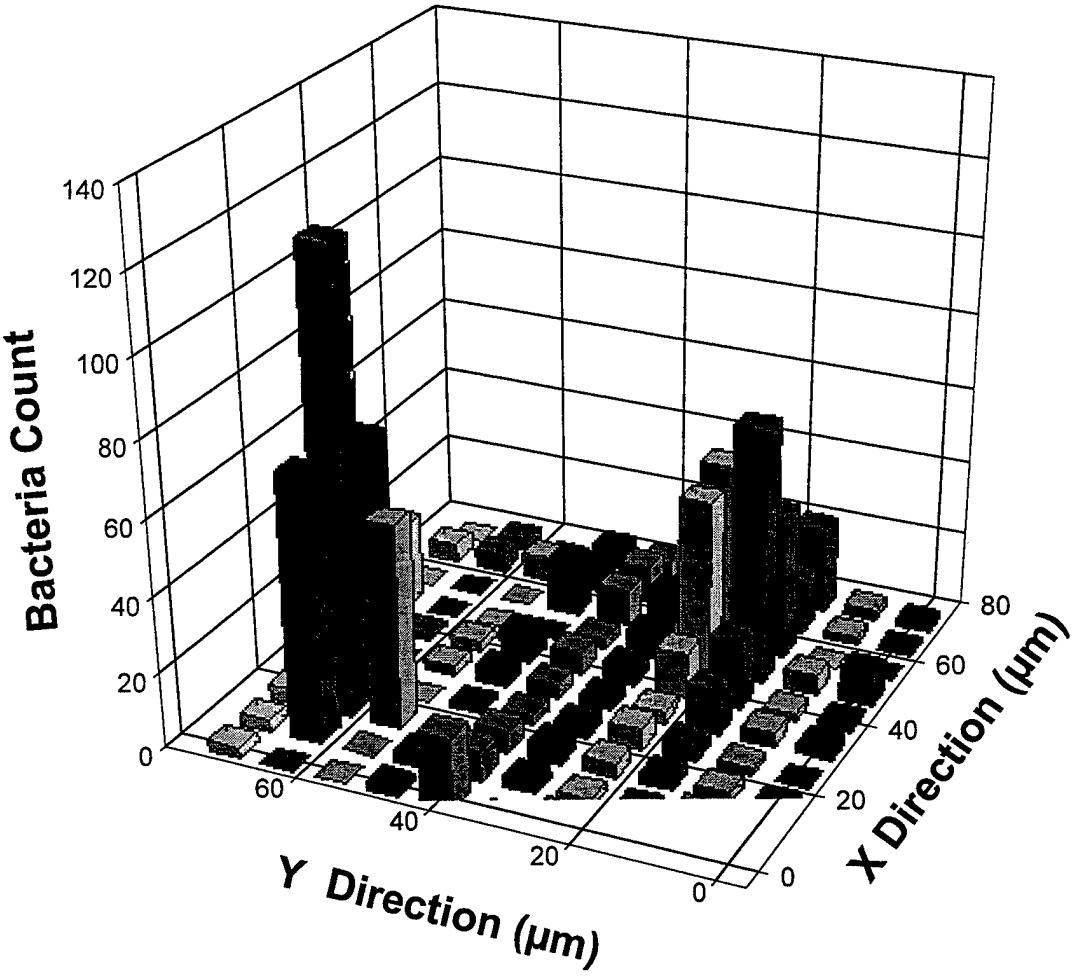


Figure V.E.11. The distribution of microorganisms settling on a Nitronic 50 metal surface immersed in natural seawater for one month as counted under an epifluorescent microscope.

## V.F. Correlation of the Community Structure with Chemical Measurements

Scanning Laser Confocal microscopy was used in conjunction with the voltammetric microelectrodes described in Section IV to establish the physical relationship of microbial microcolonies within the biofilm and chemical concentration profiles through the biofilm thickness. In order to establish this spatial relationship, a Hg-Au microelectrode was used to measure the chemical microprofile at a given location. That location was then recorded as an X-Y coordinate relative to a corner of the metal coupon using a computerized three-dimensional micromanipulator. The coordinates were used to find the same area for confocal imaging as described in Section IV.

The following sections provide data correlating biofilm chemistry obtained with voltammetric microelectrodes and images of microbial community structure obtained with confocal microscopy. Four biofilm samples were tested. The first two biofilm samples were developed on coupons of the Nitronic 50 alloy, which had ennobled open circuit potentials by the end of the exposure. The third biofilm was grown on a Nitronic 33 coupon, on which localized corrosion had initiated by the end of exposure. The fourth biofilm was also grown on Nitronic 50. Three-dimensional images of these biofilms were taken through a series of parallel X-Y scans along the Z axis using confocal microscopy. For each biofilm sample, chemical microprofiles, square wave voltammograms and confocal biofilm images will be presented.

### V.F.1. Biofilm sample one

The first two chemical microprofiles were measured within a biofilm grown on a Nitronic 50 coupon in natural seawater for 3 months. The biofilm showed a light brown color, and the open circuit potential of the coupon was +406 mV SCE. When withdrawn from seawater, some loosely associated biomass sloughed off the surface. The thickness of the biofilm was measured using stereomicroscopy. It ranged from 20 to 120 μm.

As shown in microprofile A in Figure V.F.1, oxygen concentration in seawater was 210 μM. It decreased with increasing depth into the biofilm. At the bottom of the biofilm, oxygen concentration was about 60 μM. No other redox species were detected at this specific location. Figure V.F.2 shows the square wave voltammogram of oxygen generated within the biofilm at this location. Oxygen was reduced to peroxide at –0.28 V, and peroxide was further reduced to water at –1.23 V. There was no net production of peroxide measured within the biofilm at this location. Figure V.F.3 shows the biofilm picture taken at this specific location. The white circle represents the center of the most probable location of microelectrode measurements. The 80% confidence limit is represented by the white square in Figure V.F.3. This means that chemical microprofile A was taken inside the white square with 80% probability. Since the entire picture has a size of 231 μm x 231 μm ($> 6\sigma$), it covers the location of microprofile A with 99% confidence. Figure V.F.3 indicates that there were many coccoidal shaped and some filamentous microorganisms in this part of the biofilm. In some areas, the density of the cocci was relatively high ($> 10^7$ cells/cm$^2$). But no significant microcolony was found at the center of location A.

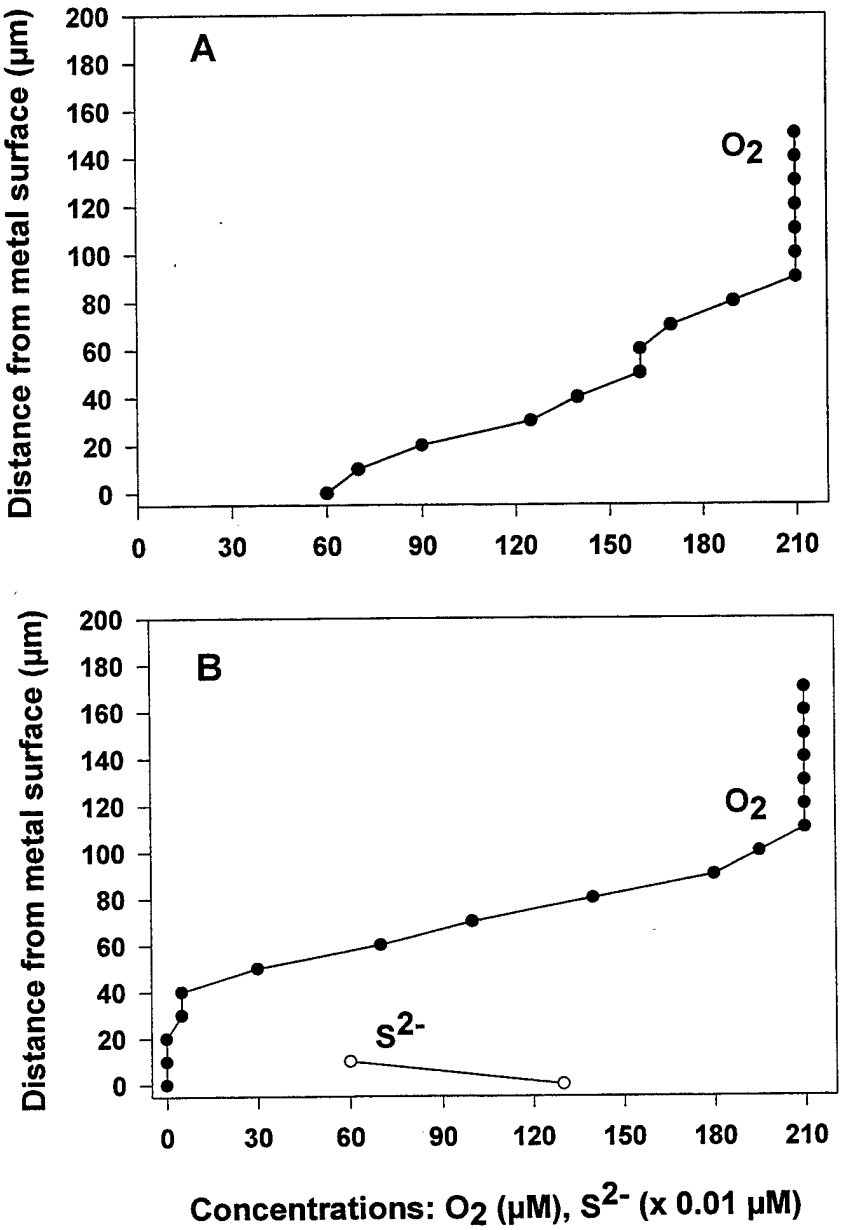


Figure V.F.1. Vertical microprofiles of redox chemical species measured at two different locations (A and B) in a marine biofilm formed on Nitronic 50. Concentrations of chemical species not plotted in profiles were below detection limits. The differences in the microelectrode calibration before and after the measurements were within 5%.

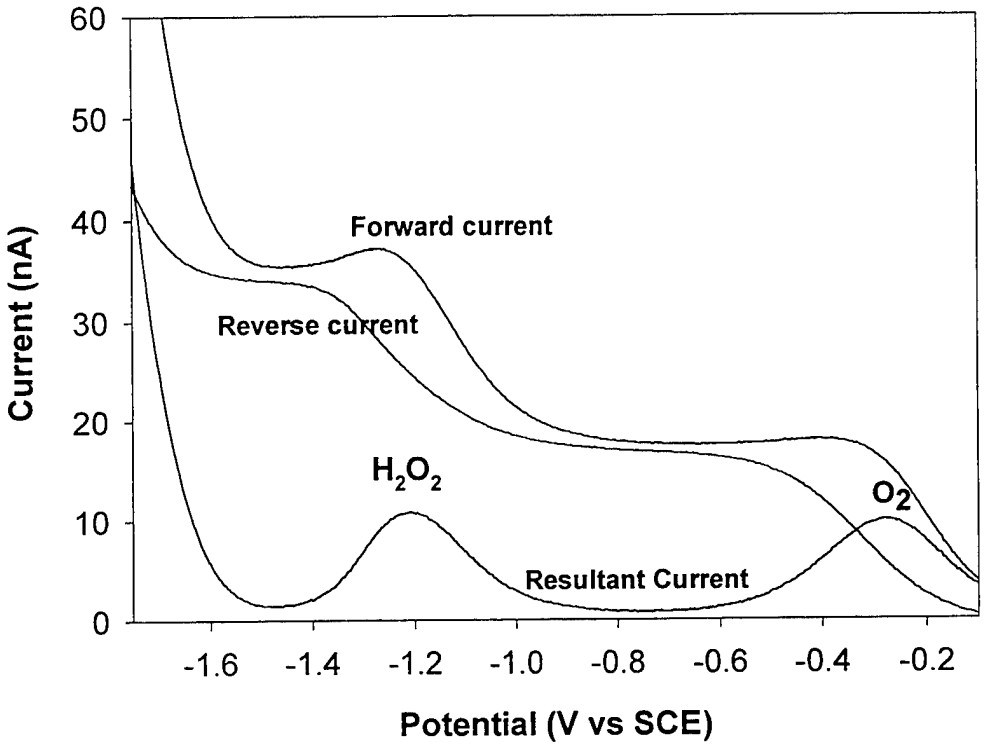


Figure V.F.2. Square wave voltammogram generated with a Hg-Au microelectrode deployed at location A in a marine biofilm. This particular voltammogram was taken at a distance of 80 μm from the metal surface where dissolved oxygen concentration was 190 μM.

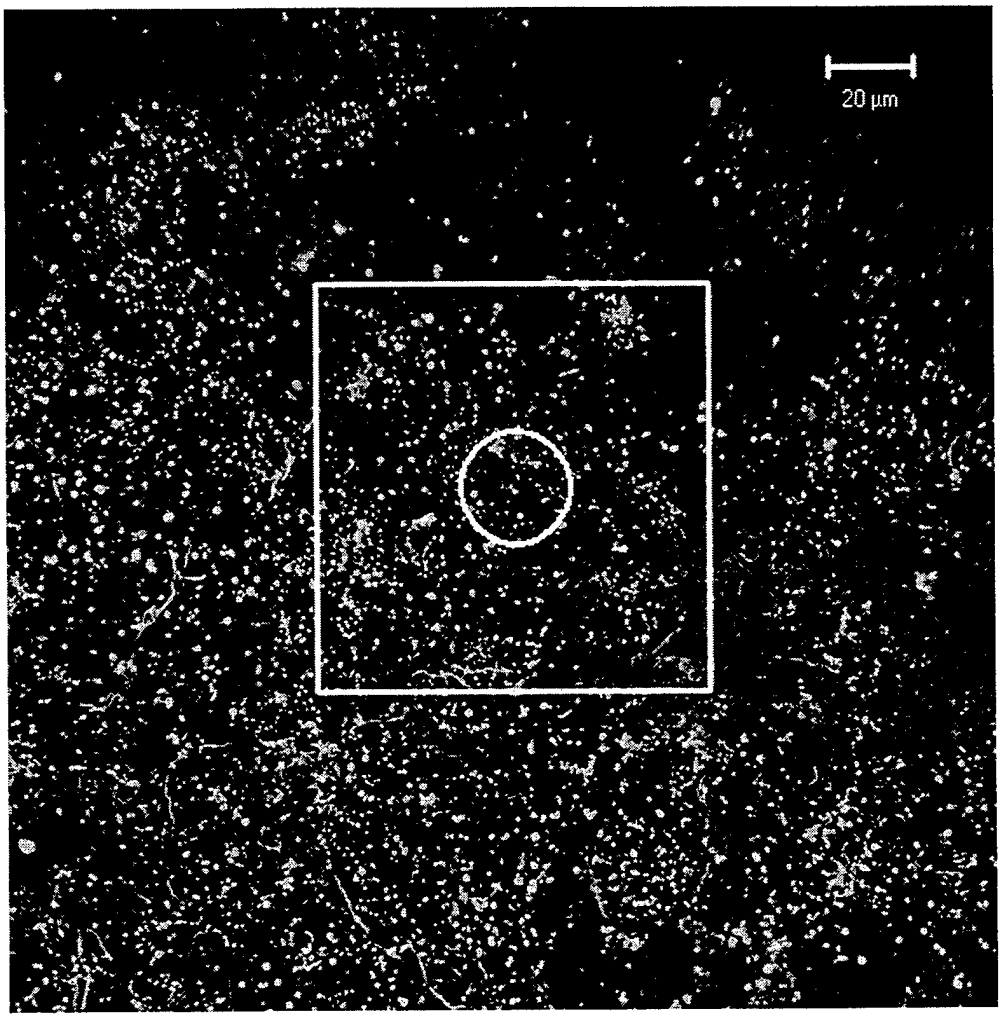


Figure V.F.3. Some coccoidal microbial cells observed at the location of microprofile A. The center of the most probable location coincides with the center of the white circle, which represents a microelectrode tip of 25 µm diameter. The square represents the 80% confident limit, within which microelectrode measurements were carried out. The entire image covers the location of microelectrode measurements with 99% confident limit.

Microprofile B was measured within the same biofilm as microprofile A but at a different location. While the bulk seawater was almost oxygen saturated, the metal surface under the biofilm was totally anoxic. Sulfide was measured at micromolar levels at a depth of 100 μm into the biofilm. Figure V.F.4 shows a square wave voltammogram of sulfide measured at this location. $H_2S$ was released reversibly at the electrode surface at the potential of –0.7 V. The microelectrode was very sensitive in detecting sulfide species. When observed under the confocal microscope (Figure V.F.5) the distribution of microorganisms was heterogeneous. Many densely packed colonies were observed throughout the field of view, and especially near the center of the most probable location (white circle in Figure V.F.5). Since sulfide chemical species were found at this location, this implies that these microorganisms might be sulfate-reducing bacteria (SRB). It is known that some SRB genera have spirilla shape (curved rods) while others such as *Desulfococcus, Desulfobacter,* and *Desulfosarcina* have spherical shapes (Krieg and Holt, 1984). While the shapes of individual organisms are hard to see in Figure V.F.5, the existance of both spirilla and cocci is consistent with the image.

### V.F.2. Biofilm sample two

The second effort in characterizing biofilm chemistry and microbiology was done in December, 1999. The second biofilm sample also was developed on Nitronic 50, this time for a period of nearly 4 months during the fall. By the end of exposure, the biofilm showed brown color, its thickness was in the range of 30 μm to 140 μm, and the open circuit potential of the coupon was +388 mV versus SCE.

Figure V.F.6. shows two chemical microprofiles measured at different locations within the biofilm. Microprofile C shows that oxygen concentration decreased with increasing depth into the biofilm, reaching a constant value of 10 micro-molar for the last 20 micrometers above the metal surface. Where oxygen concentration was below 30 μM, peroxide and dissolved Mn species were found. Figure V.F.7. is a square wave voltammogram indicating the coexistence of dissolved Mn and peroxide under suboxic conditions at the depth of the biofilm. Peroxide and Mn were reduced at the potentials of -1.23 V and -1.52 V, respectively. Microprofile D shows similar trends for oxygen and peroxide, but there was no dissolved Mn at that location. Figure V.F.7. shows a clear peroxide peak at a potential of -1.23 V with a very low oxygen peak at –0.3 V. The peroxide peak is even more pronounced in Figure V.F.8. By comparing these peroxide and oxygen peaks with standard square wave voltammograms generated in seawater, net peroxide concentration was calculated at the level of 50 μM. Peroxide might have been produced by marine diatoms.

In Figures V.F.7 and V.F.8, the broad current peak extending from –0.2 V to –0.6 V could be due to the presence of Fe(III) colloids in addition to oxygen. It is known that aged ferric colloids have such a characteristic peak in that potential range (Taillefert et al., 2000). Thus, microprofiles C and D may give an overestimate of the oxygen concentration if one assumes that the peaks at –0.3 V were produced by oxygen reduction only.

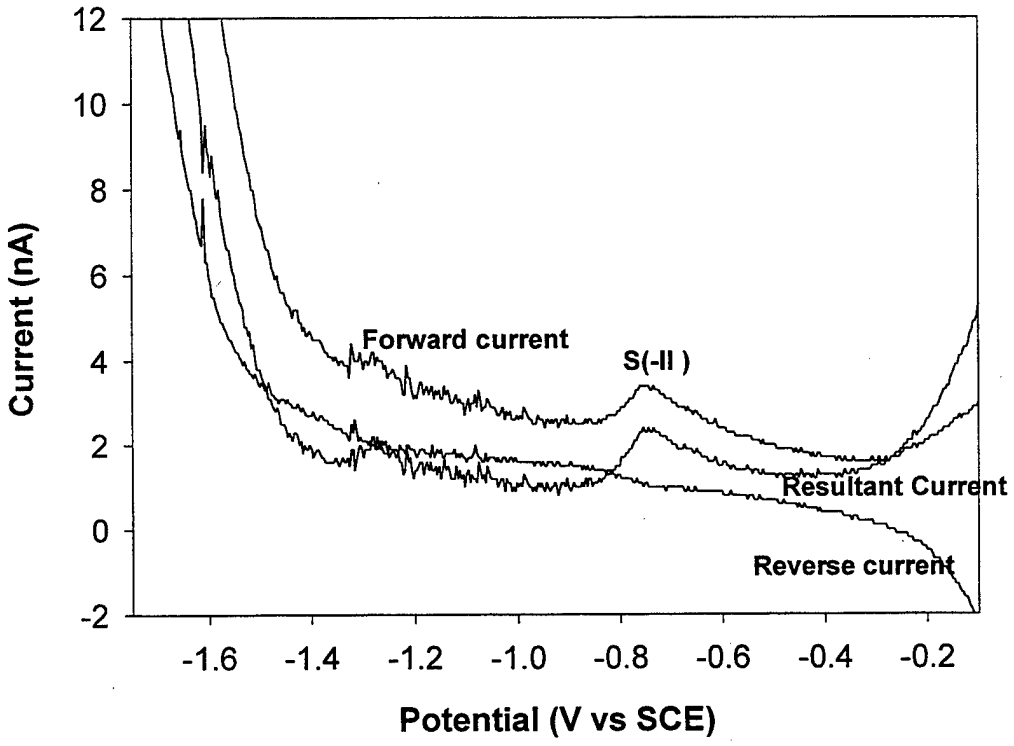


Figure V.F.4. Square wave voltammogram generated with a Hg-Au microelectrode deployed at location B in a marine biofilm. This particular voltammogram was taken near the metal surface where sulfide concentration was 1.3 μM under anoxic conditions.

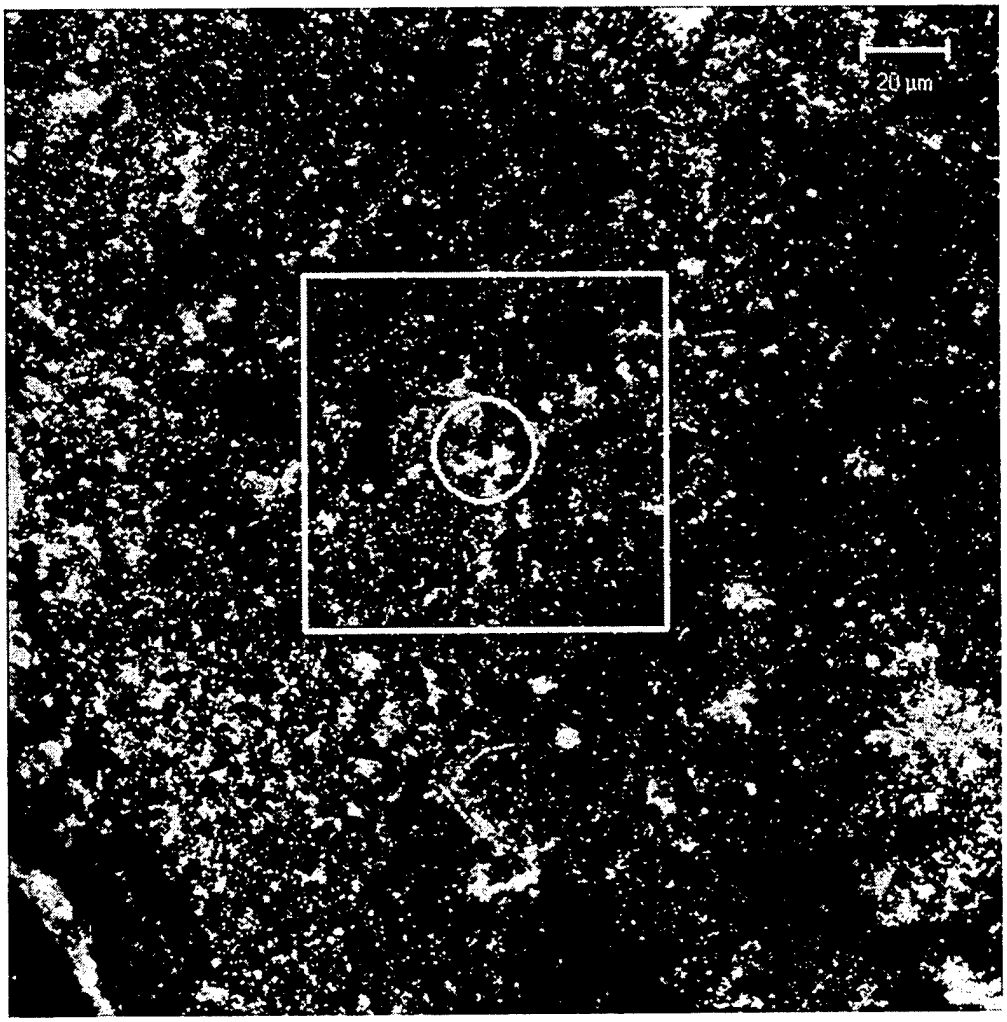


Figure V.F.5. Coccoidal microbial colonies observed at the location of microprofile B. The center of the most probable location coincides with the center of the white circle, which represents a microelectrode tip of 25 µm diameter. The square represents the 80% confident limit, within which microelectrode measurements were carried out. The entire image covers the location of microelectrode measurements with 99% confident limit.

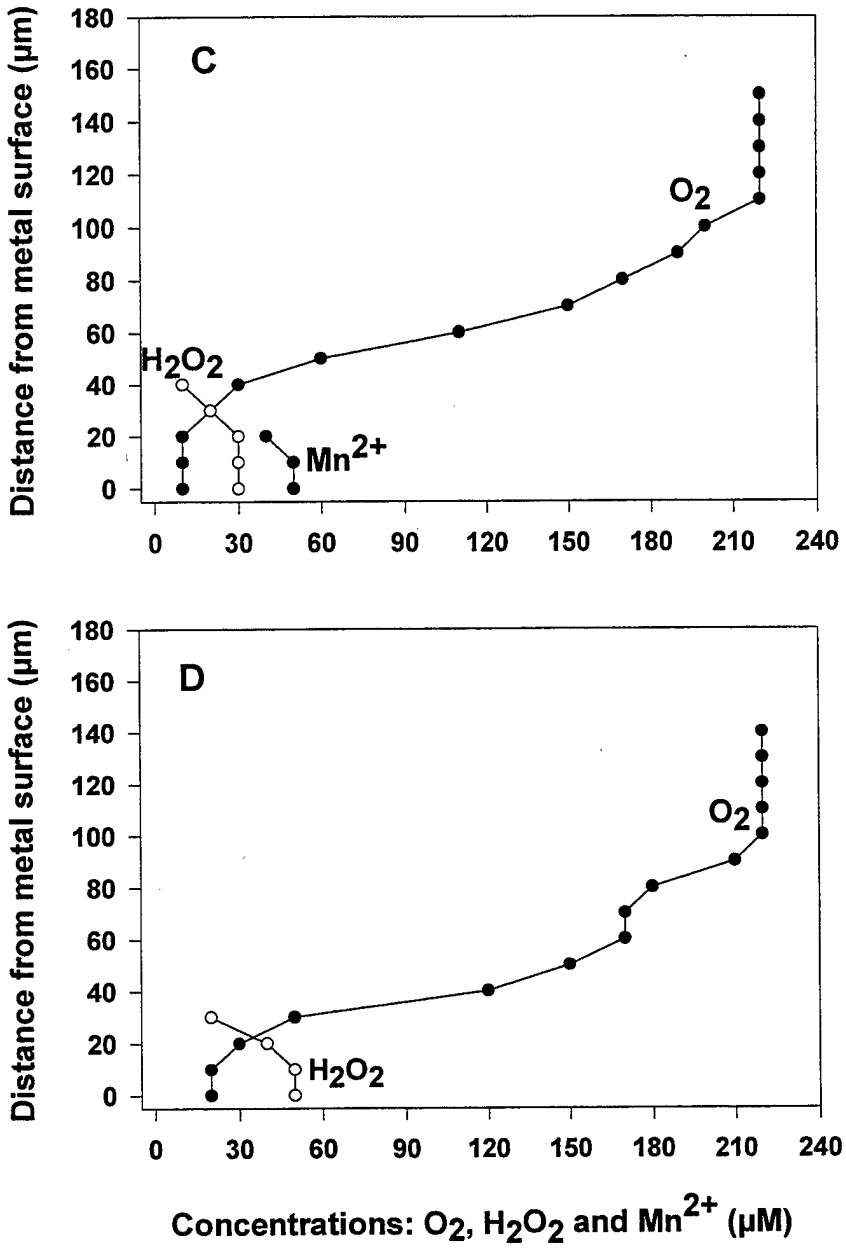


Figure V.F.6. Vertical microprofiles of redox chemical species measured at two different locations (C and D) in a marine biofilm formed on Nitronic 50. Trace amounts of ferric colloids were also detected at the bottom of the biofilm. The differences in the microelectrode calibration before and after the measurements were within 5%.

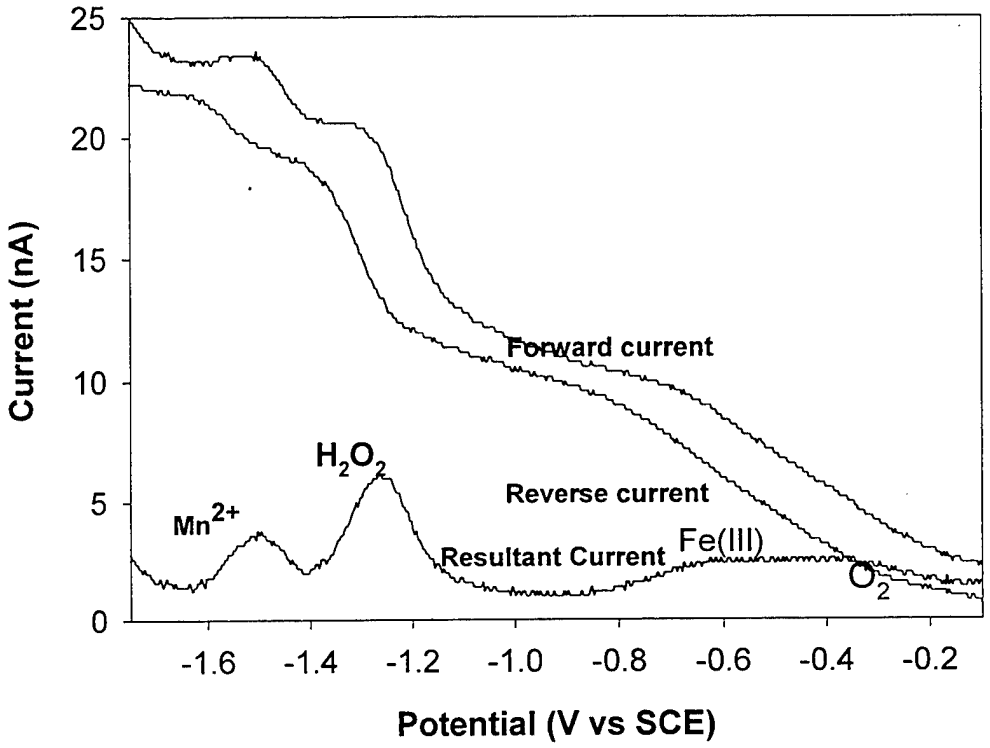


Figure V.F.7. Square wave voltammogram generated with a Hg-Au microelectrode deployed at location C in a marine biofilm. Dissolved Mn, peroxide, and trace amount of ferric colloids were detected simultaneously at the metal surface under low oxygen conditions.

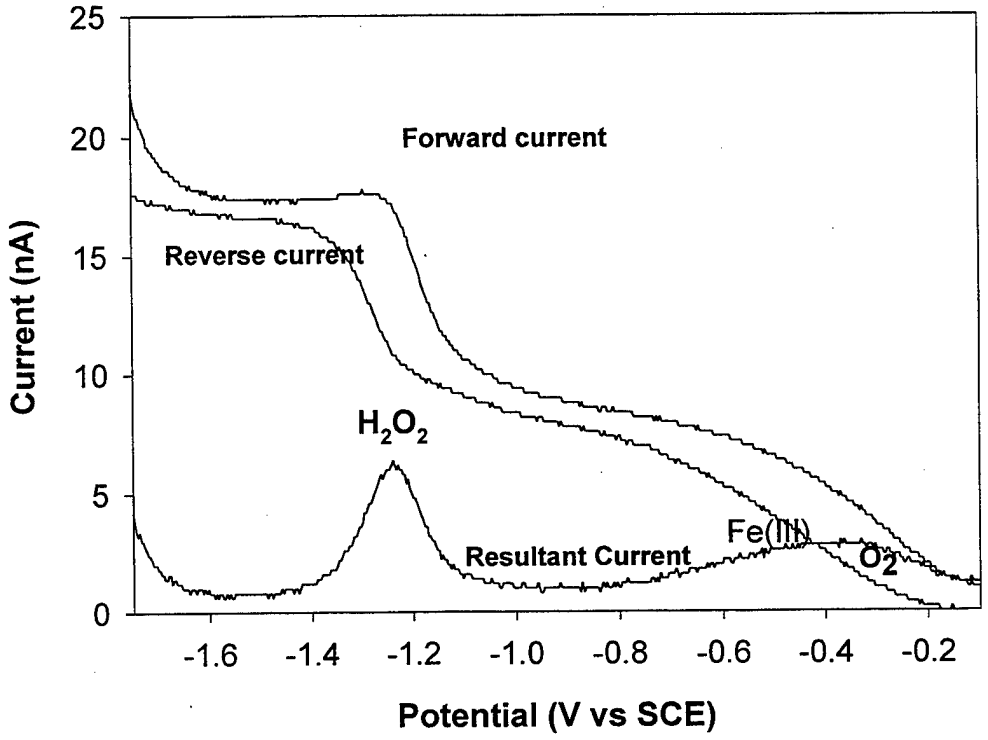


Figure V.F.8. Square wave voltammogram generated with a Hg-Au microelectrode deployed at location D in a marine biofilm. Fifty micromolar peroxide and trace amount of ferric colloids were at the metal surface under low oxygen conditions.

Microscopic observations at the locations of microprofiles C and D (Figures V.F.9 and V.F.10) showed heterogeneous distributions of microbial colonies mixed with detrital materials and EPS within the biofilm. At the location of microprofile C there also were many filamentous microorganisms associated with the colonies and EPS (Figure V.F.9). Since these filamentous microorganisms were found at the location where dissolved manganese was measured, they were assumed to be Mn-reducing/oxidizing microbes. It is well known that some Mn-oxidizing microorganisms including *Gallionella, Leptothrix, Sphaetotilus, Siderocapsa, Clonothrix,* and *Crenothrix* species have filamentous shapes (Lutey, 1992). At the location of microprofile D where dissolved manganese was not found, clumps of biomass were observed, but there were no filamentous microorganisms (Figure V.F.10).

### V.F.3. Biofilm sample three

Another series of experiments was carried out on a biofilm formed on a Nitronic 33 coupon. This coupon had been immersed in natural seawater for 5 months from September to January. At the end of the exposure, the coupon was brought back to the laboratory and examined under stereomicroscopy. It was found that the metal had suffered localized corrosion at several spots. At each localized corrosion spot, the biofilm showed red color, while at all other locations it had the usual dark brown color. The open circuit potential of the coupon was -178 mV versus SCE, and this was consistent with a corroding electrode.

Figure V.F.11 displays two chemical microprofiles measured at different locations within this biofilm. Microprofile E shows data measured at the center of a corrosion spot. To avoid damaging the microelectrode tip, a glass capillary of 25 μm diameter was used to puncture through the corrosion products before inserting the microelectrode. The result shows that the oxygen profile decreased rapidly with depth, and ferric colloids were measured at a concentration level of 160 μM over a depth of 50 μm near the metal surface. It is possible that the ferric colloids were produced by ferrous ions reacting with $MnO_2$. Figure V.F.12 shows a square wave voltammogram of ferric chemical species generated within the biofilm. The reduction of ferric colloids at the microelectrode surface occurred over a broad potential range from –0.2 V to –0.8 V. The forward current and reverse current have positive and negative peaks respectively indicating that the reduction of ferric colloids at the microelectrode surface was reversible.

Microprofile F was measured at a location about 1 cm away from the corrosion site. Low millimolar sulfide was found near the metal surface under anoxic conditions. Location F may have been a future corrosion initiation site due to the presence of sulfide. However, corrosion had not begun at that location at the time of the measurements. Figure V.F.13 shows a voltammogram measured at this specific location.

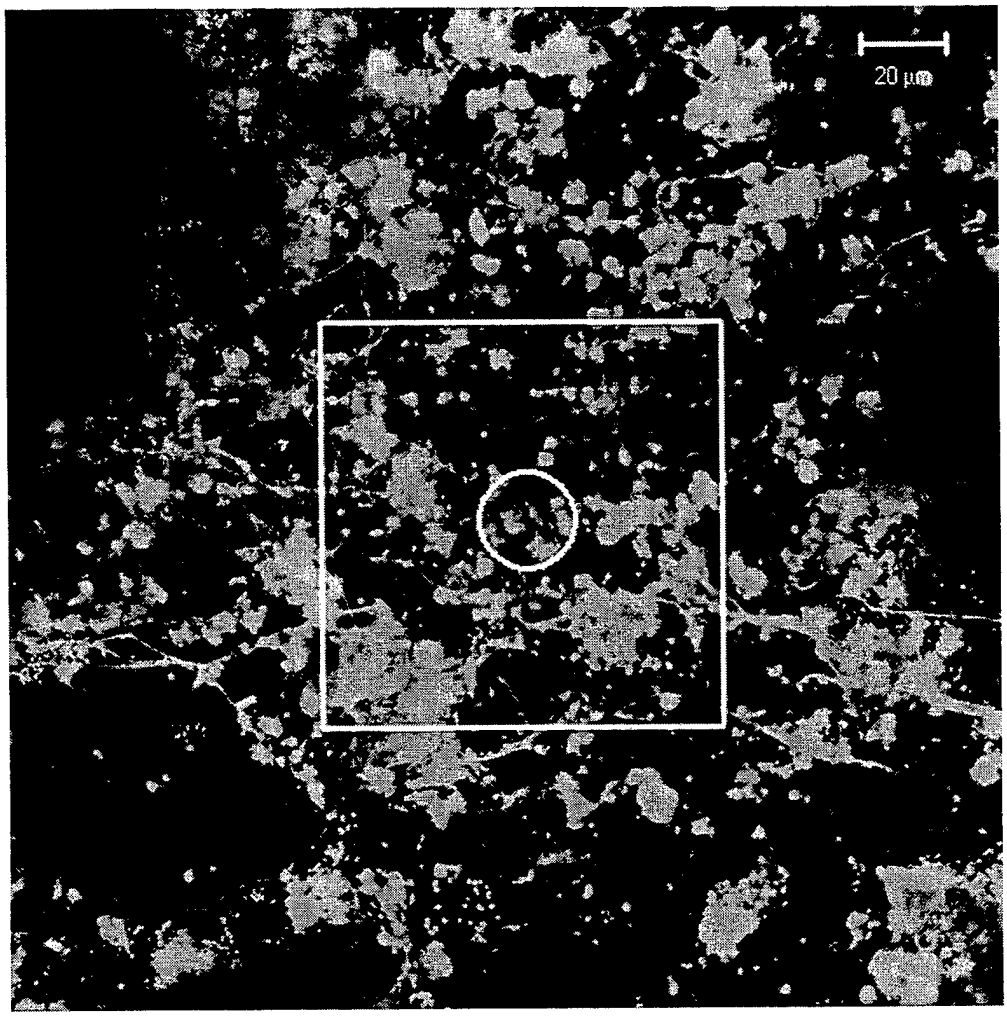


Figure V.F.9. Some filamentous microorganisms associated with biomass observed at the location of microprofile C. The center of the most probable location coincides with the center of the white circle, which represents a microelectrode tip of 25 µm diameter. The square represents the 80% confident limit, within which microelectrode measurements were carried out. The entire image covers the location of microelectrode measurements with 99% confident limit.

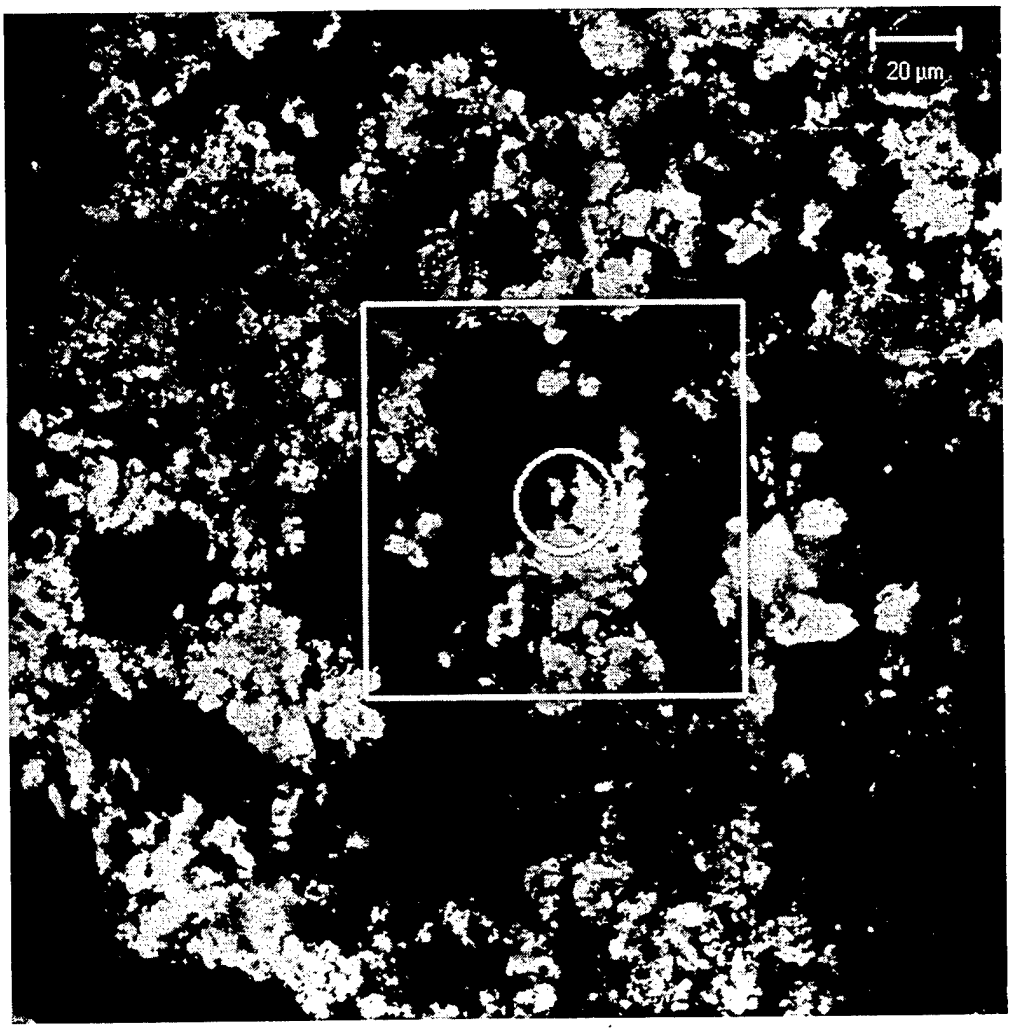


Figure V.F.10. Biofilms observed at the location of microprofile D. The center of the most probable location coincides with the center of the white circle, which represents a microelectrode tip of 25 µm diameter. The square represents the 80% confident limit, within which microelectrode measurements were carried out. The entire image covers the location of microelectrode measurements with 99% confident limit.

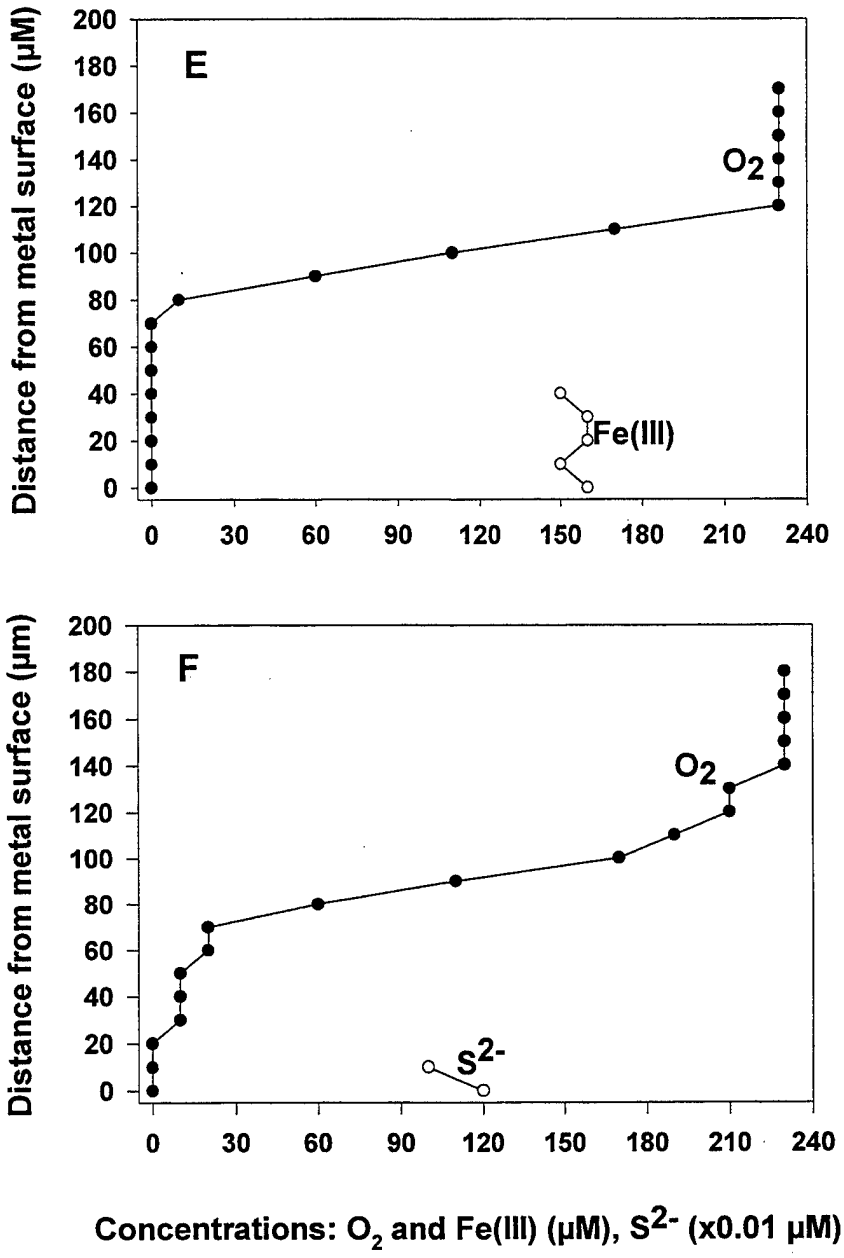


Figure V.F.11. Vertical microprofiles of redox chemical species measured at two different locations (E and F) in a marine biofilm formed on Nitronic 33. Concentrations of chemical species not plotted in profiles were below detection limits. The differences in the microelectrode calibration before and after the measurements were within 8%.

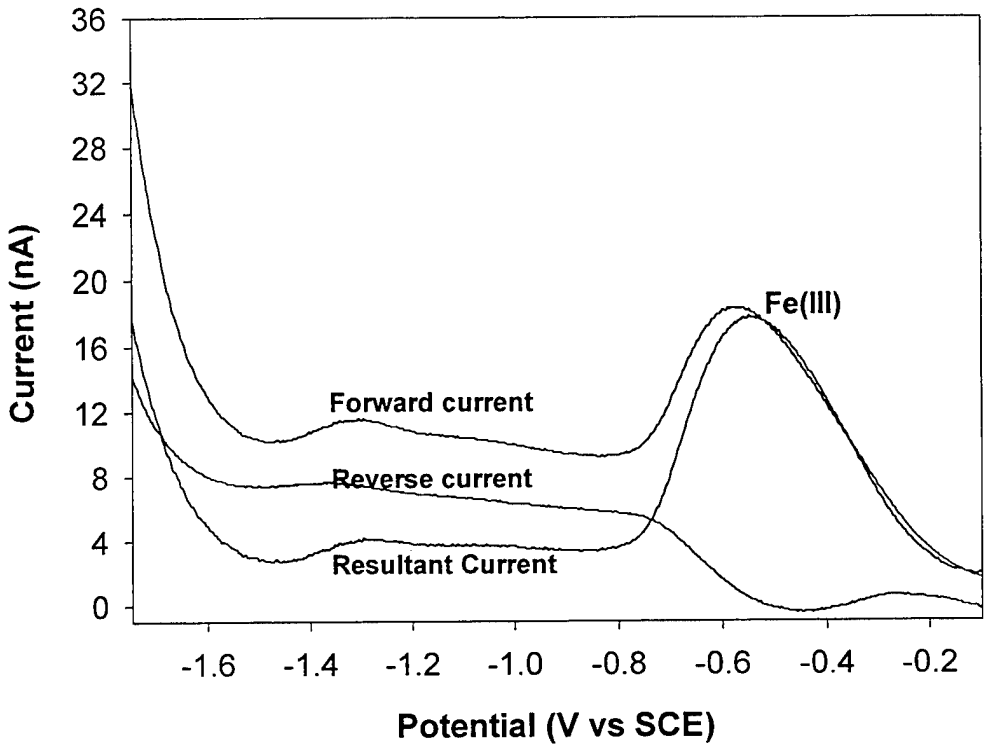


Figure V.F.12. Square wave voltammogram generated with a Hg-Au microelectrode deployed at location E at the center of a localized corrosion site in a marine biofilm. This particular voltammogram was taken at a distance of 30 μm from the metal surface where Fe(III) concentration was 160 μM under anoxic conditions.

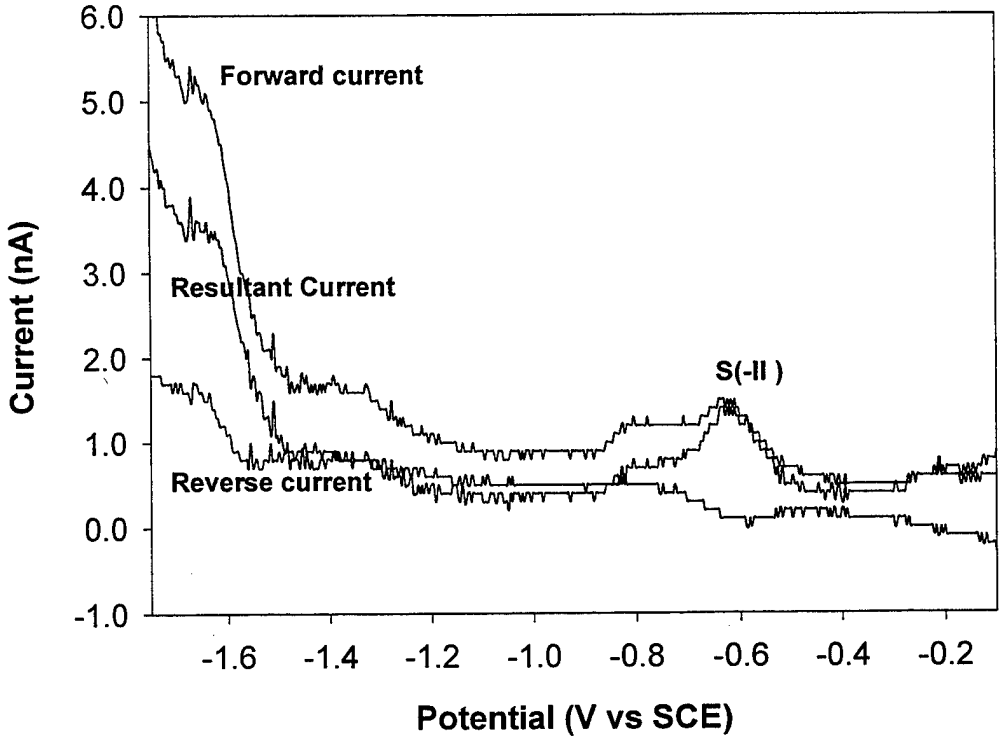


Figure V.F.13. Square wave voltammogram generated with a Hg-Au microelectrode at location F deployed in a marine biofilm. Low micromolar sulfide was found at the metal surface under anoxic conditions.

After the biofilm was fixed with paraformaldehyde and stained with Syto 13, it was observed under the confocal microscope. The locations of microprofiles E and F were tracked through their X-Y coordinates recorded by microelectrode measurements. It was found that high densities of microorganisms were associated with corrosion products at location E (Figure V.F.14). A three dimensional image was taken under the confocal microscope at location F. It is composed of 15 consecutive X-Y slices along the Z-axis, each slice being 2 μm in thickness. Figure V.F.15 shows the composite image of all 15 slices. Figure V.F.16 shows the 15 slices in sequence from the outer biofilm surface (upper left) downward. There were many layers of biomass at this specific location. Similar to the biofilm at the location of microprofile B, microbial microcolonies were found at the center of the most probable site of the chemical measurements for location F. It is reasonable to infer that those organisms were sulfate-reducing bacteria since sulfide chemical species were found there at the same location. Figure V.F.17 shows higher magnification images of slices 4 to 7 from Figure V.F.16, and Figure V.F.18 shows the same for slices 8 to 11. Because the biofilm was compressed vertically when covered with a coverslip and mounted on the confocal microscope, it is difficult to establish the spatial relationship between a specific chemical microprofile point and a slice of the image.

## References Cited


Krieg, N. R and J. G. Holt. 1984. Bergey's manual of systematic bacteriology, Vol. 1, Williams & Wilkins.

Lutey, R. W. 1992. Identification and detection of microbiologically influenced corrosion. Proc of NSF-CONICET workshop, Biocorrosion & Biofouling, edited by H. A. Videla, Z. Lewandowski, and R. W. Lutey. Nov, 1992, Argentina, pp. 146-158.

Taillefert, M., A. B. Bono, and G. W. Luther III. 2000. Reactivity of freshly formed Fe(III) in synthetic solutions and porewaters: voltammetric evidence of an aging process, Environ. *Sci. & Technol.*, Vol. 34, No. 11, pp. 2069-2300.

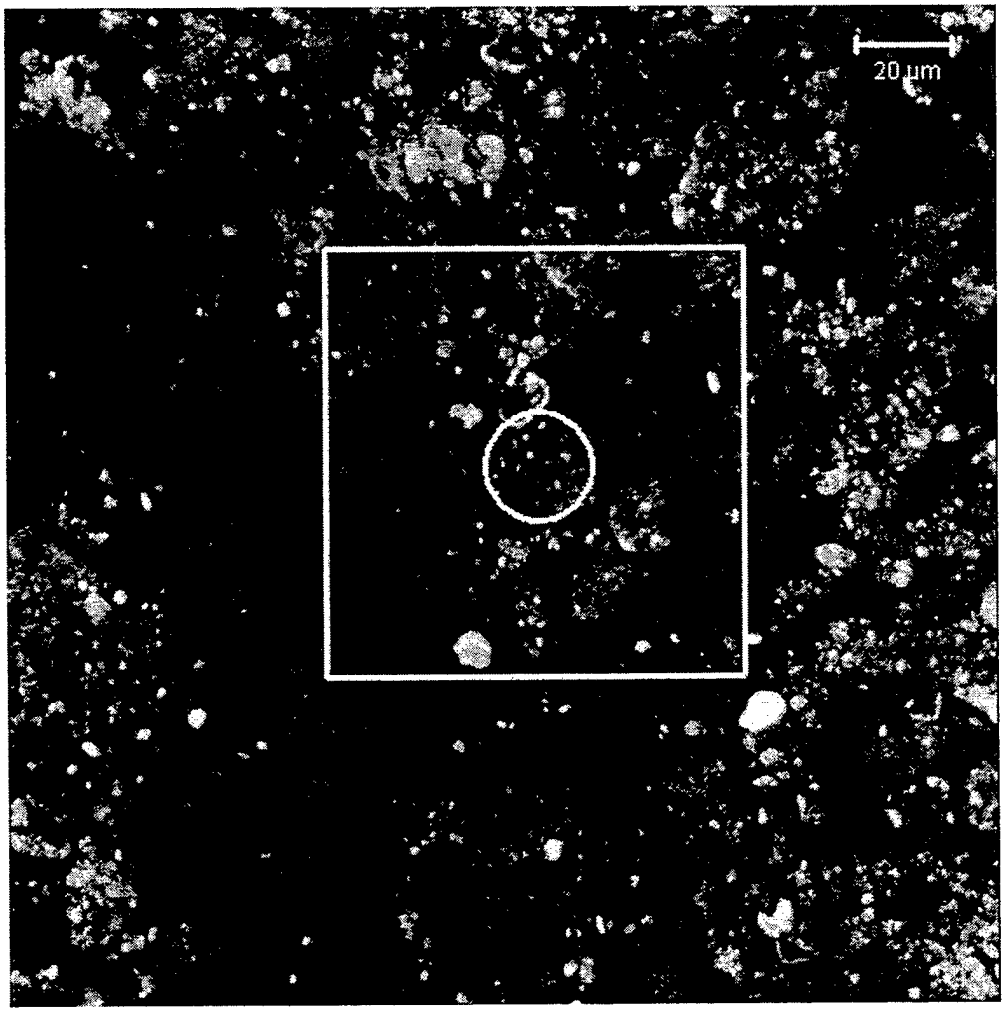


Figure V.F.14. High densities of cocci associated with corrosion products observed at the location of microprofile E. The center of the most probable location coincides with the center of the white circle, which represents a microelectrode tip of 25 µm diameter. The square represents the 80% confident limit, within which microelectrode measurements were carried out. The entire image covers the location of microelectrode measurements with 99% confident limit.

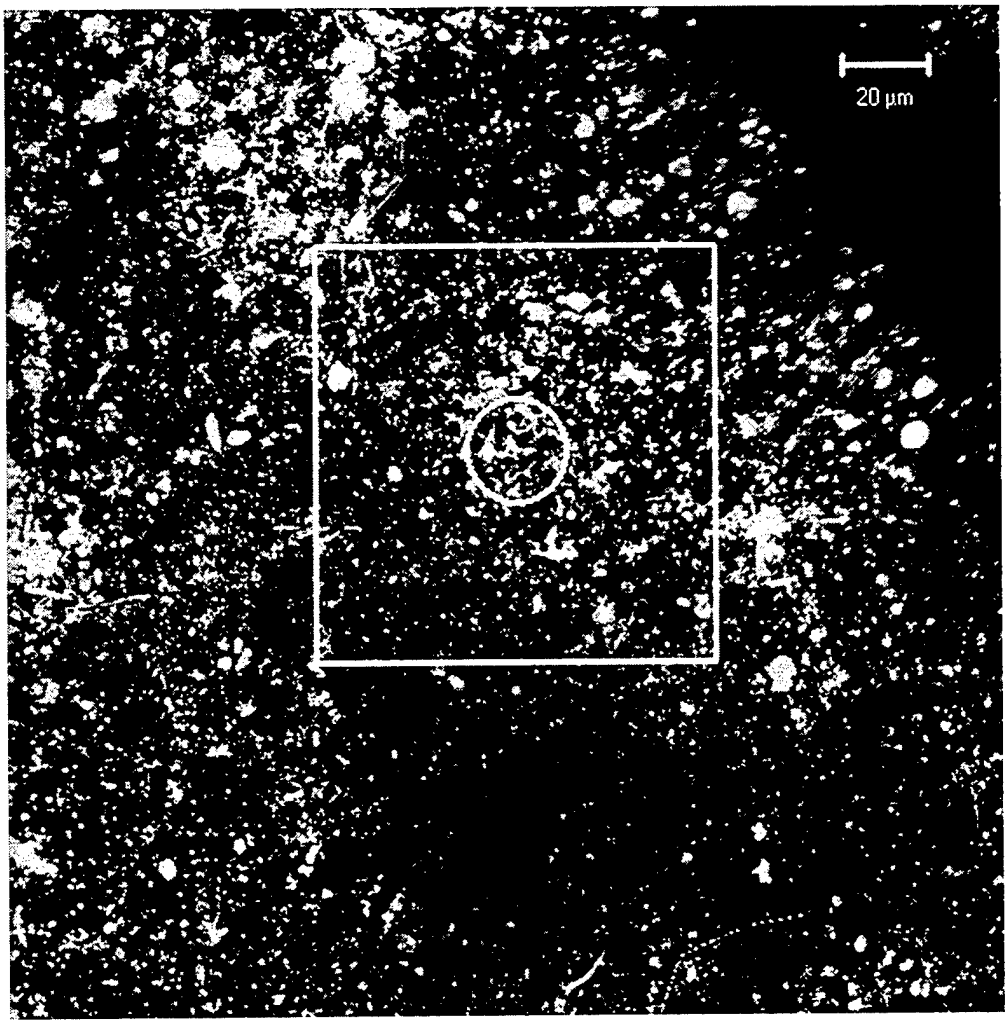


Figure V.F.15. Coccoidal and filamentous microcolonies observed at the location of microprofile F. The center of the most probable location coincides with the center of the white circle, which represents a microelectrode tip of 25 µm diameter. The square represents the 80% confident limit, within which microelectrode measurements were carried out. The entire image covers the location of microelectrode measurements with 99% confident limit.

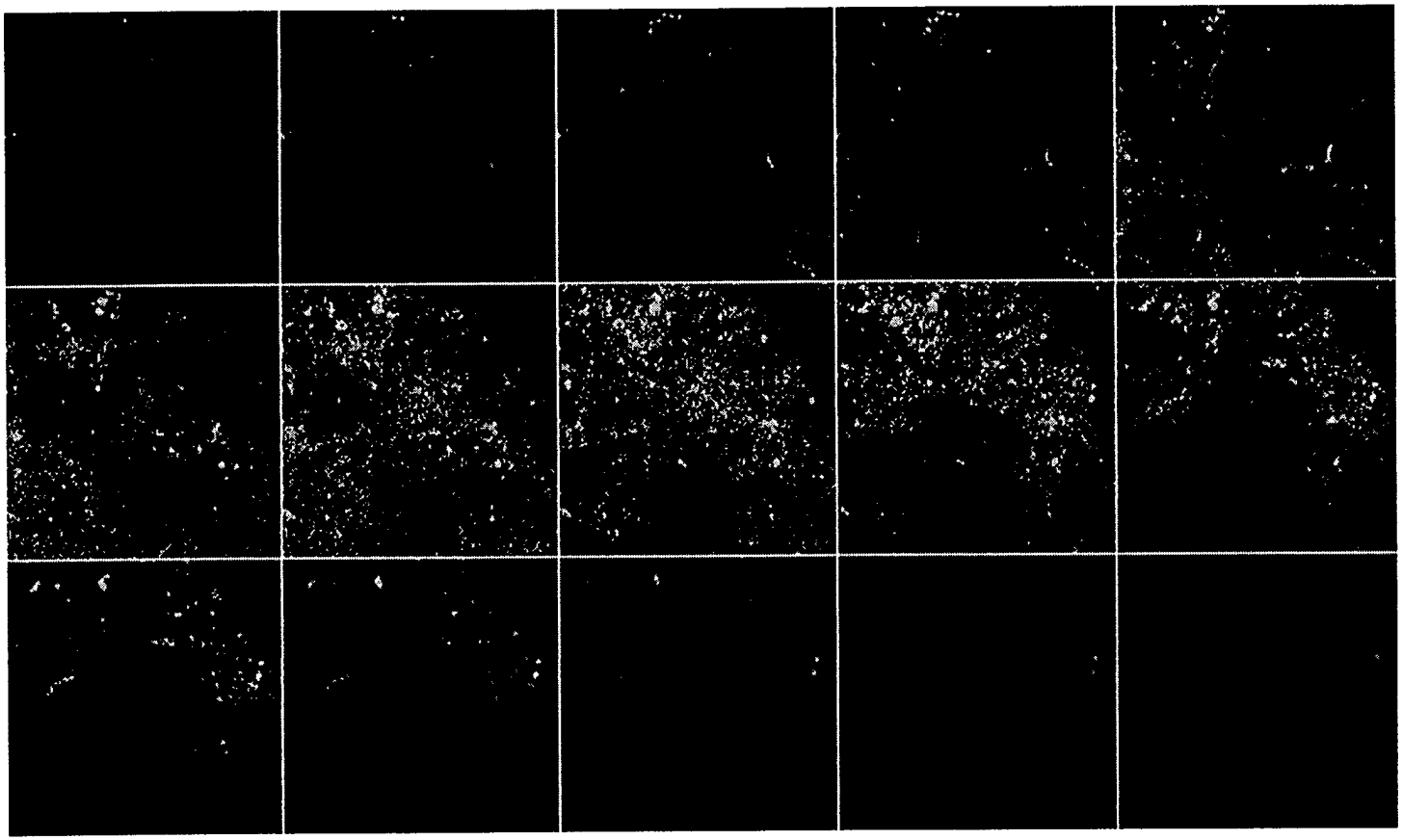

Figure V.F.16. Fifteen parallel X-Y slices of biofilm images taken at the location of microprofile F from the biofilm surface downward, each slice being in 2 μm interval along the Z-axis.

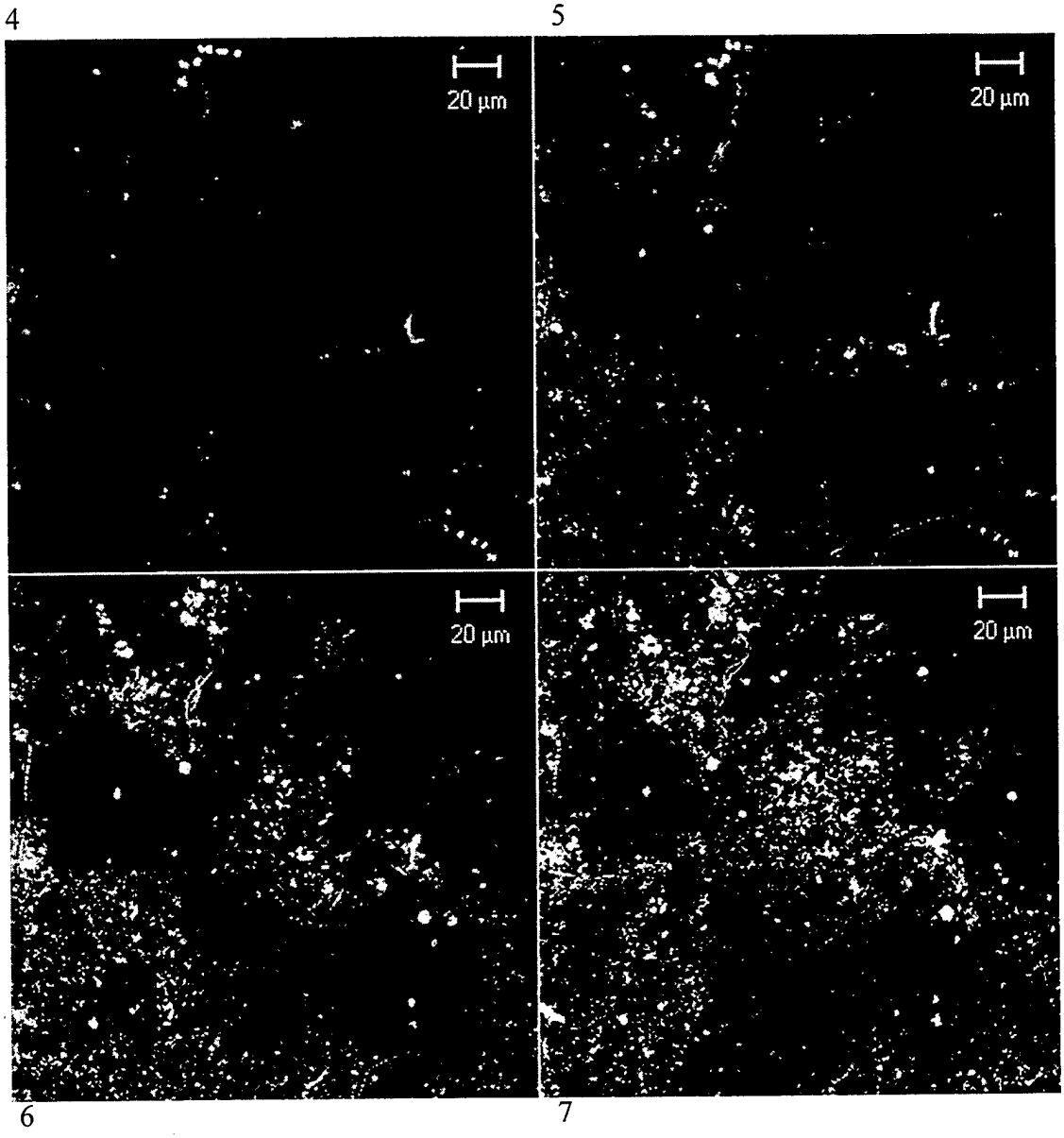


Figure V.F.17. Four X-Y slices of biofilm images taken at the location of microprofile F near the biofilm surface. These are slices 4 to 7 in Figure 3.48.

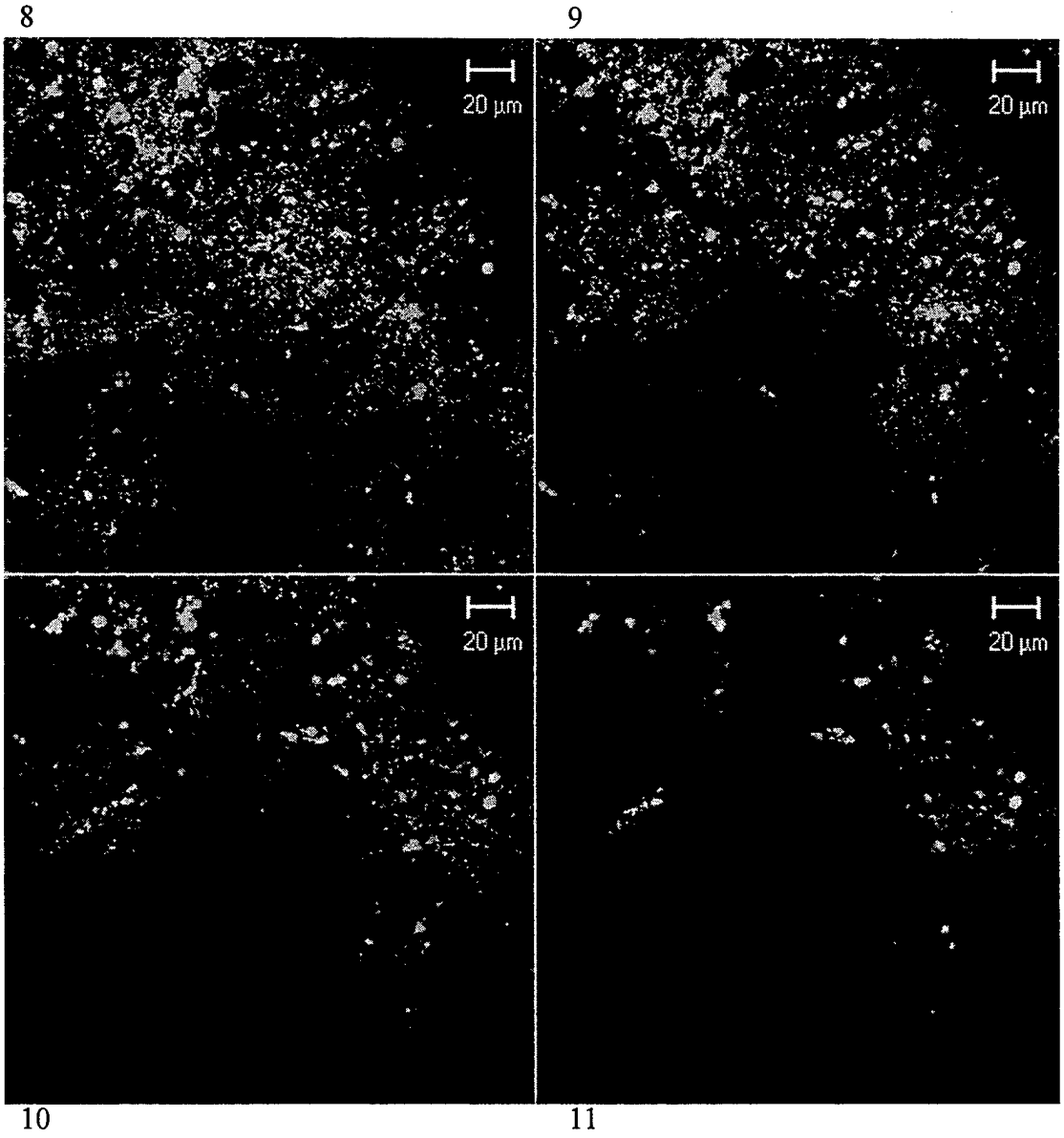


Figure V.F.18. Another four slices of biofilm images taken at the location of microprofile F. These are slices 8 to 11 in Figure 3.48.

### V.F.4. Biofilm sample four

The fourth experiment was carried out on a biofilm grown on a Nitronic 50 coupon from October through March. The biofilm had a dark brown color. The surface of the film was rough, and the thickness ranged from 10 μm to 120 μm. The metal substratum had an OCP value of + 367 mV versus SCE at the end of exposure period.

Two vertical chemical microprofiles are shown in Figure V.F.19. In microprofile G, dissolved oxygen was the only chemical specie found, and its concentration decreased only slightly within the last 40 μm above the metal surface. Figure V.F.20 shows a square wave voltammogram obtained near the metal surface at this location. In microprofile H, oxygen concentration decreased rapidly with depth, and dissolved Mn was found within the last 20 μm above the metal surface. Figure V.F.21 displays a square wave voltammogram showing dissolved Mn at location H. The current peak at the potential of –1.5 V is characteristic of Mn reduction.

Under the confocal microscope, three-dimensional biofilm images were taken at locations G and H. For Location G the composite image constructed from 15 parallel X-Y images as shown in Figure V.F.22. Many spherical and a few filamentous microbes were found at location G. However, at the center of the most probable location, there was no significant microcolony. Figure V.F.23 shows the 15 separate images in sequence from the outer biofilm surface at the upper left and proceeding downward toward the metal surface. Each slice is 2 μm thick along the Z-axis. Examination of these images in sequence reveals variations of the biofilm mass and community structure with depth into the biofilm. Figure V.F.24 shows higher magnification images of slices 8 to 11 from Figure V.F.23.

The biomass at location H was denser than that at location G. There were many filamentous microorganisms as well as the spherically shaped cocci at location H (Figure V.F.25). As was the case for microprofile C, filamentous microorganisms were observed at the X-Y location where dissolved Mn was detected. It stands to reason that those filamentous microorganisms might be capable of physiological Mn oxidation or reduction. In a manner similar to that for location G in Figure V.F.23, Figure V.F.26 shows the 15 parallel X-Y image slices for location H. Figures V.F.27 and V.F.28 show higher magnification views of four slices each from Figure V.F.26. Note particularly in Figure 3.60 that the filamentous organisms at location H are more densely packed than at location G (Figure V.F.24) where there was no manganese.

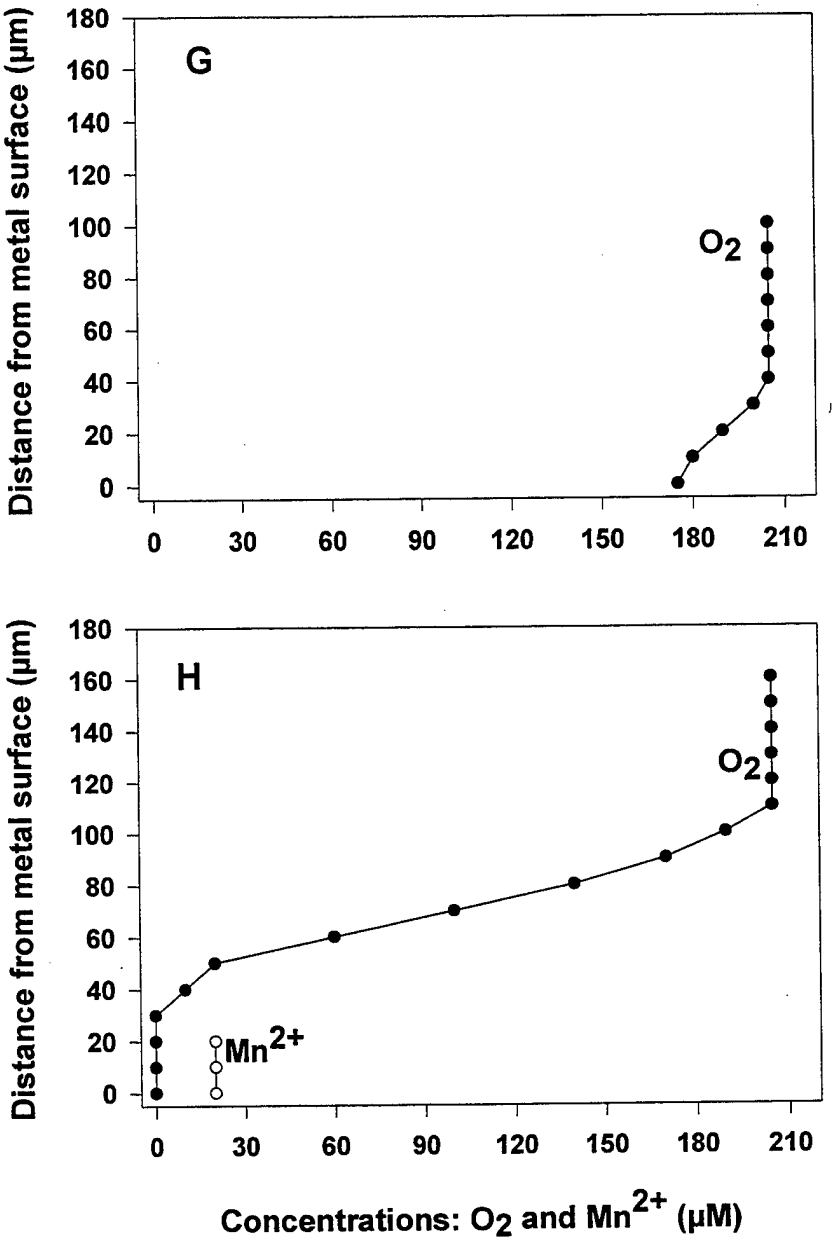


Figure V.F.19. Vertical microprofiles of redox chemical species measured at two different locations (G and H) in a marine biofilm formed on Nitronic 50. Concentrations of chemical species not plotted in profiles were below detection limits. The differences in the microelectrode calibration before and after the measurements were within 5%.

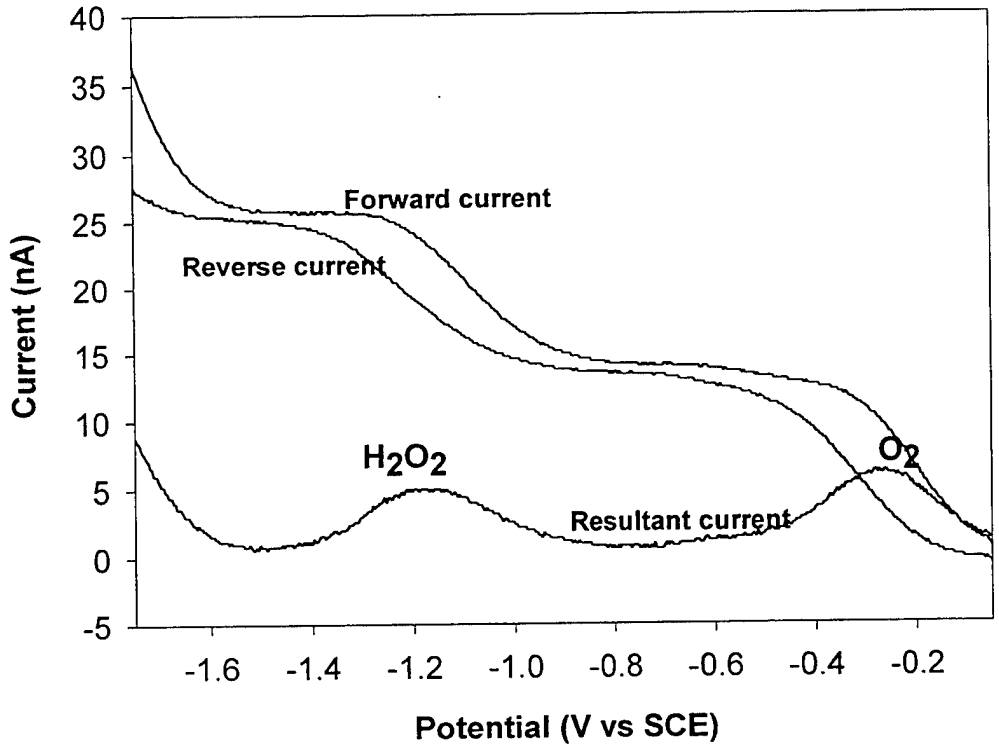


Figure V.F.20. Square wave voltammogram generated within 10 μm of the metal surface using a Hg-Au microelectrode deployed at location G in a marine biofilm. Dissolved oxygen concentration was 170 μM at this position. No other redox chemical species were detected at this location.

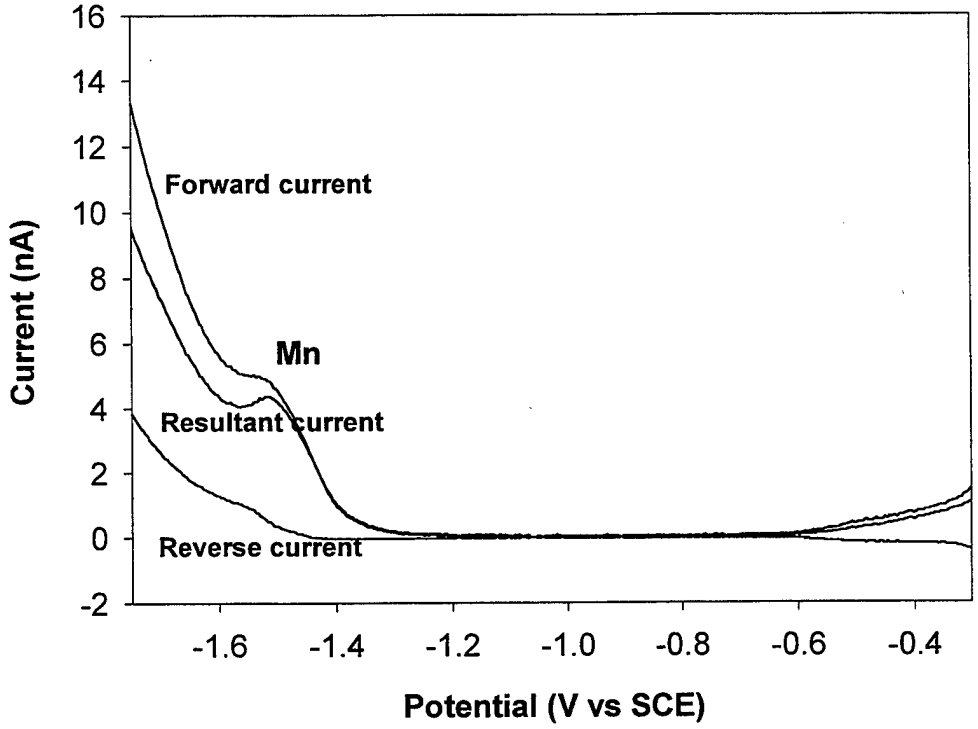


Figure V.F.21. Square wave voltammogram generated within 10 μm of the metal surface using a Hg-Au microelectrode deployed at location H in a marine biofilm. Dissolved Mn concentration was 20 μM at this position.

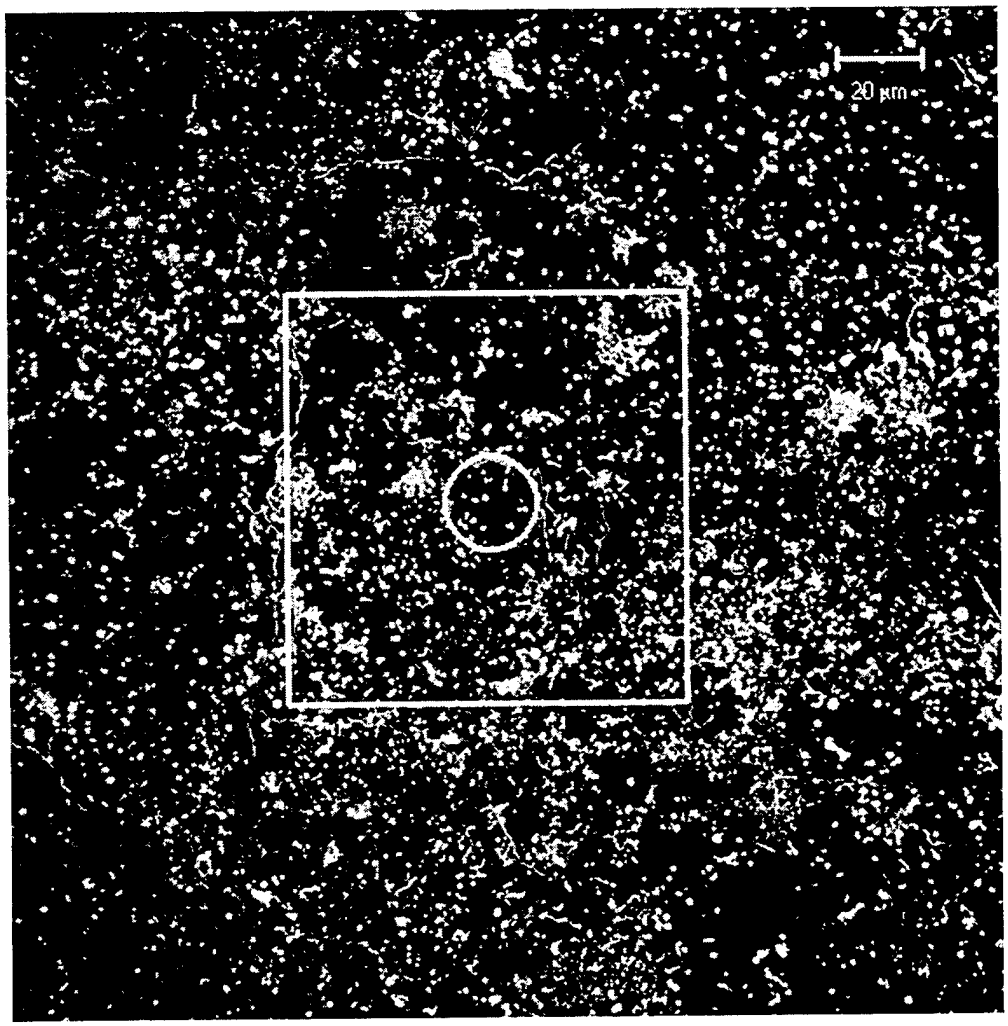


Figure V.F.22. Some cocci and filamentous microorganisms observed at the location of microprofile G. The center of the most probable location coincides with the center of the white circle, which represents a microelectrode tip of 25 µm diameter. The square represents the 80% confident limit, within which microelectrode measurements were carried out. The entire image covers the location of microelectrode measurements with 99% confident limit.

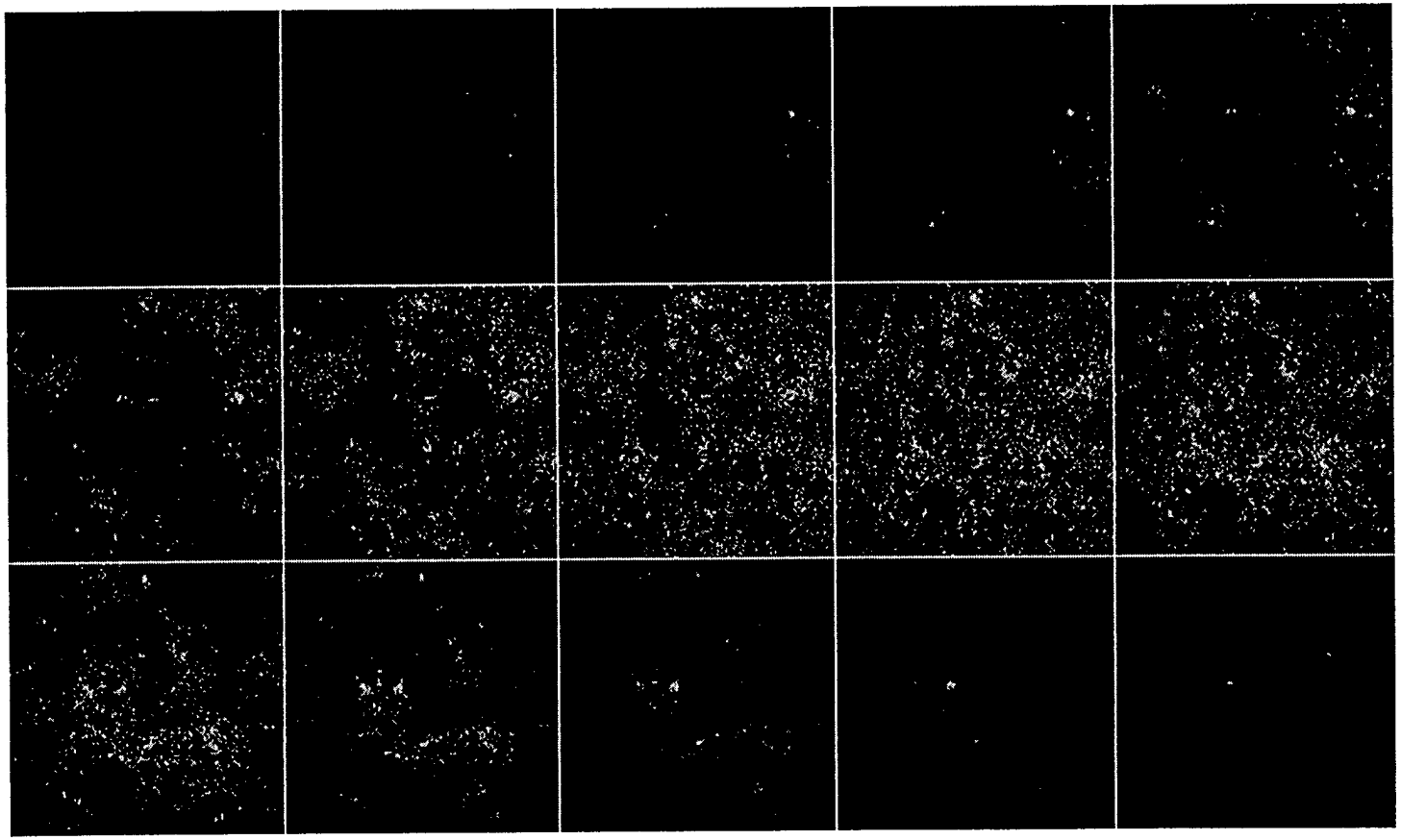

Figure V.F.23. Fifteen parallel X-Y slices of biofilm images taken at the location of microprofile G from the biofilm surface downward, each slice being in 2 μm interval along the Z-axis.

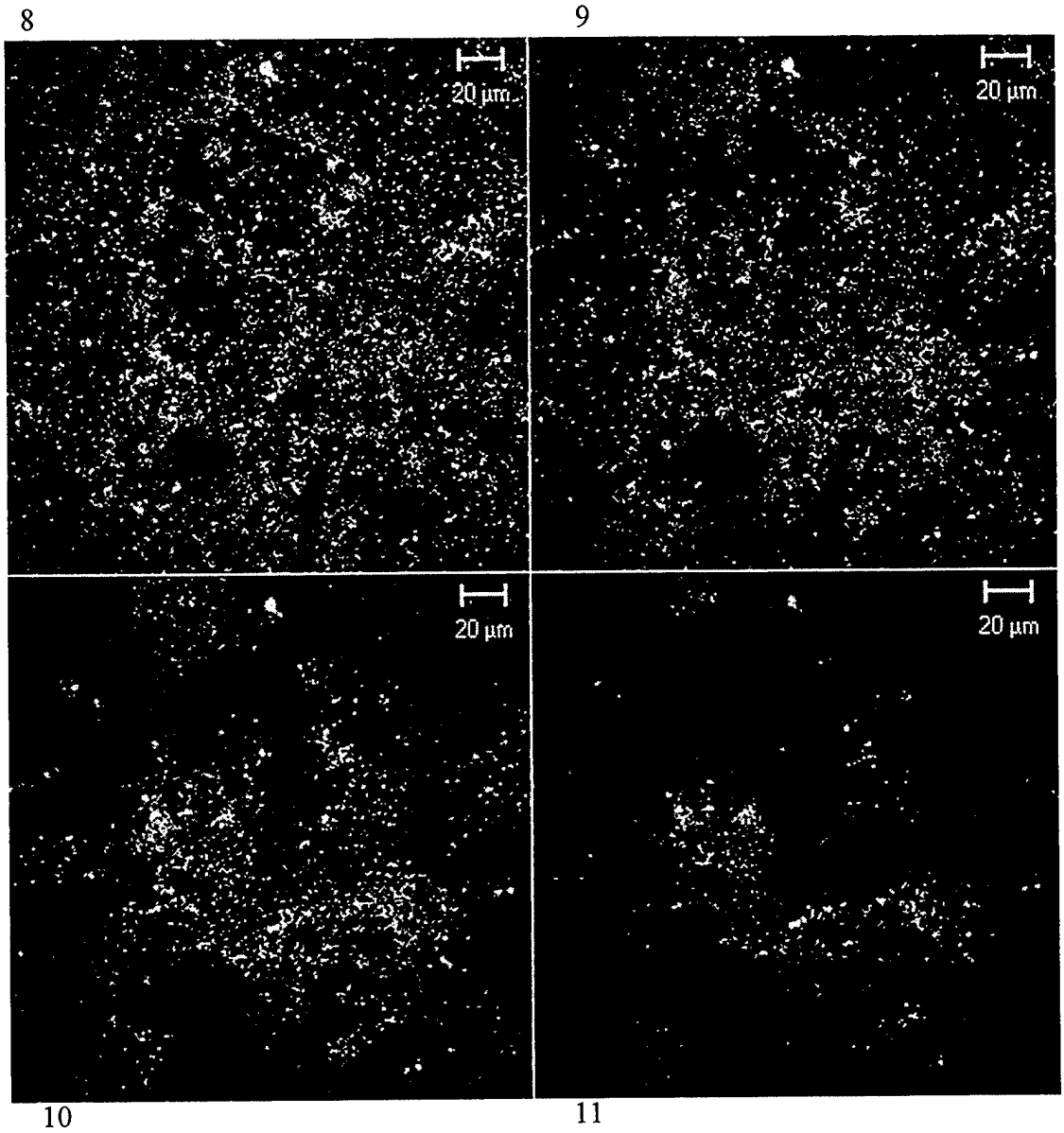


Figure V.F.24. Four slices of biofilm images taken at the location of microprofile G. These are slices 8 to 11 in Figure 3.55.

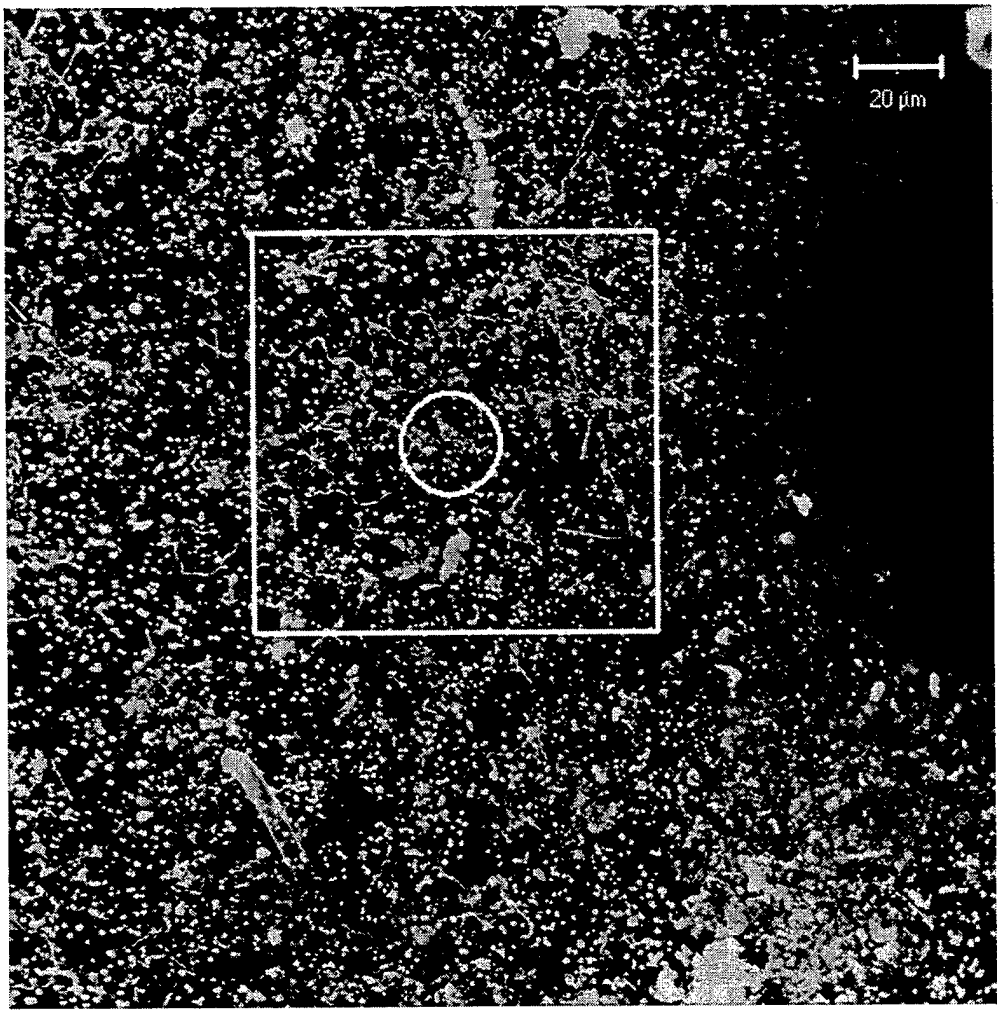


Figure V.F.25. Coccoidal and filamentous microcolonies observed at the location of microprofile H. The center of the most probable location coincides with the center of the white circle, which represents a microelectrode tip of 25 µm diameter. The square represents the 80% confident limit, within which microelectrode measurements were carried out. The entire image covers the location of microelectrode measurements with 99% confident limit.

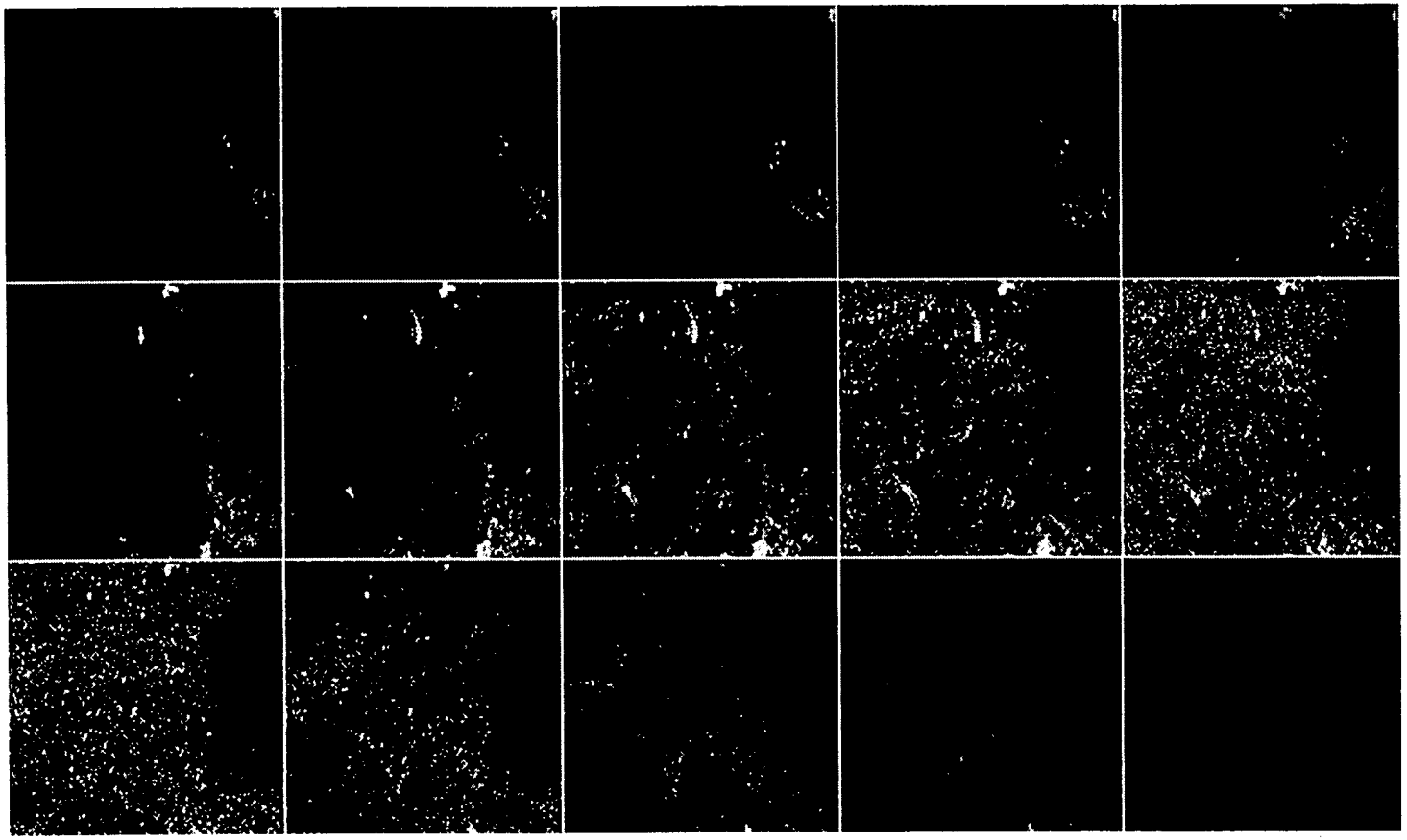

Figure V.F.26. Fifteen parallel X-Y slices of biofilm images taken at the location of microprofile H from the biofilm surface downward, each slice being in 2 μm interval along the Z-axis.

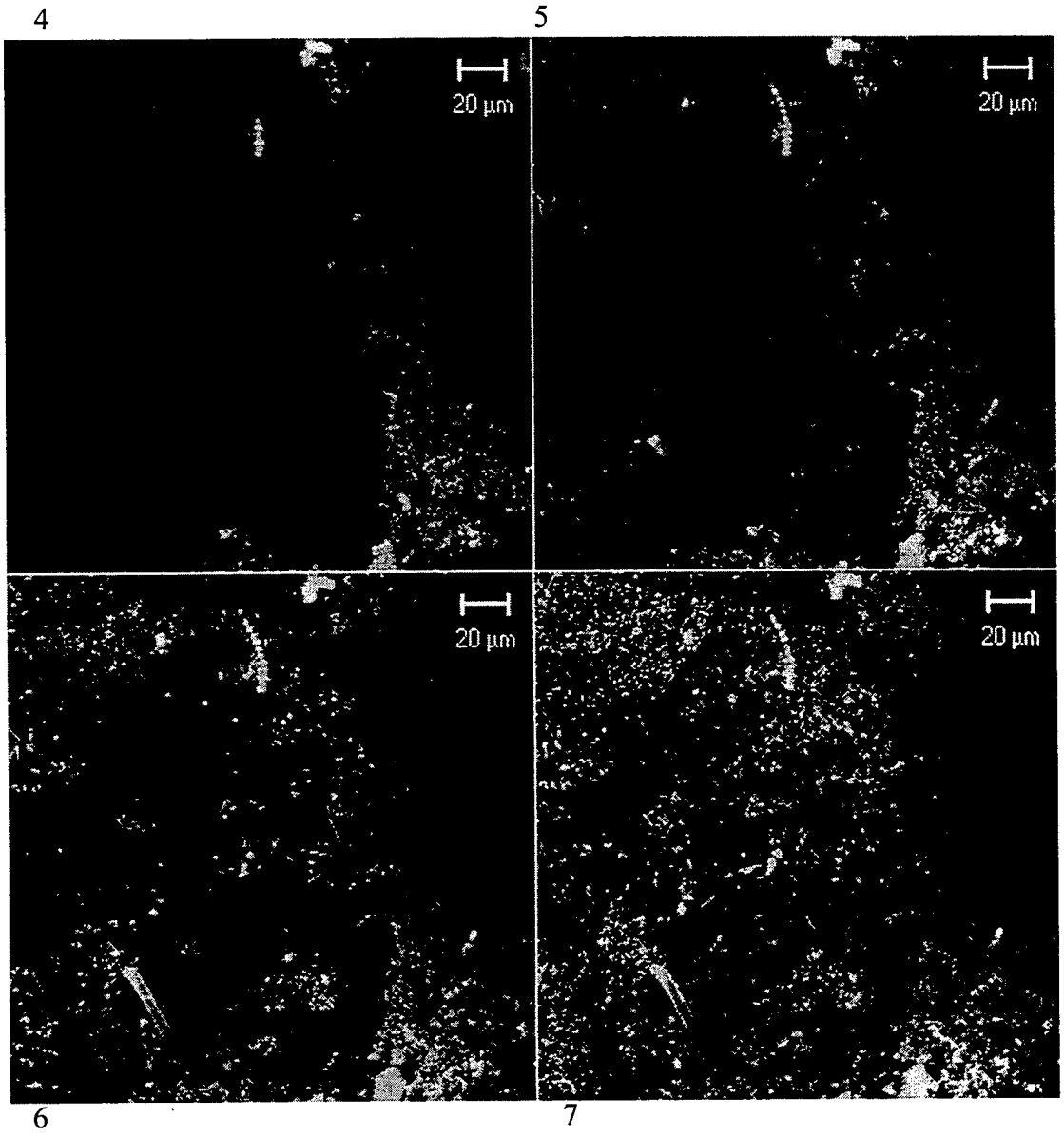


Figure V.F.27. Four X-Y slices of biofilm images taken at the location of microprofile H near the biofilm surface. These are slices 4 to 7 in Figure 3.58.

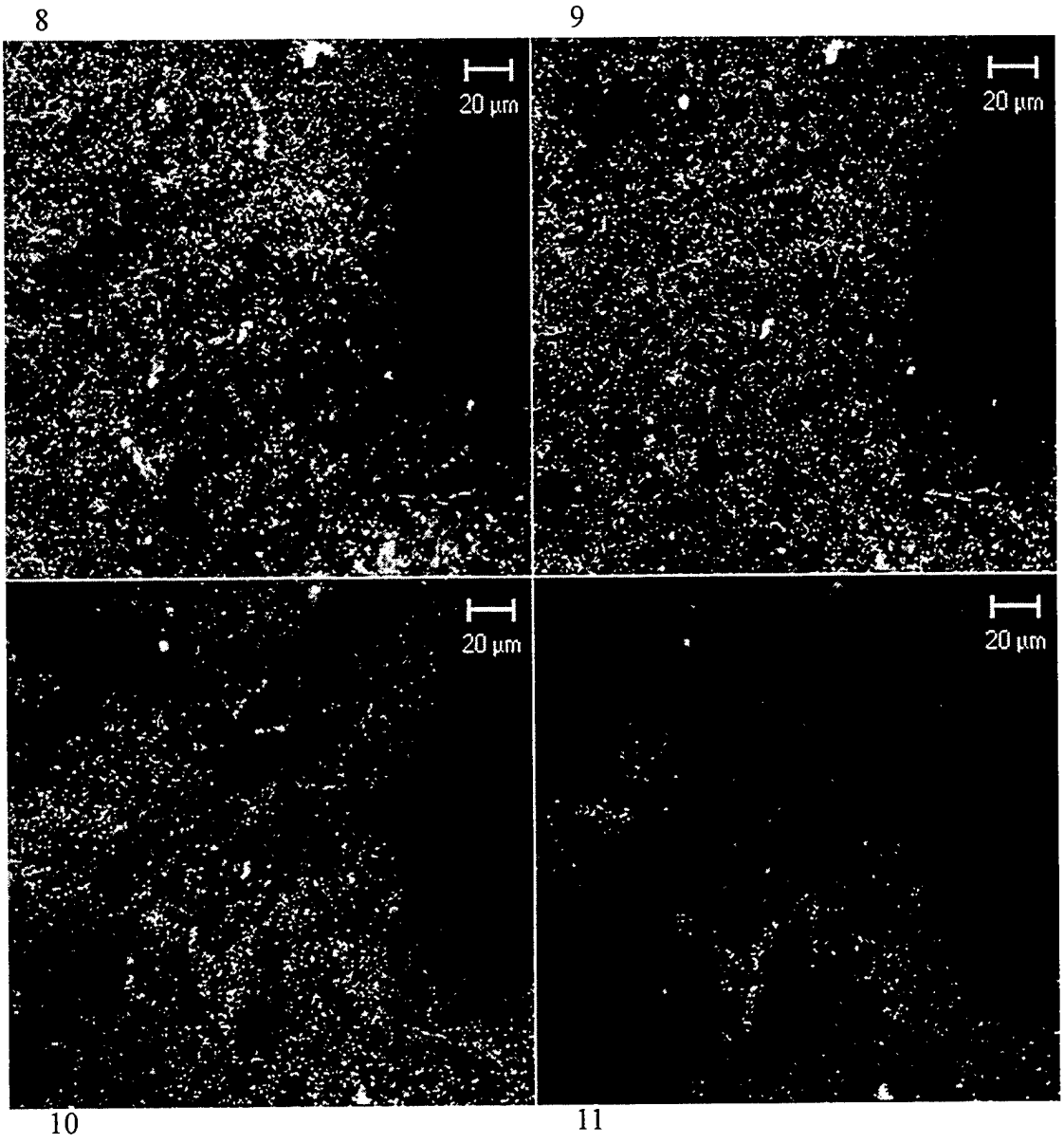


Figure V.F.28. Another four slices of biofilm images taken at the location of microprofile H. These are slices 8 to 11 in Figure 3.58.

## V.G. Summary of Ennoblement Mechanisms

This section discusses the implications of our recent work for the mechanisms of OCP ennoblement and the formation of differential potential cells under biofilm forming conditions.

### V.G.1. Conditions for OCP Ennoblement

It is now well documented that biofilms formed on passive metals and alloys drive the open circuit potential in the noble direction (See for example: Mollica and Trevis, 1976; Scotto et al., 1985; Johnsen and Bardal, 1985; Dexter and Gao, 1988; Eashwar et al., 1995; Dickinson and Lewandowski, 1996). As has been shown in many of our publications, the OCP of all active-passive metals with n-type passive films tested at our site to date typically ennoble to over +350 mV versus SCE within the first month of immersion during the summer season. Unless localized corrosion is initiated, that potential stays high with some minor fluctuations.

Let us first examine the conditions under which the OCP typically becomes ennobled. First, microbial activity within the biofilm is involved in the ennoblement process. The mere presence of microorganisms does not cause the effect. It was shown that OCP ennoblement disappeared when sodium azide, a respiration inhibitor, was added to the bulk water (Scotto et al., 1985).

Second, some dissolved oxygen at the metal surface is a prerequisite for OCP ennoblement. During the processes of biofilm development and ennoblement the dissolved oxygen concentration typically becomes highly variable from point to point along the metal surface. The concentration (as shown in earlier sections of this report) can range from nearly the air saturated value for the bulk water to unmeasurably small within only a few hundred micrometers translation along the surface. Nevertheless, Chandrasekaran and Dexter (1993) showed that established OCP ennoblement disappeared upon either depletion or saturation of oxygen in the system in which the biofilm was growing. Ennoblement could not be sustained under either anaerobic or oxygen saturated conditions.

Third, biofilms developed in natural seawater have generally accumulated elevated amounts of manganese and iron (Dexter and Chandrasekaran, 1995; Little et al., 1998). As was shown in Table V.1 above, total concentrations of manganese and iron within biofilms grown at our exposure site are on the order of 10 mM, a small fraction of which is in the dissolved form. Dissolved Mn(II) and Fe(III) were measured within biofilms by microelectrode techniques at the level of 10 to 100 μM (See Sections IV.B and V.F above). It was demonstrated by Dr. Xu during his Dissertation work (See Figure V.G.1) that Mn-complexes and Fe hydroxides could ennoble metal OCP to the extent of +300 mV, and MnO2 coatings could ennoble metal OCP to over +500 mV (see also the work of David Ruppel in Section V.D above). This agrees with the work of Dickinson and Lewandowski (1996).

Finally, due to microbial respiration, seawater biofilms also accumulate hydrogen peroxide. Previously, Chandrasekaran and Dexter (1994) measured peroxide

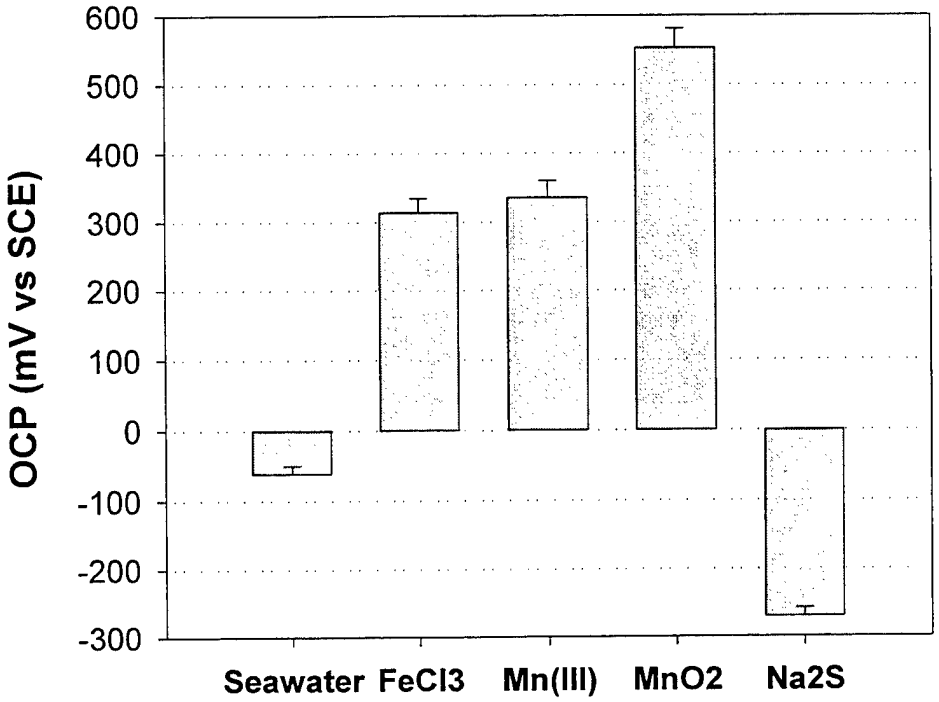


Figure V.G.1. The effects of $FeCl_3$, $(CH_3COO)_3Mn$, $MnO_2$ colloids, and sulfide on the open circuit potential of Nitronic 50 stainless alloy in seawater.

concentrations using enzyme strips with ferrothiocyanate indicator. They found peroxide at the level of 100 μM. Eashwar et al. (1995) also measured peroxide within marine biofilms at the level of 10 μM using the same methods. During Dr. Xu's work, peroxide was detected using voltammtric microlectrodes. Its concentration was often in proportion to dissolved oxygen as shown in Figure V.F.2. However, under low oxygen conditions it was also measured at 30 to 50 μM within the biofilm (Figures V.F.6 and7). This concentration was in excess of oxygen, and it was often present at the same location where $MnO_2$ detected. It is known that peroxide may be involved in the redox cycle of Mn in natural environments (Glenn, et al., 1986).

In Section V.D above it was shown that much of the increased current capacity required for the observed ability of biofilms to increase the rates of galvanic and crevice corrosion can be explained by abiotic reoxidation of $MnO_2$. It was noted however that the abiotic system could only reproduce the cathodic currents available from natural biofilms under

oxygen saturated conditions. It has already been shown above that ennoblement in general cannot be sustained in an oxygen saturated natural system, thus an additional contribution to manganese reoxidation is required. In the following section we propose that the well-known peroxidatic manganese oxidation process is compatible with all the conditions under which ennoblement occurs, and that it may provide the needed contribution.

### V.G.2. Peroxidatic Mn oxidation mechanism for OCP ennoblement

Peroxidatic Mn(II) oxidation by microorganisms plays an important role in the regeneration of Mn(III) organic complexes in the natural manganese cycle (Glenn, et.al., 1986). As shown in Figure V.G.2, this model calls for several steps to be involved in the OCP ennoblement processes. First, manganese chemical species must be accumulated within the marine biofilm. The source of manganese could be insoluble $MnO_2$ particulates as well as dissolved Mn(II) species. In open ocean seawater, the majority of dissolved manganese is the ion $Mn^{2+}$, followed by $MnCl^+$ and $MnSO_4$ (Baturin, 1988). Dissolved Mn(II) can be oxidized and deposited as $MnO_2$ into biofilms by Mn-oxidizing microorganisms (Ghiorse, 1984). The EPS of a biofilm also entraps insoluble $MnO_2$ bearing particulates from the bulk seawater.

Insoluble $MnO_2$ may be reductively dissolved through microbial catalysis or chemical reaction. It is well known that microorganisms may use $MnO_2$ as an electron acceptor during the oxidation of organic compounds under low oxygen conditions. However, organic matter can chemically dissolve $MnO_2$ as well. Stone and Morgan (1984) have examined the reduction and dissolution of Mn(III, IV) oxide suspensions by 27 aromatic and nonaromatic compounds resembling natural organics. At neutral pH, one millimolar formate, fumarate, glycerol, lactate, malonate, phthalate, propanol, propionaldehyde, propionate, and sorbitol dissolved appreciable amounts of the oxide after 3 hours of reaction. The most reactive compounds tested were phenols (e.g., catechol), phenolic acids (e.g., hydrobenzoic acid) and quinones (e.g., hydroquinone), which form the core structures of humic acids. These studies show conclusively that humic residues, which are ubiquitous in marine aquatic environments, can greatly influence $MnO_2$ reduction.

After Mn(II) becomes present in biofilms, Mn-oxidizing microorganisms can play a major role in Mn(II) reoxidation. It is known that enzymatic oxidation is the major mechanism for Mn(II) oxidation. Long-term Mn(II) oxidation experiments have demonstrated that the rate of the chemical reaction:

$$Mn(II) + 0.5\ O_2 + H_2O \rightarrow MnO_2 + 2H^+$$

at pH less than 8 is negligible in the absence of Mn-oxidizing bacteria or surface catalysts (Stumm and Morgan, 1981; Diem and Stumm, 1984). One explanation of Mn(II) resistance to oxidation at $pH < 8$ is the high energy of activation required by the reaction. At $pH > 9$, Mn(II) oxidation is autocatalytic due to formation of $MnO_2$ surfaces, which serve as catalysts. The inhibition of oxidation rates by sodium azide (Johnston and Kipphut, 1988) further suggests that Mn(II) oxidation is a microbially mediated process.

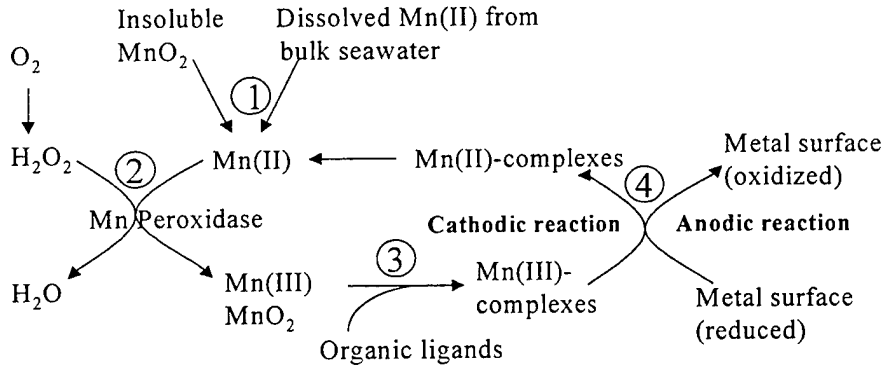


Figure V.G.2. Schematic diagram of proposed peroxidatic reoxidation of Mn(II) during Mn redox cycling on passive metals under marine biofilms.

One well established mechanism for Mn(II) oxidation is peroxidatic oxidation. Marine microorganisms release peroxide during aerobic respiration (Fridovich, 1974; Brock and Madigan, 1988). Mn-oxidizing microorganisms catalyze the oxidation of Mn(II) to Mn(III) by producing manganese peroxidase (MnP). Such peroxidatic Mn oxidation has been reported to occur in the fungi species *Phanerochaete chrysosporium* (Kirk and Farrell, 1987; Glenn et al., 1986), *Pleurotus ostreatus* (Kerem and Hadar, 1993; 1995), and *Pleurotus pulmonarius* (Camarero et al., 1996) as well as in *Leptothrix pseudochracea, Leptothrix discophora* and several other Mn-oxidizing bacteria (Ghiorse, 1989). As was shown above in Figures V.F.6 and 7, chemical measurements indicated that peroxide was present at some locations within biofilms at 30 to 50 μM. Moreover, the physical location of peroxide often coincided with that of dissolved Mn within biofilms. These data support the idea of the peroxidatic Mn oxidation mechanism. Dissolved free Mn(III) species were not measured directly by the microelectrodes within biofilms because they are unstable and may disproportionate or be reduced quickly.

The connection between Mn(II) oxidation and extracellular manganese peroxidase activity of fungi has been well-studied. Kerem and Hadar (1995) have shown that the addition of Mn(II) to cotton stalks enhances the preferential lignin degradation by *Pleurotus ostreatus*. Such enhancement was believed to be the result of manganese peroxidatic oxidation. Mn(III) then supposedly associated with organic ligands to form Mn(III)-complexes, which in turn oxidized aromatic structures in lignocellulosic complex in lignin.

The third step in the Mn redox cycle is the involvement of organic ligands. The presence of an organic ligand is necessary to maintain the stability of Mn(III). In the absence of organic ligands, Mn(III) will quickly disproportionate into Mn(II) and insoluble $MnO_2$ and lose its reactivity (Glenn et al., 1986; Roy et al., 1994; Ruppel 1999). Magers et al. (1978) have shown that carboxylic acids and hydroxyl ligands can form complexes with Mn(III), Mn(IV) and Fe(III). For the case of Mn(III), at least two types of complexes can form: $MnL_3$ and $L_2Mn\text{-}O\text{-}MnL_2$ (Richert et al., 1988). The organic ligands (amino acids, carboxylic acids, sugars, and other unsaturated compounds) are supplied by the decomposition of the organic matter at the oxic/anoxic interface (Cooper and Calvin, 1977).

The fourth step is for the Mn(III)-complex to act as a cathodic oxidizer on the metal surface. For free ions at pH 1, Mn(III)/Mn(II) standard redox potentials are very high:

$$Mn^{3+} + e^- \rightarrow Mn^{2+} \qquad E^o = 1.258 \text{ V (SCE)}$$

$$MnOOH + 3H^+ + e^- \rightarrow Mn^{2+} + 2H_2O \qquad E^o = 1.257 \text{ V (SCE)}$$

These redox potentials generally decrease with increasing pH. In the presence of complex formers, the stable Mn(III) / Mn(II) redox couple potential may vary over a wide potential range from 0.2 to 0.9 V (SCE) depending on the chelated organic ligands and oxygen availability (Stumm and Morgan,1996).

It has been known that dissolved Mn(III) plays an important role in the biogeochemical cycles of Mn, Fe, S, and C (Kosta et al., 1995; Burkhard, 1995). Canfield et al. (1993) have demonstrated that Fe(III) and Mn(III, IV) reductions can be the dominant processes for organic matter decomposition in certain marine sediments. Evidence for complexed Mn(III) has been presented for agricultural soils where Mn reacts rapidly with organic root exudates (Jauregui and Reisenauer, 1982). In fact, the involvement of Mn(III)-complexes in the lignin biodegradation processes has now been well accepted (Roy et al., 1994). Therefore, it is reasonable to suggest that Mn(III)-complex reduction may be a strong contributor to OCP ennoblement and increased cathodic current capacity on passive metals with natural biofilms.

It can be seen from Figure V.G.2 that as long as manganese accumulates within biofilms, microbially catalyzed Mn redox cycling may continue endlessly. Mn(III) reduction would drive the metal OCP in the noble direction, whereas peroxidatic Mn(II) oxidation would replenish the supply of Mn(III) forming a complete Mn redox cycle. Since the microbially catalyzed Mn redox cycle is most active at or near the oxic/anoxic interface, this model meets the conditions under which ennoblement occurs. It involves microbial activity, low oxygen conditions, peroxide, and manganese redox cycling in establishing ennoblement of passive metals in the presence of biofilms.

It should be clear that a continuous Mn cycling is not needed if one is only concerned about ennoblement of the OCP and localized corrosion initiation. No current is drawn in those processes. Continuous Mn cycling is essential, however, to sustain an increased corrosion current, and hence, the elevated galvanic and crevice corrosion rates that have

been documented by the research in our Group (Zhang and Dexter, 1995; Dexter, 1996; Dexter and LaFontaine, 1998) These results implied that some oxidizers must persist within the biofilm to maintain high corrosion current over a long period of time. The peroxidatic Mn oxidation model provides a biological mechanism for regenerating Mn(III, IV) within biofilms. Together with the abiotic mechanisms discussed above in Section V.D, we believe that this is sufficient to account for the increased corrosion rates observed.

### V.G.3. Related mechanisms

Johnsen and Bardal (1985) suggested that the mechanism of potential ennoblement might involve the catalytic action of organometallic complexes on the oxygen reaction at the metal surface. They thought that organo-metallic complexes from bacterial exopolymers within the biofilm would react with metal species, such as Fe, Co, Ni and Mn, from the corroding metal substrata to catalyze the oxygen reduction reaction in a manner similar to that shown for fuel cells (Van den Brink, 1980). However, there are two questions with this mechanism. First, it has been found that OCP ennoblement also occurred with non-corroding metals, such as titanium and platinum (Mansfeld and Little, 1989; Dexter et al., 1994). Moreover, OCP ennoblement has been shown to depend on microbial activity, and it is independent of the composition of passive metals (Dexter et al., 1994). Thus, the metal species would have to come from the bulk seawater, rather than the alloy. This would limit the metal species manganese and iron, which are the only two metals present in sufficient amounts in marine environments. Second, the organo-metallic complex model can not explain why OCP ennoblement occurs only under suboxic conditions. If oxygen reduction was the reaction that was catalyzed, why then does OCP ennoblement disappear when the solution is saturated with oxygen?

Dexter and Chandrasekaran (1995) proposed that OCP ennoblement was the combined effect of low oxygen, low pH and peroxide. They also documented the presence of heavy metals, but they thought that the heavy metals were involved in maintenance of the low pH. While this mechanism was quite capable of producing an ennoblement of the OCP on any passive alloy, it could not account for a sustained increase in the current capacity. Nevertheless, all the important elements of today's model were represented in that mechanism.

### References Cited

Baturin, G. N. 1988. The geochemistry of manganese and manganese nodules in the ocean, Chapter 2, Kluwer Academic Publishers, pp. 25-41.

Brock, T. D. and M. T. Madigan. 1988. Biology of Microorganisms, Fifth edition, Prentice Hall Inc., Englewood Cliff, NJ, pp.1-450.

Burkhard, C. A. 1995. Speciation and reactivity of manganese with reduced sulfur in the marine environment, Master's thesis, University of Delaware.

Camarero, S., B. Bockle, M. J. Martinez, and A. T. Martinez. 1996. Manganese-mediated lignin degradation by Pleurotus pulmonarius, Appl. Environ. Microbiol. 62: 1070-1072.

Canfield, D. E., B. Thamdrup, and J. W. Hansen. 1993. The anaerobic degradation of organic matter in Danish coastal sediments: Fe reduction, Mn reduction, and sulfate reduction. Geochim. Cosmochim. Acta 57: 3867-3883.

Chandrasekaran, P. and S. C. Dexter. 1993. Factors contributing to ennoblement of passive metals due to biofilms in seawater, Proc. 12th International corrosion congress, Vol. 5B, NACE, International, Houston, TX, pp. 3696-3707.

Chandrasekaran, P. and S. C. Dexter. 1994. Bacterial metabolism in biofilm consortia, CORROSION/94, paper No. 276, NACE International, Houston, TX.

Cooper, S. R. and M. Calvin. 1977. Mixed valence interaction in Diuoxo-bridged manganese complexes. *J. Amer. Chem. Soc.* 20: 6623-6630.

Dexter, S. C. and G. Y. Gao, 1988. Effect of seawater biofilms on corrosion potential and oxygen reduction of stainless steel, *Corrosion,* 44: 717-723.

Dexter, S. C., H-J. Zhang, and P. Chandrasekaran. 1994. Biofouling effects on corrosion of stainless alloys in seawater, *Biodeterioration Research 4*, edited by G. C. Llewellyn, Plenum Press, New York.

Dexter, S. C. and P. Chandrasekaran. 1995. Chemical changes at the metal surface under biofilms, effect on localized corrosion, in *Critical factors in localized corrosion II,* edited by P. Natishan, R. Kelly, G. Frankel and R. Newman. The Electrochemical Society, Pennington, NJ, pp. 188-200.

Dexter, S. C. 1996. Effect of biofilms on crevice corrosion, Proc. COR/96 Tropical Research Symposium on Crevice Corrosion, NACE International, Houston, TX.

Dexter, S. C. and J. P. LaFontaine. 1998. Effect of natural marine biofilms on galvanic corrosion, Corrosion, 54: 851-861.

Dickinson, W. H. and Z. Lewandowski. 1996. Manganese biofouling and the corrosion behavior of stainless steels, *Biofouling*, 10: 79-94.

Diem, D. and W. Stumm. 1984. Is dissolved Mn(II) being oxidized by oxygen in the absence of Mn-bacteria or surface catalysts? *Geochim. Cosmochim. Acta* 48: 1571-1573.

Eashwar, M., S. Maruthamuthu, S. Sathiyanarayanan, and K. Balakrishnan. 1995. *Corrosion Science*, Vol. 37, No. 8, pp. 1169-1176.

Fridovich, I. 1974. Chapter 11, Molecular mechanisms of oxygen activation, edited by O. Hayaishi. Academic Press, New York, pp. 453-477.

Ghiorse, W. C. 1984. Biology of iron- and manganese-depositing bacteria. *Annu. Rev. Microbiol.* 38: 515-550.

Ghiorse, W. C. 1989. Manganese and iron as physiological electron donors and acceptors in aerobic-anaerobic transition zones, in *Microbial mats — physiological ecology of benthic microbial communities,* edited by Y. Cohen and E. Rosenberg, pp. 163-169.

Glenn, J. K, L. Akileswaran, and M. H. Gold. 1986. Mn(II) oxidation is the principal function of the extracellular Mn-peroxidase from *Phanerochaete chrysosporium. Arch. Biochem. Biophys.* 251: 688-696.

Jauregui, M. A. and H. M. Reisenauer. 1983. *Soil. Sic. Soc. Am. J.* 46: 314-317.

Johnsen, R. and E Bardal. 1985. Cathodic properties of different stainless steels in natural seawater, *Corrosion,* 41: 296-304.

Johnston, C. G. and G. W. Kipphut. 1988. Microbially mediated Mn(II) oxidation in an oligotrophic Arctic Lake, *Appl. Environ. Microbiol.* 54, 1440-1445.

Kerem, Z., and Y. Hadar. 1993. Effect of manganese on lignin degradation by *Pleurotus ostreatus* during solid-state fermentation. *Appl. Environ. Microbiol.* 59: 4115-4120.

Kerem, Z. and Y. Hadar. 1995. Effect of manganese on preferential degradation of lignin by *Pleurotus ostreatus* during solid-state fermentation. *Appl. Environ. Microbiol.* 61: 3057-3062.

Kirk, T. K. and R. L. Farrel. 1987. Enzymatic "combustion": the microbial degradation of lignin. *Annu. Rev. Microbiol.* 41: 465-505.

Kosta, J. E, G. W. Luther III, and K. H. Nealson. 1995. Chemical and biological reduction of Mn(III)-pyrophosphate complexes: potential importance of dissolved Mn(III) as an environmental oxidant. *Geochim. Cosmochim. Acta* 59: 885-894.

Little, B. J., P. A. Wagner, and Z. Lewandowski. 1998. The role of biomineralization in microbiological influenced corrosion, CORROSION/98 paper No. 294, NACE international, Houston, TX.

Magers, K. D., C. G. Smith, and D. T. Sawyer. 1978. Polarographic and spectroscopic studies of the manganese (II), (III), and Manganese (IV) complexes formed by polyhydroxy ligands. *Inorg. Chem.* 17 : 515-523.

Mansfeld, F. and B. J. Little. 1989. *Corrosion* 45: 786-795.

Mollica, A. and A. Trevis. 1976. *Proc. of the 4th Intl. Cong. On Marine Corrosion and Fouling*, pp. 351-365.

Richert, S. A., P. K. S. Tsang, and D. T. Sawyer. 1988. Ligand-centered oxidation of manganese (II) complexes. *Inorg. Chem.* 27: 1814-1818.

Roy, B. P., M. G. Paice, F. S. Archibald, S. K. Misra, and L. E. Misiak. 1994. Creation of metal-complexing agents, reduction of manganese dioxide, and promotion of manganese peroxidase-mediated Mn(III) production by cellobiose: quinone oxidoreductase for *Trameters versicolor. J. Biol. Chem.* 269: 19745-19750.

Ruppel. T. D. 1999. The effect of manganese in biofilms on galvanic corrosion currents. Master's thesis, University of Delaware.

Scotto, V., R. DiCintio, and G. Marcenaro. 1985. *Corrosion Science*, Vol. 25, No. 3, pp. 185-200.

Stone, A. T. and J. J. Morgan. 1984. Reduction and dissolution of Manganese (III) and Manganese (IV) oxides by organics: 2. Survey of the reactivity of organics. *Environ. Sci. & Technol.* 18: 617-624.

Stumm, W. and J. J. Morgan. 1996. *Aquatic Chemistry*. John Wiley & Sons, Inc., New York.

Van den Brink, F., E. Barendrecht, and W. Visscher, 1980. Rec. Trav. Chim. Pays-Bas, 99: 253-263.

Zhang, H-J. and S. C. Dexter. 1995. Effect of biofilms on crevice corrosion of stainless steels in coastal seawater, *Corrosion,* 51: 56-66.

# VI. Status of Questions and Answers

Since 1990, the research with ONR support in Dr. Dexter's Corrosion Lab at the University of Delaware has concentrated on determining how natural marine biofilms affect corrosion of passive alloys immersed in seawater and estuarine environments.

In this section the research hypotheses tested during that research will be restated as questions. For each question, a summary statement will be given as to the status of the answers determined and what still needs to be done. The questions will be organized into four sub-sections on the open circuit potential, corrosion initiation, corrosion rates and mechanisms.

## A. Ennoblement of the Open Circuit Potential

By the beginning of our ONR funded work it was already well established that biofilms were able to raise (or ennoble) the open circuit corrosion potential of many alloys. In our own work funded by other agencies, we had already asked the questions:

What is the effect of alloy composition on ennoblement of the OCP?
What is the effect of water salinity and temperature?
What is the effect of daylight and light/dark cycling?
What happens to the ennobled OCP when corrosion initiates?

The answers to those questions were summarized in Section II of this Report. Several new questions were asked during the course of the ONR work:

### A.1. *How can one do the proper control experiment, and how do you know if it is effective or not?*

This subject was dealt with in Section IV.A. All control experiments are difficult, and they require much attention on a continuous basis. The objective is to eliminate the electrochemical effect of the biofilm without changing the bulk water chemistry, not necessarily to keep the metal surface "sterile." One knows that the control is effective if the test coupon behaves like a bare sample, as if the biofilm were absent, for the desired duration of the experiment. Treating the water by filtering and low temperature pasteurization works well for experiments of less than one week duration and when small volumes of water are needed. For longer durations, or for volumes of water larger than one liter, treating the water becomes tedious. In that case, and if anode and cathode reactions can be separated, cleaning and recycling cathode panels once a day becomes preferable.

**A.2.** *Do biofilms cause the OCP of manganese-bearing alloys, such as Nitronic 50, Nitronic 40 and Nitronic 33 to ennoble?*

Yes, Nitronic alloys 40 and 50 ennoble similarly to other passive alloys that we have tested over the years. Likewise, ennoblement begins on Nitronic 33. However, localized corrosion initiates readily on that alloy, so it cannot sustain ennobled potentials for very long. See Section III.E.

**A.3.** *If manganese is not available in the environment, will manganese in the alloy accumulate in the biofilm and cause accelerated corrosion?*

In Section III.E, page 41, experiments on the source of manganese were described. In tests conducted to date, Mn in the alloy seems to have no effect when Mn is present in the water at concentrations of 1 μM or higher. Data obtained to date fail to show any statistically significant impact of manganese in the alloy. We have used test waters with two different manganese concentrations (1 to 3 and 6 to 8 μM). Biofilms grown from both these waters accumulated Mn to about the same concentration. We have also tested alloys with Mn concentrations ranging from zero to 4 wt. % (Nitronic 50), but the effect of the biofilm for those alloys did not vary systematically with the concentration of Mn in the alloy. While these results are encouraging for the Navy's proposed use of the Nitronic 50 alloy, we cannot make a definitive conclusion until we test a higher Mn alloy, such as Nitronic 40 (8 wt. %) in a water with low nano-molar level Mn concentrations.

**A.4.** *What is the effect of the electronic structure of the passive film (n-type vs. p-type) on OCP ennoblement?*

Most structural passive alloys have n-type semiconducting passive films. On those alloys ennoblement of the OCP occurs readily, and it persists until the initiation of localized corrosion. Alloys such as N06455 (C4) with p-type passive films, however, do not ennoble as quickly, or to as great an extent, as the n-type alloys. We have suggested that this is due to slow kinetics of electron transfer across the electron-poor p-type passive film. That hypothesis will require further testing before it can be given the status of a conclusion, however. See Section III.B.

## B. Effect of Biofilms on Corrosion Initiation

It is well established that any shift of the OCP in the noble direction increases the probability of passivity breakdown and localized corrosion initiation of passive metals immersed in chloride bearing solutions. Thus, for immersion of such alloys in estuarine and seawater environments we have asked the following questions:

**B.1.** *What is the effect of OCP ennoblement on the initiation time for crevice corrosion?*

There is a lot of inherent scatter in data on crevice initiation time for any passive alloy under any set of testing conditions. This makes it difficult to give a definitive answer to the question. Nevertheless, the extensive testing that has been done on alloys S30400 and S31600 favors the conclusion that OCP ennoblement reduces crevice initiation time. In contrast, no decrease in crevice initiation time has been found for the superaustenitic alloys (eg. 6XN) and superferritic alloys (eg. 29-4C). The case for intermediate alloys, such as N08904 and S31700 is undecided. The manganese bearing alloy, Nitronic 50 has a resistance to corrosion initiation similar to that of S30400. Thus, one would expect the effect of biofilms on crevice initiation of Nitronic 50 to be similar to that of S30400. However, this expectation should be tested by experiments on the Nitronic 50 and 40 alloys before any conclusions are drawn.

**B.2.** *What is the practical significance of a decrease in initiation time?*

Our conclusion is that the significance is more academic than practical. The initiation time for alloys like S30400 is already much shorter than their desired lifetimes in structural applications. Thus, a further decrease in initiation time is of little importance. The significance is also low for the most resistant alloys, since they do not readily initiate localized corrosion with or without biofilms. Alloys with intermediate resistance such as S31700 and N08904 tend to start corroding at lower salinities with biofilm formation than without. At one time, we proposed that this type of data could be used to formulate guidelines for the use of various alloys based on their salinity tolerance in the presence of biofilms. Today we consider this to be impractical due to variations in salinity with time a any given location in typical estuarine environments and due to salinity gradients within structures from fluctuations in flow rate and temperature.

**B.3.** *How does the chemistry developed within biofilms affect the critical pitting and breakdown potentials?*

The effect of biofilm chemistry on pitting and breakdown potentials has been discussed in Section III.A. From this work we concluded that biofilms significantly increased the critical pitting potential for alloy S30400 in seawater, while there was little effect on alloy S31600. The clear implication from that work was that something produced within the biofilm matrix is acting as a pitting inhibitor. Several compounds such as nitrates, phosphates and sulfates are known to be pitting inhibitors. Moreover, it is reasonable to expect that they would be found within biofilms. Further research, however, will be needed to make specific identifications. The reason why there was no

measurable effect on S31600 was not identified. It was thought, however, that the level of inhibition produced in the biofilm was probably not enough to raise the Ecpp value for S31600, which is already higher than that of S30400.

From this work it also was concluded that critical pitting potentials for low resistance stainless steels such as S30400 should be measured using samples with biofilms if the results will be used to predict the initiation of pitting in natural seawater.

**B.4.** *What is the effect of biofilms on localized corrosion initiation on passive alloy weldments?*

We have always maintained that in marine systems the first step is formation of the general microbial biofilm in which initial settlement is random across the submerged metal surface. That biofilm causes a noble shift in the OCP. This in turn leads to an increase in electrochemical activity at the most vulnerable sites as the OCP reaches the breakdown potential at those locations. On weldments, the least resistant sites are usually associated with the weld bead or the heat affected zone. Our data in Section III.C showed clearly that microorganisms are attracted to sites of electrochemical activity. Preferential colonization at those sites then helps to stabilize and localize them, leading to the initiation of stable localized corrosion. All data we have taken in marine systems supports that view.

**B.5.** *How should one understand the spatial relationship between sites of microbial settlement and corrosion initiation?*

There has been a tendency for many investigators to focus on organisms at the corrosion site as the cause of corrosion. The evidence we have gathered in marine systems says that organisms in the general biofilm remote from the corrosion site are also important. While there is a clear relationship between the organisms found at the corrosion site and electrochemical activity coming from that site, the organisms at the site may not always be the first cause of corrosion. Moreover, the organisms are probably at that site because they were attracted to the corrosion that had already started there, rather than the common view that colony formed first and then initiated corrosion.

**B.6.** *How do the effects on weldments in marine environments relate to those in industrial fresh- and waste- waters?*

This is a difficult question because marine systems typically have much higher chloride concentrations and a more diverse microbial population than their industrial water counterparts. However, the process of OCP ennoblement in response to biofilm formation takes place in both fresh and

marine waters. Years ago Kobrin observed that the classical MIC problem on stainless steel weldments in fresh hydrotest waters tended to occur mostly when manganese metabolizing organisms, permanganates and chlorides were all present in the water. Thus, it is reasonable in those systems to expect the process to begin by general biofilm formation and the concentration of chlorides and manganese compounds. This would cause a general ennoblement of the OCP, in turn leading to electrochemical activity around the welds. Formation of biomounds at those sites would then serve to stabilize high concentrations of ferric and manganic chlorides, which are highly corrosive.

This illustrates the need to address more carefully the progression of bacterial attachment before, during and after corrosion initiation if one wants to convincingly establish the mechanism of biological effects on corrosion. Further work needs to be done to precisely address the nature of bacterial attraction to sites of anodic electrochemical activity.

## C. Effect on Cathodic Kinetics and Corrosion Rates

Work done by many investigators, including our lab, in the 1980s showed that cathodic kinetics in the upper portions of cathodic polarization curves were increased due to biofilm formation along with ennoblement of the OCP. This lead us to ask the following questions, and the results were a prime factor in our realization that many of the mechanisms proposed for OCP ennoblement could not account for such kinetic effects.

### C.1. *Does the presence of natural biofilms on passive metal surfaces change the cathodic polarization curves?*

Shifts toward higher currents in the upper part of cathodic polarization curves (above –0.2 V SCE) in the presence of biofilms had been published by Scotto and Johnsen and Bardal as well as ourselves in the 1980s. More recently the Thesis work of John LaFontaine (see Figure III.D.4) showed that biofilms could enhance cathodic kinetics in the –0.3 to –1.0 V range as well.

Manganese within the biofilm is now believed to be responsible for both the shift in potential and the increase in kinetics, but additional work on the electrochemical reactions and microorganisms involved will be necessary to fully understand the mechanism.

### C.2. *Does this change in cathodic polarization result in an increase in crevice corrosion propagation rate?*

Hong-Ji Zhang used both weight loss and remote crevice assembly techniques to demonstrate increased crevice propagation rates in the presence of natural marine biofilms, vs. controls without the biofilm. Other measures

of the effect, such as maximum and average depths of attack and percentage of area attacked under the crevice former also indicated an increased severity of attack in the presence of biofilms.

## C.3. *Are galvanic corrosion rates affected by the presence of biofilms on the cathode member of the couple?*

The work of LaFontaine has established that biofilms on cathodes constructed of passive alloy cathodes do cause higher galvanic corrosion rates on a variety of anode materials. This has been verified by both weight loss and galvanic current measurements.

Tests have not yet been done, however, to see if biofilms on non-passive alloy cathode materials, such as steel and copper alloys will have similar effects. It is known that steel and copper alloys do not usually experience OCP ennoblement upon biofilm formation due to the shapes of their anodic polarization curves. There is no data that we are aware of, however, on whether the cathodic properties of non-passive alloys may be enhanced.

## C.4. D*oes the galvanic corrosion effect depend on the anode material?*

Based on the early cathodic polarization curves published by Scotto and co-workers, we had predicted that galvanic corrosion of copper anodes coupled with passive alloy cathodes would be accelerated by formation of a natural biofilm on the passive alloy. We also predicted that such acceleration would not occur for zinc anodes, while we considered the situation to be uncertain for anodes of steel and structural aluminum alloys.

The predictions for copper and zinc were verified by the Thesis work of John LaFontaine as described in Section III.D. His data showed that galvanic corrosion of mild steel and 3003 aluminum anodes were also increased by natural marine biofilms on the cathode member of the couple. These results on galvanic corrosion of steel anodes agree with experience in the North Sea Oil Industry, where steel anodes are routinely used to protect structural stainless steel from localized corrosion. Steel anode consumption in this application has been higher than expected based on oxygen reduction as the cathode reaction.

In our tests with a cathode to anode area ratio of 10, we thought that zinc was not affected due to the basic pH that would have been generated near the passive alloy cathode surface at the zinc potential. pH values greater than 9 are considered to have an inhibitive effect on the metabolism of many marine microorganisms. If that hypothesis is correct, then one would expect that consumption of aluminum anodes with potentials more active than zinc also

would not be affected. It is not clear, however, that this would still be the case for either zinc or aluminum anodes at higher cathode to anode area ratios, where the cathodic current density would be lower. Thus, further work will be needed to see if these results hold up for aluminum anodes and higher cathode to anode area ratios.

## C.5. *How does the effect of biofilms on cathodic current density compare to that of dissolved oxygen?*

For many decades the common understanding was that corrosion rates in seawater were usually limited by the mass transport rate of oxygen to the cathode surface. This was dependent on the diffusion path length, which was in turn inversely related to velocity of flow past the surface.

This indeed seems to be the case for laboratory tests in simulated seawaters. There is also much data to support it in natural seawater when the tests are done under conditions where biofilms do not form. These would be time periods less than one or two days or at high (or low) temperatures or high velocities.

Under biofilm forming conditions, however, corrosion rates from 2 to 8 times higher than those sustainable by oxygen alone have been repeatedly verified. These results lend credence to contention by the late Frank LaQue and others that natural seawater is more corrosive that artificial saline solutions used to simulate it in the laboratory. Our data show that recycling of Mn in natural biofilms can account for the crevice and galvanic corrosion rates measured.

Additional work will be needed to determine if biofilms have any effect on self-corrosion rates of steel, copper alloys and aluminum alloys when not connected to passive metals in galvanic couples.

## C.6. *How do biofilms affect the cathodic properties of the manganese bearing Nitronic series alloys?*

As described in Section III.E on page 35, the effect of biofilm development on cathodic polarization curves for the Nitronic 50 alloy was similar to that of other alloys tested. Galvanic currents for structural aluminum alloys connected to Nitronic 50 with biofilms were elevated vs. control in a manner similar to that for the same aluminum alloys connected to N08367. Quantitatively, the accelerating effect of biofilms was slightly smaller for Nitronic 50 than for N08367. However, insufficient data have been gathered to date to allow for the statistical significance of that difference to be evaluated.

## D. Mechanisms

One of the main purposes for our ONR funded work has been to investigate mechanisms by which marine biofilms on passive alloys could shift the OCP in the noble direction, thus enhancing corrosion initiation and propagation. Following is a list of question that we have asked during the course of that work and the current status of the answers.

### D.1. *What mechanisms could affect the OCP and how do they do it?*

This summary is not intended to be a comprehensive survey of all possible mechanisms, just the ones we have worked on during our ONR sponsored research.

**D.1.a. Effect of pH on oxygen reduction.** Quite early in the 1990s several investigators showed that a systematic decrease in pH within the biofilm would be sufficient to explain the observed ennoblement of the OCP. We have recently published data showing that the pH within natural biofilms can indeed be below 2. That same data, however, showed that the pH is highly variable both along the metal surface and perpendicular to it. The very low pH values were found to be quite localized. This finding was in agreement with the new heterogeneous model of biofilm structure. Thus, we concluded that there is probably never enough total acidity to account for ennoblement by the pH mechanism alone. We also realized that the pH mechanism alone could not account for the sustained increase in cathodic currents observed for crevice and galvanic corrosion in the presence of biofilms.

**D.1.b. Bacterial enzymes.** Several investigators have proposed that bacterial enzymes might be involved in the ennoblement process. At one time we proposed that bacterial enzymes used in regulating oxygen reduction derivatives, such as superoxide and peroxide, during respiration could be involved in establishing a limited concentration of hydrogen peroxide within the biofilm matrix. This may still be correct, but we now see peroxide as one of several agents by which $MnO_2$ may be reoxidized, rather than a primary component of the ennoblement mechanism.

Other investigators proposed that bacterial enzymes might be involved in enhancement of the oxygen reduction reaction. We do not currently think that any form of oxygen catalysis can be the primary mechanism of ennoblement. The reason for this judgement is that microelectrode measurements of oxygen concentrations in biofilms from several labs (including ours) have shown that it is usually quite low near the metal surface. Thus, direct catalysis of oxygen seems unlikely to be able to explain ennoblement of the OCP, let alone sustained increases in corrosion rate.

**D.1.c. Heavy metal catalysis of oxygen.** While we did not work directly on this mechanism, our chemical measurements of oxygen with microelectrodes have a bearing on it. As stated in the above paragraph, we now believe that any mechanism based on catalysis of oxygen cannot explain the observed

experimental data on increased corrosion rates. The aspect of that mechanism calling for heavy metal involvement, however, we do believe is correct.

**D.1.d. Low oxygen, pH and peroxide.** During the mid-1990s Chandrasekaran's work showed that a combination of low oxygen, low pH and milli-Molar concentrations of peroxide developed in a biofilm could account for the observed ennoblement of the OCP for many passive alloys. This mechanism was consistent with the layered biofilm development model generally accepted at that time.

Two factors worked against the credibility of that model, however. First was the proposal of a new heterogeneous model for biofilm development by Lewandowski and co-workers. We quickly realized that the images we saw when observing biofilms in the epi-fluorescent microscope fit the new model far better than the old layered one. Moreover, the new model made it harder to accept that the combination of oxygen, pH and peroxide could be as uniformly distributed as would be required by the ennoblement model.

Second, our work on the effects of biofilms on corrosion propagation rates made it increasingly obvious that the oxygen-pH-peroxide mechanism could not sustain an elevated cathodic current even though it could ennoble the OCP. Ennoblement of the potential does not require a net current flow, while an elevated corrosion rate does. Since we could not envision any way to maintain the chemical combination required by the model in the face of a sustained current draw, we were forced by our own data to abandon that model. Note, however, that the $MnO_2$ model now favored by many investigators, including ourselves, incorporates many of the features of the earlier model.

**D.1e. New redox reactions.** We originally proposed that we would consider that the biofilm might introduce new redox reactions if other mechanisms that had been proposed proved inadequate. We are now convinced that this is indeed the most viable mechanism, although it contains elements of several earlier mechanisms that proved unable to account for observational data on their own. We had known for several years that biofilms grown from several natural environments tended to accumulate heavy metals, especially iron and manganese. It is now thought that reduction of $MnO_2$ is able to account for both ennoblement of the OCP and the observation of sustained, cathodic currents leading to elevated corrosion rates. Many chemical reactions have been proposed by which a small amount of manganese in the biofilm can be recycled repeatedly through the redox cycle to account for these observations. Further discussion of this mechanism can be found under Item D.2 below.

**D.1.f. Mechanism of day/night light cycling effects.** Data from our pre-ONR work had shown that the OCP of many passive alloys held steadily in

the +350 to +500 mV SCE range when biofilms were grown under darkened conditions. When the same alloys underwent biofilm formation exposed to the daily light/dark cycle, however, the potential cycled between very noble values at night and several hundred mV less noble in the daytime. We attributed these effects to variations in pH within the biofilm caused by photosynthesis. At night when the OCPs were high, the organisms in the biofilm would be producing $CO_2$ during respiration, keeping the pH slightly acidic. In the daylight hours, however, we proposed that photosynthetic organisms in the biofilm would produce oxygen, thus making the pH more basic, and interfering with the ennoblement mechanism. Since we have better tools today for both chemical measurements and biofilm imaging, this question should be revisited. During that work the effect of UV irradiation on the photosynthetic ability of cyanobacteria in the biofilm should also be evaluated.

**D.1.g. What about the structure of the passive film itself?** One of our early thoughts was that the biofilm could be causing a change in thickness or defect structure of the passive film that would affect the OCP through a change in the passive current density, $i_p$. For most alloys we do not currently believe that this is the case. The data from repeated experiments with several student investigators have always failed to show any systematic and reproducible variation of $i_o$ with OCP of the sample in the presence of natural biofilms.

The recent work of Maruthamuthu, however, has shown conclusively that alloys with p-type passive films respond differently to the action of natural biofilms than those with n-type passive films. This difference has become particularly noticeable when alloys of the two types are compared in how they respond to manganese dioxide. During Maruthamuthu's research the reaction kinetics of alloys with electron poor p-type passive films were shown to be slower in reacting to manganese compounds than those with n-type films. Anodic polarization experiments to measure $i_p$ , however, have not yet been run on the p-type alloys. Although the p-type alloys are not as prominently used as structural marine alloys as the n-types, additional work on response of the p-types to OCP ennoblement by biofilms will help us to understand the mechanism.

The work of Maruthamuthu and Ruppel showed that, while alloy C4 ennobles much less due to the p-type structure of the passive film, the galvanic corrosion rate is still increased vs. control for anodes connected to it in the presence of biofilms. Thus, the two effects of biofilms, ennoblement of the OCP and increased cathodic current may not always go together. It still looks, however, like Mn may be able to account for both effects. The reaction kinetics for Mn are just slower on the p-type oxide surface of the C4 alloy than they would be on an n-type alloy.

**D.2.** *What mechanisms could affect a sustained cathodic current and how might they work?*

We now believe that biomineralization and recycling of Mn (and perhaps Fe) compounds within the matrix of natural biofilms from marine, brackish and fresh water systems can account for the ennoblement phenomenon. We have presented direct experimental evidence that recycling of $MnO_2$ in natural marine biofilms can account for the observation of both ennobled open circuit potentials and increased corrosion rates associated with biofilm formation on passive alloys relative to those on bare control samples of the same alloys.

Numerous specific chemical reactions that may be involved have been proposed from our own work and that of other investigators. It has become clear that the amount of Fe and Mn compounds within biofilms is small enough that the electrochemical reactions involved in corrosion would quickly deplete all available oxidized species. Thus, recycling of the available chemical species by a continuous reoxidation mechanism will be necessary to account for the observation of sustained corrosion currents. Several investigators have proposed reactions by which such recycling may be possible. The work of Ruppel in our lab has produced direct experimental evidence that $MnO_2$ cycling actually occurs, and that it can account for the observed corrosion rates. That work also showed that there are both chemical and biological ways of reoxidizing manganese in biofilm environments, and that both types of mechanisms are probably necessary.

Much work remains to be done to show which reactions are actually taking place in various environments and what microbial consortia are for them to be maintained for long periods of time.

**D.3.** *What are the relative proportions of the cathodic current carried by various reactions involving Fe, Mn and other ions within the biofilm matrix?*

The experimental work needed to answer this question has not been done yet, but the data are important to a full understanding of the mechanism by which biofilms affect corrosion rates.

**D.4.** *What methods can be used to relate the chemistry in the biofilm to the colonies of organisms?*

Development of the Au-Hg solid state microelectrodes with tip diameters of 25 μm has given us a tool for measuring concentrations of soluble species of oxygen, oxygen derivatives (eg., peroxide), Fe, Mn and sulfur using square wave voltammetry. Combination of these microelectrodes with a computer controlled micromanipulator has made it possible to measure chemical

profiles through the thickness of the biofilm matrix at any desired point along the metal surface.

Three-dimensional imaging of the microbial community structure in the biofilm is now being done in our lab by scanning laser confocal microscopy. A protocol has been worked out to match the areas at which chemical measurements are made to images from the confocal microscope. A summary of results from the combination of these techniques has been given in Section V.F starting on page 104. The value of this type of data for understanding the mechanism can be increased by the following refinements to the technique:

a) Increase the accuracy and reliability of relocating the area at which chemical profiles were measured for confocal imaging.

b) Increase the resolution of chemical measurements by decreasing the tip diameter of the microelectrodes. We think a reduction to 10 μ m is possible.

c) Optimize the imaging system for deeper penetration into the biofilm matrix, allowing for analysis of thicker and more mature biofilms.

The present imaging system is capable of providing information on microbial community structure, but it cannot provide for identification of micro-organisms beyond the morphological type level. Thus, to confirm that Mn, Fe or sulfur metabolizing organisms are present at the locations where such compounds are found in the chemical profiles, methods must be found for sampling and culturing organisms from specific points in the biofilm.

## **D.5.** *What remains to be done on the effects of biofilms on manganese bearing alloys?*

Data obtained to date indicate that manganese up to 4 % in the alloy (Nitronic 50) does not contribute measurably to the effect of biofilms. This result cannot be stated as a general conclusion, however, until experiments have been done, first with higher Mn alloys and, second in waters that cannot themselves contribute manganese to the biofilm matrix. The Nitronic 40 alloy with 8% Mn should have sufficient resistance to crevice initiation to be a suitable test material. Nitronic 33 has even more manganese, but its corrosion is too low.

The expectation that biofilms should accelerate crevice initiation of Nitronic 50 in a similar way to that of S30400 (see Section VI.B.1) should be tested experimentally.

The differences between corrosion rates of anodes connected to Nitronic 50 and 6XN with biofilms should be tested further to see if it is statistically significant.

## VII. Summary of Students Graduated and Degrees Granted

### A. Magisterial and Doctoral Students

Sakhuja, Dheeraj
Degree: M.S. (1997)
Thesis Title: "Corrosion Initiation Mechanisms on Stainless Steel Weldments"

Xu, Kunming
Degree: M.S. (1997)
Thesis Title: "Development of Hg-Au Microelectrodes for the Determination of Dissolved Mn, Fe, O2 and S(-II) in Marine Biofilms"

LaFontaine, John
Degree: M.S. (1998)
Thesis Title: "Effect of Biofilms on Galvanic Corrosion"

Ruppel, David
Degree: M.S. (1999)
Thesis Title: "The Effect of Biofilms on Galvanic Corrosion"

### B. Doctoral Students

Zhang, Hong-Ji
Degree: Ph.D. (1993)
Dissertation Title: "The Effect of Biofilms on Localized Corrosion of Stainless Alloys"

Chandrasekaran, P.
Degree: Ph.D. (1995)
Dissertation Title: "Mechanism of Potential Ennoblement on Passive Metals Due to Biofilms in Seawater"

Xu, Kunming
Degree: Ph.D. (2000)
Dissertation Title: "Effect of Biofilm Heterogeneity on Corrosion Behavior of Passive Alloys in Seawater."

### C. Post Doctoral Students

Zhang, Hong-Ji

Eashwar, M.

Maruthamuthu, S.

## VIII. Summary of Papers Published With ONR Support

### A. Journal Papers:


Dexter, S. C., 1993, "Role of Microfouling Organisms in Marine Corrosion", Biofouling, Vol. 7, pp. 97-127.

Dexter, S. C., 1996, "Biofouling and Biocorrosion," Bulletin of Electrochemistry (India), Vol. 12, No. 1-2, Jan-Feb, 1996, pp. 1-7.

Xu, K., S. C. Dexter and G. W. Luther, III, 1998, "Voltammetric microelectrodes for biocorrosion studies," Corrosion, Vol. 54, No. 10, p. 814.

Dexter, S. C. and J. P. LaFontaine, 1998, "Effect of natural marine biofilms on galvanic corrosion," Corrosion, Vol. 54, No. 11, p. 851.

Dexter, S. C. and P. Chandrasekaran, 2000, "Direct Measurement of pH Within Marine Biofilms on Passive Metals," Biofouling, Vol. 15, No. 4, pp. 313-325.


### B. Book Chapters:


Edyvean, R.G.J. and S. C. Dexter, 1993, "MIC in Marine Industries," in Microbiologically Influenced Corrosion, A Practical Manual, G. Kobrin, Ed., NACE International, Houston, TX, pp. 47-63.

Dexter, S. C., 1995, "Effect of Biofilms on Marine Corrosion," in Bioextraction and Biodeterioration of Metals, C. Gaylarde and H. Videla, Eds., Cambridge University Press, pp. 129-167.

Dexter, S. C., 1995, Chapter 43, Microbiological Effects, in: Corrosion Tests and Standards, ASTM Manual 20, R. Baboian, Ed., American Society for Testing and Materials, Philadelphia, PA, pp. 419-429.

Dexter, S. C. and P. Chandrasekaran, 1996, "Chemical Changes at the Metal Surface Under Biofilms, Effect on Localized Corrosion," in Critical Factors in Localized Corrosion II, P. M. Natishan, et al., eds., The Electrochemical Society, Pennington, NJ, 1996, pp. 188-200.

Dexter, S. C., 1999, "Role of Biofilms in Determining the Rate of Localized Marine Corrosion," in Critical Factors in Localized Corrosion III, A Symposium in Honor of the 70th Birthday of Jerome Kruger, R. G. Kelly, P. M. Natishan, G. S. Frankel, and R. C. Newman, Eds., PV 98-17, The Electrochemical Society, Pennington, NJ, 1999, pp. 339-352.

## C. Reviewed Conference Papers:


Chandrasekaran, P. and S.C. Dexter, 1993, "Mechanism of Potential Ennoblement on Passive Metals by Seawater Biofilms," CORROSION/93, Paper No. 493, NACE, International, Houston, TX.

Zhang, H-J. and S.C. Dexter, 1993, "Effect of Biofilms on Crevice Corrosion of Stainless Alloys in Coastal Seawater, Proc. 12th International Corrosion Congress, Vol. 5B, NACE, International, Houston, TX, pp. 3761-3772.

Chandrasekaran, P.and S.C. Dexter, 1993, "Factors Contributing to Ennoblement of Passive Metals Due to Biofilms in Seawater," Proc. 12th International Corrosion Congress, Vol. 5B, NACE, International, Houston, TX, pp. 3696-3707.

Dexter, S. C., P. Chandrasekaran, H-J Zhang and S. Wood, 1993, "Microbial Corrosion in Marine Environments: Effect of Micro-fouling Organisms on Corrosion of Passive Metals", Proc. 2nd USA/Argentina Workshop on Biocorrosion and Biofouling, Buckman Laboratories International, Inc., Memphis, TN, pp. 171-180.

Chandrasekaran, P. and S. C. Dexter, 1994, "Bacterial Metabolism in Biofilm Consortia," Paper # 276, CORROSION/94, NACE, Intl., Houston, TX.

Chandrasekaran, P. and S. C. Dexter, 1994, "Thermodynamic and Kinetic Factors Influenced by Biofilm Chemistry Prior to Passivity Breakdown," Paper # 482, CORROSION/94, NACE, International, Houston, TX.

Zhang, H-J. and S. C. Dexter, 1995, "Effect of Biofilms on Critical Pitting Potentials for Stainless Steels S30400 and S31600 in Seawater," Proc. 1995 International Conference on Microbiologically Influenced Corrosion, New Orleans, LA, May, 1995, P. Angel, et al., eds., NACE International, Houston, TX, pp. 70/1 - 70/8.

Dexter, S. C., "Effect of Biofilms on Crevice Corrosion," Proc. COR/96 Topical Research Symposium on Crevice Corrosion, NACE, Houston, TX, 1996, pp. 367-383.

Xu, K., S.C. Dexter and G.W. Luther, 1997, "Development of Voltammetric Microelectrodes for use in Corrosion Studies," Paper No. 300, CORROSION/97, NACE, International, Houston, TX.

Dexter, S.C. and J.P. LaFontaine, 1998, "Effect of Natural Marine Biofilms on Galvanic Corrosion Predicted Using Potentiodynamic Polarization Curves, CORROSION/98 Paper No. 288, NACE, International, Houston, TX.

Eashwar, M. and S. C. Dexter, 1999, "Relation of Bacterial Settlement Patterns to Anodic Activity on Stainless Steel Weldments," Paper No. 174, CORROSION/99, NACE, International, Houston, TX.

## D. Non-Reviewed Conference Papers:

Dexter, S. C., 1994, "Mechanism of Ennoblement by Biofilms on Active/Passive Alloys Immersed in Seawater," in Proc. Tri-Service Conference on Corrosion, June, 1994, Orlando, FL.

LaFontaine, J.P. and S.C. Dexter, 1997, "Effect of Marine Biofilms on Galvanic Corrosion," in Proc. Tri-Service Conference on Corrosion, November, 1997, Wrightsville Beach, NC.

Dexter, S. C., 1998, "Contribution of Biofilms to the Rate of Marine Corrosion," LATINCORR 98 Paper No. S19-08, 3rd Latin American Region Corrosion Congress, Cancun, Mexico, August, 1998.

## E. Other Collaborative Publications Made Possible by ONR Support:

Tatnall, R. E., R. A. Corbett, B. D. Krantz and S. C. Dexter, 1994 "Electrochemical Studies Related to the Proposed Role of Sulfate Reducing Bacteria in Corrosion under Tubercles," Paper # 274, CORROSION/94, NACE, International, Houston, TX.

Tatnall, R.E., R.A. Corbett, B.D. Krantz and S.C. Dexter, 1995, "Electrochemical Response to Acid Production Under a Simulated Tubercle," CORROSION/95 Paper, NACE International, Houston, TX.

Angel, P., S. Borenstein, R. Buchanan, S. Dexter, N. Dowling, B. Little, C. Lundin, M. McNeil, D. Pope, R. Tatnall, D. White and H. Ziegenfuss, Editors, 1995, Proceedings of the 1995 International Conference on Microbially Influenced Corrosion, NACE, Houston, TX, 1995.

Buchanan, R. A., A. L. Kovacs, C. D. Lundin, K. K. Khan, J. C. Danko, P. Angell and S. C. Dexter,1996, "Microbially Influenced Corrosion of Fe, Ni, Cu, Al and Ti Based Weldments in a Marine Environment," CORROSION/96 Paper No. 274, NACE, International, Houston, TX, 1996.

Buchannan, R.A., A.L. Kovacs, C.D. Lundin, K.K. Khan, J.C. Danko, P. Angell and S.C. Dexter, 1997, Microbially Influenced Corrosion of Fe-, Ni-, Cu-, Al- and Ti-Based Weldments, Materials Performance, Vol. 36, No. 6, pp. 46-55.

## F. Papers Currently in Progress From ONR Sponsored Work:

Ruppel, D.T., S.C. Dexter and G.W. Luther, III, 2001, "Role of Manganese dioxide in Corrosion in the Presence of Natural Biofilms," submitted to Corrosion Journal, January, 2001.

Dexter, S.C. and S. Maruthamuthu, 2001, "Response of Passive Alloys with n- and p-Type Passive Films to Manganese in Biofilms," To be presented as Paper No. 256 at Corrosion/2001, March, 2001, Houston, TX.

Dexter, S.C., K. Xu and G.W. Luther, III, 2001, "Sensors for Relating Microbial Colonies and their Chemistry to Localized Corrosion," To be presented at the 199$^{th}$ Meeting of the Electrochemical Society, March, 2001, Washington, D.C.

Dexter, S.C., S. Maruthamuthu and D.T. Ruppel, "Effect of Manganese in Biofilms on Cathodic Properties of Passive Alloys with p-Type Passive Films." In Preparation.

Eashwar, M. and S.C. Dexter, "Polarization Characteristics Of Stainless Alloys In Natural Waters: Time, Biofilm-Mass And Material Dependency" In Preparation.

Eashwar, M. and S.C. Dexter, "Effect Of Material Composition On The Corrosion Potential Of Stainless Alloys In Natural Waters" In Preparation.